Experimental Investigations on the Physics of Streamers

PROEFSCHRIFT

ter verkrijging van de graad van doctor
aan de Technische Universiteit Eindhoven,
op gezag van de rector magnificus, prof.dr.ir. C.J. van Duijn,
voor een commissie aangewezen door het College voor Promoties
in het openbaar te verdedigen
op donderdag 3 februari 2011 om 16.00 uur

door

Sander Nijdam

geboren te Nuenen, Gerwen en Nederwetten

Dit proefschrift is goedgekeurd door de promotoren:

prof.dr. U.M. Ebert
en
prof.dr.ir. G.M.W. Kroesen

Copromotor:
dr.ir. E.M. van Veldhuizen

Contents

Summary

Experimental Investigations on the Physics of Streamers

Streamers are rapidly extending ionized fingers that can appear in gasses, liquids and solids. They are generated by high electric fields but can penetrate into areas where the background electric field is below the ionization threshold. Streamers occur in nature as a precursor to sparks and lightning, but also independently as sprites (large discharges high above thunderclouds) or St. Elmo's fire. Their main applications are gas and water cleaning, ozone creation, particle charging and flow control. Streamers are very efficient in creating active chemical species as no energy is lost in heating of the background gas and surrounding materials. Furthermore, as streamers are the first phase of sparks, they are relevant for any application of sparks, e.g. in the ignition process in a combustion engine or a discharge lamp. Finally, streamers can occur in high voltage applications, like switch-gear. In this thesis, a number of aspects of the physics of streamers are investigated experimentally.

In our study, we have created streamers by applying a high voltage pulse to a wire or sharp tip that is located 40 to 160 mm above a grounded plate. These experiments were conducted inside a vacuum chamber at various pressures between 25 and 1000 mbar, with various gasses and gas mixtures, most of high purity (up to less than 0.1 ppm contaminations).

We create the voltage pulses by two different high voltage pulse sources. The C-supply can give pulses between 5 and 60 kV with a minimum risetime of about 15 ns and an exponential decay of varying duration. The newly built Blumlein pulser creates quasi-rectangular pulses with an amplitude between 20 and 35 kV, a duration of about 130 ns and a risetime of about 10 ns. Both pulse sources can produce pulses of positive and negative polarity but have primarily been used with positive polarity.

First, the interaction of individual streamer channels and the streamer branching angles are analysed by stereo-photography. Then insight into the propagation mechanism of positive streamers (i.e. against the electron drift direction) is gained by changing the gas composition and the repetition frequency of voltage pulses. Finally, morphology, channel diameters, propagation velocities and spectra of laboratory streamer discharges in a variety of gasses and gas mixtures are studied. Some of these studies are used as a "simulation" of sprite discharges on earth as well as on other planets.

Interaction and branching of streamers

Pictures show that streamer or sprite discharge channels emerging from the same electrode sometimes seem to reconnect or merge even though their heads carry electric charge of the same polarity; one might therefore suspect that reconnections are an artifact of the two-dimensional projection in the pictures. We have used stereo-photography to investigate the full three-dimensional structure of such events. We analyse reconnection, possibly an electrostatic effect in which a late thin streamer reconnects to an earlier thick streamer channel, and merging, a suggested photo-ionization effect in which two simultaneously propagating streamer heads merge into one new streamer.

We find that reconnections as defined above occur frequently. Merging on the other hand was only observed with a double tip electrode at a pressure of 25 mbar and a tip separation of 2 mm, i.e. for a reduced tip distance of $p \cdot d = 50 \, \mu\text{m}$ bar. In this case the full width at half maximum of the streamer channel is more than 10 times as large as the tip separation. We have also investigated streamer branching with the stereo-photography method and have found that the average branching angle of streamers under the conditions that were investigated is about 42° with a standard deviation of 12°.

The role of photo- and background ionization in streamer propagation

Positive streamers in air are thought to propagate against the electron drift direction by photo-ionization whose parameters depend on the nitrogen:oxygen ratio. Therefore we study streamers in nitrogen with 20%, 0.2% and 0.01% oxygen and in pure nitrogen and argon. Our new experimental set-up guarantees contamination to be below 0.1 ppm for our purest nitrogen. Streamers in pure nitrogen and in all nitrogen/oxygen mixtures look generally similar, but become thinner and branch more with decreasing oxygen content. In pure nitrogen the streamers can branch so much that they resemble feathers. This feature is even more pronounced in pure argon, with approximately 10^2 hair tips/cm^3 in the feathers at 200 mbar; this density can be interpreted as the density of free electrons that create avalanches

towards the streamer stem.

It is remarkable that the streamer velocity is essentially the same for similar voltage and pressure in all nitrogen/oxygen mixtures as well as in pure nitrogen, while the oxygen concentration and therefore the photo-ionization lengths vary by more than five orders of magnitude. This is supported by recent modelling results by Wormeester *et al.* in 2010.

To study the effects of background ionization on streamers, we have used two methods: variation of pulse repetition frequency (0.01–10 Hz) and addition of about 9 parts per billion of radioactive ^{85}Kr gas to pure nitrogen. We found that higher background ionization levels lead to smoother and thicker streamers. This is similar to the effect of increased photo-ionization close to the streamer tip, created by increasing the oxygen concentration.

Again, we do not see any major effects on streamer properties, except that initiation probabilities go down significantly in pure nitrogen with low (0.01 Hz) repetition frequency. At 200 mbar, the estimated background ionization level from the ^{85}Kr was about $4 \cdot 10^5 \, \mathrm{cm}^{-3}$, which corresponds to the theoretical level in non-radioactive gas at a pulse repetition frequency of about 1 Hz under similar conditions. This fits with the observed variations in streamer morphology as function of repetition frequency for both pure nitrogen and the nitrogen-krypton mixture.

Furthermore, we have found that streamers do not follow the paths of streamers in preceding discharges for pulse repetition frequencies around 1 Hz. This can be explained by the combination of recombination and diffusion of ionization after a discharge pulse which nearly flattens any leftover ionization trail in about 1 second.

Streamers in other gasses and streamer spectra

In order to get more insight in positive streamer propagation, we have studied more than just nitrogen-oxygen mixtures. We have studied pure oxygen, argon, helium, hydrogen and carbon dioxide. Each of these gasses has different properties like ionization levels, excitation levels, cross sections and electronegativity. Furthermore, we have studied streamers in binary gas mixtures that simulate the atmospheres of Venus (CO_2–N_2) and Jupiter (H_2–He). Streamers in these gasses, as well as in air are physically similar to large scale sprite discharges on the corresponding planets. Therefore, the results of our measurements can be used to better equip (space) missions that study sprites on earth and other planets and can help in the interpretation of the observations of these missions.

For all gasses and mixtures, overall morphology, velocities, diameters and emission spectra have been investigated. We have found that it is possible to create streamers in all gasses. Streamer diameters are more or less the same for all gasses, except for pure helium and the Jupiter atmosphere where minimal streamers are respectively 3 and 5 times thicker than in the other gasses. The physical similarity between streamers at different pressures has been confirmed for all gasses that enabled us to measure streamer diameters; the minimal diameters in air and other nitrogen-oxygen mixtures are smaller than in earlier measurements.

Streamer velocities are even more similar; for a given combination of pressure and pulse voltage all propagation velocities are within a factor 2. Streamer brightness on the other hand is very different for the different gas mixtures. Streamers are brightest in nitrogen-oxygen mixtures, nitrogen, argon and helium and dimmest in oxygen, CO_2 and the venusian mixture. The difference between the brightest and dimmest gasses is about three to four orders of magnitude in the optical range.

Streamer spectra from molecular gasses are characterized by molecular bands. In gasses containing a significant amount of nitrogen (including the venusian mixture), the nitrogen second positive system dominates the emission spectrum. In contrast, spark-like discharges in the same gasses are dominated by radiation from neutral and ionized atoms.

Spectra in atomic gasses (argon and helium) are different: the argon spectrum contains mainly atomic argon lines, but the helium spectrum also contains many lines of impurities, while we have no indication that the gas purity is below specification. The reason for the many impurity lines in helium are the high excitation and ionization levels of helium compared to the impurities. These high levels (and low cross sections for electron-atom collisions at low energies) may also explain the large diameter of streamers in pure helium.

Samenvatting

Experimenteel onderzoek aan de fysica van streamers

Streamers zijn geïoniseerde vingers die zich snel voortplanten door gassen, vloeistoffen en vaste stoffen. Ze worden opgewekt door hoge elektrische velden, maar kunnen zich ook voortbewegen door gebieden waar het elektrisch veld lager is dan het zogenaamde ionisatie-veld. Streamers komen in de natuur voor als de eerste fase van vonken en bliksem, maar ook apart als zogenaamde *sprites* (zeer grote ontladingen boven onweerswolken) of het Sint-Elmusvuur. De belangrijkste toepassingen van streamers zijn gas- en waterreiniging, ozonproduktie, het opladen van deeltjes en het beïnvloeden van gasstromingen. Streamers zijn erg efficiënt in het produceren van actieve chemische deeltjes omdat ze geen energie verliezen aan het opwarmen van de omgeving. Omdat streamers ook de eerste fase van vonken zijn, zijn ze ook relevant voor toepassingen van vonken, zoals de ontsteking in een verbrandingsmotor of een ontladingslamp. Als laatste komen streamers voor in de hoogspanningstechniek. In dit proefschrift onderzoeken we enkele aspecten van de fysica van streamers met experimentele technieken.

In het onderzoek produceren we streamers door een hoogspanningspuls toe te passen op een draad of een scherpe punt die 40 tot 160 mm boven een geaarde plaat hangt. Dit is gedaan in een vacuümvat bij drukken tussen 25 en 1000 mbar met verschillende gassen en gasmengsels, veelal met hoge zuiverheid (tot minder dan 0.1 ppm onzuiverheden).

De hoogspanningspulsen worden gemaakt door twee verschillende pulsbronnen. De zogenaamde *C-supply* kan pulsen produceren met een amplitude van 5 tot 60 kV, met een stijgtijd van minimaal 15 ns en een exponentiële afval met instelbare lengte. De nieuw gebouwde *Blumlein pulser* maakt quasi-rechthoekige pulsen met een amplitude tussen 20 en 35 kV, een lengte van ongeveer 130 ns en een stijgtijd van ongeveer 10 ns. Beide bronnen kunnen zowel positieve als negatieve pulsen maken, maar wij hebben voornamelijk positieve pulsen gebruikt.

Als eerste analyseren we de interactie tussen individuele streamer-kanalen en

de vertakkingshoeken door middel van stereofotografie. Hierna bekijken we het precieze voortbewegingsmechanisme van positieve streamers (die tegen de elektronendriftrichting bewegen) door middel van variatie van de gassamenstelling en de pulsfrequentie. Als laatste bekijken we morfologie, kanaaldiameters, voortbewegingssnelheden en spectra van streamerontladingen in een grote variëteit aan gassen en gasmengsels. Een deel van dit werk wordt gebruikt als een simulatie van spriteontladingen op aarde en op andere planeten.

Interactie en vertakking van streamers

Plaatjes van streamerontladingen laten vaak zien dat twee streamers uit dezelfde elektrode zich later weer met elkaar lijken te verbinden of samensmelten, ondanks het feit dat ze beide dezelfde polariteit hebben. Het lijkt dan ook dat dit effect een artefact is van de inherent tweedimensionale projectie in de foto's. Om deze redn hebben we stereofotografie toegepast om de volledige driedimensionale structuur van deze ontladingen te bestuderen. We analyseren re-connectie, waarschijnlijk een elektrostatisch effect waarbij een late streamer verbindt met een dik eerder kanaal, en samensmelting, een effect dat veroorzaakt lijkt door foto-ionisatie waarbij twee naast elkaar voortbewegende streamers samensmelten tot één nieuwe.

We hebben vastgesteld dat re-connecties zoals hierboven gedefinieerd inderdaad regelmatig voorkomen. Samensmelten is echter alleen gezien bij een elektrode met twee punten met een onderlinge afstand van 2 mm bij een druk van 25 mbar, oftewel, een gereduceerde puntafstand van $p \cdot d = 50\,\mu$m bar. In dit geval is de breedte van het streamerkanaal al ruim tien keer zo groot als de puntafstand. Verder hebben we ook de vertakkingshoeken van streamers onderzocht met de stereofotografie methode. We hebben gevonden dat in ons geval de gemiddelde vertakkingshoek ongeveer 42° is met een standaarddeviatie van 12°.

De rol van foto- en achtergrondionisatie bij streamer propagatie

Omdat positieve streamers zich voortbewegen tegen de elektronendriftrichting in, hebben ze een bron van elektronen nodig voor zich. In het algemeen wordt aangenomen dat foto-ionisatie deze bron is. Foto-ionisatie hangt sterk af van de verhouding tussen stikstof en zuurstof in het gas. Daarom hebben we experimenten gedaan in stikstof met 20%, 0.2% en 0.01% zuurstof en in zuivere stikstof en argon. Onze nieuwe opstelling garandeert zuiverheden tot lager dan 0.1 ppm voor de zuiverste stikstofvariant. We hebben gezien dat streamers in zuivere stikstof en alle stikstof/zuurstofmengsels behoorlijk op elkaar lijken. De streamers worden wel dunner en ze vertakken meer naarmate er minder zuurstof in het gas zit. In zuivere stikstof beginnen de streamers zelfs op vogelveren te lijken. Dit effect is nog sterker in zuivere argon met ongeveer 10^2 haartjes/cm^3 in de veren bij 200 mbar. Deze

dichtheid kan worden geïnterpreteerd als de dichtheid van vrije elektronen die lawines veroorzaken richting de streamerstam.

Het is opvallend dat de voortbewegingssnelheid van de streamers vrijwel hetzelfde is in alle stikstof/zuurstofmengsels en in zuivere stikstof (bij dezelfde druk en spanningspuls), terwijl de zuurstofconcentratie en dus ook de foto-ionisatie lengtes meer dan vijf ordegroottes variëren. Dit effect is recentelijk ook gevonden in modelberekeningen door Wormeester *et al.* in 2010.

Om de effecten van achtergrondionisatie op streamers te bestuderen hebben we twee methodes gebruikt: variatie van de pulsfrequentie (0.01–10 Hz) en toevoeging van ongeveer 9 ppb radioactief ^{85}Kr gas aan zuivere stikstof. We hebben gevonden dat hogere achtergrondionisatieniveaus leiden tot dikkere en gladdere streamers. Dit is vergelijkbaar met het effect van meer foto-ionisatie bij de streamerkop door verhoging van de zuurstofconcentratie.

Ook hier vinden we geen grote effecten op de eigenschappen van de streamers, behalve dat de kans op streamer-initiatie flink lager is in zuivere stikstof bij een lage pulsfrequentie (0.01 Hz). Bij 200 mbar is het geschatte achtergrondionisatieniveau veroorzaakt door de ^{85}Kr toevoeging ongeveer $4 \cdot 10^5$ cm^{-3}, wat overeenkomt met het theoretisch geschatte niveau in niet-radioactief gas bij een pulsfrequentie van ongeveer 1 Hz onder dezelfde omstandigheden. Dit klopt met de geobserveerde variaties in streamermorfologie voor verschillende pulsfrequenties bij zowel zuivere stikstof als het stikstof-krypton mengsel.

Verder hebben we gevonden dat streamers niet hetzelfde pad volgen als hun voorgangers in voorgaande ontladingen bij pulsfrequenties rond de 1 Hz. Dit kan worden verklaard door een combinatie van recombinatie en diffusie van achtergebleven ionisatie na een ontlading. Beide effecten samen zorgen er voor dat het achtergebleven ionisatiepad vrijwel verdwijnt in 1 seconde.

Streamers in andere gassen en streamerspectra

Om meer inzicht te verkrijgen in de voortbewegingsmechanismes van positieve streamers hebben we meer onderzocht dan alleen stikstof/zuurstof mengsels. We hebben gebruik gemaakt van zuivere zuurstof, argon, helium, waterstof en koolstofdioxide. Al deze gassen hebben verschillende eigenschappen zoals ionisatie- en excitatieniveaus, botsingsdoorsnedes en elektronegativiteit. Verder hebben we streamers onderzocht in binaire gasmengsels die de atmosferen van Venus (CO_2–N_2) en Jupiter (H_2–He) nabootsen. Streamers in deze gassen, en in lucht, zijn fysisch vergelijkbaar met grootschalige sprite-ontladingen in de atmosferen van deze planeten. Daarom kunnen de resultaten van onze metingen gebruikt worden voor de uitrusting van toekomstige (ruimte)missies die sprites op deze planeten willen bestuderen. Ook kunnen de resultaten helpen in de interpretatie van de

observaties van dit soort missies.

Van alle hierboven genoemde gassen en mengsels hebben we de algemene morfologie, voortplantingssnelheden, diameters en emissiespectra onderzocht. We hebben gevonden dat het in alle gassen en mengsels mogelijk is om streamers op te wekken. Streamer diameters zijn min of meer gelijk voor alle gassen, behalve voor zuiver helium en het Jupitermengsel waarin de dunste streamers respectievelijk 3 en 5 maal dikker zijn dan in de andere gassen. De fysische schaling van streamerdiameters bij verschillende drukken is bevestigd voor alle gassen waarin we de diameters hebben kunnen meten. De gevonden minimale diameters in lucht en stikstof/zuurstof mengsels zijn kleiner dan in eerdere metingen.

Voortplantingssnelheden zijn nog meer gelijk dan diameters voor de verschillende gassen. Bij een gegeven combinatie van druk en spanningspuls vallen alle snelheden binnen een factor twee. De helderheid van de streamers daarentegen varieert behoorlijk. Streamers in stikstof/zuurstofmengsels, stikstof, argon en helium zijn het helderst terwijl streamers in zuurstof, CO_2 en de Venusatmosfeer het minste licht uitstralen. Het verschil tussen de helderste en lichtzwakste gassen bedraagt drie tot vier ordegroottes (voor het zichtbare golflengtegebied).

Streamerspectra van alle moleculaire gassen worden gekarakteriseerd door de moleculaire banden. In gassen met een significante hoeveelheid stikstof (waaronder de Venusatmosfeer), wordt het spectrum gedomineerd door het *second positive system*. Vonk-achtige ontladingen in dezelfde gassen daarentegen worden gedomineerd door straling van neutrale en geïoniseerde atomen.

Spectra van streamers in atomaire gassen (argon en helium) zijn anders: het argonspectrum bevat vooral atomaire argonlijnen terwijl het heliumspectrum ook veel lijnen van onzuiverheden bevat (we hebben geen aanwijzing dat er veel onzuiverheden in zitten). Dit kan worden verklaard door de hoge excitatie- en ionisatieniveaus van helium vergeleken met de onzuiverheden. Deze hoge niveaus (en bijbehorende kleine botsingsdoorsnedes voor elektron-atoombotsingen bij lage energieën), kunnen waarschijnlijk ook de grote diameters van streamers in zuiver helium verklaren.

Chapter 1

Introduction

1.1   What are streamers?

Streamers are rapidly extending ionized fingers that can appear in gasses, liquids and solids. They are generated by high electric fields but can penetrate into areas where the background electric field is below the ionization threshold. This is possible because the interior of the streamer channel consists of a conducting plasma. Therefore the electric field in this interior is largely screened. This is only possible when the interior is surrounded by a space charge layer. At the front of the ionized finger, the space charge layer is strongly curved and therefore significantly enhances the electric field in the non-ionized area ahead of it. This self-organization mechanism makes the streamer a well-defined non-linear structure. The non-linearity is caused by space charge effects as explained above while gas heating is negligible in most cases. Electron and ion density, space charge and field distribution in a simulated streamer are shown in figure 1.1.

Streamers occur as a precursor to sparks, but can also exist independently, depending on conditions. In nature they create the path for lightning, and also occur as large discharges, called sprites, far above thunderclouds. This will be discussed in more detail below. As a precursor to sparks, streamers are of interest in any high voltage application where they are often to be avoided. However, they also have many useful applications themselves, which will also be discussed below.

We want to study streamers to gain insight in their properties, relate this to our theoretical understanding of streamers and thereby help the development of applications of streamers. Furthermore, good experiments and better understanding of laboratory streamers helps in the detection and interpretation of naturally
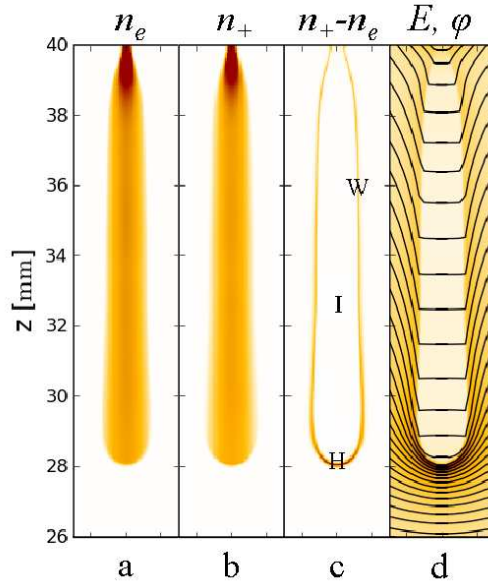
Figure 1.1: Structure of positive streamers shown by zooming into the relevant region of a simulation by Ratushnaya *et al*. The panels show: a) electron density n_e, b) ion density n_+, c) space charge density $(n_+ - n_e)$, d) electric field strength E and equipotential lines φ. The letters in panel c indicate the streamer regions: H - streamer head, I - interior and W - wall of the streamer channel. Image from [175].

occurring discharges like sprites and lightning on earth and other planets.

1.2   Streamers in nature

Sparks

As was mentioned above, sparks are preceded by streamers. The streamers can propagate through virgin air and create an ionized channel that can evolve into a spark. Without this ionized channel, no spark can occur.

Lightning leaders

A cloud-to-ground lightning stroke creates its path towards earth through a leader. This is a hot conducting channel of air that propagates to the ground in a stepped way. These channels are therefore often called stepped leaders. Each step is typically 50 meters in length [219]. At the front of each of these leaders, a corona of streamers creates the first ionized path like for a spark (which is closely related to a
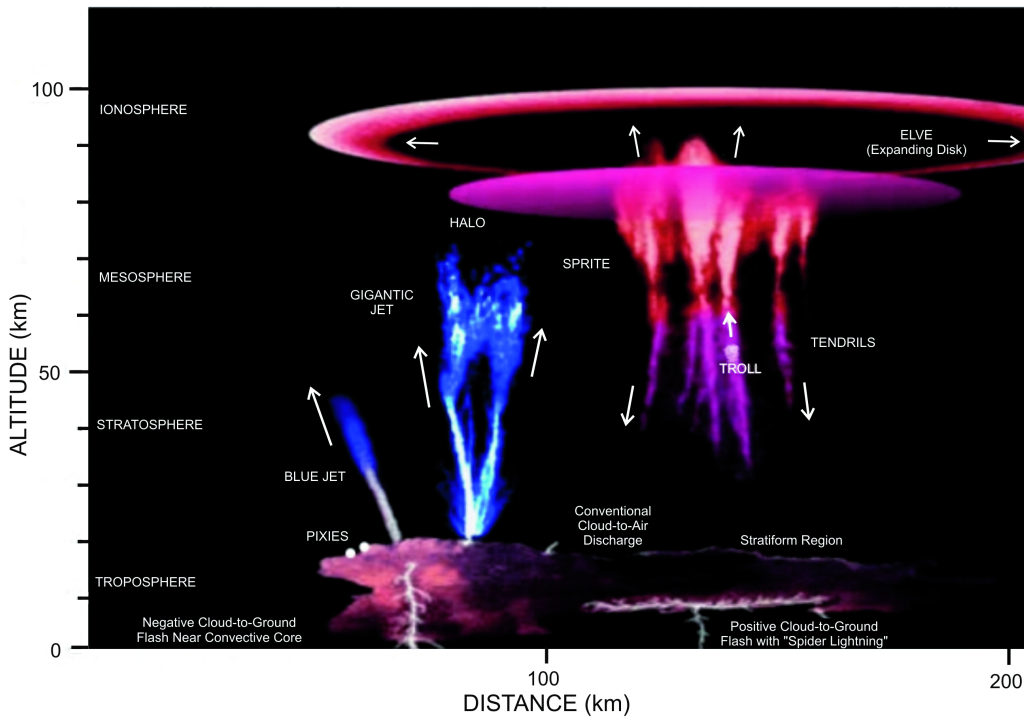
Figure 1.2: Artist impression of lightning, sprites and other TLE's. Figure by D.D. Sentman, Univ. Alaska in Fairbanks.

leader). When a leader has found the ground, or attaches to a leader coming from the ground, a complete conducting path is formed and the so-called return-stroke commences. The strong current in the return stroke produces most of the light and sound associated with lightning.

Sprites and other TLE's

Lightning is often accompanied by electric discharges in the upper atmosphere, known as TLE's (transient luminous events); they were first described in the scientific literature in 1990 [57]. The various TLE's observed in the terrestrial atmosphere consist of several distinct phenomena, which are known as sprites, ELVES, blue jets, as well as several other sub-species (see figure 1.2). Red sprites are an impressive display of light above the thunderclouds which span a vertical range of 50 to 90 km above the surface and take many forms. They are red in colour, although their lowermost, tendril-like part can be blue, see Sentman *et al.* [185]. It is now commonly accepted that sprites are in fact large streamer discharges that have many similarities to laboratory scale discharges at higher pressures [52, 165].

St. Elmo's fire

St. Elmo's fire is a phenomenon that was first observed on masts of ships during thunderstorms. Under such conditions, a glowing ball of light could sometimes be observed at the tips of the masts. This glowing ball of light is in fact a (DC) streamer corona discharge that is formed due to the field enhancement at the tip of the masts. The same phenomenon can also be observed on lightning rods, chimneys, aircraft wings and, in reduced form, on power lines or other high-voltage wires or pins. In the latter cases no thunderstorm is required. St. Elmo's fire can often be heard by a distinct buzzing sound.

1.3   Application of streamers

Streamers are used in a variety of applications. Their advantage over hot discharges like sparks and arcs is that they are more energy efficient in the production of chemical active species. Because streamers are very far from thermodynamic equilibrium, they do not heat up the gas or surrounding materials. Below is an (incomplete) list of streamer applications:

Gas and water cleaning The chemical active species that are produced by streamers can break up unwanted molecules in industrially polluted gas and water streams. Contaminants that can be removed include organic compounds (including odours), NO_x, SO_2 and tar. See [40, 70, 220, 232].

Ozone generation By simply applying a streamer discharge in air, first O* radicals and then ozone is created. The low temperature in a streamer discharge limits the destruction of produced ozone. The ozone can be used for different purposes like disinfection of medical equipment, sanitizing of swimming pools, manufacturing of chemical compounds and more. See [220].

Particle charging A negative DC corona discharge can charge dust particles in a gas flow. These charged dust particles can now be extracted from the gas by electrostatic attraction. Similar charging methods are used in copying machines and laser printers. See [90, 220]

Flow control A streamer discharge can have a (small) influence on gas flows. This can be used to improve the flow around an air-plane wing, better control a flame or cooling electrical components. The main advantage of such flow control over conventional methods is that no moving parts are needed. See [138, 198].

1.4   Major topics in this thesis

In this work we we study aspects from the physics of streamer discharges which are relevant for all applications and occurences of streamers. We focus on laboratory experiments on pulsed positive streamers in a variety of gasses at pressures between 25 and 1000 mbar. Our most important diagnostic technique is streamer imaging by means of a fast camera.

Results from this study can be used in a variety of fields: improvement of streamer models (both macroscopic and microscopic), improvement of streamer application research and better understanding of naturally occurring streamer discharges. We explicitly compare our laboratory experiments with sprites.

Streamers can be generated by high voltage of positive or negative polarity. Although these positive and negative streamers have much in common, they also have some fundamental differences. Streamers propagate so fast that the heavy particles do not significantly contribute to streamer propagation. Therefore, the only moving particles are the electrons. In a negative streamer, the electrons drift in the same direction as the streamer propagates, while in a positive streamer, they drift against the propagation direction. This difference has many implications on streamer properties. Negative streamers provide their own free electrons while positive streamers need a source of free electrons ahead to continue to propagate. There are two likely candidates for this source of electrons: photo-ionization and background ionization.

Most modern streamer models only treat streamers in air and therefore use photo-ionization as the only source of these free electrons. In this photo-ionization mechanism, a UV-photon emitted by an excited nitrogen molecule can directly ionize an oxygen molecule. It therefore depends on the presence of both nitrogen and oxygen. However, if only photo-ionization is responsible for propagation of streamers, it is unclear what will happen in pure gasses like nitrogen. Is there still enough photo-ionization possible because of trace amounts of oxygen or is another electron source needed, and if so, is it available? The other suggested source would be background ionization. Not much work has been published about the exact effects of (lack of) photo-ionization in streamers and the effects of background ionization. In this thesis we investigate both mechanisms by means of laboratory experiments in air, other nitrogen-oxygen mixtures, pure nitrogen (up to 99.99999% purity) and pure nitrogen with addition of a small amount of radioactive krypton-85.

Another issue in predicting streamers is the interaction between streamers. The branching of streamers has never been studied extensively, while it is an important ingredient for macroscopic models of the streamer-tree. Many of these macroscopic

models now rely on wrong assumptions regarding the branching mechanism (see section 2.4.1) and are therefore in need of revision. An even less studied topic is the interaction between two existing streamers. Can they merge or connect to each other? We study all these branching and interaction mechanisms by means of stereo-photography of streamer discharges.

The final topics treated in this thesis are morphology and emission spectra of streamer discharges in a variety of gasses. As was mentioned above, most streamer research is focused on air or gas mixtures that are close to air (e.g. contaminated air). In order to get more insight in the processes that occur in a streamer discharge in general, it can help to also look at other gasses. We have investigated streamer discharges in pure argon, oxygen, CO_2, hydrogen and helium. For these gasses we have looked at important streamer properties like diameters, propagation velocities and general morphology. Furthermore, we have recorded the emission spectra of streamer discharges in these gasses. These help us understand which species are present in the discharge and thus which processes occur in the streamer. We also briefly compare the emission spectra of (cold) streamer discharges with (hot) spark discharges.

Related to this work is the prediction of sprites and their light emissions on other planets by means of streamer laboratory experiments. Knowledge about sprites on other planets can help in selecting proper equipment for spacecraft missions that are designed to detect and image these extraterrestrial discharges. Here we focus on streamer discharges in gas mixtures that represent the atmospheres of Venus and Jupiter.

Part of the work in this thesis builds on the work of Tanja Briels [32]. She studied fundamental aspects of streamers with methods that are equal or similar to many of the methods discussed here. She focused on effects of pulse polarity, amplitude and shape on streamer evolution and morphology as well as on quantifiable parameters like propagation velocity and diameter. By doing this, she confirmed the similarity laws (see section 2.3.2) and started investigations into the differences between air and pure nitrogen.

1.5   Organization of the thesis

The theoretical background of streamers will be treated in chapter 2. Here we will also explain the similarities and differences between streamer discharges and related discharges like avalanche, glow and arc discharges. Furthermore, we will discuss the commonalities between laboratory streamer experiments and sprites.

Most aspects of our experimental set-ups and measurement techniques are discussed in chapter 3 although also chapters 4 and 8 contain substantial sections regarding the specific techniques employed in the measurements discussed there.

Chapter 4 is dedicated to stereoscopic investigations of streamer discharges to better understand the interaction between streamers. We look at streamer branching angles and merging and reconnection of streamer channels.

In chapters 5 and 6 we investigate the effects of respectively photo- and background ionization on propagation of positive streamers in air and other nitrogen-oxygen mixtures.

Chapters 7 and 8 treat measurements on streamers in a variety of gasses and gas mixture, where the former is focused on general streamer morphology and properties and the latter on emission spectra.

We conclude with chapter 9 that summarizes the most important results and gives ideas for future work.

Finally, we have added two appendices. Appendix A describes and explains a peculiar streamer discharge morphology that was found during the course of the investigations. Appendix B contains some additional images to support chapters 5 and 7.

1.6   Related publications

Parts of the work described in this thesis have been published by or submitted to scientific journals. Chapter 4 is largely based on

S. Nijdam, J. S. Moerman, T. M. P. Briels, E. M. van Veldhuizen and U. Ebert, *Stereo-photography of streamers in air*, Appl. Phys. Lett. **92**, 101502 (2008).

and

S. Nijdam, C. G. C. Geurts, E. M. van Veldhuizen and U. Ebert, *Reconnection and merging of positive streamers in air*, J. Phys. D: Appl. Phys. **42**, 045201 (2009).

Chapter 5 is largely based on

S. Nijdam, F. M. J. H. van de Wetering, R. Blanc, E. M. van Veldhuizen and U. Ebert, *Probing photo-ionization: Experiments on positive streamers in pure gases and mixtures*, J. Phys. D: Appl. Phys. **43**, 145204 (2010).

The work related to extraterrestrial sprites that is part of chapters 7 and 8 was published as

D. Dubrovin, S. Nijdam, E. M. van Veldhuizen, U. Ebert, Y. Yair and C. Price, *Sprite discharges on Venus and Jupiter-like planets: a laboratory investigation*, J. Geophys. Res. - Space Physics **115**, A00E34 (2010).

A shortened version of appendix A can be found in

S. Nijdam, K. Miermans, E. van Veldhuizen and U. Ebert, *A peculiar streamer morphology created by a complex voltage pulse*, 2011 special issue of the IEEE Transactions on Plasma Science, Images in Plasma Science, submitted.

Related work is also published or in press:

V. Yordanov, A. Blagoev, I. Ivanova-Stanik, E. M. van Veldhuizen, S. Nijdam, J. van Dijk and J. J. A. M. van der Mullen, *Surface ionization wave in a plasma focus-like model device*, J. Phys. D: Appl. Phys., **41**, 215208 (2008).

E. M. van Veldhuizen, S. Nijdam, A. Luque, F. Brau and U. Ebert, *3D properties of pulsed corona streamers*, Eur. Phys. J. Appl. Phys., **47**, 22811 (2009).

U. Ebert, S. Nijdam, C. Li, A. Luque, T. M. P. Briels and E. M. van Veldhuizen, *Recent results on streamer discharges and their relevance for sprites and lightning*, J. Geophys. Res. - Space Physics, **115**, A00E43 (2010).

G. Wormeester, S. Pancheshnyi, A. Luque, S. Nijdam and U. Ebert, *Probing photoionization: Simulations of positive streamers in varying N_2:O_2-mixtures* J. Phys. D: Appl. Phys., **43**, 505201 (2010).

S. Nijdam, E. M. van Veldhuizen and U. Ebert, *Comment on "NO_x production in laboratory discharges simulating blue jets and red sprites" by H. Peterson et al.*, J. Geophys. Res. - Space Physics, **115**, A12305 (2010).

U. Ebert, F. Brau, G. Derks, W. Hundsdorfer, C.-Y. Kao, C. Li, A. Luque, B. Meulenbroek, S. Nijdam, V. Ratushnaya, L. Schäfer and S. Tanveer, *Multiple scales in streamer discharges, with an emphasis on moving boundary approximations*, NonLinearity, in print.

Finally, the following related paper has been submitted:

G. Wormeester, S. Nijdam and U. Ebert, *Feather-like Structures in Positive Streamers*, Jpn. J. Appl. Phys.

Chapter 2

DC and pulsed discharges: Observations and concepts

2.1 Streamers, Townsend, glow and other discharge types

We define a streamer as a moving ionization finger which screens its interior by means of space charge. The space charge in the curved tip of the streamer locally amplifies the background electric field ahead of it.

A simple classification of common DC and pulsed discharge types, including a streamer discharge, is given in table 2.1. Here, the discharges are classified by their time-dependence (transient or stationary) and by the importance of effects of space charge and heating (of neutral gas species) on the discharge. Pulsed streamer discharges, the main topic of this thesis, are characterized as transient discharges in which space charge effects play an important role but where no heating occurs. In contrast to stationary DC discharges they do not depend on boundary conditions.

Of course a classification like this is never complete; it does not include discharges that are close to stationary but are still influenced by a varying external

Table 2.1: Classification of DC and pulsed discharge types by dividing them in transient and stationary discharges and in cold discharges with and without space charge and hot discharges.

	Without space charge	With space charge	With heating
Transient	Avalanche	Streamer	Leader
Stationary	Townsend	Glow	Arc/spark
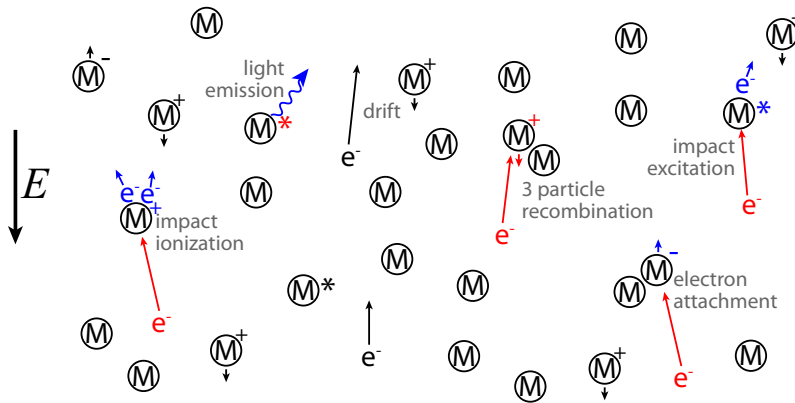
Figure 2.1: General mechanisms present in most gas discharges. The Ⓜ-symbol indicates atoms or molecules (neutral, excited (*) or ionized (+ or -)). A red colour indicates species or properties before a reaction, a blue colour after this reaction. The direction of the electric field is indicated on the left. Dimensions, velocities and ratios are not drawn to scale. Diffusion of heavy particles is not indicated.

electric field (e.g. radiofrequent discharges). Furthermore, many discharges are operated with a stationary external field, but still occur as transient discharges. The most prominent example (for this work) of such a discharge is the "intermittent" DC corona discharge.

In longer electrical pulses, the discharge types from table 2.1 can occur after each other. The discharge starts as an avalanche, then becomes a streamer, which can develop into a glow and finally an arc discharge. Which discharge exactly occurs depends on many parameters like pressure, gap distance, electrode geometry and gas type and on electrical parameters like pulse duration and shape, voltage amplitude and maximal provided current. The most important mechanisms of cold discharges and their transitions will be discussed below.

All of these discharges operate in "bulk" gas, but can under specific conditions also operate over surfaces. Dielectric barrier discharges, in contrast, always operate on or near a (dielectric) surface, hence the name.

Avalanche discharges and transition to streamer

In an avalanche discharge, electrons are accelerated in a high externally applied electric field. At a certain kinetic energy, they can ionize background gas atoms or molecules and create more electrons. These and a few other important microscopic processes that are important in most gas discharges are indicated in figure 2.1. The number of electrons generated per unit length per electron by this impact

ionization is called the Townsend impact ionization coefficient α_i:

$$\alpha_i\left(|\boldsymbol{E}|\right) = \alpha\left(|\boldsymbol{E}|/E_0\right) = \sigma_i \cdot n_0, \tag{2.1}$$

where $|\boldsymbol{E}|$ is the electric field, σ_i the cross section for electron impact ionization, n_0 the background gas density and E_0 is a parameter for the effective cross section at given gas density [136]. A special form of this equation for stationary discharges in homogeneous fields was proposed initially by Townsend:

$$\alpha_i\left(|\boldsymbol{E}|\right) = \alpha_0 \exp\left(-E_0/|\boldsymbol{E}|\right), \tag{2.2}$$

where α_0 is a second parameter related to the effective cross section at given gas density. The ionization length $1/\alpha_i$ determines an intrinsic length for the plasma. This length is the mean length that an electron drifts in the fields before it creates an electron-ion pair by impact. Therefore, in geometries smaller than this length, no gas discharge can occur. Both the electron mean free path between any collision and the ionization length scale with inverse gas density. The subsequent scaling of streamers and other discharges will be discussed in section 2.3.2.

As long as the charge produced by the impact ionization process does not significantly change the electric field, the discharge is called an avalanche. When the electric field is significantly enhanced, the discharge changes into a streamer. This transition is discussed in more detail in section 2.2.

Townsend and glow discharges

Like streamer and avalanche discharges, Townsend and glow discharges are cold discharges. They usually occur as a stationary discharge but have to be preceded by another discharge like a streamer or avalanche discharge to ignite. In Townsend and glow discharges, electrons are emitted from the electrode and are then multiplied in the gap. In the case of a Townsend discharge the electron multiplication takes place in the whole gap, while in a glow discharge, space charge concentrates the multiplication in the cathode sheath region. Electrons are freed from the cathode by the temperature of the cathode itself or by secondary emission either due to the impact of energetic positive ions or due to photons or heavy neutrals.

The sheath region of a glow discharge has a high electric field due to charge separation between fast electrons and slow positive ions (causing the so-called cathode fall). The fast electrons emitted by the cathode and accelerated by the high field multiply by impact ionization on the sheath edge. In many glow discharges, most space between the electrodes is occupied by the positive column, a region with a relatively low, constant, electric field. However, the discharge can contain up to eight distinguishable regions [172]. See also Šijačić and Ebert [190] for a detailed description and numerical model about the Townsend to glow discharge transition. In their one dimensional model (equivalent to a plate-plate discharge)

they find that depending on $p \cdot d$ (pressure times distance) and the secondary emission coefficient of the cathode γ, the transition can occur according to the textbook sub-critical behaviour or for smaller values of $p \cdot d$ it can also behave supercritical or have some intermediate "mixed" behaviour.

Transition to sparks, arcs or leaders

Avalanches, Townsend, streamer and glow discharges are all examples of cold discharges. This means that the heavy particle temperature is not much above room temperature and definitely far below the electron temperature ($T_e \gg T_i \approx T_n$ where e, i and n stand for electron, ion and neutral respectively). At even higher currents, at higher pressures or with longer pulse durations, these discharges can transform into spark, arc or leader discharges. These are all hot discharges, the heavy particle temperature is close to the electron temperature and can reach thousands of Kelvin ($T_e \approx T_i \approx T_n$). In applications, heating of the gas is often problematic and therefore cold discharges are preferred in many plasma treatment applications. Furthermore, the heating itself leads to higher thermal losses and thereby is a waste of energy that reduces the chemical efficiency of hot plasmas [58].

Continuous versus pulsed corona

Corona discharges can be separated in two different categories: continuous and pulsed coronas. Continuous corona discharges occur at DC or low frequency AC voltages. In such a discharge, there is a continuous initiation of streamers. However, if the circuit providing the voltage can support high currents, these will transform into a stationary glow or spark discharge. Therefore, continuous corona discharges can only occur if the current is limited. One example is a continuous corona discharge around high voltage power lines, where the large gap to ground limits the current. A recent example of work on DC corona discharges is by Eichwald *et al.* [54].

A pulsed corona is produced by applying a short voltage pulse to an electrode. Its practical advantages are that the short duration of the pulse ensures that no transition to spark takes place and therefore it can be used at higher voltages and currents than a continuous corona. Energy is only put into electrons that create chemical transitions, not in any inefficient thermal heating. Furthermore, electron energies can be very high, which can be beneficial for the transitions. These effects are very useful in applications like gas treatment. Such applications also benefit from the much higher power densities that are possible for pulsed coronas compared to DC or AC coronas. Another advantage of the pulsed corona is that it can be triggered with a high time accuracy, which makes it possible to study the discharge with fast cameras. For these reasons, all streamers discussed

in this thesis are pulsed corona discharges.

2.2   Streamer initiation

Streamers always start in the form of an avalanche as discussed above. When a first electron is accelerated in a high electric field, it creates more free electrons by impact ionization, that again liberate more electrons.

In a homogeneous field, according to the Raether-Meek criterion (a classical estimate from the late 1930's), space charge effects set in when the total number of free electrons reaches $10^8 - 10^9$ under standard temperature and pressure conditions [130, 171][1]. At this point a streamer can initiate. If we assume that in a constant electric field the electron density n_e grows by impact ionization (*ii*) like

$$[\partial_t n_e]_{ii} = \mu_e \cdot |\boldsymbol{E}| \cdot \alpha_i \left(|\boldsymbol{E}|\right) \cdot n_e, \tag{2.3}$$

with μ_e the electron mobility, and that the loss terms (mainly wall recombination and attachment) are relatively low, then one electron can lead to the required number of new electrons if

$$\exp\left(\alpha_i \left(|\boldsymbol{E}|\right) \cdot d\right) \approx 10^8 \text{ to } 10^9, \tag{2.4}$$

with d the avalanche length. In other words,

$$\alpha_i \left(|\boldsymbol{E}|\right) \cdot d \approx 18 \text{ to } 21. \tag{2.5}$$

Even though this old rule of thumb is very useful for rough approximations, recent simulation results have given more insight in the exact process of streamer initiation. Montijn and Ebert [136] have performed such simulations and combined them with analytical models. They choose that from a field enhancement of 3% above the background field, the additional field generated by the space charges can no longer be neglected. They find that the transition point $\alpha_i \left(|\boldsymbol{E}|\right) \cdot d$ depends strongly on diffusion and on the background electric field. For high fields (>100 kV/cm under standard conditions) in non-attaching gasses (e.g. nitrogen and argon), the transition point saturates towards $\alpha_i d \simeq 15$ or to about $3 \cdot 10^6$ electrons, (compare with (2.4) and (2.5)). On the other hand, for low fields where diffusion dominates and for attaching gasses (e.g. air and oxygen), $\alpha_i d$ can be above 21. Results from these calculations are used in other works like Pai *et al.* [155].

Li *et al.* [104, 105] have used a somewhat different approach with the same results. Instead of using fluid simulations and analytical models, they have used a particle model to study the avalanche-to-streamer transition. In earlier work [104]

---

[1]Although the Raether-Meek criterion is called a criterion, it is more a rule of thumb than a hard criterion.

they show that using superparticles is not a good approach to study this transition, as the superparticles can easily lead to noisy charge distributions. Therefore, in newer work [105] they switch to a hybrid model that uses a full particle model for the ionization front and a fluid model for the regions with high densities of slow electrons. They calculate the evolution of the electron density during initiation of a negative streamer in pure nitrogen under standard conditions in a homogeneous field of 100 kV/cm. In their example, they use a full particle model for the electrons up to $t = 0.32$ ns when the number of electrons reaches $1.5 \cdot 10^7$. Between $t = 0.36$ and 0.54 ns the field at the streamer head is enhanced to 1.5 to 3 times the background field. This transition agrees with (2.4) and (2.5).

The theoretical work discussed above uses a homogeneous background electric field. However, in most streamer experiments and applications, streamers are generated from a tip- or wire-like structure. At such a (sharp) tip or wire, the electric field will be greatly enhanced which makes it easier to initiate a streamer. After initiation, the streamer can propagate into the rest of the gap where the background field may be too low for streamer initiation, but high enough for streamer propagation (discussed in the next section). Such a geometry with field enhancement greatly reduces the required voltages for streamer initiation, which makes experiments and applications smaller, cheaper and easier to operate.

The lowest voltage where a streamer can initiate is called the inception voltage; it depends on electrode shape and material as well as on gas composition and density and (up to now) has no direct interpretation in terms of microscopic discharge properties.

Van Veldhuizen and Rutgers [223] have studied streamer initiation experimentally in different gasses. They investigate inception probability, streamer length and breakdown (transition to spark) voltage at atmospheric pressure in a 25 mm point-plane gap with voltages between 3 and 27 kV. They find large differences between a noble gas (argon) on the one side and molecular gasses (air, nitrogen, oxygen) on the other side. Starting a streamer in a molecular gas appears more difficult than in a noble gas. They explain this difference by the low energy levels of vibrations and rotations in molecules that can easily take up the energy of an electron in the initial stage of an avalanche. This should result in different values of α_i for these different gasses. According to the Siglo database [1], this assumption is correct for relatively low electric fields: α_i is more than 2 orders of magnitude larger for argon than for nitrogen at fields below 30 kV/cm at atmospheric pressure. In air electrons are lost by attachment to oxygen molecules. This results in a negative value of α_i for fields below 30 kV/cm.

Lock *et al.* [116] have studied initiation and breakdown in supercritical CO_2 inside a wire-cylinder geometry. They record breakdown voltages that are a
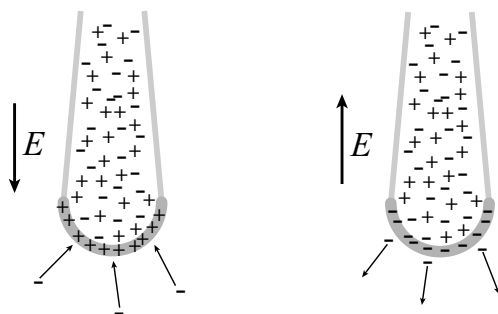
Figure 2.2: Illustration of downwards propagating positive (left hand side) and negative (right hand side) streamers. The plus-symbols indicate positive ions while the minus symbols indicate negative ions or free electrons.

factor 3 lower than extrapolation of the Paschen curve[2] for CO_2 would suggest. They explain this difference with the extensive density inhomogeneities of the supercritical fluid near the critical point. However, it is unclear why Paschen's law would be applicable for a wire-cylinder geometry operated under pulsed conditions. Paschen's law describes Townsend breakdown in stationary fields with a parallel plate geometry.

2.3   Streamer propagation

After streamer initiation, a streamer will propagate under the influence of an external electric field augmented by its self-generated field. An illustration of the mechanism of streamer propagation is given in figure 2.2. Here it is shown that around the streamer head, positive or negative space charge layers exist (for positive and negative streamers), the inside is filled with conducting plasma. In order to sustain the extension of the plasma channel by impact ionization, enough free electrons should exist in the high field region just in front of the space charge region. In negative streamers the supply of free electrons is not a problem because the electrons from the ionized region can drift in the field in the direction of streamer propagation. However, in positive streamers, the electrons can not come from the streamer itself. Therefore, for positive streamer propagation, "fresh" electrons are needed in front of the streamer head. The possible sources of these free electrons will be discussed in the next section and in chapters 5 and 6.

Most charges in a streamer discharge in air are initially produced by the impact

---

[2]Paschen's law describes breakdown voltage V_{bd} as function of pressure p times electrode distance d as $V_{bd} = \frac{a \cdot pd}{\ln(pd) + b}$ with a and b constants that depend on gas composition.

ionization of nitrogen

$$N_2 + e \rightarrow N_2^+ + e + e \tag{2.6}$$

with an ionization energy of ≥ 15.58 eV or of oxygen

$$O_2 + e \rightarrow O_2^+ + e + e. \tag{2.7}$$

with an ionization energy of ≥ 12.07 eV. Therefore, the positive charges indicated in figure 2.2 will mainly consist of positive molecular ions. According to Aleksandrov and Bazelyan [9], N_2^+ and O_2^+ will quickly change to other species according to the following scheme (for dry air under standard conditions)

$$N_2^+ \dashrightarrow N_4^+ \dashrightarrow O_2^+ \dashrightarrow O_4^+. \tag{2.8}$$
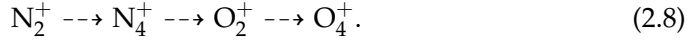
After some tens of nanoseconds, the positive ions are dominated by O_4^+.

The negative charges all start as electrons, but in air they quickly attach to molecular oxygen by three-body attachment

$$e + O_2 + M \rightarrow O_2^- + M, \tag{2.9}$$

where M can represent oxygen or water molecules depending on the moisture content of the air. M can also represent nitrogen, but with a reaction rate that is two orders of magnitude lower than for oxygen [91]. This reaction becomes important for pure-nitrogen like gas mixtures but can be neglected in air. Because of these electron loss processes, many of the negative charges indicated in the streamer tails in air in figure 2.2 will be negative molecular oxygen ions, limiting the total conductivity. Therefore streamers in pure nitrogen can become longer than in air under similar conditions as less electron attachment occurs if current flow from behind is required. The negative charges in the streamer head, as well as the moving charges in front of the streamer heads will be mostly free electrons.

Due to the electric screening layer around the curved streamer head, the electric field ahead of it is usually much higher than the external or background field. An example of this enhanced field in the streamer head is given in simulation results by Luque *et al.* [122] shown in figure 2.3. Here it can be seen that the electric field ahead of the streamer heads is more than three times higher than the background field. Depending on conditions, this enhancement can be even higher as was recently shown by Ratushnaya *et al.* [175].

Figure 2.3 also shows some other differences between positive and negative streamers. The positive streamer starts slower than the negative streamer, but quickly makes up for this. The slow initial motion of the positive streamer can be attributed to the fact that negative streamers always propagate with at least the electron drift velocity in the background electric field, while there is no lower bound for the propagation velocity of positive streamers. Later, the image shows that the positive streamer is more narrow and therefore its field enhancement is larger than in the negative streamer. This makes the positive streamer faster.
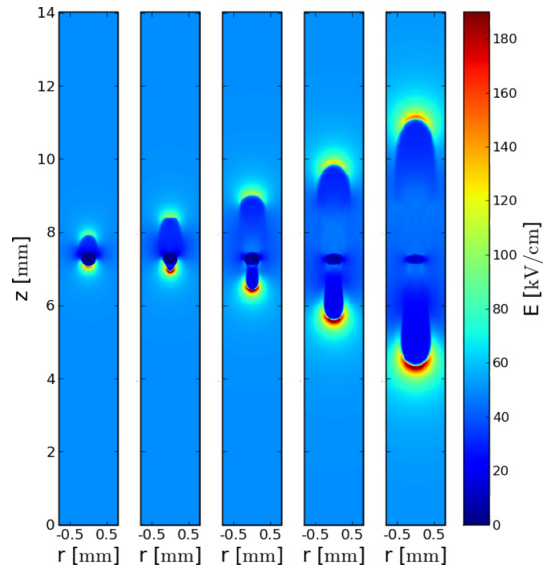
Figure 2.3: Electric field of a double-headed streamer at standard temperature and pressure in a homogeneous background field of 50 kV/cm, plotted at equal time steps of 1.2 ns. The negative front is propagating upwards, the positive front moves downwards. Note that the lateral borders of the figure do not correspond to the full computational domain, $|r| < 4$ mm. Image taken from [122].

2.3.1 Electron sources for positive streamers

As was discussed above, positive streamers need a constant source of free electrons in front of them in order to propagate. Because of the electronegativity of molecular oxygen, free electrons in air quickly attach to oxygen by reaction (2.9) if the electric field is below about 30 kV/cm. If this is the case, a high field is needed to detach the electrons so that they can be accelerated. The exact level of the detachment field depends on the vibrational excitation of the molecule. According to Pancheshnyi [156], a good value for the instant detachment field under standard conditions in air is 38 kV/cm.

Photo-ionization

Most streamer models model air and the major source of electrons in front of the streamer head is taken as photo-ionization. In air, photo-ionization occurs when a UV photon in the 98 to 102.5 nm range, emitted by an excited nitrogen molecule,

ionizes an oxygen molecule, thereby producing a free electron:

$$N_2^* \rightarrow N_2 + \gamma_{98-102.5\,nm} \tag{2.10}$$

$$O_2 + \gamma_{98-102.5\,nm} \rightarrow O_2^+ + e. \tag{2.11}$$
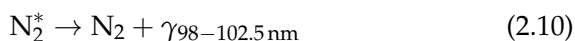
As the emitted photon can ionize an oxygen molecule some distance away from its origin, this is a non-local effect and therefore excited nitrogen molecules in the streamer head can create free electrons in front of the streamer head (as well as in other places around the streamer head). The average distance a UV photon can travel depends on the density of the absorbing species, oxygen in this case. In atmospheric air under standard conditions, this distance will be about 1.3 mm [121].

Investigations of the exact details of photo-ionization in air are quite scarce and are mostly based on the understanding of the mechanism by Teich [211, 212] and measurements by Penney and Hummert [167]. This was combined by Zheleznik *et al.* [244] into a model of photo-ionization that is now used (in original or modified form) in most streamer simulations. In recent years Aints *et al.* [6] have used the same method as Penney and Hummert to investigate the effects of water content in air on photo-ionization. Their results are similar to the results of Penney and Hummert, with small corrections for the effects of water content. Naidis [141] has investigated the cause and implications of their findings and finds that quenching of radiative states as well as absorption of UV photons by water molecules can explain the differences they find between moist and dry air.

Most measurements of photo-ionization have been performed at low pressures (Penney and Hummert used 0.1–25 mbar). When extrapolating this data to higher pressures, quenching of excited states becomes important, which makes many simpler extrapolations questionable.

Despite the lack of fundamental work on the photo-ionization mechanism, its effects on streamer discharges have been studied by a number of authors. Simulations on the role of photo-ionization have been performed by e.g. Kulikovsky [96], Morrow and Lowke [139], Bourdon *et al.* [26], Luque *et al.* [119, 121] and Wormeester *et al.* [236].

Kulikovsky postulates that the fundamental spatial scale of a streamer discharge is defined by the photo-ionization length and that this defines all other parameters. However, recent work by e.g. Wormeester *et al.* [236] has shown that this is a too simple viewpoint and that in a streamer discharge, many length scales exist that have nothing to do with photo-ionization and also appear in simulations with photo-ionization disabled.

Bourdon *et al.* and Luque *et al.* have developed fast numerical approaches to include the photo-ionization model of Zheleznik *et al.* in their numerical models. The results of their approaches are very similar. Recently, Settaouti [186] has used Monte Carlo simulations from which he concludes that photo-ionization is the

essential mechanism in streamer propagation and that no streamers develop when photo-ionization is omitted from the calculations. However, it seems that, like Kulikovsky, he does not take background ionization into account, which helps in streamer propagation without the need for photo-ionization as is discussed below and in section 6.1.

Experimental work has been done by e.g. Nudnova and Starikovskii [152] who use an Abel inversion technique to investigate streamer head radiation patterns and determine the so-called electrodynamic radius from this data. They compare this with streamer modelling and see that in their models, the streamer head shape is transformed from "elliptical" to "hemispherical" as the photo-ionization coefficient increases by an order of magnitude.

More details about the history of understanding of photo-ionization in air and other nitrogen-oxygen mixtures can be found in section 5.1.

There is hardly any literature about photo-ionization in other gas mixtures. Of course, in other mixtures it is possible as well that emitted radiation by one species can directly ionize another species. However, in the case of the combination of nitrogen and oxygen, the photo-ionization cross-section of oxygen is relatively large for the UV-photons emitted by nitrogen (compared to other possible photo-ionization combinations) as some electronic emission lines of nitrogen are very close to the ionization potential of oxygen. This does not have to be the case for other gas mixtures.

Background ionization

Besides photo-ionization, there is another source that can provide free electrons in front of a positive streamer head: background ionization. Background ionization is ionization that is already present in the gas before the streamer starts, or at least it is not produced by the streamer. It can have different sources. In ambient air, radioactive compounds (e.g. radon) from building materials and cosmic rays are the most important sources of background ionization. They lead to a natural background ionization level of 10^3–10^4 cm^{-3} at ground level (Pancheshnyi [156] and references therein).

Another source of background ionization can be leftover ionization from previous discharges. This is especially important in repetitive discharges types like DC corona discharges or repetitive pulsed discharges. Already at a slow repetition rate of about 1 Hz, leftover charges can lead to background ionization densities of order 10^5 cm^{-3} (see calculation on page 108).

Background ionization can also be created by external UV-radiation sources, addition of radioactive compounds to the gas or surfaces, electron or ion beam

injection and more.

Independently of the source of background ionization, in air the created electrons will always quickly be bound by oxygen, according to reaction (2.9). This means that they will have to be detached by the high field of the streamer before they can be accelerated and form avalanches.

Pancheshnyi [156] has published a detailed review of the importance of background ionization and negative ions on streamer properties. This work, as well as a more detailed introduction to background ionization, including reactions and reaction rates is discussed in section 6.1.

2.3.2 Similarity laws

Similarity laws for discharges in gasses of the same composition, but of different density were probably first formulated by Townsend for the so-called Townsend discharge at the beginning of the 20th century; they are discussed in many textbooks of gas discharge physics (e.g. [129, 172, 179]).

While there are many deviations from similarity in other discharges, similarity in the propagating heads of streamer discharges holds particularly well because these fast processes are dominated by collisions of single electrons with neutral molecules, while two-step processes and three-particle processes that would be density dependent, are negligible on these short time scales. This implies that the basic length scale of the streamer discharge is the mean free path of the electron

$$\ell_{mfp} = \frac{1}{4\sigma n_0} = \frac{kT}{4\sigma p},$$ (2.12)

(with the ideal gas law) where σ is the collisional cross section, n_0 the gas density, k the Boltzmann constant, T the gas temperature and p the pressure. σ is the total cross section of all collisions and therefore includes the ionization cross section σ_i from equation (2.1) but for all collisions, not just ionization. From (2.12) follows that ℓ_{mfp} is inversely proportional to the density of the medium,

$$\ell_{mfp} \propto 1/n_0.$$ (2.13)

All length scales follow the same scaling as the mean free path:

$$l \propto \ell_{mfp} \propto 1/n_0.$$ (2.14)

Streamers are similar when electrons gain the same energy while being accelerated in the electric field ($q_e \cdot |\boldsymbol{E}| \cdot \ell_{mfp}$). This means that the electric field scales as

$$|\boldsymbol{E}| \propto n_0$$ (2.15)

for similar streamers. From this, it follows that velocities of streamers v_d, as well as electron energy distributions are independent of n_0 because $v_d = \mu_e \cdot |E|$, in which the electron mobility μ_e scales with $1/n_0$ and $|E|$ scales with n_0;

$$v_d \not\propto n_0. \tag{2.16}$$

The characteristic energy of the electrons is equal to the ionization energy and therefore is constant for a specific gas and does not scale with density. From (2.14) and (2.16) it follows that many characteristic times t scale with inverse density

$$t \propto 1/n_0. \tag{2.17}$$

The dielectric relaxation time is $\tau = \varepsilon_0 / (q_e \cdot n_e \cdot \mu_e)$, with ε_0 the permittivity of vacuum and q_e the electron charge. As τ (according to (2.17)) and μ_e both scale with $1/n_0$, n_e scales like

$$n_e \propto n_0^2. \tag{2.18}$$

As velocities do not scale with gas density, current density also scales with n_0^2 while the total current does not scale with gas density. However, the total current can depend on the applied voltage, on the number of streamer channels and on the gas type. Combining (2.14) and (2.18) shows that the total number of electrons scales with $1/n_0$. At constant temperature and for ideal gasses, we can replace n_0 in all similarity laws by the pressure p.

Scaling laws can only be applied under specific conditions. Corrections need to be applied for the following conditions [52] (we only list the conditions that are relevant for our experiments):

Multi-particle processes: When reactions including more than two particles or more than one charged particle dominate the discharge, scaling laws no longer apply. When such reactions are significant but not dominant, corrections can be applied. Examples of these multi-particle processes are quenching of excited nitrogen molecules (which decreases photo-ionization above pressures of about 80 mbar), three body-attachment (reaction 2.9) and two-step ionization.

Stochastic effects: When charge densities are so low that stochastic processes play an important role, the scaling laws no longer apply. One important streamer process that can be influenced by such stochastic processes is streamer branching (see section 2.4). Although branching is a nonlinear bifurcation process that can occur without any fluctuations, it can be accelerated by electron density fluctuations. Also streamer inception can be greatly influenced by stochastic availability of electrons.

Electrodes or other material boundaries: Shape and surface properties of such boundaries can not be rescaled with changing gas density.
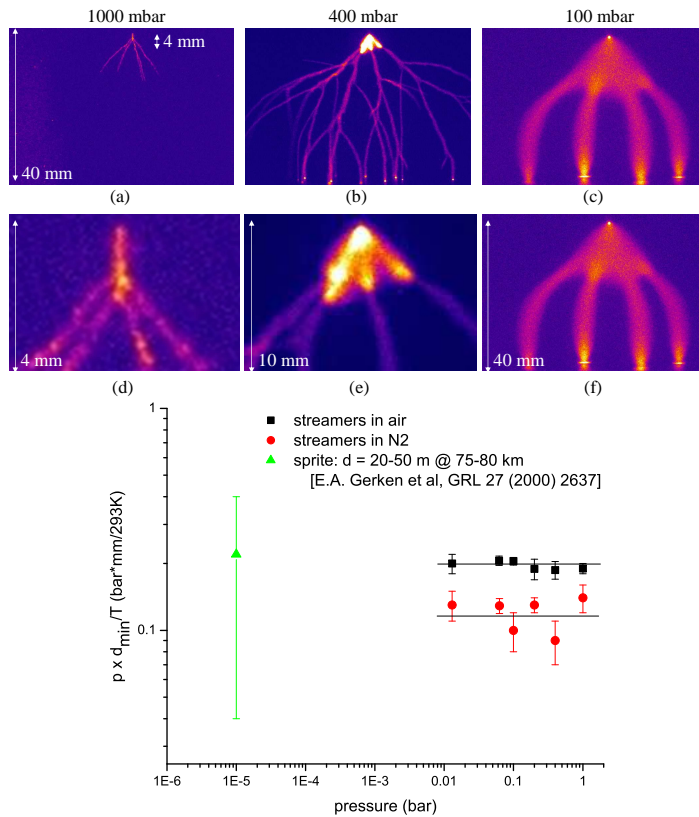
Figure 2.4: Illustrations of scaling of streamer features with pressure. In the top row, complete overview images of the full 40 mm gap of ~10 kV streamer discharges in air are shown for three pressures. In the second row, the central parts of the same images are shown scaled so that $p \cdot h$ is the same (with h the height of the imaged section). This shows that the central part of a streamer discharge in air has a similar shape independent of pressure when scaled according to the similarity laws. The graph on the bottom shows that the reduced minimal streamer diameter in air and pure nitrogen is independent of pressure over a large pressure range and even fits with measurements of sprite channel thickness by Gerken *et al.* [63]. Figures taken from [32], also published in [34].

Nevertheless, the scaling laws can be applied to most streamer experiments as well as to geophysical discharges. This has recently been confirmed experimentally for the overall morphology including diameters and velocities of streamers and sprites in terrestrial air of varying density by Briels *et al.* [34]. Figure 2.4 shows some of her results. Similarity laws for streamers have been applied to many fields. Pasko *et al.* have studied them with regard to sprites and other transient luminous events [110, 161, 164, 165]. Luque *et al.* [123, 124] have done this as well

(see also section 2.7 of this work for the relation between sprites and laboratory streamer discharges). Tardiveau *et al.* [210] have used the similarity laws to infer properties of streamers at high pressures and densities in combustion engines from measurements at atmospheric and elevated pressures. In their experiments, they find deviations from the similarity laws at high pressures (several atmospheres at room temperature). A leader structure (a hot channel) starts to show up before the gap is bridged. They argue that this is due to reduced heat diffusion but we have argued that the primary reason is a higher rate of heat generation at higher density [52].

2.3.3 Initiation cloud, primary, secondary and late streamers

Most pulsed positive streamer discharges with a tip-like electrode start with a so-called initiation cloud. In fact, what on time integrated images of the discharge seems like a cloud, is in fact often a smaller cloud that transforms into a thin expanding shell of ionization. After a certain distance, this shell breaks up in multiple streamer channels, except when the gap is so small that the initiation cloud extends into roughly half the gap distance, then it usually breaks up in only one channel. An initiation cloud that breaks up into multiple channels can be seen in figure 2.4, especially in the 100 mbar images. The size of the initiation cloud depends on gas density according to the similarity laws ($l \propto 1/n_0$) but it also depends on gas composition and, of course, on the applied voltage. For example, in air the initiation cloud is much larger (up to a factor 10 or more) than in pure nitrogen [34].

The maximal possible size of the initiation cloud can be estimated by assuming that the initiation cloud is a good conductor and therefore shields the electrode pin. The potential on the outside of the initiation cloud will now be equal to the pin potential. The potential ϕ at radius r outside of a conducting sphere will be

$$\phi(r) = V \cdot R/r \quad \text{for } r > R, \tag{2.19}$$

with V the applied voltage and R the radius of the conducting sphere. The electric field is

$$E(r) = V \cdot R/r^2. \tag{2.20}$$

Therefore, at the edge of the sphere where $r = R$ the field is

$$E(R) = V/R. \tag{2.21}$$

If we also assume that the field should be larger than the breakdown field ($E_{crit} \approx$ 30 kV/cm in air under standard conditions), we can estimate the maximum size of the initiation cloud as

$$R_{max} = V/E_{crit}. \tag{2.22}$$
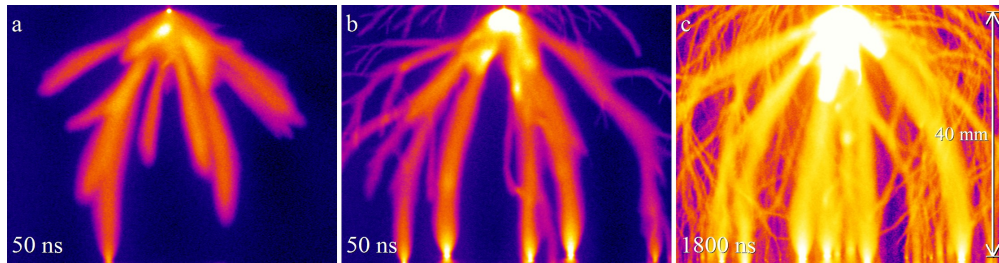
Figure 2.5: Streamer discharges in a 40 mm gap in atmospheric air with a 54 kV pulse. The images are acquired with short (a and b) and long (c) exposure times. The exact image start delay is varied between a and b (exact values unknown). Images by Tanja Briels, originally published in figure 6 of [31].

The theoretical upper bound for the cloud size from equation (2.22) matches quite well with measurement results in air by Briels *et al.* [34, 35]. It should be noted that she studied positive streamers which destabilize and branch much easier than negative streamers as negative streamers are stabilized by the electron drift (see [122]). Therefore it is expected that the actual size of the initiation cloud will be closer to the theoretical maximum size for negative pulses than for positive pulses. This is demonstrated in appendix A of this thesis.

The first streamers coming from the initiation cloud are called primary streamers. A primary streamer starts from the initiation cloud and then traverses the gap towards the other electrode (the cathode for a positive streamer discharge). Example of such streamers are shown in figures 2.5a and b. However, for long gaps, low voltages or short pulse durations, the primary streamers often do not reach the other side and extinguish somewhere between the electrodes (see figure 2.4a). Most of the work in this thesis treats positive primary streamers.

If the primary streamer has connected to the other side, more light is emitted by the streamer channel. Often a new bright front is observed that translates from the anode towards the cathode through the same channel as its preceding primary streamer. Marode [126] suggests that this so-called secondary streamer corresponds to a moving equivalent of the positive column of a glow discharge; this phenomenon is currently under investigation by Ebert *et al.* Here, we did not investigate the secondary streamer phase in detail. Therefore, in this thesis, we will treat the secondary streamer phase and the glow phase together and refer to them as the glow phase.

A detailed analysis of the processes occurring in primary and secondary streamers is given by Sigmond [189]. He notes that moving secondary streamer fronts in centimetre scale gaps in atmospheric air do not perturb the smoothly decaying streamer current and that they are only reported in air. Ono and Oda [153] have

compared primary and secondary streamers. They observe that emission from the first negative system of N_2^+ (391.4 nm) is only observed in primary streamers and not in secondary streamers. This is attributed to the fact that higher electron energies are required for propagation of primary streamers than for secondary streamers as primary streamers have to create ionization while secondary streamers propagate along the ionized channel created by the primary streamers. Furthermore, they find that secondary streamers only occur at higher voltages (15 kV in air and 20 kV in pure nitrogen). Van Heesch *et al.* [81] found that O* radical yield from primary steamers is up to two times higher than from secondary streamers. They explain this by higher local electric fields and electron energies in the primary streamers.

A third category of streamers besides primary and secondary streamers are the so-called late streamers. These are in fact primary streamers but they either start later than the dominant streamers, or are so slow that they seem to have started later. Late streamers propagate along completely different paths than the other (primary) streamers before them. They are often very thin, which is related to their slow propagation velocity (see e.g. Briels *et al.* [33]). In most cases they do not appear from the sharp electrode tip itself but instead from (less sharp) edges of the electrode or electrode holder because the tip is already screened by a glow region and therefore no longer enhances the electric field as much. Examples of these late streamers are visible in figures 2.5b and c. In figure 2.5b the late streamers have just started and are visible on the top of the image. In figure 2.5c, a much longer camera exposure is used. Therefore the primary streamers are now overexposed as their secondary and glow phase is also included in this exposure. However, many (thin) late streamers are clearly visible crisscrossing all corners of the image.

2.4   Streamer branching and interaction

Most streamer discharges contain more than one streamer channel. Therefore, interactions between streamers are important when studying streamer behaviour. One important aspect is streamer branching where one streamer channel splits in two (or more) channels. Other interactions are attraction and repulsion of streamer channels. Furthermore, neighbouring channels influence each others' field configuration. If attraction occurs, this may lead to streamer merging or (re-)connection. We define merging streamers as two streamer channels moving in a nearly parallel direction and then merging into one. Connection occurs when two streamer channels coming from different directions connect to each other, mostly one tip ends on an existing channel. A special case of connection is reconnection, where both connecting channels originate from the same electrode.
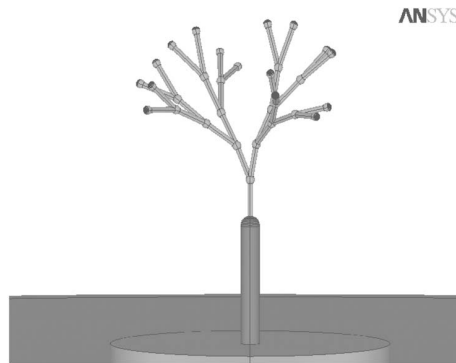
Figure 2.6: Results of simulations of a streamer tree by Akyuz *et al.* when the applied voltage on the needle is 5 kV. Taken from [8].

The streamer interaction mechanisms discussed above are an important ingredient for building models of a complete streamer discharge. However, a complete model based on measurements or theoretical understanding of the microscopic processes is not available yet. All existing models are based on phenomenological assumptions. An early example of such a model of a complete discharge tree is by Niemeyer *et al.* [146]. They use a simple fractal model to approximate sliding surface discharges. This model includes streamer branching and the distribution of the electric field in a phenomenological manner. A similar, but more sophisticated model has been used by Akyuz *et al.* [8]. They simulate a 3 dimensional streamer tree up to about 16 separate streamer filaments (see figure 2.6). We will discuss their assumptions about branching angles below. Pasko *et al.* also use similar 2D [162] and 3D [163] fractal models, but they apply them to sprite discharges instead of laboratory-scale discharges. They claim that their models can reproduce the large scale sprite phenomena that are reported and demonstrate differences between sprites created by positive and negative polarity lightning strokes. They find that simulated sprites produced by a negative cloud-to-ground stroke extend down to altitudes ~10 km higher than positive ones. However, the number of observed sprites generated by negative lightning strokes is very low compared to sprites generated by positive strokes [18]. Furthermore their general comparison with sprite properties was rather limited as the quality and quantity of sprite observations was still low at that time.

More recently, there have been some publications regarding simulation of the strongly branched structure of lightning strikes [79, 207, 209, 217] and other streamer-like discharges [11, 97, 218], but no attempts to improve the understanding of complete streamer discharges by applying all streamer interactions in a model.

2.4.1 Streamer branching

The most important streamer "interaction" is branching of a single streamer channel into two channels. Branching is observed in most streamer discharges except when the gap is so short that the streamer has reached the other side before it has branched. Furthermore, minimal streamers (see below) do not branch either but eventually extinguish. This is the main argument why streamer discharges never are real fractals.

The exact mechanism of streamer branching has been under discussion for quite a long time now. One, now widely accepted, explanation is that it occurs due to a Laplacian instability similar to viscous fingering [12, 132, 178], without the need for photo-ionization or stochastic effects. In this explanation, Laplacian instability is a requirement for branching, but branching can be accelerated by stochastic processes. This concept is further evaluated by Montijn *et al.* [137] by using adaptive grid refinement techniques. They find that streamers can also branch in sufficiently undervolted gaps but that they show fewer branching modes than in higher fields. Liu and Pasko [108] argue that photo-ionization is very important for streamer branching in air and that a streamer branches when its radius becomes greater than $1/\chi_{min} \cdot p_{O_2}$ with χ_{min} the photo-ionization absorption cross section of molecular oxygen and p_{O_2} its partial pressure. Their models show a lower threshold radius for positive streamers than for negative streamers. In a later paper [110], they reconfirm this mechanism and extend it by stating that quenching effects facilitate easier branching at higher pressures, again because less UV-photons lead to less free electrons and thus more noise. A similar explanation of streamer branching by fundamental instabilities in the streamer front is used by Sinkevich [193]. Arrayás *et al.* [13] use an analytical approach to calculate the Laplacian instability of a negative streamer. They propose an equation to estimate the spacing between different branching positions as function of the external electric field and the diffusion coefficient. Derks and Ebert [46] also use an analytical approach to study the same problem. They point out some inconsistencies in Arrayás *et al.* [13].

Another, older, explanation for streamer branching was already proposed by Loeb and Meek in 1940 [118] based on concepts of Raether [171]. It uses the stochastic behaviour of secondary avalanches in front of the streamer head. However, this concept has never been shown to agree with the expected distribution of seed electrons in front of the streamer. In air, the number of free electrons created by photo-ionization just in front of the streamer head is so high that it can not explain the stochastic occurrence of avalanches. However, in other gas mixtures (e.g. nearly pure nitrogen) this can be different. In chapters 5, 6 and 7 we investigate effects of gas type and purity on branching. An elaborate discussion about the observed phenomena can be found in section 5.4.

Despite the problems with the avalanche-branching model in air, this mechanism is still used by many authors to explain streamer branching. For example, Akyuz *et al.* [8] use two equivalent avalanches in front of an "old" streamer channel in order to simulate branching angles. They find an angle of about 39° for branching in two dimensions, which is within the range of observed angles in Lichtenberg figures. For three dimensions, they use a more sophisticated method but it is still based on two wrong assumptions, namely that secondary avalanches in front of a streamer head directly lead to streamer branching in air and that there are not more than two avalanches at the same time.

Van Veldhuizen and Rutgers [222] have experimentally investigated streamer branching in argon and ambient air for different discharge geometries and pulse characteristics. They find that streamers in a point-wire discharge branch about 10 times more often than in a plane-plane discharge. They can not explain this difference from the properties of the streamer heads like size and maximal field. They therefore suggest that electrostatic repulsion plays an important role in streamer branching. This electrostatic repulsion is part of the Laplacian instability theory discussed above. Furthermore, they conclude that the impedance of the power supply must be taken into account when studying branching, as it has a significant influence on the number and thickness of the branches. Briels *et al.* [30, 31] have investigated this effect further. They characterize four different types of streamers although they realize and later show [33] that there is no phase transition between these types. Nevertheless, they propose that two of their streamer types are so-called minimal streamers that have a diameter at which streamers no longer branch. This minimal diameter is density dependent (see section 2.3.2) but independent of background field or other pulse parameters. This concept was proposed by Ebert *et al.* [51].

Different experimental results [35, 153, 243] have all shown that in nitrogen-oxygen mixtures, decreasing the oxygen content leads to more branching. Briels *et al.* [35] attribute this to differences in photo-ionization. Luque *et al.* [119] get similar results from their simulations; under certain conditions, photo-ionization can suppress branching because it leads to a smoother particle distribution and therefore is less susceptible to Laplacian instabilities. Similar reasoning is followed by Hallac *et al.* [75]. Pancheshnyi [156] also notices similar effects. He states that high pulse repetition frequencies lead to higher background ionization levels (see also section 6.1.2) and therefore smoother, less stochastic streamer propagation which results in less branching.

Babaeva *et al.* [15, 16] investigate the role of stochastic behaviour and inhomogeneities on streamer branching on a more macroscopic level. They investigate the influence of not only inhomogeneities but also of dust particles and bubbles (for streamers in liquids). They find that larger particles and bubbles can intercept

and re-initiate streamers and thereby increase the chance of branching. However, this mechanism differs significantly from "normal" streamer branching as it is involves macroscopic processes, while streamer branching in bulk gas only involves microscopic processes.

2.4.2 Streamer attraction/repulsion

Compared to branching, not much work has been published on other streamer interactions. We can identify three different physical mechanisms for interaction between two streamer channels:

Electrostatic As streamer channels have a net charge, they can attract or repel each other by their electric field.

Magnetic Streamer channels do carry current and therefore create a magnetic field that could attract or repel other current carrying channels through Lorentz forces.

Photo-ionization Streamers can influence the ionization levels around them by (non-local) photo-ionization. If they are close enough, photo-ionization from one streamer can affect the other one.

A possible fourth interaction mechanism can be the leftover ionization or charge in a previous streamer but this only affects streamers that occur (much) later in time and will not be treated in this section. We discuss this mechanism in detail in chapter 6. For all streamer discharges discussed in this thesis, the current carried by the streamer is too low to induce any significant Lorentz force. Therefore we will also disregard magnetic interaction.

In air, the photo-ionization length is short compared to inter-streamer distances (about 1.6 mm at atmospheric pressure [167, 244]) and therefore will only affect streamers that are already very close to each other. However, in other gas mixtures with longer photo-ionization lengths, it can have an effect on neighbouring streamer channels, albeit that the effect will be small if the amount of photo-ionization is low.

This leaves us with only one candidate for significant streamer interactions: electrostatic attraction and repulsion. Examples from electrostatic attraction of streamers are most clearly observed with streamers of different polarity that can occur in e.g. point-point discharges like lamp ignition [45, 196] or connection of up- and downwards moving leaders in lightning strikes [19]. In nearly all cases where streamers originate from the same electrode (and therefore have the same polarity), it is observed that they repel each other, as is expected from an electrostatical viewpoint.

Nevertheless there have been multiple reports that late streamers can bend towards earlier channels [31, 71] as well as similar observations in sprites [44]. Briels *et al.* [31] propose that streamer channels change polarity once they have crossed the gap and can then electrostatically attract other streamer channels. Similar reasoning is used in the results presented in chapter 4 of this thesis where we investigate this effect in more detail. Sprite streamer polarization along the length of the channel may explain the observed attraction in sprites and was proposed recently by Luque and Ebert [124] and Liu [113].

2.5   Streamer optical emission

As streamers propagate, fast electrons excite species in the streamer head. Many of these excited species can fall back to lower excitational levels or the ground level and thereby emit a photon. These photon emissions are by far the most important property of streamers that are studied experimentally. They are used in streamer imaging and in optical emission spectroscopy, which together comprise most of the experimental results presented in this thesis.

In order to have good insight in the streamer properties from optical emissions, one needs to know which excited species are responsible for which emission lines or bands and how this is related to other streamer properties like electron density and local electric field.

Liu *et al.* [109, 112] have modelled optical emission from positive streamers in air at ground level and high altitude (70 km) pressures. They show that emissions from different band systems in nitrogen molecules will have different spatial intensity distributions in and around the streamer for different altitudes. Emissions from the first negative system of N_2^+ (FNS, upper state $B^2\Sigma_u^+$) are located very close to the high electric field region, while emissions from the first and second positive systems of N_2 (FPS and SPS, upper states $B^3\Pi_g$ and $C^3\Pi_u$) are distributed over a much wider area. This can mainly be attributed to the longer lifetimes of the excited states of the FPS and SPS systems. At ground level, the highest intensity emission is produced by the second positive system while at high altitude, the first and second positive systems have nearly equal intensities. This difference between ground level and high altitude can be attributed to density-dependent quenching of the different molecular systems.

This is consistent with many observations by e.g. Gallimberti *et al.* [62], Stritzke *et al.* [202], Tochikubo and Teich [215] and Simek *et al.* [191, 192] as well as with other modelling results [111, 165] and with observations of sprite emission spectra [199].

As quenching can play an important role in the emitted spectra, good knowledge of quenching rate coefficients is needed to understand these spectra. Recently, Dilecce *et al.* [49] have investigated these rate coefficients by means of laser induced

fluorescence measurements.

Besides radiated intensity, quenching also influences the effective lifetime of the different excited states. Shcherbakov and Sigmond [187] have performed experiments on the lifetimes of the SPS and FNS bands and have found emission durations with a full width at half maximum of 1.4–1.5 ns and 0.5–0.6 ns respectively in atmospheric density air. These times include the passing of the streamer front as well as the lifetime of the excited species. In another paper [188], they use results from such sub-nanosecond spectroscopic measurements to determine streamer properties like the electron density and the electric field in the streamer head. Similar methods are often employed to study properties of laboratory streamers [159] and sprites [80, 111], although in the case of sprite observations, it is impossible to achieve high time or wavelength resolutions.

2.6   Streamers in different gasses

Most of the topics discussed above, as well as most streamer literature is focused on streamers in air and, to a lesser extent, on other nitrogen-oxygen mixtures or pure nitrogen. There has been some experimental work on other gasses (e.g. pure noble gasses and industrial gas mixtures), but there is not much theoretical work on these non-air-like gasses and mixtures.

Properties of a gas which are important for streamer discharges are:

Ionization energy and cross sections determine the electron energy that is needed for impact ionization in the streamer head. This level is much higher in helium than in most other gas mixtures.

Vibrational, rotational and electronic excitational levels and cross sections determine how much energy an electron loses by inelastic collisions. There is a large difference in the amount and height of these levels between molecular gasses (e.g, oxygen, nitrogen) and atomic gasses (e.g. argon, helium). Molecular gasses have many rotational and vibrational levels as well as electronic levels, while atomic gasses only have a few electronic levels. In practice all atomic gasses that are regularly studied for streamer discharges are noble gasses.

Electronegativity determines if and how many free electrons are lost by attachment to other molecules. Of the gasses studied here, only oxygen and CO_2 are electronegative. All other gasses are electropositive. Nevertheless, even trace amounts of oxygen (below 1 ppm) are able to attach most electrons after a discharge and can therefore have a big influence on background ionization levels (1 ppm under standard gas conditions is still 10^{13} cm^{-3}, which is much higher than background ionization levels under most circumstances).

Photo-ionization determines how much non-local production of electrons can occur. As was briefly discussed above, there is hardly any data on photo-ionization mechanisms in other gas mixtures than oxygen-nitrogen.

Other (chemical) reactions and reaction rates (e.g. quenching, recombination) determine what happens with excited states, ions, dissociation and more during and after a streamer discharge. Especially in mixtures of molecular gasses, the number of reactions can be huge. For example, Sentman *et al.* [184] include over 800 reactions and over 80 species in their models of sprite chemistry in air. Often, the number of reactions and species can be reduced by only including the most important ones, but still a large number will remain.

A good reason for the low amount of theoretical work on streamers in non-air-like gasses is lack of input data. Some input data, like cross sections are available from sources like the Siglo database [1], but others, like photo-ionization data is only available for air (but can be extrapolated to other nitrogen-oxygen mixtures).

2.7 Similarities between streamers and sprites

The mechanism of sprite production on earth is now being understood with increasing precision [83, 84, 123, 160, 165, 173, 200]. The charge separation within the thundercloud is slow enough that the conductivity in the mesosphere and the ionosphere can screen the emerging electric fields (see figure 1.2 for the atmospheric layers). However, a lightning stroke changes the charge content of the cloud and the surface so rapidly, that the newly generated electric fields are not screened immediately and appear up to the ionosphere. These fields are typically calculated in quasi-electrostatic approximation. As the breakdown electric field E_k depends on atmospheric density, it decreases exponentially with altitude, and therefore the lightning generated electric field can exceed the breakdown field at a sufficiently high altitude as was predicted by Wilson in 1925 [230]. This is a necessary condition for the emergence of a sprite a few to several tens of milliseconds after the parent lightning [44, 84, 183], but sprites do not always appear in the mesosphere even if the quasi-electrostatic field is there [123]. According to recent triangulations by Stenbaek-Nielsen *et al.* [201], sprites emerge at altitudes of 66 to 89 km. High-speed imaging showed that sprites start with downward moving streamer heads [44, 128, 199], and telescopic imaging by Gerken *et al.* [63] shows that single channels have diameters of tens to hundreds of meters. These observations are reproduced by simulations [123]. A review of sprite properties on earth can be found in [200].

2.7.1 Lightning and sprites on other planets

Lightning discharges are the energetic manifestation of the microphysical and thermodynamical processes occurring within clouds that reside in a planetary atmosphere. In the solar system, lightning has been detected by spacecraft via direct optical imaging on Earth, Saturn and Jupiter, and by electromagnetic remote sensing on Earth, Venus, Jupiter, Saturn, Neptune and Uranus. Recently, Ruf *et al.* [180] reported ground-based detection of non-thermal emission from a Martian dust storm, which they attributed to electrical discharges, although no radio signals from lightning have been found by the Mars Express spacecraft [74]. No signature of lightning activity had been discovered on Titan, Pluto and Mercury. We refer the reader to the recent comprehensive reviews on planetary lightning by Desch *et al.* [47] and Yair *et al.* [239]. We will elaborate here on the findings that concern lightning on Venus and on Jupiter. On Venus, lightning activity had been deduced based on the VLF emission detected by the Soviet landers Venera 11 and 12 (Ksanfomality *et al.* [95]). However, the data from top-side observations by various spacecraft have not shown un-equivocal optical or electromagnetic signatures, especially after the fly-bys of the Galileo and Cassini spacecraft [72, 73]. Krasnopolsky [94] reported earth-based measurements of high-resolution spectra of Venus in the NO band at 5.3 µm and found an NO content of 5.5 ± 1.5 ppb below 60 km altitude. Such a concentration cannot be explained by cosmic-ray induced chemistry and the suggested mechanism is production by lightning. Russel *et al.* [181] have analysed the Venus Express magnetometer data and have inferred a global flash rate on Venus which is comparable to that on Earth, $\sim 50/s$. It is hard to explain how such a high flash rate can occur in the stratiform clouds on Venus. Based on conventional charge-separation processes which occur in terrestrial thunderclouds, Levin *et al.* [102] have shown that the charging rate of the clouds on Venus should be considerably slower than on Earth, and the resulting flash rate should be of the order of few per hour. This does not rule out the possibility that other, unknown charging mechanisms do operate within the clouds, leading to rapid electrification and frequent lightning. Recently, Russel *et al.* [182] have compared Venus lightning processes with terrestrial lightning. They find that although many observed lightning properties seem different between Venus and Earth, many of these differences can be attributed to effects during the ionospheric propagation to the spacecraft and are therefore observation artefacts.

On Jupiter, the Voyager, Galileo, Cassini and New-Horizons missions found clear indications that lightning discharges are prevalent [17, 24]. They are thought to occur in the deep H_2O clouds that exist in the Jovian atmosphere and are estimated to be roughly 100 times more energetic than on Earth (Yair *et al.* [238]). Recent observations by the Cassini mission have shown visible lightning on Saturn as well [50].

Since lightning has been found in planetary atmospheres, it seems reasonable

to assume that some form of TLE, like sprites, occur there as well. Yair *et al.* [240] estimated the altitude in which breakdown can occur above the cloud deck in various planetary atmospheres, using the quasi-electrostatic approximation first proposed by Wilson [230]. Yair *et al.* [240] predict that for sufficiently large charge moments, sprites can form in the atmospheres of Venus and Jupiter.

The Japanese Climate Orbiter, Akatsuki (formerly known as Planet-C), launched on 20 May 2010, will search for lightning on Venus (see [142, 204]). However, the Venusian thick cloud layers might inhibit optical observations. Sadly, on 7 December 2010, the Venus orbit injection of the craft failed. The expected next possible orbit injection will be in 2015 or 2016. Therefore we do not expect to see new measurement results on lightning and sprites on Venus in the near future.

Yair *et al.* [240] expect that, if lightning exists, sprites may form above the upper-most cloud deck, and thus could be easily observed by an orbiting spacecraft, both on Venus and on Jupiter. The altitude, diameter, shape and light emission of the observed sprites could yield valuable information about the charge configuration in the clouds below, as well as about the gas composition of the upper atmosphere of the planet. In this work we investigate the expected spectrum of sprites (in chapter 8) and their morphology (section 7.7) via laboratory experiments. This information can be useful in finding and identifying sprites in upcoming observations.

2.7.2 Laboratory experiments on sprites

It is by now well understood that the large sprite discharges at low air density are essentially up-scaled versions of small streamer discharges at high air density that dominate the initial breakdown of large gas volumes in a sufficiently strong electric field. As discussed by [34, 51, 52, 165] and supported by observations by [64, 127, 128] and by simulations by [108, 119, 121, 123, 164], streamers and sprites are essentially related through the similarity or scaling laws.

As was discussed above, the basic arguments for the similarity laws between streamers at different gas densities do not depend on the gas composition, and indeed the similarity laws are confirmed experimentally in air. This opens a possibility to simulate planetary sprites through laboratory experiments in the corresponding gas mixtures. To the best of our knowledge such simulations were never performed in gas mixtures specifically chosen to simulate planetary atmospheres other than earth.

Chapter 3

General experimental set-up

3.1 Introduction

To produce and analyse a streamer discharge, an experiment with several components is required. The most important ones are listed here.

Vacuum vessel contains the discharge and, together with a pump and gas handling system, provides the gas composition and pressure for the discharge. This is treated in section 3.2.

Voltage pulse generator needed to provide a fast positive or negative voltage pulse to produce the streamer discharge. The two different types that have been used are treated in section 3.3.

Faraday cage and other shielding to ensure that the electronics required for triggering, gas handling and diagnostics are not influenced or damaged by the strong electro-magnetic radiation produced by the voltage pulse generator and the streamer discharge itself. Our Faraday cage contains a window of electrically conducting ITO glass between the vacuum vessel and the camera.

Diagnostic system which, in our case, consists of an ICCD camera or a small spectrometer combined with voltage and current probes. The spectrometers used in this work are treated in section 8.2, while the other diagnostics and processing techniques are discussed in section 3.4.
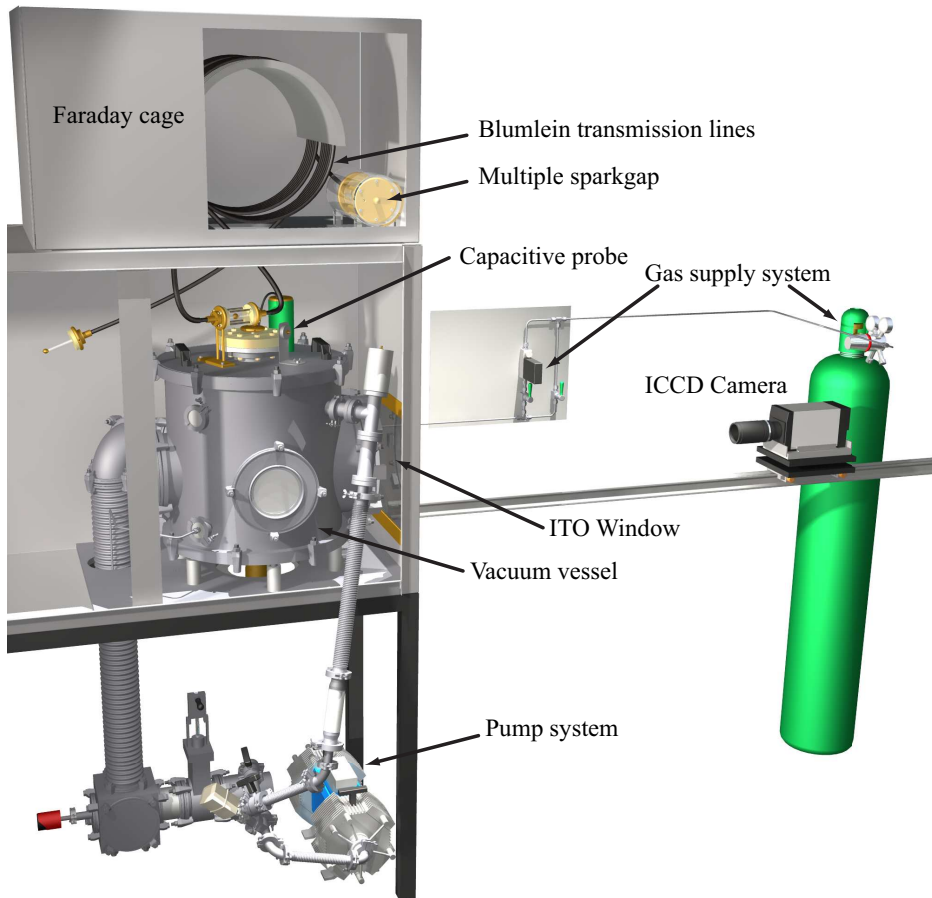
Figure 3.1: Overview of the complete set-up with various components indicated. In this case the new vessel (see section 3.2.3) is shown, together with the Blumlein voltage pulse source (see section 3.3.2).

3.2 Vacuum vessels and systems

Streamer experiments are often performed in ambient air. However, when we want to investigate streamers at other pressures and in other gasses or gas mixtures, a closed vessel is needed. The easiest way to fill such a vessel with the required gas (mixture), is to pump it down to a (near) vacuum and then fill it. This ensures the highest purity of the required gas. Therefore a vacuum system is preferred for these measurements.

The experiments discussed in this thesis have been performed in two different vacuum vessels. The old vessel was used in previous experiments by Briels *et*
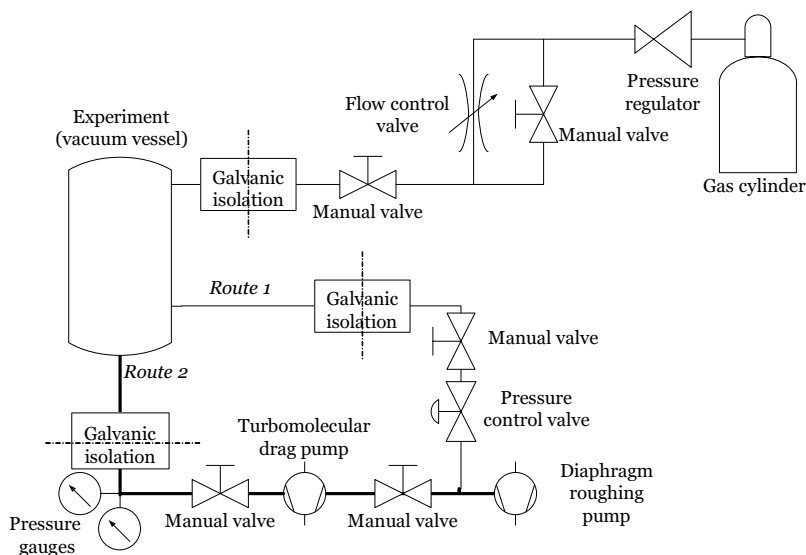
Figure 3.2: Schematic representation of the vacuum system, including the gas filling and flushing system and the two (parallel) routes of the vacuum system. Note that in most cases two different gas cylinders were connected side by side, while in some other cases gas from the building infrastructure was used. In the latter case, the scheme is exactly the same except that the gas cylinder should be replaced by the building gas pipeline and some extra manual valves and pipes are included.

al. [30, 31, 34], and a new vessel which was specifically designed for operation with very pure gasses (with contaminations below 1 ppm).

3.2.1   Gas handling and pump system

Figure 3.2 shows a schematic representation of the vacuum system of the new set-up. Gas can enter the vacuum vessel from the cylinder either through a flow controller (controlled by a Brooks Instrument Read Out & Control Electronics 0154) or through the manual bypass valve next to it. The former method is used to flush gas during an experiment in order to keep a fixed refreshment rate. The latter method is used to quickly fill the vacuum system to the required pressure.

On the vacuum side of the system, the roughing pump is a Pfeiffer Diaphragm Vacuum Pump (MVP 160-3) which is always turned on. It is connected to the main vacuum vessel via two routes. Route 1 is used during an experiment to maintain a fixed pressure while gas is flushed in the vacuum vessel. This is achieved by a Pfeiffer EVR 116 control valve in combination with a Pfeiffer RVC 300 control unit. The required pressure is entered on the control unit, which controls the valve in such a way that the required pressure is reached. This is only possible if the flow
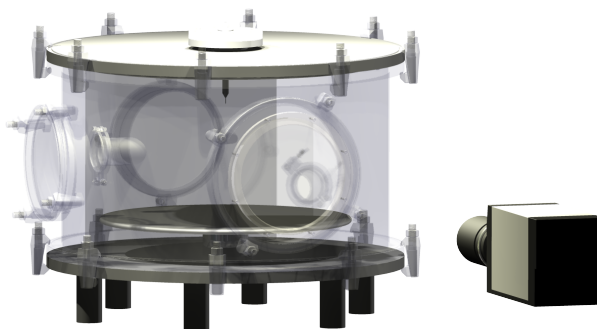
Figure 3.3: Overview of the old vacuum vessel with the ICCD camera. The wall of the vessel has been rendered transparent so that the anode tip and cathode plane are visible.

into the vessel is not too high, but there should be some flow.

Route 2 is used to evacuate the set-up when changing gas filling, or after usage. This route consists of thick (ISO-100) pipes and bellows up until the turbo-molecular drag pump (a Pfeiffer Compact Turbo TurboDrag Pump, TMH 261 P). The thick pipes can support much higher flow rates than the much smaller piping and pressure control valve in route 1. Therefore this route is preferred when one wants to evacuate the vessel quickly, or when a high vacuum is needed.

Before the start of a typical experiment, the vacuum vessel is filled with the desired gas to atmospheric pressure, evacuated and re-filled twice before finally filling the vessel to the desired pressure. This procedures effectively removes any remaining traces of other gasses from previous experiments, leakage or out-gassing. During an experiment, the gas is refreshed with a typical full refresh time of 25 minutes.

The design of the gas handling system of the old set-up is similar as described above, except that it does not contain a turbo-molecular pump and the roughing pump is not oil free.

3.2.2 Old vessel

The old vacuum vessel (see figure 3.3) consists of a cylindrical tank with an inner diameter of about 500 mm and an inner height of about 300 mm. At the bottom of the vessel, a 390 mm diameter cathode plate is mounted. For small gap distances (e.g. less than 80 mm), a smaller cathode plate can be placed on top of this cathode plate.

A high voltage feedthrough is mounted at the top flange of the vessel. Inside
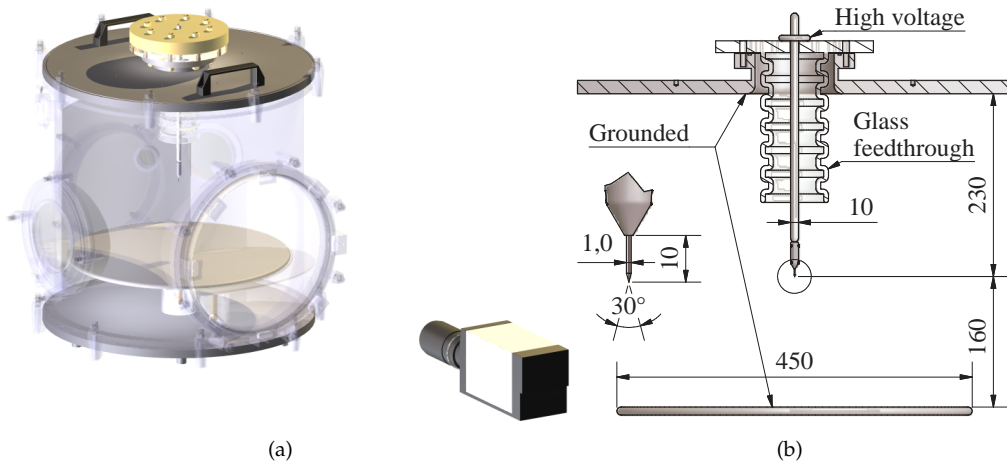
Figure 3.4: Overview (a) and schematic view (b) of the new high purity vacuum vessel with the ICCD camera. The wall of the vessel has been rendered transparent in the overview so that the anode tip and cathode plane are visible. In the schematic view, dimensions are given in mm. The bottom of the tip holder and the tungsten anode tip are shown enlarged on the left side of (b).

the vessel it is surrounded by plastic plates to prevent discharges between the feedthrough and the grounded vessel. However, the gaps between these plates and the feedthrough itself have always led to problems with discharges, even when filled with insulating grease.

At the bottom of the feedthrough, a small rod is connected to which the electrode tip can be attached. The geometry of the tip and bottom plate can be adapted for different experiments. See section 4.2.2 for some examples of electrode geometries.

The discharge can be imaged through a window mounted on the ISO-K DN200 flange on the front of the vessel. Usually a quartz window with a diameter of 150 mm was mounted on this flange, although in some cases, when ambient air was investigated, the whole flange has been removed in order to have a better view of the discharge. The quartz window slightly limits the view of the camera for large gap distances (140-160 mm) resulting in dark areas (without streamers) on the edges of the camera images.

3.2.3   New vessel for pure gasses

The new vacuum vessel (see figure 3.4) addresses three shortcomings of the old vessel, namely the quality of the vacuum (and thereby the purity of the gas fill), the electrical insulation of the high voltage feedthrough and the size of the main

viewport. We will treat the quality of the vacuum and the resulting purity of the gas (mixture) in detail below.

The main viewport of the new vessel consists of an ISO-K DN320 port with an inner diameter of 330 mm, covered with a 25 mm thick quartz plate. This window is significantly larger than the one in the old vessel. The increase in window diameter makes it possible to image the complete discharge area between the electrode tip holder and the cathode plate without any dark corners.

The inner diameter of the new vessel is equal to that of the old vessel (~500 mm), but the inner height is increased to about 500 mm to make room for better electrical insulation. The high voltage feedthrough at the top of the vessel consists of a glass feedthrough produced by the GTD service of the Eindhoven University of Technology. It insulates a 10 mm diameter metal rod from the surrounding (grounded) stainless steel vessel and top flange. Besides improving the electrical insulation, the glass feedthrough should also perform better under vacuum conditions than the plastic shielding that is used in the old set-up (less out-gassing), although this has not been specifically tested. A fixed sharp tungsten tip electrode is attached at the end of the metal rod, 160 mm above the cathode plate.

Gas purity in the set-up

As was mentioned above, the new set-up is specifically designed to ensure the purity of the enclosed gasses. For this reason, the set-up can be baked to reduce out-gassing, it contains no plastic parts, except for the o-ring seals and it stays closed all of the time. When not in use, the set-up is pumped down to a pressure of about $2 \cdot 10^{-7}$ mbar.

The leak rate of the vessel was tested by closing all valves of the system at high vacuum and monitoring the pressure increase as function of time. The result of this measurement is shown in figure 3.5. The resulting leak rate (including out-gassing) under vacuum is about $8 \cdot 10^{-7}$ mbar/min, which is considerably lower than the $5 \cdot 10^{-3}$ mbar/min reported by e.g. Yi and Williams [243]. We have used a helium leak tester to check for leaks, but have not found any.

During use, the gas inside the set-up is flushed with such a flow rate that all gas is replaced every 25 minutes. The absolute flow rate is controlled by a mass-flow controller and depends on pressure. The flow rate is sufficiently high such that the contamination caused by the leak/out-gassing rate is significantly below 1 ppm for all used pressures.
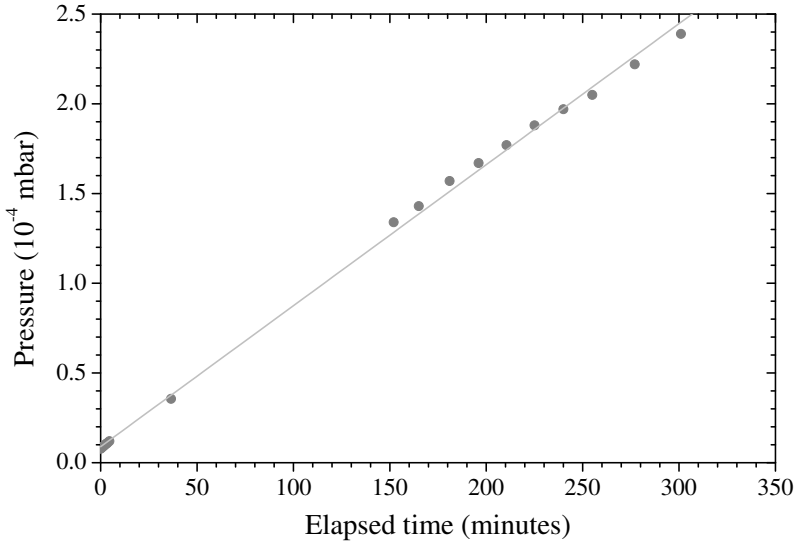
Figure 3.5: Pressure rise of the (closed) system without flow and at sub-atmospheric pressures. The measured rate of out-gassing and or leakage of the system is $(7.86 \pm 0.07) \cdot 10^{-7}$ mbar/min.
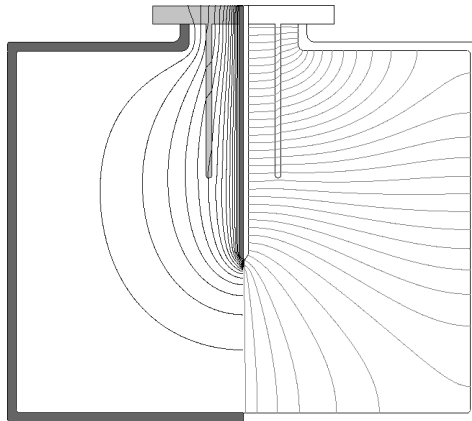
Figure 3.6: Potential distribution (left hand side) and streamlines (right hand side) in a simplified model of our new vacuum vessel. Calculations have been performed with the Integrated Engineering Software Electro 2D v90 field simulator program. The internal diameter is 500 mm, the internal height 390 mm and the tip radius is 15 µm.

3.2.4 Potential distribution in vessel

In order to get an idea on the potential distribution of the background electric field in the geometry of our new vessel, we have performed some calculations. With the help of dr. P. Wouters, we have used the Integrated Engineering Software Electro 2D v90 field simulator program to calculate the electric field and potential distribution in a simplified version of the new vessel. Some results of these calculations are plotted in figure 3.6.

We have not plotted the electric field magnitude itself, as this only has a very high spike close to the electrode tip (we have used a 15 µm tip radius) and is quite low everywhere else. Halfway between the electrode tip and the plate, the background electric field is about 10^3 V/cm for a tip potential of 50 kV. At the tip, the calculated field reaches a level of about $8 \cdot 10^6$ V/cm for the same potential. This is a bit lower than the theoretical field close to a 15 µm radius tip at this potential ($E = U/r = 3.3 \cdot 10^7$ V/cm) but this may be attributed to discretization errors near the tip.

In general, we observe that the paths of streamers in the vacuum vessel roughly follow the calculated streamlines (see for example figures 3.17, 5.1 and 6.6).

3.3 Pulse forming networks

In order to create a streamer discharge, a high voltage is needed. For the study of aspects of the physics of streamers, it is most practical to generate this high voltage in the form of fast pulses with a low (0.01-100 Hz) repetition frequency (see section 2.1 for a comparison of pulsed versus continuous corona discharges). In our case, most experiments have been performed at 1 Hz pulse repetition frequency.

We have used two different pulse forming networks to generate the pulses, namely the C-supply that has also been used in previous experiments by Briels *et al.* [31] and the Blumlein pulser that has been newly built. Both pulse forming networks will be treated below.

3.3.1 C-supply

The C-supply consists of a 0.5–2 nF capacitor that is charged by a high voltage negative DC source (see figure 3.7). Now a trigger circuit triggers a spark gap, which acts as a fast switch. The capacitor is discharged and creates a positive voltage pulse on the anode tip. This pulse has a risetime of at least 15 ns and a fall time of about 10 µs, depending on discharge impedance and choice of resistors (see also sections 3.3.3 and 3.5). This circuit is treated extensively in [31].
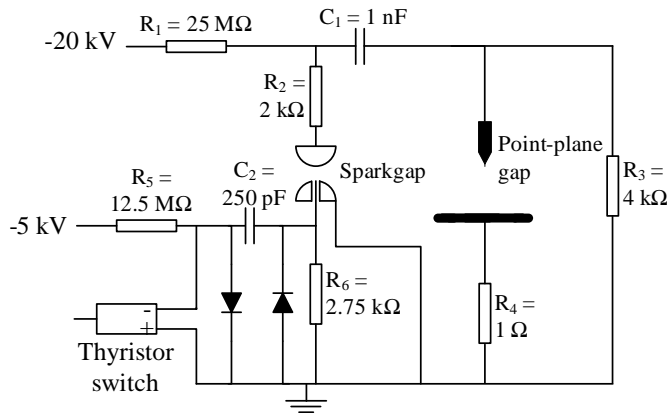
Figure 3.7: Schematic circuit of the C-supply for the generation of positive voltage pulses. The values of most components are not fixed and have been varied during the experiment. The amplitude of the pulse in the point-plane gap is mainly determined by the input voltage (-20 kV in the drawing). The resistors in series (R_2) and in parallel (R_3) with the discharge determine the pulse risetime and duration.

3.3.2   Blumlein pulser

Advantages of short pulses

Past measurements by Briels *et al.* [31, 33, 34, 35] and others [10, 153, 243] have been performed with voltage pulses with durations of many hundreds of nanoseconds up to many microseconds and with risetimes of tens of nanoseconds or more. This approach has two disadvantages: firstly, the often slow risetime means that the streamers may initiate at a significantly lower voltage than the reported maximum voltage. Therefore, they may not exhibit the properties (like diameter and propagating velocity) that are representative for this voltage, but for a lower voltage [31, 33]. Secondly, a long pulse duration may lead to a streamer-to-spark transition. Because a spark is usually much brighter than a streamer, it may damage the photo-cathode of an ICCD camera.

One way to overcome these two problems is to use a power supply based on a Blumlein pulser [114, 194]. With such a circuit, it is possible to make pulses with a well defined duration (depending on the cable length) and a fast risetime (order from 1 to 10 ns).

Design of the Blumlein pulser

The Blumlein pulser is a new design based on existing knowledge about such circuits [114, 194]. It produces a more or less rectangular pulse with a short
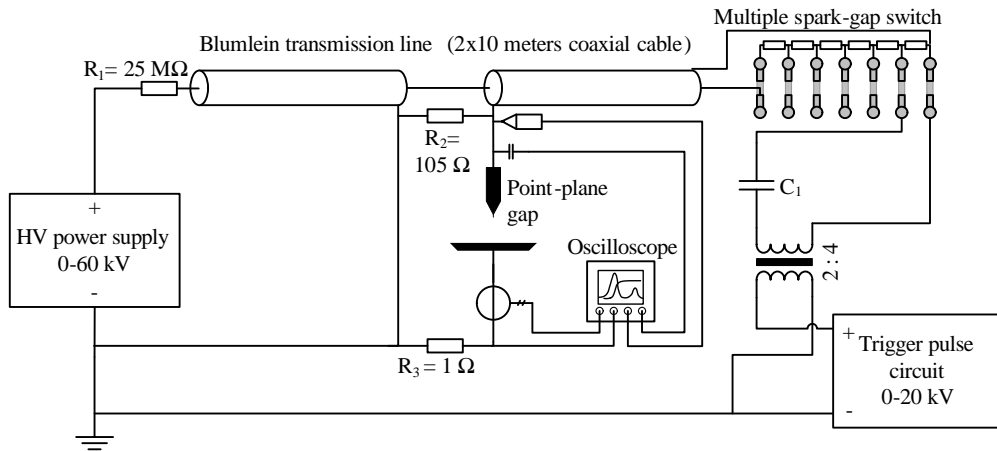
Figure 3.8: Schematic circuit of the Blumlein pulser design for the case of a positive voltage pulse. The oscilloscope is connected to four probes. From left to right: current transformer, current measurement by shunt, North star high voltage probe and capacitive voltage probe. The exact trigger pulse circuit has been omitted for sake of simplicity. It is given in two different versions in figure 3.11.

risetime and a fixed duration. This is achieved by charging two coaxial cables (see figure 3.8) with a DC voltage source. The cores of the two coaxial cables are connected directly, while the mantles are connected via the load. The impedance of the load should be equal or close to $2 \cdot R_c$ with R_c the cable impedance.

When a switch at the end of one of these cables is closed, a voltage pulse will travel along the cable mantles. This voltage pulse will arrive at the load (and the anode tip). After traversing the second cable back and forth, the voltage pulse at the anode tip will be nullified.

This new design has three advantages compared to the C-supply: The faster risetime ensures that the voltage during initiation and early propagation is closer to the reported maximum voltage; therefore thicker streamers are generated [31]. The short duration of the pulse enables us to use overvolted gaps without the risk of spark formation (this can damage the camera). The short duration also helps to ensure that only primary streamers are produced (see section 2.3.3). This makes it much easier to perform spectroscopic measurements on only these primary streamers; we can use long integration times without capturing other phenomena like secondary streamers or glow discharges. However, this last advantage is only valid if the streamers do not bridge the gap long before the end of the pulse duration. In our measurements this is not always the case, as is shown in figure 5.8.

We have implemented the Blumlein pulser on top of the discharge vessel, as
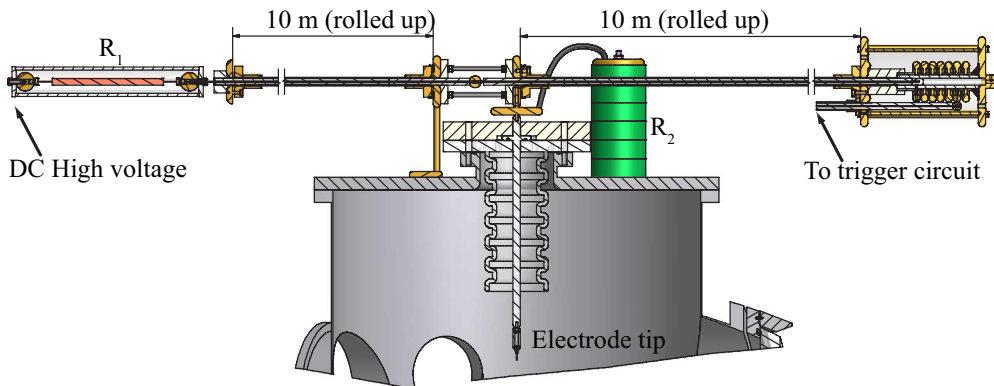
Figure 3.9: Schematic drawing of the Blumlein pulser layout on top of the discharge vessel. The high voltage charging resistor (R_1) is shown on the left. A more realistic image of the physical layout of this circuit is presented in figure 3.1.

is schematically presented in figure 3.9 and more realistically but less detailed in figure 3.1. The load is represented by the discharge itself parallel to a resistor with an impedance of 105 Ω. A multiple sparkgap is used as the switch (see below).

The present design allows for a risetime of about 10 ns and a pulse duration of 130 ns. The pulse duration is determined by the cable length; it is twice the pulse delay time of a single 10 m long cable. We see only one reflected pulse occurring after the first pulse. This indicates that our system is quite well matched. More details on pulse shape and risetime are given in section 3.3.3. The length of the pulse can be varied by using other lengths for the two coaxial cables, although this takes some time and is not easy to implement during a measurement series.

Multiple sparkgap switch

The multiple spark gap switch has been around for quite some time [115]. It is based on the principle of the sparkgap. In a sparkgap, a high voltage is applied over two electrodes that are separated by a small gap. This voltage should be just below the breakdown voltage of the gap. When the sparkgap is triggered, breakdown occurs, thereby closing the switch. The triggering can be performed with a variety of methods, among which are small secondary discharges and lasers. The main advantages of a sparkgap switch are that it can close quickly, that it can withstand very high currents and that it can withstand reflected pulses without problems.

A multiple sparkgap does not have one gap, but, as the name suggests, multiple gaps, in a serial layout. The high voltage (that needs to be switched) is applied over all the gaps. Again, this high voltage should be just below the breakdown
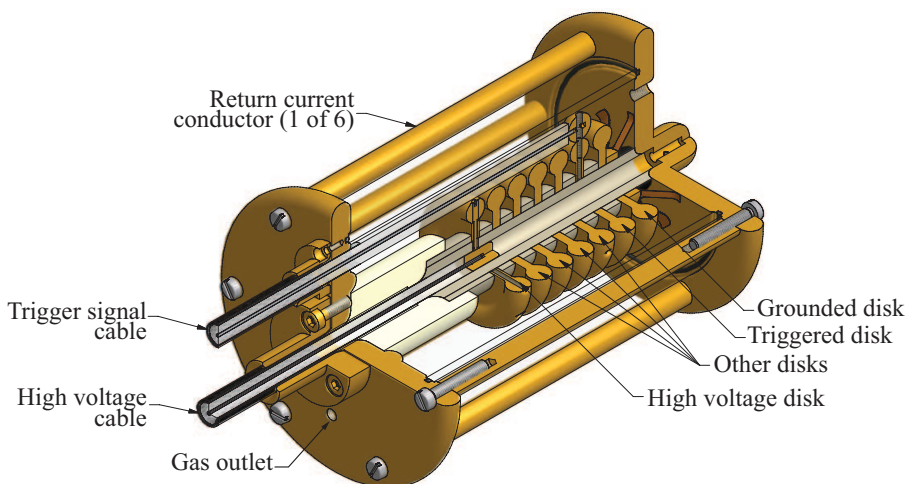
Figure 3.10: Three quarter section view of the multiple sparkgap switch. In the centre of the switch the seven disks around the six spark-gaps are visible. The main current path is through the central conductor of the high voltage cable, across the seven disks and then back via the back plate, the six cylindrical return current conductors, the front plate and finally the mantle of the high voltage cable. Most metal parts in the set-up are made of brass. The gas inlet is connected directly to the perspex cover around the sparkgap and is not visible in this view.

voltage of the switch. Now one gap is triggered, in our case by applying an extra external voltage. This will lead to breakdown in this first gap. The high voltage is now divided over one gap less. Therefore it is above the breakdown limit of the remaining gaps. These remaining gaps will now break down one by one. When breakdown occurs in the last gap (not necessarily the one furthest away from the trigger gap), the complete switch is closed. The main advantage of this multiple sparkgap layout is that the last gap is vastly overvolted just before breakdown. This means that the breakdown will be very fast and therefore leads to a very fast (nanosecond) switch.

During the investigations discussed in this thesis, different lay-outs of the switch have been used. The version shown in figure 3.10 is the latest design with 6 gaps and a coaxial design. In this design the inflowing gas (pure nitrogen) is directed straight between the brass disks (to efficiently remove reaction products). The pressure in the sparkgap can be regulated between atmospheric and 3 bar overpressure as a means to vary the breakdown voltage of the switch. The gas outflow is regulated by a needle valve.

Previous designs had different gas flow connections, a different position of the trigger cable and even a completely reversed layout with a central conductor
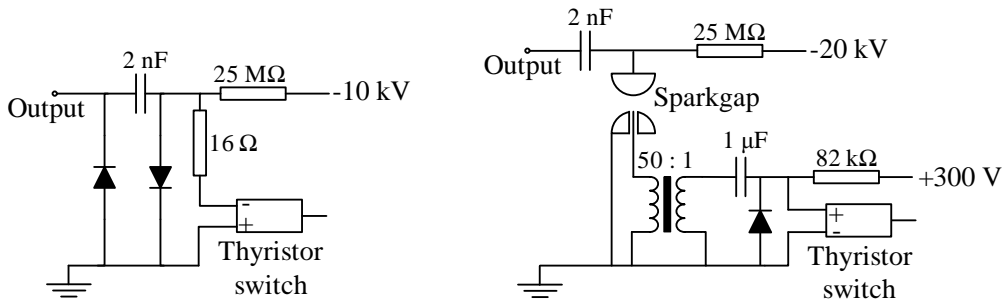
Figure 3.11: Two different lay-outs of the trigger circuits used with the Blumlein pulser. The indicated output is connected to the Blumlein pulser as shown in figure 3.8.

through the axis instead of the brass coaxial rods on the outside of the switch. This latter design had 7 gaps. However, the performance of all the different layouts is very similar and we will not treat them in detail. More details regarding the multiple sparkgap switch can be found in the trainee reports by Blanc and Miermans [21, 133].

Sparkgap triggering

Our multiple sparkgap switch is triggered by applying an extra voltage pulse to the triggered first gap. The trigger circuit is separated from the high voltage pulse of the main Blumlein circuit by means of a transformer (see figure 3.8). A capacitor is placed in series with the secondary transformer to prevent DC current between the triggered disks of the Blumlein pulser.

Different layouts of the trigger circuit have been used. The two main topologies are given in figure 3.11. In both cases a capacitor is slowly charged and, when triggered, quickly discharged. This leads to a fast voltage pulse, that is used to trigger the multiple sparkgap switch. This operation method is similar to the generation of the voltage pulse with the C-supply discussed in section 3.3.1.

The difference between the two trigger circuits is in the way how they discharge the main capacitor. The first layout uses a high voltage thyristor to accomplish this, while the second layout makes use of a secondary sparkgap, that itself is triggered by a smaller capacitive circuit triggered by a low voltage thyristor. This capacitive circuit is coupled to the secondary sparkgap by means of a 1:50 high voltage transformer.

The main advantages of the first trigger circuit are its simplicity and the low jitter. However, we have experienced three failures of the Behlke high voltage thyristor switches used in this circuit. These switches are quite expensive and have

a long delivery time. We do not know why exactly these switches have failed or how to prevent it. Therefore, we have decided to stop using this circuit and change to another layout.

The second circuit shown in figure 3.11 is our final topology, and has been used since April 2010. This topology is very similar to the C-supply, except that we do not produce the trigger of the secondary sparkgap by means of a high voltage thyristor and capacitor, but instead by means of a low voltage thyristor and capacitor. This 300 V pulse is then up-transformed to about 15 kV, which can trigger the secondary sparkgap. The main advantage of this topology is that all parts that can break down easily (mostly semiconductors like the thyristor and diodes) are now cheap low voltage components instead of the expensive high voltage ones. The disadvantage of this circuit is that it has a somewhat higher jitter (~5-10 ns), caused by the secondary sparkgap. This jitter is added to the jitter of the multiple sparkgap to get the total jitter of the Blumlein pulser.

The new topology with the low-voltage thyristor/capacitor combination and a 1:50 transformer can also be used to replace the high voltage switch in the C-supply. We therefore recommend to use this topology in the C-supply as well. In fact, the trigger circuit can be directly connected to the discharge vessel and then serve as a C-supply pulse source by itself, replacing the Blumlein pulser (when combined with appropriate resistors to determine pulse length and risetime).

3.3.3   Pulse shapes

As was discussed in the previous sections, the Blumlein pulser and the C-supply create quite different pulse shapes. Two characteristic pulse shapes of roughly similar amplitude are given in figure 3.12.

In general, the Blumlein pulser creates a more or less rectangular pulse with a risetime of about 10 ns and a duration of about 130 ns. This pulse is followed by one reflected pulse of reversed polarity and an amplitude that is about one third of the original pulse. After this reflected pulse, the voltage returns to 0 kV within about 500 ns. A peculiar side-effect of this pulse shape is discussed in appendix A.

The C-supply creates a pulse with a roughly exponential rise and decay. However, not all pulses have exactly the same shape as the ones shown in the figure. In the case of the C-supply, the pulse shape depends largely on the choice of resistors. Especially the resistors in series and in parallel with the discharge are important (R_2 and R_3 respectively in figure 3.7). The resistor in series (R_2) with the discharge determines the risetime. This time can vary between about 15 ns, when no resistor is used (~0 Ω) to hundreds of nanoseconds when a resistor of multiple kilo-ohms is used. Unfortunately, a fast risetime (low series impedance) usually is paired with oscillations of the voltage, as is shown in figure 3.19.
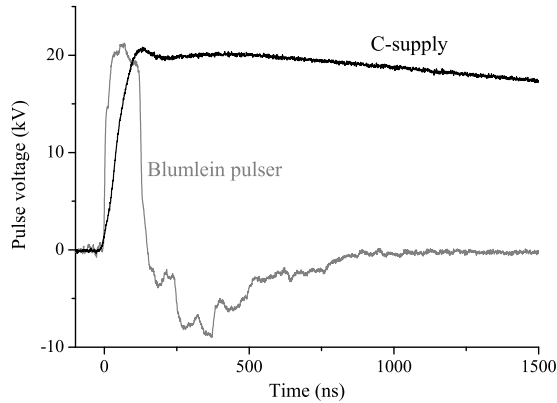
Figure 3.12: Comparison of the voltage pulses produced by the two different pulse sources. Note that the duration of the pulse from the C-supply depends largely on the impedance of the discharge and can therefore vary significantly according to gas type and pressure. Because the Blumlein pulser contains a low-ohmic resistor in parallel to the discharge, it is hardly influenced by the discharge impedance.

The resistor in parallel (R_3) determines the decay of the pulse as long as the impedance of the discharge is significantly higher than the impedance of this resistor. In this case, the decay is exponential with a time constant equal to $R_3 \cdot C_1$. The voltage of the C-supply can be chosen between +5 kV and about +55 kV. To change the voltage, one should adapt the DC source voltage as well as the electrode separation or gas pressure of the spark-gap switch. We have used the C-supply only with positive polarity pulses.

The pulse shape produced by the Blumlein pulser is more or less constant. Its amplitude and polarity are determined by the DC source voltage and can be tuned at will, but its general shape can not easily be modified. The only changes we have performed consisted of fine-tuning of the parallel resistor (R_2 in figure 3.8) to minimize reflections and optimize the risetime. One can change the duration of the pulse by changing the length of the transmission lines of the Blumlein pulser, but this is quite some work and was not done during the experiments discussed here. The voltage limits of the Blumlein pulser are mostly determined by the multiple sparkgap switch. In its final lay-out with 5 gaps of 0.5 mm and 1 (trigger)-gap of 1 mm, the switch can operate at pulse voltages between roughly 15 and 35 kV (by varying gas pressure in the switch). These limits can be adapted by changing the ceramic spacers between the discs.

3.4 Diagnostics and processing

We use multiple diagnostic methods to investigate the streamer discharges. The most important three are electrical diagnostics, streamer imaging and spectroscopy. The former two are treated below, while the latter one is treated in chapter 8. In some cases we have used stereoscopic imaging of the streamer discharge. This method is explained in detail in section 4.2.1.

3.4.1 Electrical diagnostics

The two most important electrical parameters that are needed when investigating streamer discharges are the pulse voltage and the discharge current, both as function of time. For both parameters we have used two different measurement probes which we will all discuss below. All four measurement probes were connected to a four-channel LeCroy WaveRunner 6100 digital oscilloscope with 1 GHz bandwidth although never all together.

Northstar PVM voltage probes

Our main probe used to measure the voltage pulse produced by our pulse forming networks is a Northstar PVM-4 1:1000 high voltage probe. This probe has a bandwidth of 110 MHz and can withstand pulsed voltages up to 60 kV. Most voltage pulse shapes (e.g. the ones in figure 3.12), and all absolute voltage values have been determined with this probe. The voltage probe is connected to the electrode feedthrough on top of the vacuum vessel.

Besides the PVM-4 probe, we have also used a very similar PVM-1 probe. The main difference between this probe and the PVM-4 probe is that its bandwidth is limited to 80 MHz. We have mainly used the PVM-1 probe to monitor voltage pulse shapes in other parts of the circuit, e.g. in the trigger-circuit.

Capacitive voltage probe

We have used a capacitive probe designed by Ad Kemper to more accurately measure risetimes of the voltage pulses produced by the Blumlein pulser. Because these risetimes are between 5 and 15 ns, they can not be accurately determined by the PVM-4 probe (with 110 MHz bandwidth). The bandwidth of the capacitive probe is over 1 GHz. Therefore this probe is fast enough to accurately determine the risetime of a fast voltage pulse. This probe is also attached to the top of the vacuum vessel, in close proximity, but without direct electrical connection, to the electrode feedthrough.
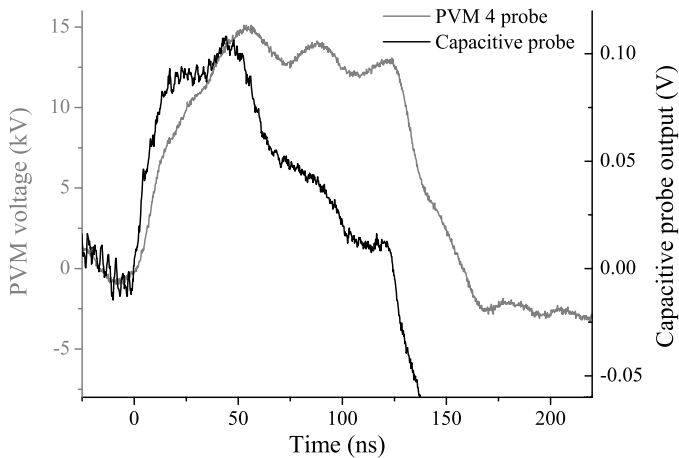
Figure 3.13: Comparison of the output of the PVM probe and the capacitive probe when measuring the same voltage pulse.

In order to reduce electro-magnetic noise picked up from the pulse forming network and the experiment itself, we have installed so-called handformable cables with a shielding of about 130 dB. These cables are grounded to both the Faraday cage encasing the experiment and the Faraday cage encasing the oscilloscope.

The capacitive probe has two disadvantages compared with the PVM probes: it is not calibrated and it has some differentiating action on the measured voltage signals. We could calibrate the probe against the PVM probe (or another probe). However, this would require that the probe is mounted in a fixed position with respect to the high voltage feedthrough. We chose not to do this so we could move the probe closer or further away from the high voltage parts to either get more signal or prevent sparking to the probe. An example of the differentiating action of the capacitive probe is shown in figure 3.13. Here it can be seen that the capacitive probe measures a faster risetime, but that it does not fully reproduce the pulse shape as acquired by the PVM probe.

Both these problems of the capacitive probe can be overcome by combining the capacitive probe with a PVM probe. The capacitive probe is then only used to measure the risetime, while the PVM is used to determine the rough shape of the pulse and the absolute pulse amplitude.

Current shunt

The simplest way to measure a current is to measure the voltage over a resistor (a shunt) in series with the load (the discharge). We have implemented such a current shunt between the cathode plane at the bottom of the discharge vessel and

51
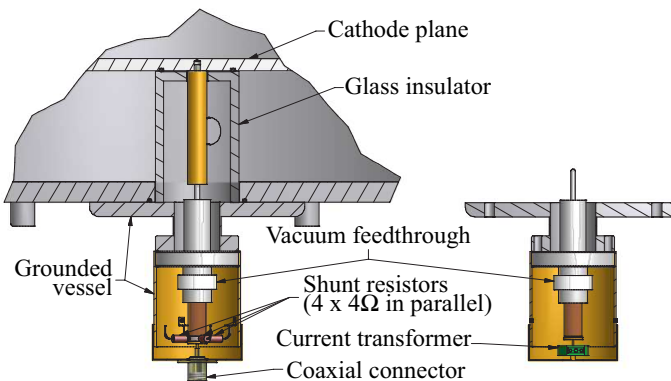
Figure 3.14: Schematic cross sections of the two current-measurement probes. Both are mounted on the bottom of the vacuum vessel. The left image depicts the current shunt method and the right image the current transformer.

the grounded discharge vessel itself (see figure 3.14). The shunt is mounted in a coaxial construction, fully surrounded by a grounded metal enclosure. The voltage over the shunt resistors (4 parallel resistors of 4 Ω each) is measured through an N-type connector that is connected to the oscilloscope via a handformable cable.

Current transformer

An alternative to the shunt is a current measurement by a current transformer. We have used a Pearson current monitor (model 2877) positioned in roughly the same position as the current shunt. The four resistors are now replaced by one straight (axial) metal conductor around which the current probe is mounted. Again, the voltage signal over the current probe is measured by the oscilloscope through a handformable cable.

Current measurement and electrical distortion

Unfortunately, both current measurement methods result in a signal that includes a large amount of distortion and oscillations. Only at high currents (order of 1 A and larger), we can measure the real discharge current with some degree of accuracy. At lower currents the oscillations dominate.

We are quite sure that these oscillations do not represent a real current inside the vacuum vessel. Even under high vacuum conditions, the current oscillations are still present, with the same amplitude and frequency as under streamer and glow discharge conditions. In such vacuum conditions, only displacement current should occur, which has a waveform shaped like the derivative of the voltage pulse
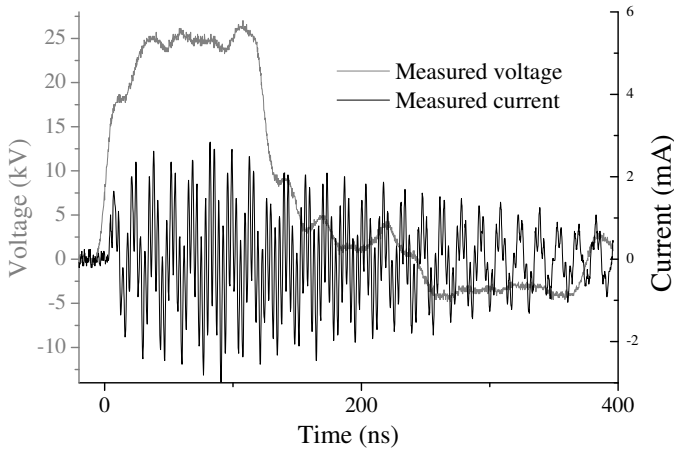
Figure 3.15: Current oscillations measured with the current transformer under vacuum conditions (no discharge). The voltage curve measured with the Northstar PVM probe is included for comparison.

waveform. However, as can be seen in figure 3.15, the current oscillations are not shaped like the derivative of the voltage waveform.

Nevertheless, the current oscillations are probably initiated by the displacement current or other real current phenomena. They then trigger a resonance in the cable or somewhere else in the measurement system. But, even after replacement of the thick coaxial cable by handformable cables (which greatly improved the signal-to-noise ratio for the capacitive voltage probe) and replacement of the current shunt by the current transformer, the oscillations are still present with roughly the same amplitude and frequencies (we did not measure the exact amplitude and frequencies in all situations). Measurements have shown that in the final layout (handformable cables and current shunt), the frequency spectrum of the oscillations has peaks at 67 and 300 MHz [133].

3.4.2 Camera system

A propagating streamer head emits light and the path of these heads can therefore be imaged onto a camera with a lens. Because the emitted light is often weak an intensified CCD (ICCD) camera is needed. The intensifier also enables us to take images with very short (nanosecond) exposure times. As (in air and nitrogen) only the propagating streamer heads emit light, these images only show a small section of the streamer propagation and can therefore be used to measure the velocity of the streamers [33].

In our case, streamer discharges are imaged by a Stanford Computer Optics
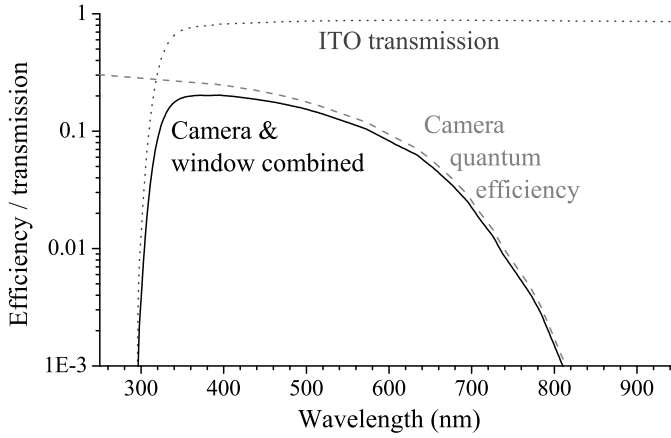
Figure 3.16: Curves of the ICCD camera photo-cathode quantum efficiency, the ITO window transmittance and the product of these curves (the effective system wavelength respondence). Note that these curves do not include the transmittance of the quartz window of the vacuum vessel and the quartz camera lens.

4QuikE ICCD camera. This camera has a minimum gate time of 2 ns and produces 1360 by 1024 pixel, 14 bit grey-scale images. We use two different lens assemblies: a Nikkor UV 105 mm f/4.5 camera lens mounted directly on the camera and a 250 mm focal length, 50 mm diameter achromatic doublet on an optical rail. The latter is used to zoom in on a specific region of the discharge in order to measure small streamer diameters. We use a window of conducting ITO (Indium tin oxide) glass as part of the Faraday cage to protect the camera against the high voltage pulses.

Mf value

In many of the images presented in this thesis, the original brightness is indicated by the multiplication factor *Mf*, as introduced similarly by Ono and Oda [153]. This value is a measure for the gain of the complete system, it includes lens aperture, ICCD gain voltage and maximum pixel count used in the false-colour images. An image with a high *Mf* value is in reality much dimmer than an image with similar colouring but with a lower *Mf* value (the real brightness is proportional to Mf^{-1} for an image with the same colours). We have normalized the *Mf* value in such a way that the brightest image presented in [150] has an *Mf* value of 1. This has resulted in the following equation for the *Mf* value,

$$Mf = 500 \cdot e^{\frac{V_g}{68.9\,V}} \cdot \frac{1}{D^2 \cdot (C_{max} - C_{min})},$$

(3.1)

54

with V_g the gain voltage of the camera, D the inverse aperture (e.g. 4.5 for f/4.5) and C_{max} and C_{min} the maximum and minimum count values used in the image representation. The factor 500 comes from the normalization procedure and the camera gain factor of 68.9 V is a property of our camera. This calculation is only valid for images from this specific camera together with our set-up (lenses and windows) and a specific false-colour palette. Therefore our exact definition is different from the one by Ono and Oda [153] although the general concept is the same.

Note that we improved our fitting procedure of the camera calibration data since publication of [150]. Therefore the data presented there has a somewhat different definition of the *Mf* value. In the old definition, we used a camera gain factor of 58.4 V and a normalization value of 99 instead of 500. This means that images with *Mf* values around 1 will be virtually the same between [150] and this thesis, but high *Mf* values can be up to a factor of 2 lower in this thesis than in [150].

Effects of diffusion on camera images

In gas mixtures containing nitrogen, most radiation is produced by molecular nitrogen. It is well known that the streamer heads only emit light for a very short time (less than 2 ns) in these mixtures [22, 33, 187]. We can assume that the atoms or molecules that emit the radiation have not moved significantly between excitation and emission. For example, the thermal velocity of a nitrogen molecule at room temperature is about 500 m/s between collisions. This means that the maximum distance it can travel within 10 ns is 5 μm if it is not scattered on its path; this is clearly below our resolution. Therefore, the image represents a mapping of the production of the relevant excited states in nitrogen.

In some other gasses, like argon, the streamer channels remain bright tens to hundreds of nanoseconds after the streamer head has passed. However, even in this case the maximum distance travelled by an excited atom or molecule before it decays will still be smaller than the imaged pixel size of our camera. Therefore, in all cases, the images represent a map of the locations where the excited molecules or atoms are created and the images are not influenced by diffusion of these excited species after excitation.

3.4.3   Measuring streamer diameter and velocity

From the images taken, the streamer diameter is determined with the following method:

- A straight streamer channel section is selected.
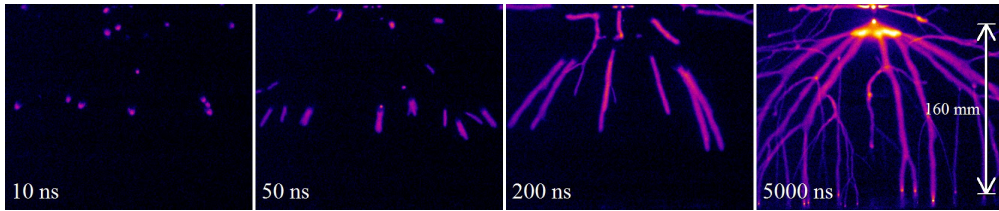
Figure 3.17: Example of ICCD images for discharges under the same conditions using different gate (exposure) times, as indicated on the images. The camera delay has been varied so that the streamers are roughly in the centre of the image. In this example, the second and third image could be used to determine the streamer propagation velocity. The velocity is calculated by dividing the length of the longer streamer sections by the exposure time. This example shows images of artificial air at 200 mbar with a C-supply pulse of about 24.5 kV.
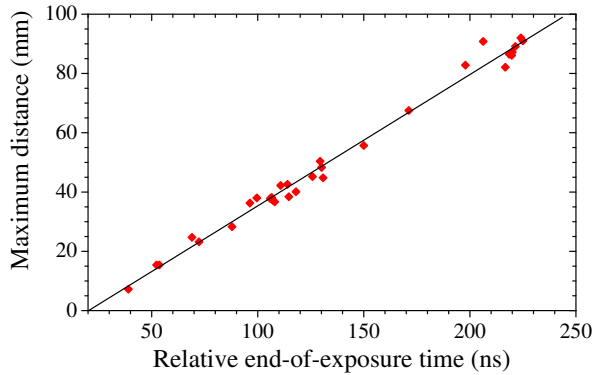
(a)
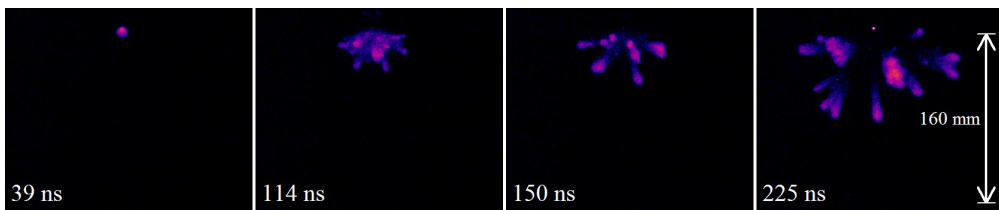
(b)

Figure 3.18: (a) the maximum distance of the streamer fronts versus the end-of-exposure time and (b) example images from the same measurement series. The end-of-exposure times are indicated on the images. They are calculated as $t = t_{camera-delay} + t_{exposure} - t_{oscilloscope}$ where $t_{oscilloscope}$ is the start of the voltage pulse according to the oscilloscope. Not all corrections discussed in section 3.5 are used because only relative time values are needed to calculate the propagation velocity. The velocity is defined as the slope of the fitted line, in this case $4.4 \cdot 10^5$ m/s. This example shows positive streamers in 25 mbar nitrogen 7.0 with a 10 kV pulse from the C-supply.

56

- In this section, several perpendicular cross sections of the streamer are taken (one per pixel).

- These cross sections are averaged to form one single mean cross section.

- The streamer diameter is determined as the full width at half maximum (FWHM) of the maximal streamer intensity.

A streamer diameter of at least 10 pixels in the image is required to ensure that the streamer diameter is measured correctly and camera artifacts due to cross-talk of camera pixels are negligible [31, 34]. For higher pressures (with thinner streamers), we have used the doublet lens in order to zoom in on a small specific region of the discharge.

The streamer propagation velocity has been measured with two different methods. The first method is as follows: we take short exposure images of streamers while they propagate in the middle of the gap (see figure 3.17). We then choose the thinner, straighter and longer streamer sections in each picture. The thinner streamers are insured to be in focus, the longer streamers are assumed to propagate almost in the photograph plane. The length of each such streamer section is measured (we use a similar FWHM method as for the diameter measurement), and the velocity is calculated as the ratio between length and exposure time, corrected for head size. Streamer sections that contain a branching event are ignored.

This method could be improved by using stereo-photographic techniques as demonstrated in [148, 149]. However, for sake of simplicity, we have chosen not to do this in the measurements presented here.

In the case of measurements on streamer velocity in argon, this first method does not work because of the long lifetimes of the exited states of argon. Even when using a very short integration time and a delay long enough to start observing when the streamers are halfway through the gap, one will still see the entire trail between the streamer head and the anode tip. Therefore we have to measure the velocity by measuring the distance travelled by the fastest streamer heads as function of time. When we now differentiate this curve we have the velocity as function of time. For this method to work we need to have little jitter in the streamer initiation. This method has previously been used by Winands *et al.* [33, 234] to measure streamer propagation velocities. An example of a velocity measurement with this method is shown in figure 3.18.

With both methods one should keep in mind that streamer velocity is not always constant in the strongly non uniform field of our point-plane discharge gap (see e.g. figure 7 and accompanying discussion in [34]). However, after roughly half of the gap, the velocity does not change much, except when the streamers get close (a few streamer widths) to the cathode plate. Therefore, we have chosen to use images in
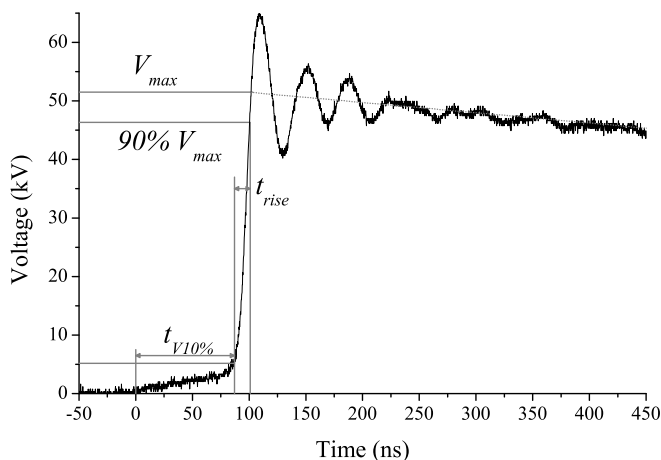
Figure 3.19: Typical voltage curve of streamer discharges as described in chapter 4 with definitions of important characteristics.

which the streamers are roughly halfway into the gap (for both methods). We have verified that both methods described above give the same results for gasses that support the first method.

3.5   Timings

In order to properly correlate the timing of camera images to the voltage curve, a full analysis of all delays in our experimental set-up has been conducted. With the results of this analysis we can define an absolute timescale for all measurements. We define the origin of the time scale ($t = 0$ ns) as the moment when the voltage imposed on the anode starts to increase above 0 V. This is illustrated in figure 3.19.

The maximum voltage (V_{max}) is defined as the crossing point of the increasing voltage slope with a linear fit of the beginning of the decreasing voltage slope. In the case of figure 3.19 this leads to $V_{max} = 52$ kV. The duration of the slow voltage increase just after $t = 0$ ns (here about 80 ns) depends mainly on the pressure in the spark gap switch and, to a lesser extent, on the streamer vessel pressure and anode geometry. Therefore we have defined another important point: $t_{V10\%}$, the time when the voltage has reached $V = 0.1 \cdot V_{max}$. The risetime (t_{rise}) of the voltage slope is also important. We have defined it as the time between $V = 0.1 \cdot V_{max}$ and $V = 0.9 \cdot V_{max}$. These characteristic values of the voltage pulse are influenced by resistors in the power supply and the impedance of the discharge and therefore vary between experiments.
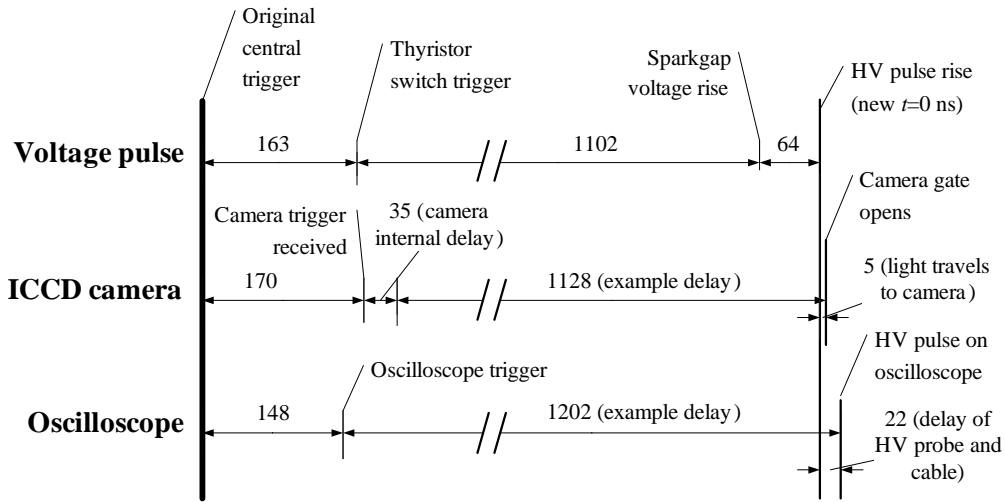
Figure 3.20: Timing scheme of the three parallel time-paths in the set-up. The scheme starts at the central trigger on the left hand side and ends at the occurence and measurement of the streamer on the right hand side. All arrows indicate a signal delay with the delay times indicated in ns. The length of the arrows is drawn to scale, except for the longest durations (>1000 ns), which are broken up.

The camera delay (t_{start}) is related to the same origin of the time scale as the voltage pulse. The camera gate is opened at t_{start} and stays open for a specified time (t_{gate}). This is discussed in more detail below.

Timing schemes

In order to determine the timing characteristics of the set-up, a full analysis of all timings and delays has been performed. In this analysis, the delays of all cables, optical fibres, probes and other equipment has been determined and combined. A sketch is shown in figure 3.20. In this figure, three time paths for different parts of the set-up are shown. These three time paths are all initiated by a central trigger from a function generator. Details of the time paths will be discussed below.

Note that the values given here are only valid for one exact layout of the set-up. They depend on many things, including the lengths of all measurement and triggering cables. These cables are often changed when working on the set-up. The values given here are from the state of the set-up in summer 2008 when the measurements that are discussed in chapter 4 were performed. These measurements were performed with the C-supply. The ICCD camera was placed inside an aluminium box and triggered through an optical fibre. For any other layout of the set-up, all values given in figure 3.20 and mentioned below should be

rechecked.

Voltage pulse   From the central trigger, the trigger pulse is fed through coaxial cables and an optical fibre to the thyristor switch in the high voltage circuit. This takes 163 ns. The thyristor switch in turn triggers the spark-gap 1102 ns later. The spark-gap then causes the rise of the high voltage pulse on the anode with a 64 ns delay. All three sections in this time-path have fixed delays with jitter of maximum 2-3 ns. These delays are intrinsic properties of the cables and equipment.

ICCD Camera   The ICCD camera is also triggered from the central trigger through coaxial cables and an optical fibre. This takes 170 ns. After receiving this trigger, the camera has an internal delay of 35 ns before it can open the gate. From this moment, the gate is opened after a user-specified delay. In the example from figure 3.20, this delay is set to 1128 ns in order to capture the beginning of the voltage pulse and the streamer initiation. Because of the short time-scales involved, we must account for the path-length of the light rays travelling from the discharge to the camera.

Oscilloscope   Again, the oscilloscope is triggered from the central trigger through coaxial cables and an optical fibre. This takes 148 ns. The rise of the high voltage pulse will occur some time after this trigger; in our example 1180 ns. Because the oscilloscope is connected to a high voltage (HV) probe with a long coaxial cable, the voltage rise will be detected on the oscilloscope 22 ns later.

Resulting timing

By using the known and set delays of the set-up, we can redefine a new origin of the time-scale that is the same for both the oscilloscope and the camera as is explained in section 3.5. In the example from figure 3.20, we have to subtract 74 ns from the time as shown on the oscilloscope to convert this to the time-scale of the camera. In other words, an event occurring at the new $t = 0$ ns will be registered on the oscilloscope at 1128 ns and on the camera at 1202 ns.

Chapter 4

Streamer branching and interaction

4.1   Introduction

Streamers penetrate into undervolted gaps due to space charges and local field enhancement at their heads [51]; frequently they break up into shapes reminding trees with many branches. Streamer branches stretching out from the same electrode carry head charges of equal polarity and repel each other electrostatically. Such self avoiding behaviour is incorporated in phenomenological dielectric breakdown models, see, e.g. [8, 146, 147, 163]. On the other hand, streamers and leaders emerging from oppositely charged electrodes carry opposite head charges; therefore when propagating towards the opposite electrode, they attract each other electrostatically and frequently join one another along the way; this is seen, e.g. in lamp ignition [45, 196] as well as in the counter leaders stretching from tall structures upwards towards an approaching lightning leader [19].

However, there are three recent observations [31, 44, 71] that seem to violate this scheme: streamer or sprite channels emerging from the same polarity electrode or atmospheric region do not repel each other, but they seem to merge or reconnect.

The first type of events was reported by Briels *et al.* [31] in pulsed power experiments in a needle-to-plane electrode geometry. Here thick and thin positive streamers emerged from the needle anode. The thick ones are much faster than the thin ones (as quantified in [31, 33]) and start somewhat earlier, they reach the cathode plate and then seem to attract thin streamers that arrive later. The streamers seem to approach the early ones in an almost perpendicular direction. Such an event is shown in figure 6 of [31] and will be called reconnection; a similar

event is shown in figure 4.8 below and in figure 7 of [231] and figure 10 of [234]. A physical mechanism for such an event is given in [31]: the originally positive thick streamer channel charges negatively after connecting to the cathode and therefore attracts the late positive streamer electrostatically.

The second type of events was seen by Grabowski *et al.* [71] and Winands *et al.* [231] in pulsed power experiments of either positive or negative polarity: many streamers emerged from a wire electrode, and sometimes two almost parallel streamers seemed to merge into a single one while propagating away from the wire. Such an event is shown in figure 5B of [71] and will be called merging; a similar event is shown in figure 4.13 on page 74 of this thesis. It was also reported orally for the experiments discussed in [231, 234]. A physical mechanism for such merging was recently proposed by Luque *et al.* [121]: the non-local photo-ionization reaction in nitrogen-oxygen mixtures like air could generate so much ionization in the space between the streamer heads that the heads merge despite their electrostatic repulsion; the mechanism was demonstrated in three-dimensional computations of two streamers for varying gas density and nitrogen-oxygen ratio.

A third type of event was reported by Cummer *et al.* [44] in high speed images of sprite discharges above thunderclouds; the figures are reproduced in figure 4.12 below. Here sprite channels propagating downwards seem to connect to each other, often accompanied by a bright spot. Sprite discharges have been established to be large versions of streamers at low gas densities, related to each other by similarity laws [34, 165, 200]. This phenomenon looks quite similar to the reconnection described above, however, the sprite streamers do not reach any electrodes to change the channel polarity. A possible explanation of the reconnection in sprites was recently given by Luque and Ebert [124]. They find from simulations that charge conservation in combination with varying air density along the channel creates a negative charge in the streamer tail while the streamer head carries a growing positive charge, thereby creating a polarization along the channel. The negative charging of the tail may attract newer positive streamer heads. Similar results have been found by Liu [113].

These three events were imaged with normal photography, i.e. in a two-dimensional projection of the full three-dimensional events. Therefore it is impossible to determine from the figures whether two streamer branches really do join, or whether they pass behind each other, and only the statistical analysis of many pictures can lead to such a conclusion. However, the true three-dimensional event can be reconstructed from stereo photography. In this chapter, stereo photography is applied to several situations where streamers appear to reconnect or merge.

Another largely unexplored issue in streamer research is the breakup of single channels. Such branching events are commonly seen in experiments [31, 35, 222]; multiple branching actually determines the gas volume that is crossed by streamers and consecutively chemically activated for plasma processing purposes. However,
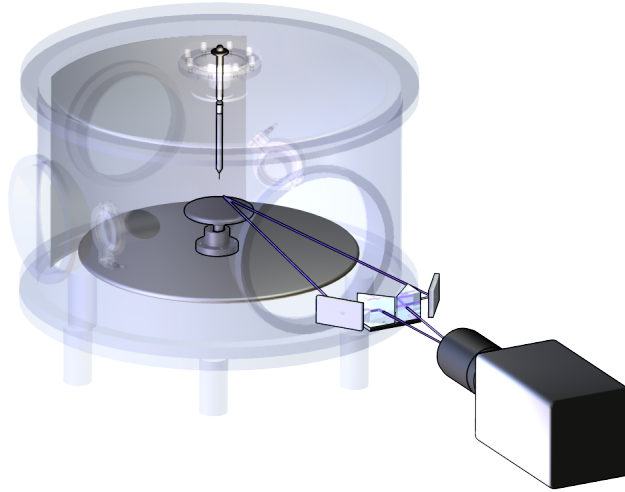
Figure 4.1: Schematic overview of the stereoscopic measurement set-up with the two image paths indicated. In this example an anode with a single tip is installed inside the discharge vessel.

up to now, only the conditions of the first branching event have been resolved in microscopic models [12, 108, 119, 136, 156]. On the other hand, the distribution of branching lengths and angles is an ingredient of models for the complete branching tree on larger scales [8, 146, 163]. In section 4.3, we resolve these lengths and, in particular, the angles in experiments. Additional details about the measurements discussed in this chapter can be found in the traineeship reports by Joeri Moerman [134] and Christian Geurts [65].

4.2   Methods and diagnostics

All experiments presented in this chapter have been performed in ambient air with a cathode-anode gap of 40 to 140 mm. Although the experiments have been conducted inside a vacuum-vessel (the old vacuum vessel described in section 3.2.2), in many cases the front window of this vessel was removed so that the air was identical to the ambient air inside the laboratory. In cases where pressures below 1000 mbar were used, the front window was mounted and the vessel contents were flushed with ambient air.

We use the electric circuit called the C-supply treated in section 3.3.1. In this set-up a capacitor is charged negatively with a DC power supply. This capacitor is then discharged by means of a spark-gap switch. This results in a voltage pulse on a pointed tip or wire with a risetime of about 20 ns, a maximum voltage between 6
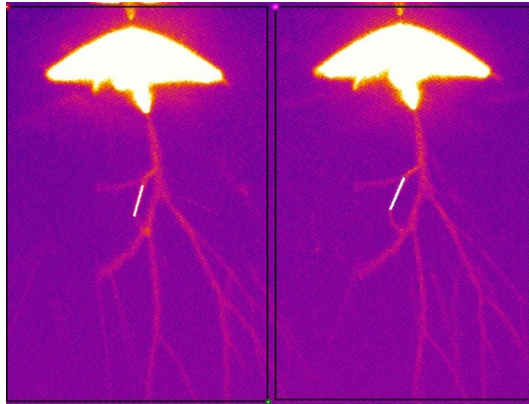
Figure 4.2: Stereo image as recorded by camera. Settings: positive voltage on tip, $U = 47\,$kV, $p = 200\,$mbar, $\alpha = 13°$, $d = 140\,$mm. The intensity has been scaled so that the structure in the bottom part can be clearly seen. One streamer section has been marked with a white line in both images.

and 55 kV and a decay time of a few microseconds. A positive corona discharge then propagates from the needle or wire to the grounded plate. Both needle and plate are highlighted in figure 4.1. The different anode geometries that have been used to study reconnection and merging are discussed in section 4.2.2.

The corona discharge produced by the circuit is imaged onto an intensified CCD-camera (Stanford Computer Optics 4QuickE) with a minimum gate time of 2 ns. The original camera frames of all images are 1360 by 1024 pixel, 14 bit grey-scale images. The camera images presented are false-colour representations of these original camera frames. Image processing and measurements (e.g. of streamer diameters) were done on the original full resolution 14 bit grey-scale frames.

4.2.1 Stereo photography method

Streamer discharges are usually imaged with conventional or digital cameras [31, 156, 229]. This leads to two-dimensional (2D) representations of what is essentially a three-dimensional (3D) phenomenon. These 2D representations can cause problems of interpretation. For example, it is impossible to see whether an apparent loop or reconnection is really what it seems to be. It is also impossible to get a complete picture of the 3D spatial structure and to measure branching angles. For this purpose, we have implemented a stereo-photography method which makes it possible to image streamer discharges in 3D. In this way, we resolve the imaging ambiguities in the fundamental physical phenomena, help understanding which gas volumes are actually treated by the discharge, and supply

(a) front view   (b) left view
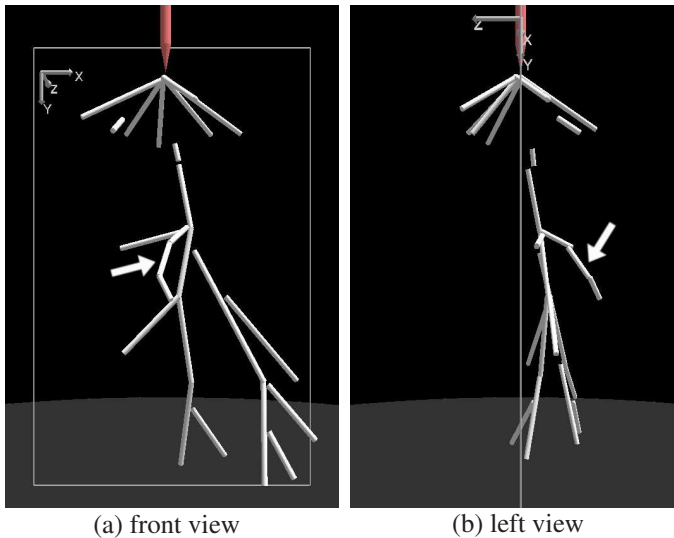
Figure 4.3: Orthogonal views of the 3D reconstruction of the streamer structure shown in figure 4.2. The section originally marked with the white line is now marked with an arrow in both views.

experimental data for larger scale models. The stereoscopic technique that we use has been around for a very long time [29, 55] and has been used for a large variety of topics. Some phenomena similar to streamers that have been studied with stereo-photography are sparks [125], flames [144] and dusty plasmas [214].

MacAlpine *et al.* [125] have studied sparks with a camera and a prism. In this study two images were taken using a prism to form an image at a right angle to the directly-observed one. In this way the complete 3D-structure of the spark path can be reconstructed with great accuracy. Similar work was reported by Agneray *et al.* [5] and Beckers *et al.* [20]. However, this method only works well for structures that have very few channels (e.g. the one spark of MacAlpine *et al.*). When there are many channels, it is very difficult to correlate them pairwise from two images taken at an angle of 90°.

In our case, we want to study streamer discharges that contain many (10–100) streamers. For this purpose a similar method can be used, but with a much smaller angle between the two image paths so that the two images of one streamer can be recognized. To achieve a smaller angle, one camera has been used in combination with two prisms and two flat mirrors as shown in figure 4.1. With this set-up two images (from different viewing angles) are captured on one camera frame; therefore they are temporally perfectly synchronized. An example of such a camera frame is shown in figure 4.2.

From the two 2D-images the 3D structure of the streamer channels can be

reconstructed in the following manner: Custom built software is used in which a line segment is placed manually over identical straight sections of a streamer channel in both left and right views The end points of these two line segments are now translated from 2D (xy) to 3D (xyz). We have used two different methods for this conversion: a simple method and a more exact trigonometric method (pinhole method). These two methods will be discussed below.

After the two 2D lines have been translated into one 3D streamer section, we can repeat this procedure for all other suitable streamer sections in the image. When all these 3D streamer sections are now plotted in 3D-space, we get some insight in the real structure of the streamer discharge. The 3D reconstruction of the example from figure 4.2 is shown in figure 4.3. Here it can clearly be seen that the streamer section marked with the white lines in figure 4.2 is not part of a loop. This information can not be derived from just one of the original 2D images. One of the measurements that can be performed now is measuring branching angles. The measured angles are the inner angles between two 3D streamer sections, represented as vectors. The technique described here also has some limitations, the most important one is that it is not possible to process discharge images that contain more than about 50 streamer channels.

The measurements of the branching angle (section 4.3) have been performed in a 140 mm gap with a full angle between the two optical paths of about 13°. Because the measurements regarding reconnection and merging (sections 4.4 and 4.5) are performed in a 40 mm gap instead of the 140 mm gap, the camera, prisms and mirrors have been placed closer to the vacuum vessel. The full angle between the two optical paths is 10° in these measurements.

An easy method to check if reconnection or merging occurs, is to look if it is visible in both images of a stereoscopic photo. Furthermore, the vertical position of the merging/reconnection location should be the same in both images. If this is clearly the case then it can be concluded that the merging or reconnection really takes place. In many cases, this method has been used instead of the more labour intensive complete 3D reconstruction.

Simple reconstruction method

In first instance, we have employed a very simple method to reconstruct 3D geometries from 2D images. It assumes that the cameras are far from the system and have a very large focal length. This introduces significant errors in absolute positions, but only small errors in local observables (branching angles and lengths). Indeed, the distance between the camera and the discharge is about 1 m, while distances between recently splitted streamer branches never exceed 2 cm in our measurements. Therefore, we can use this method without introducing errors larger than 1%.
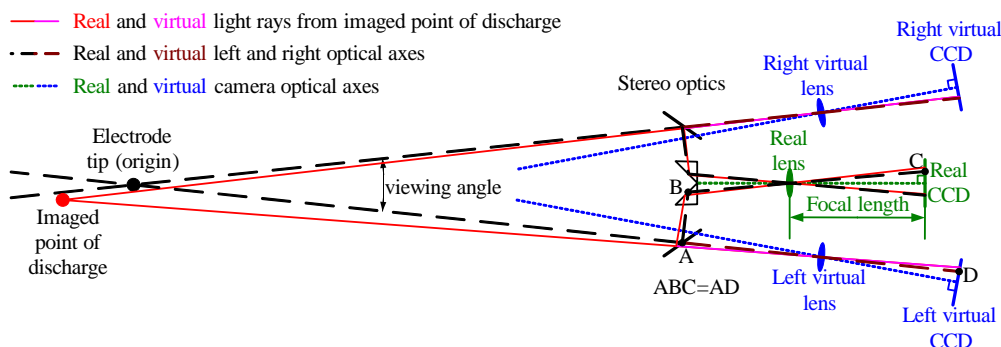
Figure 4.4: Schematic overview (top view) of the pinhole stereoscopic reconstruction technique. Both the real optics and camera and the two virtual cameras are shown. The imaged point is imaged on the two virtual CCD's and the real CCD. It can be seen that the distance between the optical axis and the imaged point on the CCD differs on the left and the right hand side. In the actual reconstruction, the third dimension is also used.

The simple method starts from the 2D coordinates (x_l, y_l) and (x_r, y_r) of identical streamer parts within the left or right image respectively, where the origins of the respective coordinate systems are chosen in the electrode tip. The depth coordinate z is then approximated as $z = (x_r - x_l) / (2 \cdot \sin(\alpha/2))$, where α is the full angle between the two optical paths (in most measurements processed with this method $\alpha = 13°$). The 3D x and y-coordinates are calculated as $x = (x_r + x_l)/2$ and $y = (y_r + y_l)/2$.

The error in streamer distances after splitting that results from this simplification is less than 0.2 mm. The dominant error comes from the visual determination of the locations of streamer section end points on the stereoscopic images. In many situations it is difficult to locate the exact point of branching, especially where two streamers are very close to each other. The total error is approximately 1 mm for local observables and 5 mm for absolute locations.

We have used the simple calculation method to determine the branching angles presented in section 4.3.

Pinhole reconstruction method

A more exact calculation method for the 3D reconstruction is obtained by using a complete 3D geometrical computation assuming an ideal pinhole camera. In this method, two virtual cameras are placed so that they will produce the left and right images without the prisms and mirrors as shown in figure 4.4. In other words, the distance between these cameras and the origin (on the vertical axis of the vacuum

vessel) is equal to the total path length of one of the two paths drawn in figure 4.1. The angle between the two virtual cameras and the origin is equal to the angle between the two paths (10° in most cases).

Both virtual cameras are represented as ideal pinhole cameras; they consist of an infinitely small hole and a screen (the ICCD). Such an ideal pinhole camera represents a camera aperture that is described as a point and no real lenses or apertures are involved. It does not include geometric distortions, diffraction or unfocused objects due to finite apertures. Therefore it can only be used as a first order approximation for a real camera system.

In order to reconstruct a 3D location of a point, the vector from the pixel location of this point to the pinhole location is calculated for both cameras. The crossing point of these two vectors now determines its real 3D location. In real life measurements the vectors will, of course, never really cross in full 3D; therefore the point halfway between their closest points is used.

The assumption of a pinhole camera neglects lens artifacts like chromatic aberration and pincushion or barrel distortion. The pinhole method reduces the absolute position errors of points far away from the origin (here defined as the position of (one of) the electrode tips or an arbitrary position on the wire, see figure 4.4). The local errors (relative position errors of two points close together) have not changed significantly by employing the new method.

The pinhole reconstruction method has been used to determine reconnection and merging as discussed in sections 4.4 and 4.5.

4.2.2   Anode geometries

Four different anode geometries have been used; they are shown in figure 4.5: (a) a single tip, (b) symmetrical double tips, (c) asymmetrical double protrusions from a plane and (d) a wire. The difference between the double tip geometry (b) and the double protrusion geometry (c) is that in the double tip geometry, both tips extend from a pointed holder, while in the double protrusion geometry, the tips extend from a plane similar to the cathode plate. In this geometry, the background electric field at some distance from the protrusions is quite similar to a plane-plane geometry; it is quite homogeneous in contrast to a point plane geometry. This protrusion geometry (c) is roughly similar to a needle-array electrode [93, 206], but it has only two needles. In particular, we will use an asymmetric configuration where one tip extends significantly further out of the plane than the other.

The distance between the tip(s) or the wire and the cathode plate was always set to 40 mm except for the measurements of the branching angle, where a 140 mm tip-to-plate distance was used. In the asymmetric geometry (c), 40 mm is the distance between the tip of the longer protrusion and the plane. The same tips
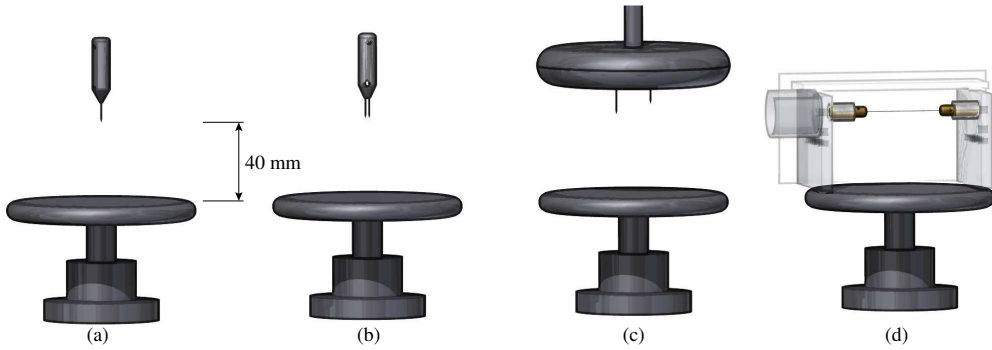
Figure 4.5: Schematic drawing of the four different anode geometries above the cathode plane. a) single tip; b) symmetrical double tips; c) asymmetrical double protrusion from a plane; d) wire. In the image of the wire geometry, all non-metal components are shown as semi-transparent. The drawing is to scale.

(a) 220 mbar	(b) 565 mbar	(c) 1000 mbar	(d) All pressures combined
average: $(46.0 \pm 10.8)°$	average: $(43.4 \pm 12.4)°$	average: $(39.7 \pm 13.2)°$	average: $(43.0 \pm 12.3)°$
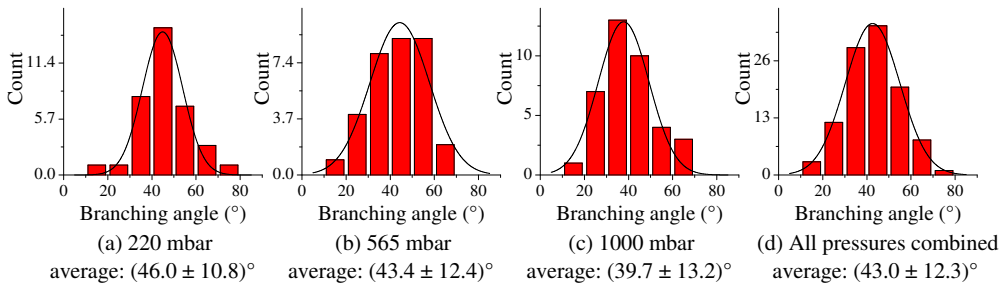
Figure 4.6: Histograms with Gaussian fits for branching angles for three different pressures and for all pressures combined.

have been used in all geometries, made of 1 mm diameter tungsten rods, with a conical pointed end. The wire in the wire geometry is a 0.2 mm diameter kanthal wire.

4.3 Streamer branching

As can be observed in most streamer images presented in this thesis: streamers do often branch and thereby form tree-like structures. We have investigated the branching angle of positive streamers in air by means of the stereoscopic techniques discussed in section 4.2.1. The 3D streamer morphology has been reconstructed by means of the simple reconstruction method. In these measurements, a positive voltage pulse of 47 kV with a risetime of about 30 ns was applied with the C-supply to the point, 14 cm above the plate. The atmosphere in the vacuum vessel consisted
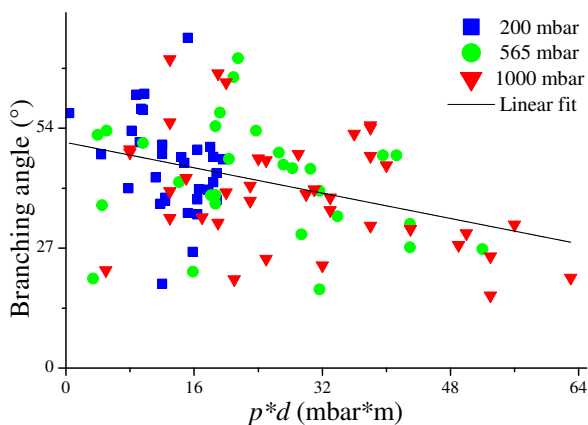
Figure 4.7: Measured branching angle as function of $p \cdot d$ where p is the pressure and d the vertical distance from the tip (the y-coordinate) at the point of branching.

of ambient air at different pressures (200, 565 and 1000 mbar).

Figures 4.6a-c show histograms of the measured branching angles for 200, 565 and 1000 mbar and figure 4.6d combines the results for all pressures into one histogram. As can be seen, the distribution is roughly Gaussian, with average values between 39° and 46° and standard deviations of 11° to 13°. The average branching angle shows a slight decrease as a function of pressure. However, it is not clear whether this is statistically significant due to the limited amount of data points (about 35 points per pressure).

The length scales of streamers are expected and observed to scale quite well with pressure. However, density fluctuations do not scale with density [34, 51]; if they play a significant role in streamer branching, one would expect the branching distribution to depend on pressure. Therefore, in figure 4.7 the branching angle is plotted as function of $p \cdot d$ where p is the pressure and d the vertical distance from the tip (the y-coordinate) at the point of branching. If the branching behaviour would differ for streamer sections close to the tip from sections close to the cathode plane, this would be visible in this plot. Also a pressure dependence would be visible. However, only a small dependence on $p \cdot d$ can be observed. This dependence is statistically not significant given the large spread and measurement error in the data set (correlation coefficient $R^2 = 0.15$).

The ratio of streamer length between branching events over streamer width has also been measured. This ratio is about 15 for all pressures. This is a bit higher than the ratio of 12 found by Briels *et al.* [34].

4.4 Reconnection

We define streamer reconnection as the case where one streamer channel connects with another streamer channel originating from the same electrode in a near perpendicular manner. In other words, it approaches the other streamer channel from the side and then connects with it.

Streamer reconnection is studied in the single tip geometry (a) and in the double protrusion geometry (c) (see figure 4.5). Apparent reconnections in the single tip geometry (a) were observed and discussed before by Briels *et al*. [31], based on normal (2D) photography. A stereo image of a single tip streamer discharge with apparent reconnection(s) is shown in figure 4.8. A partial 3D reconstruction of this discharge is shown in figure 4.9.

The original stereo image already shows that reconnection occurs in both the left and right hand views at the same vertical position. This indicates that there is indeed a thin streamer channel reconnecting to a thick streamer channel. This is confirmed in the 3D reconstruction. It was found that reconnections as the one shown are observed in about 50% of the images taken under the conditions of figure 4.8. Because some images are not very clear and in some cases reconnecting streamer channels are obscured by other streamer channels, we conclude that reconnections occur in the majority of discharge events under these conditions.

Streamer reconnections can also be observed in the double protrusion anode geometry (c). In this geometry, the thickest and earliest streamer channels originate from the tip that protrudes farthest from the plane. An example of such a discharge event is shown in figure 4.10. This image shows multiple reconnections from streamer channels originating from the right tip to streamer channels originating from the left tip. (We continue to use the term reconnection as these streamers originate from the same electrode assembly.) All these reconnections are clearly visible in both views and are therefore interpreted as real reconnections. The width (full width at half maximum, FWHM) of the thick, early channels is about 1.1 mm, the width of the thin channels about 0.6 mm. In figure 5 of [33], Briels *et al.* have reported similar values for the width of streamers created under these conditions.

Reconnections as shown in figures 4.8 and 4.10 are observed frequently under these experimental conditions. We find that reconnection only occurs to streamer channels that have crossed the entire gap and end on the cathode plate.

In figure 4.12, a sprite discharge is shown that remarkably resembles the streamer discharge shown in figure 4.10. Similar reconnection events are visible although it can not be proved that they are real because no stereo-photographic images are available. The similarities and differences between sprite and streamer reconnections will be discussed in more detail in section 4.6.

Briels *et al*. [34] have reported that thick streamer channels are always faster
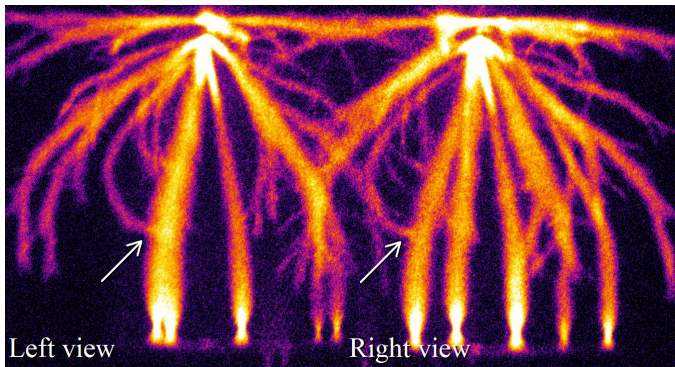
Figure 4.8: A stereo image of a streamer reconnection in single tip anode geometry (a). The two views of the single tip event overlap a bit in the middle of the figure. The most striking reconnection location is marked with an arrow in both views. Experimental settings: gas fill: 1000 mbar ambient air; $V_{max} = 52$ kV; $t_{V10\%} = 87$ ns; $t_{rise} = 24$ ns; $t_{start} = 52$ ns; $t_{gate} = 50$ ns (as defined in section 3.5). The voltage curve in this experiment is very similar to the one shown in figure 3.19. As can be seen from the timing parameters of this experiment, the complete image is shot before the voltage pulse reached its maximum.
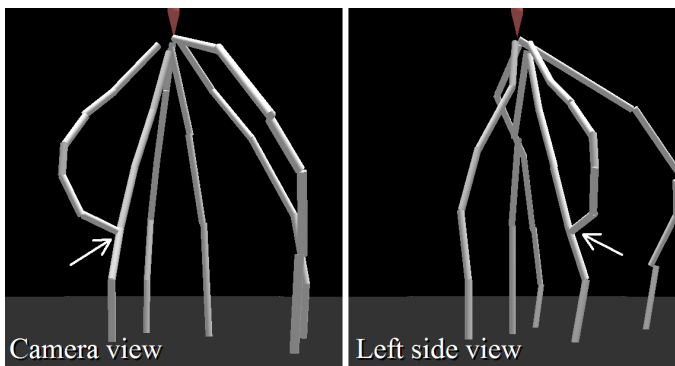
Figure 4.9: Orthogonal views of the 3D reconstruction of the reconnection event from figure 4.8. Again the reconnection location is marked with an arrow in both views. Not all streamer channels from the original images are represented in this reconstruction.

than thin streamer channels. In our experiments, tens to hundreds of nanoseconds after the thick channels have bridged the gap, thinner and slower streamers can connect to the conducting traces left behind by the early thick streamers. This has been confirmed by increasing the delay of the camera so that only the late streamers are visible. An example of such an image can be seen in figure 4.11. It shows that most of the length of the thick channels seen in figure 4.10 is no longer visible. Only
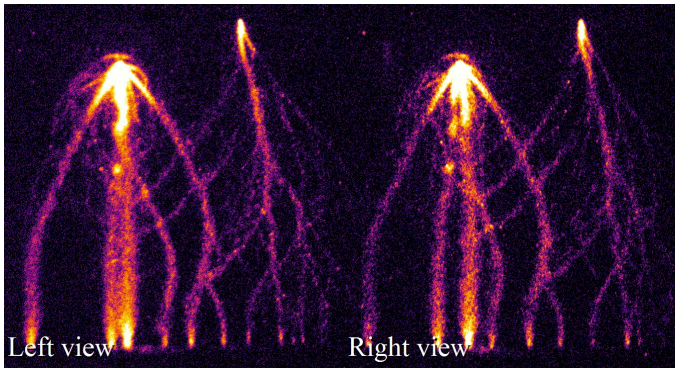
Figure 4.10: A stereo image of multiple streamer reconnections in the double protrusion-plane anode geometry (c). The horizontal distance between the two tips is 18 mm, the left tip protrudes 14 mm from the plane and the right tip protrudes 8 mm from the plane. Other experimental settings: gas fill: 1000 mbar ambient air; $V_{max} = 50\,\text{kV}$; $t_{V10\%} = 15\,\text{ns}$; $t_{rise} = 35\,\text{ns}$; $t_{start} = 10\,\text{ns}$; $t_{gate} = 100\,\text{ns}$.
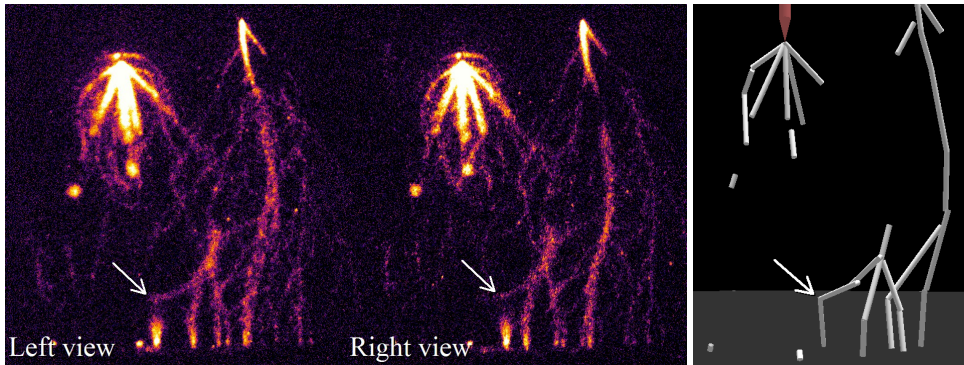
Figure 4.11: A stereo image and its 3D reconstruction of multiple streamer reconnections in the double protrusion-plane anode geometry (c). The experimental conditions are the same as in figure 4.10 except for the longer camera delay $t_{start} = 50\,\text{ns}$. Note that the streamer channel indicated with the arrow makes a nearly 90° turn.

the upper part (secondary streamers or glow discharge) and the cathode spots of these channels remain clearly visible. This can easily be understood from the fact that only the propagating head of a streamer channel emits a significant amount of radiation; therefore the channel behind the head is usually invisible or very dim after the head has passed, see figure 3.17.

A striking feature in figure 4.11 is the streamer channel indicated with the arrow. This streamer channel seems to change direction instantaneously by about 90°. These direction changes are observed in most images with longer delays under these experimental conditions. They appear very similar to the shape of
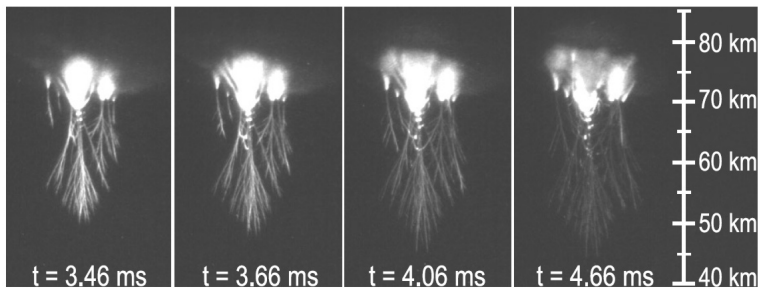
Figure 4.12: High speed sprite discharge images from 13 August 2005 at 03:12:32.0 UT showing apparent reconnection between different channels. These discharges occur above thunderclouds. The picture is reproduced from [44] (courtesy of Steve Cummer).
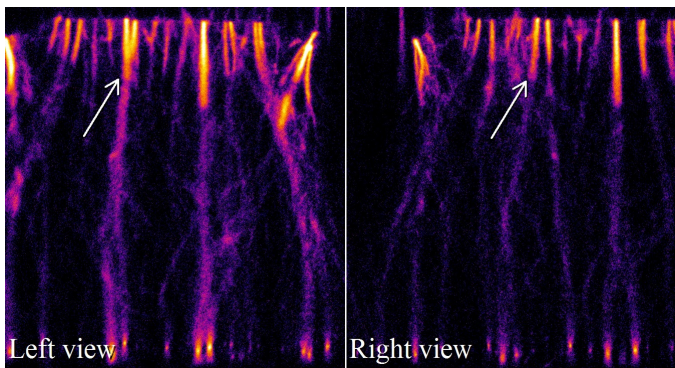
Figure 4.13: Stereo image of a wire-plate discharge. A possible merging location in the left hand view is indicated with an arrow. However, the right hand view clearly shows that in reality no merging occurs. Experimental settings: gas fill: 1000 mbar ambient air; $V_{max} = 45$ kV; $t_{V10\%} = 15$ ns; $t_{rise} = 22$ ns; $t_{start} = 0$ ns; $t_{gate} = 1000$ ns. The vertical white line indicates the rough position of the transition between the two views.

the streamers reconnecting as in figure 4.10. Therefore, these direction changes are interpreted as streamer reconnection consisting of the approaching streamer and the already existing channel. This confirms that reconnection is indeed the attraction of a late streamer channel towards an earlier streamer channel.

4.5   Merging

Streamer merging was first suggested as an interpretation of experiments in a wire-plate discharge. 2D pictures of Grabowski *et al.* [71] and Winands *et al.* [231]

show possible merging of streamer channels close to the wire. We have reproduced such experiments with the wire-plate electrode geometry as shown in figure 4.5d. During this investigation, we have never found a definite case of merging of streamer channels in the hundreds of discharge events studied. Often channels seem to merge in one of the images, but are clearly not merging in the other image. An example of such an event is shown in figure 4.13. Here, in the left image two streamer channels seem to merge. However, the right image clearly shows that this is not the case.

The left image also shows that two channels propagate downwards from the apparent merging location towards the cathode plate. This is already an indication that no real merging occurs. In rare cases (less than 1% of the images), the image quality around an apparent merging location was not good enough to definitely conclude that no merging occurred, but the propagation of multiple channels from these locations again indicates that no merging occurs. The same conclusion is drawn from measurements at 400 mbar ambient air.

The average separation between streamers initiating from the wire in figure 4.13 is just below 2 mm. This value is in agreement with streamer observations in a wire-plane geometry of Winands *et al.* [235] and Creyghton *et al.* [43].

The streamer channels are more parallel in the wire-plate discharge images than in the (double) tip-plate discharges images. This is because the electric field lines diverge around the needle electrode in the projection plane of the picture while they are parallel for the wire electrode. However, in the direction perpendicular to the image plane, the streamers do diverge significantly and show similar spatial distributions as in the point-plane discharges. This divergence has been observed before by Winands *et al.* ([233], figure D6).

A more controllable method to investigate streamer merging is to use two tips close to each other as shown in figure 4.5b. In this case streamer channels originate from both of these tips simultaneously (within 2 ns). These two streamer channels will now propagate in a more or less parallel direction towards the cathode plate and may merge or repel each other. Depending on pressure and other parameters, the two original streamer channels may also branch once or more. The chosen tip separation distance of 2 mm is similar to the average distance between streamers in the wire experiments at 1 bar.

Images of streamer discharges originating from double tips are compared to images of streamers originating from a single tip in figure 4.14; the pressure varies from 25 mbar to 1000 mbar between the columns; the rows show single and double tip experiments with long exposure times and double tip experiments with short exposure times. The figure shows that for the double tip discharges, always two initial streamer channels are formed. These two channels repel each other for all pressures, except for 25 mbar where they merge. The width of the streamer (FWHM) is 23 mm at 25 mbar. This is 11.5 times as large as the distance between
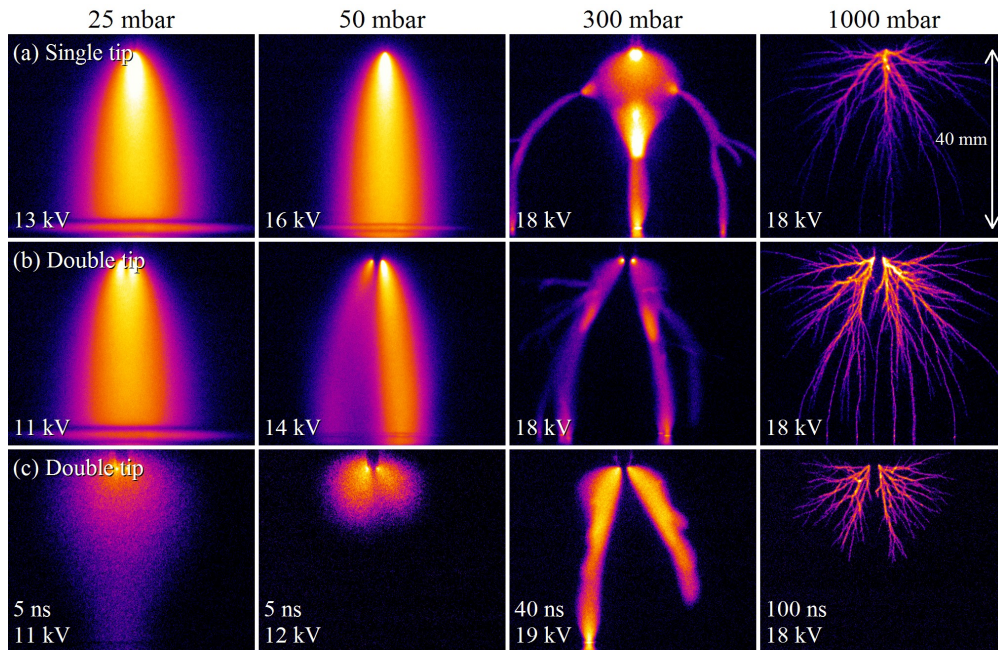
Figure 4.14: Images of streamer discharges with the single tip anode geometry (a) in the top row, and with the symmetrical double tip anode geometry (b) and (c) in the middle and bottom rows. Within the columns, the pressure varies from 25 mbar to 1000 mbar as indicated. The two upper rows show time integrated images ($t_{gate} > 1000$ ns), the bottom row shows images with shorter gate times as indicated in the panels. In all images V_{max} is indicated. The horizontal distance between the two tips is 2 mm. Voltage risetimes varied between 15 and 25 ns, the camera opens at $t_{start} \cong t_{V10\%}$. The camera gain varies significantly between the images; discharges are much brighter at lower pressures than at higher pressures.

the two tips. At 50 mbar, the width of the single tip streamer is still 18 mm, 9 times the tip distance, but the streamers do not merge.

In cases when one of the streamers initiates shortly before the other (by any reason, randomly or systematically), it can shield the second streamer from the background electric field. This causes the second streamer to be less powerful than the first streamer. This can be observed in the 50 mbar double tip images. Here, it is clear that one streamer channel dominates the discharge and the other channel moves away from the central vertical axis. Which tip or side is dominant changes randomly from discharge to discharge and in some cases both channels are equally bright and symmetrically shaped. Such behaviour with one dominant side is observed for pressures between 50 and 250 mbar.

The images of figure 4.14 are taken with peak voltages of about 12 kV for the

25 mbar images to 18 kV for the 300 mbar and 1000 mbar images[1]. Also for other voltages the same merging behaviour as function of pressure was observed. At 25 mbar, merging still occurs with 6 kV peak voltage, while at higher pressures no merging is observed at both lower and higher voltages than the ones shown in figure 4.14.

4.6   Discussion and conclusions

In conclusion, we have built a stereographic set-up that enables reconstruction of the 3D spatial structures of streamer discharges. This enables us to get more insight into what really happens in such a discharge. For example, we are now able to see if a streamer really does reconnect to another streamer. Up to now, such statements relied on multiple observations from 2D images [31]. We are also able to measure branching angles and distances of streamers.

The reconstruction methods described in this chapter all rely on manual processing of the data (assisted by software). However, for large amounts of images, such a manual process can be very time-consuming. In theory it should be possible to automate the 3D reconstruction process, but the often low image quality makes this a difficult task. Recently, Kocik *et al.* [89] have shown some of the first steps needed to automate such a reconstruction task. They demonstrate two methods to recognize streamer paths from a streamer image and thereby convert the bitmap image to 2D streamer path vectors. However, their methods are not yet able to fully reconstruct a 3D streamer tree and need further work.

We have found that the branching angle for streamers in an overvolted gap of 14 cm does not significantly depend on pressure and $p \cdot d$ and is distributed normally with an average of 43° and a standard deviation of 12°.

Furthermore, it can be concluded that reconnection of late streamer channels on earlier streamer channels occurs frequently in streamer discharges with many streamer channels. It is suggested [31] that the reconnection is caused by electrostatic attraction of a late streamer to a conducting channel left by an early streamer that already has reached the oppositely charged electrode and has changed polarity. The late streamer approaches the early channel almost perpendicularly — like an electrode plate or wire — which is another argument in favour of an electrostatic mechanism. In order to study reconnection of streamers theoretically, a complete three dimensional model would be required. Such streamer simulations, however, are only in the first stages of development [120, 121].

Besides electrostatic attraction, two other interaction mechanisms between

---

[1]It was attempted to use a fixed V_{max} of 18 kV for all images. However, for pressures below 100 mbar, V_{max} had to be decreased to prevent sparking in the top feedthrough of the set-up.

streamers can be imagined as the reason for reconnection: magnetic attraction and photo-ionization. However, magnetic attraction between current channels only occurs when these channels are more or less parallel and would not lead to the near perpendicular reconnections that are observed. Besides, the currents in these streamer channels are low and would not lead to any significant Lorentz force. Photo-ionization can also be excluded because it decays exponentially like $e^{-r/\ell}$ for distances r larger than the photo-ionization length $\ell = 1.6\,\mathrm{mm}$ (at atmospheric pressure in air according to [167, 244]), while electrostatic attraction decays as $\frac{1}{r^2}$. Therefore photo-ionization is much weaker at distances exceeding ℓ, and can not turn the streamer path over large distances as in figures 4.8–4.11.

The reconnections in sprites [44] show a very similar signature, as a comparison of figures 4.12 and 4.10 shows: the head of a late sprite streamer is attracted to an earlier formed channel. However, no stereoscopic imaging is available in this case to decide whether the effect is real.

The similarity of sprites and streamers by now is well established, see [34, 165, 200]. However, there is another important difference, namely the early attracting sprite channel is not connected to some electrode to explain its polarity change. A possible mechanism is charge separation along the sprite streamer channel as was recently suggested by Luque and Ebert [124] and Liu [113].

Merging of more or less parallel, simultaneously propagating streamer channels was only observed at low pressures (25 mbar), but not at higher pressures under the conditions of these experiments (overvolted 40 mm gaps, ambient air, 2 mm or more tip separation). Only when the streamer diameter (FWHM) is at least 10 times larger than the tip separation, we observe merging. And even in this case, it can be debated if this is really merging, or that only one streamer initiates from a complex electrode tip. All observations show that thinner streamer heads always do repel each other and will remain separate while propagating between anode and cathode.

A mechanism for streamer merging was recently proposed by Luque *et al.* [121] (see figure 4.15); as photo-ionization in air is a non-local ionization reaction acting over a reduced length scale of about 1.6 mm bar at normal temperature, the ionization cloud around the streamer heads decays smoothly over this length scale. (The unit mm bar is used because the length scales of streamers are expected and observed to scale quite well with pressure [34, 51].) When the streamer heads get so close that their photo-ionization zones overlap, impact ionization can further enhance the ionization in the area between the heads and the streamer heads can merge. Again, magnetic attraction of parallel current carrying channels is very weak because of the low currents and can therefore be excluded.

We can compare the experimental results with the simulations of Luque *et*
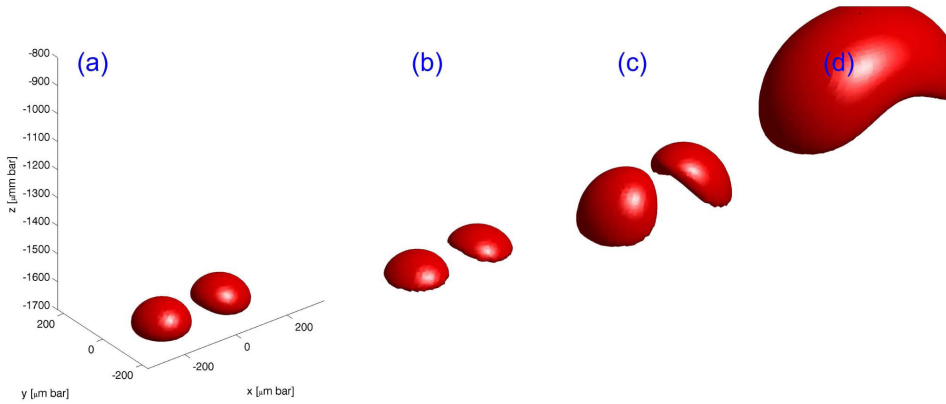
Figure 4.15: Simulation by Luque *et al.* of time evolution of the heads of two negative streamers in air at 1 bar. Time advances from left to right in equal steps. Represented is the surface where the negative charge density reaches its half maximum. The repulsion between the electrons in the space-charge layer drives the streamers heads apart. However, the ionization in the space between the two streamers due to radiation out of the high-field region in the heads makes them merge and create a single streamer. Image from [121].

al. [120] on streamer merging due to photo-ionization. In these calculations, the pressure p was varied while the reduced seed distance was fixed to $p \cdot d = 230\,\mu\mathrm{m} \cdot \mathrm{bar}$ at room temperature, here d is the seed separation. Up to $p = 1$ bar, the streamers in air always merged in these simulations. In the double tip measurements presented here, the real tip distance was fixed, therefore the reduced tip distance ranges from $50\,\mu\mathrm{m} \cdot \mathrm{bar}$ to $2\,\mathrm{mm} \cdot \mathrm{bar}$. At 115 mbar, the 2 mm tip separation gives a reduced tip separation of $230\,\mu\mathrm{m} \cdot \mathrm{bar}$, but the streamers repel each other; they merge only below $p \cdot d = 100\,\mu\mathrm{m} \cdot \mathrm{bar}$. However, the streamers in the theoretical work emerge from an avalanche in a homogeneous electric field, while the streamers in the present experiments emerge from two needle electrodes. Therefore a discrepancy by a factor of 2 or more is not unreasonable, and we conclude that experiments and theory need to be developed further before they can be compared quantitatively. Furthermore, the theoretical prediction relies on the photo-ionization lengths that were measured by Penney and Hummert in 1970 [167] and whose accuracy is widely doubted [119, 152, 156]; but no other data are available.

Streamers in experiments are never initiated exactly simultaneously. We observe that inception of the different streamer channels occurs within 2 ns but we can not be certain that there is no jitter on smaller timescales. In the double tip experiments we can be certain that there is not one favourite tip because the dominant (largest) streamer changes from left to right and back randomly between discharge events. We can however, not be certain that there is no stochastic jitter in the inception

times. This can lead to two streamers with a small mutual delay that also could prevent merging. If this is the case, it will probably be always present in real world experiments. Numerical simulations can answer if a time delay of e.g. 1 ns between two streamers will prevent merging. Such a time delay between inception can also be responsible for the appearance of a dominant and a weaker streamer channel; the streamer that is initiated first shields the second streamer from the background electric field.

In wire-plate discharges, apparent streamer merging is occasionally observed on 2D-images. However, in these discharges we have never observed merging with any degree of certainty with stereo-photography.

Chapter 5

Effects of photo-ionization

5.1 Introduction

Streamers are the first stage of electric breakdown, when a high voltage is applied to large gas volumes [51, 172, 220]. The discharge can later develop into a spark or lightning, but it also can stay completely in the streamer phase if the voltage, current or pulse duration is limited. An example of a discharge that remains essentially in the streamer phase is a sprite discharge, a huge discharge at 40 to 90 km altitude above thunderclouds [52, 165]. In a wide field of technical applications, the voltage pulse is intentionally kept short to suppress inefficient gas heating during later stages of the discharge [81, 241], and the complete technology builds on streamers. Streamers enhance the electric field at their tip to values above the breakdown value and create a region of active local ionization dynamics; in nanosecond resolved intensified CCD-photographs, these active areas can be seen as bright spots [23, 42, 157]. For further reading on streamers and sprites, we refer to cluster issues in J. Phys. D [2] and in J. Geophys. Res. [3] as well as to the many original papers cited there.

While negative streamers naturally propagate through electron drift (possibly supported by additional mechanisms), positive streamers are typically easier to generate, but more difficult to explain [122], as they propagate against the electron drift direction with velocities comparable to the drift velocity. While Townsend [216] in 1915 still assumed symmetry between positive and negative charge carriers, it soon became clear that positive ions are not suitable for impact ionization and are too slow. The commonly accepted explanation for the propagation of positive streamers in air is photo-ionization; this was suggested in 1935 by

Flegler and Raether in Munich [56], by Bradley and Snoddy in Virginia [28] and by Cravath in California [41]: the active ionization region emits UV radiation that at some distance (in particular, ahead of the front) can generate additional electron-ion-pairs. The theoretical understanding of photo-ionization in nitrogen/oxygen mixtures was developed further by Teich [211, 212]: the energetic electrons in the high field region of the streamer excite certain levels of molecular nitrogen with energies above the ionization energy of oxygen. These levels de-excite by emission of a photon which can non-locally ionize molecular oxygen. Teich also identified quenching at higher air pressure as a mechanism suppressing photo-ionization.

There is hardly any experimental work published on measuring photo-ionization directly in the past 40 years. Cravath [41, 117] already in 1935 suggested two ionization lengths of 1 and of 5 mm in air at standard temperature and pressure, and Raether [170] measured 5 mm in 1938 where he also investigated hydrogen and oxygen. After the second world war, Przybylski and Teich continued this work in Raether's lab in Hamburg and published their results in German in 1958 and 1967 [169, 211, 212]. Penney and Hummert [167] in Pennsylvania investigated the process again and found in 1970 full agreement with the earlier measurements of Przybylski and Teich, and with those of Sroka in "pure" oxygen, "pure" nitrogen and air. The results show that photo-ionization in air is about 1 or 2 orders of magnitude more effective than in pure oxygen or pure nitrogen, but significant photo-ionization in both pure gasses is still present. However, the only information about the purity of the gasses is that "commercial-grade" gasses have been used. This probably refers to impurities in the order of 0.1% to 1%. They do not discuss which mechanisms could be responsible for the photo-ionization in any of the gasses, in contrast to Teich. In recent years Aints *et al.* [6] have used the same method as Penney and Hummert to investigate the effects of water content in air on photo-ionization. Their results are similar to the results of Penney and Hummert, with small corrections for the effects of water content.

The data of Przybylski, Teich, Penney and Hummert and the theoretical understanding of Teich were merged by Zhelezniak *et al.* [244] into a model of photo-ionization that nowadays is used in most streamer simulations [26, 96, 119, 121, 139, 141].

On the other hand, the reliability of the photo-ionization data and of the resulting Zhelezniak model has been questioned; for a recent discussion, we refer to the introduction of Nudnova and Starikovskii [152]. Background ionization has been suggested as an alternative for photo-ionization; in early simulations, photo-ionization was even replaced by background ionization to reduce the computational complexity [48]. The background ionization could either be due to radioactivity and cosmic radiation, or to left over charges at high repetition rates of the discharge as elaborated by Pancheshnyi [156]. In the present experiments, high repetition rates are avoided, we use a 1 Hz repetition frequency for all experiments.

Experiments with other repetition frequencies will be discussed in the next chapter.

As photo-ionization is a vital part of streamer theory, and as direct measurements are difficult, Luque *et al.* [121] have suggested indirect measurements through studying the interaction of two streamer heads propagating next to each other: they typically would repel each other electrostatically, but could merge through the non-local effect of photo-ionization. In an attempt to confirm this theory, we have performed experiments with two streamers emitted from adjacent needles as was discussed in the previous chapter, but a common parameter regime has not yet been explored for theory and experiment, and the photo-ionization could not yet be investigated along these lines. Kashiwagi and Itoh have shown that UV and VUV radiation from a surface streamer discharge can trigger a synchronous streamer discharge [87]. They have found that radiation around 115 nm is most effective, which is somewhat higher than the limit of 102.5 nm that is associated with nitrogen-oxygen photo-ionization. However, in the case of surface discharges, photo-electron emission from the insulator surface itself can replace photo-ionization of oxygen molecules in bulk streamer discharges. The photo-electron emission from the surface can occur at longer wavelengths than the bulk photo-ionization of oxygen molecules.

Here we follow a different experimental track. According to Teich's photo-ionization mechanism in nitrogen-oxygen mixtures, the density of emitted photons is proportional to the nitrogen concentration, and the absorption lengths of the photons are inversely proportional to the oxygen concentration. If positive streamers in air indeed propagate through this mechanism, one would expect that their properties change when the ratio of nitrogen and oxygen is changed. The main purpose of this chapter is therefore to investigate positive streamers in varying nitrogen:oxygen mixtures experimentally. To set the limits, we also investigate streamers in pure nitrogen.

5.1.1 Previous experiments on streamers in different nitrogen-oxygen-mixtures and pure gasses

Streamers in varying nitrogen-oxygen-mixtures have been investigated before by Yi and Williams [243], Ono and Oda [153], and Briels *et al.* [35, 34].

Yi and Williams use a 130 mm plane-plane with a protruding point geometry, where the protruding point is a 3.2 mm diameter rod ground to a sharp tip (radius ~100 μm). They use both positive and negative voltage pulses with amplitudes between 70 and 130 kV and risetimes of order 50 ns. Nitrogen-oxygen mixtures with oxygen fractions between "0%" and 15% are investigated. The purity of their pure nitrogen is not specified but it is presumably significantly better than 0.1%, as this is the oxygen content of their next purest gas mixture. They claim that their measurements strongly suggest that photo-ionization plays an important

role because (especially positive) streamers propagate faster at higher oxygen concentrations. For high voltages (>100 kV), the propagation velocity of positive streamers increases with roughly a factor of 5 when going from their pure nitrogen to 10% oxygen in nitrogen. In negative streamers the same concentration change leads to a velocity increase of less than 40%.

Ono and Oda also use a point-plane geometry, but with a 13 mm gap. Their tips are made by cutting a 0.3 mm stainless steel wire and have no well defined tip profile. They apply positive voltage pulses with amplitudes between 13 and 37 kV, risetimes in the order of tens of nanoseconds and durations of a few hundred nanoseconds on nitrogen-oxygen mixtures containing oxygen fractions between "0%" and 20%. Again, the purity of nitrogen used in the experiments is not specified. Their next purest mixture contains 0.2% oxygen. They claim that propagation velocity, diameter and shape of the streamers are strongly influenced by the oxygen concentration. No measured value varied by more than a factor of five when changing the oxygen concentration from 20% to 0%. The streamer diameter increases from 0.2-0.4 mm in pure nitrogen to more than 1 mm in air. At 18 kV, the propagation velocity increases from $\sim 2 \cdot 10^5$ m/s in pure nitrogen to $5 \cdot 10^5$ m/s in air. Namihira *et al.* [143] have studied streamer propagation in atmospheric air in a 76 and 152 mm diameter wire-cylinder geometry with 60–100 kV, 100 ns voltage pulses of positive polarity. They find propagation velocities of $1.8–3.3 \cdot 10^6$ m/s

Briels *et al.* have measured in air, a mixture with 0.2% oxygen in nitrogen and "pure nitrogen". They use 5 to 30 kV positive pulses with risetimes of order 150 ns in point-plane gaps of 40 and 160 mm at pressures between 100 mbar and 1 bar. They have shown that at lower oxygen concentrations, streamers branch and zigzag more, they are brighter and thinner (about 40% thinner in pure nitrogen than in air). They have not found a clear effect of oxygen concentration on propagation velocity; at 1 bar they are lowest in pure nitrogen, while at lower pressures they are the same or highest in pure nitrogen. However, the set-up that was used in these experiments is not designed for high purity gas handling. Therefore, it is not known what the exact purity of the pure nitrogen was in all of the experiments described by Briels *et al.*

In order to better investigate the effects of low oxygen concentrations, here we present results in which the purity of the gasses can be guaranteed to ppm (parts per million) levels.

5.1.2   Content of the chapter

In this chapter we present experimental measurements on streamer discharges in different gas mixtures, with an emphasis on nitrogen/oxygen mixtures. We will repeat some measurements made by Briels *et al.* [34], but with a better defined purity of the gasses and better optics to measure streamer diameters. We also

Table 5.1: Gas impurity levels of relevant pure gasses as provided by the gas supplier. Impurity levels are given as upper limits in parts per million (ppm), n/a indicates that no number is specified by the supplier. Nitrogen-oxygen mixtures like artificial air are mixed by the supplier from nitrogen 6.0 and oxygen 6.0.

Gas	N_2	O_2	Ar	H_2O	CO_2	CO	C_nH_m
Nitrogen 6.0	≈100%	0.2	n/a	0.5	0.1	0.1	0.1
Nitrogen 7.0	≈100%	0.03	n/a	0.05	0.03	0.03	30
Oxygen 6.0	0.5	≈100%	1	0.5	n/a	0.1	0.1
Argon 5.0	5	2	≈100%	3	n/a	n/a	0.2

extend the measured range to nitrogen of 0.1 ppm purity and show some results from argon of 10 ppm purity. More detailed measurements on pure argon and pure oxygen are presented in chapter 7. We discuss implications for the propagation mechanism. We measure at various pressures to test streamer similarity laws.

5.2 Experimental conditions

We use mixtures of O_2 and N_2 that are pre-mixed by the supplier. According to the specifications, the amount of contamination is below 1 ppm, except for nitrogen 7.0[1], which has a specified contamination of less than 0.1 ppm. The mixtures we have used contain nitrogen with 20%, 0.2%, 0.01% and <0.0001% oxygen (volumetric fractions). We refer to the 20% oxygen mixture as artificial air. Besides these mixtures, we have also used pure argon with not more then 10 ppm impurity (5.0 purity). See table 5.1 for information regarding impurities in the different pure gasses. The nitrogen-oxygen gas mixtures consist of nitrogen 6.0 with the specified percentage of oxygen 6.0 added by the supplier.

All experiments presented in this chapter have been performed on positive streamers in our new vacuum vessel (see section 3.2.3) with a 160 mm separation point plane geometry. Both the C-supply and the Blumlein pulser have been used.

In discharges in nitrogen-oxygen mixtures, only the streamer's head produces light. Therefore an image taken with a long exposure shows the trace left by the streamer head as it passes. With a shorter exposure just a section of the streamer's path is seen (see e.g. figure 5.9). At lower pressures, or higher voltages, the streamers can develop into glow after reaching the plate electrode, resulting in a more or less uniform light that is emitted from the entire channel. This is seen in the right column of figure 5.1. The glow phase lasts longer than the streamer phase, and emits significantly more light.

---

[1]Purity of gasses and gas mixtures is denoted as the number of nines in the notation of purity. So nitrogen 3.0 has a purity of at least 99.9% and nitrogen 6.0 a purity of at least 99.9999% (i.e. less than 1 ppm contamination).

5.3   Effects of oxygen concentration in nitrogen

5.3.1   Streamer morphology

We investigate the general morphology of the streamers by means of ICCD camera images. Previous time resolved photography in a similar set-up has established the following sequence of discharge evolution: first a glowing ball or initiation cloud appears at the needle electrode, the ball extends and transits into an expanding glowing shell that eventually becomes unstable and breaks up into many simultaneously propagating streamers (see [34, 36] as well as section 2.3.3 of this thesis). The sizes of the initiation cloud and glowing shell scale inversely with pressure. At high pressures (1000 mbar in our case), they are so small that they can not be distinguished in our images. At low pressures, or when the size of the gap is very small, the initiation cloud and glowing shell may extend over more than half of the gap. Pressure, gas mixture, gap length, voltage and voltage risetime determine whether a single, few or many streamers emerge from the glowing shell.

Results from the C-supply

Figure 5.1 shows an overview of streamers in five different gas mixtures made with the C-supply. More images at other voltages can be found in figure B.1 on page 190. The general morphology of the N_2:O_2 mixtures and pure nitrogen (both 6.0 and 7.0 purity) is very similar, although it is clear that, especially at low pressures, there are more branches in pure nitrogen and in the 0.01% O_2 mixture than in the other two mixtures. This has also been observed by Ono and Oda [153]. Their streamer channels become marginally straighter for higher concentrations of oxygen.

One striking feature in the N_2:O_2 mixtures and pure nitrogen is the maximal length of the streamers at 1000 mbar; the streamers are longest for the 0.2% O_2 mixture and shorter for nitrogen 7.0. However, the interpretation is not straightforward. In these images the exposure time of our camera was about 2 μs, and the decay time ($1/e$) of the voltage pulse was about 6 μs. On the other hand, Briels *et al.* [34] in their "pure nitrogen" have found much longer streamers under similar conditions that propagated for more than 4 μs after the start of the pulse. In those measurements the decay time of the voltage pulse was probably much longer than 6 μs because they used a higher parallel impedance in the C-supply circuit (the exact value is unclear). The lengths of our streamers in pure nitrogen therefore are determined either by the exposure time of the camera or by the decay time of the voltage pulse. In air, streamers stay short both in Briels' and in the present measurements. This is probably due to the conductivity loss inside the streamer channel due to the attachment of electrons to oxygen molecules. In air, this loss mechanism is much stronger than in pure nitrogen with a small amount of oxygen
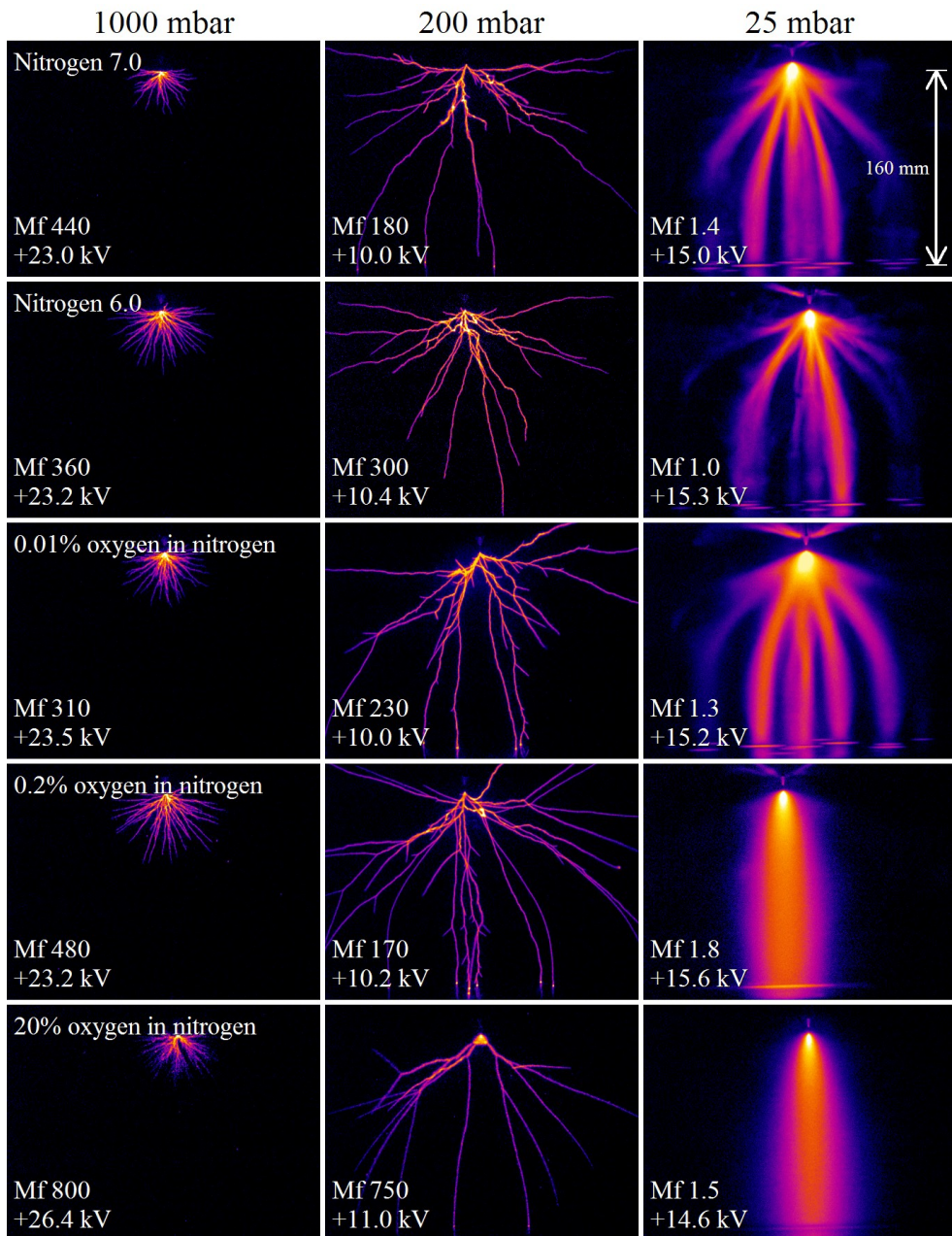
Figure 5.1: Overview of streamer discharges produced with the C-supply for five gas mixtures used (rows), at pressures of 1000, 200 and 25 mbar (columns). All measurements have a long exposure time and therefore show one complete discharge event, including transition to glow for 25 mbar. The multiplication factor (*Mf*) gives an indication of the real intensity of the discharge. The length scale is indicated with the white arrow at the top right image. Additional images with other voltages are given in figure B.1.
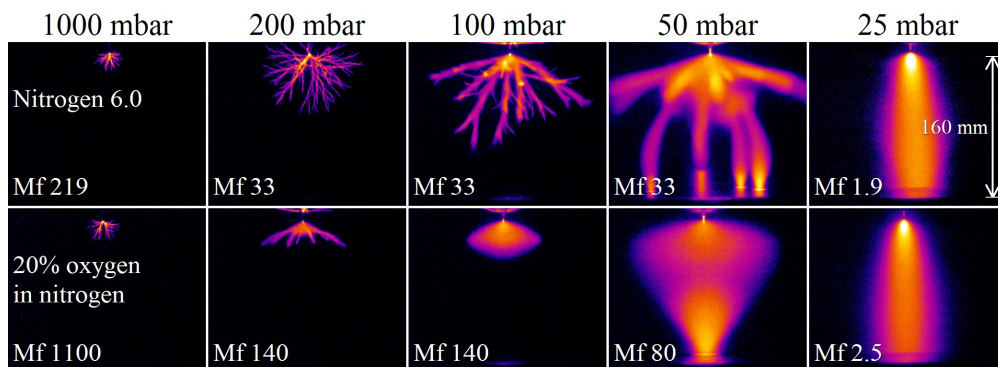
Figure 5.2: Overview of streamer discharges produced with a 20 kV pulse by the Blumlein pulser (~130 ns pulse length) for nitrogen 6.0 (top row) and artificial air (bottom row), at five different pressures. All measurements have a long exposure time and therefore show the whole discharge.

contamination.

One should be careful when comparing exact *Mf* values of our measurements. We have not conducted a statistical study into the brightness of the streamer channels. Also note that the *Mf* values reported here are somewhat different than those published in [150]. The reason for this, as well as its consequences are discussed in more detail in section 3.4.2 on page 55. More results from measurements with the C-supply can be found in the traineeship report by Ferdi van de Wetering [227]. *Mf* values discussed in that report are all calculated with the old method.

Results from the Blumlein pulser

The differences between artificial air and pure nitrogen can be studied better with the Blumlein pulser than with the C-supply. We recall that the Blumlein pulser has a faster risetime and a shorter pulse duration than the C-supply (see section 3.3). This allows us to use the same voltage at all pressures without danger of provoking a spark. Hence in figure 5.2, the background electric fields E are the same up to modifications due to the presence of the discharge while the reduced fields E/N increase with decreasing density N. The figure shows that at 25 mbar and 1000 mbar the images for nitrogen 6.0 and artificial air are quite similar, but all intermediate pressures show clear differences between the two gasses. Again, artificial air has fewer and thicker streamers, as well as a much larger "initiation cloud". Because of the limited duration of the pulse, no streamers emerge from this cloud in artificial air at 100 mbar. This limited duration is also the reason for the short streamer lengths at pressures above 50 mbar for both gasses. We have used a voltage of 20 kV in all measurements in figure 5.2; this voltage is higher

than in figure 5.1 for all pressures below 1000 mbar.

These differences in appearance between air and nitrogen 6.0 with the Blumlein pulser are also more pronounced than found by Briels *et al.* [34]. This can again be attributed to the effect of a higher voltage and faster risetime in our case, but also to the higher purity that can be achieved in the new set-up (see section 3.2). It seems that the thinnest or minimal streamers are similar in the different mixtures, but that air produces thicker streamers more easily.

The larger "initiation cloud" in artificial air can also be observed in the 200 mbar images from figure 5.1, when comparing this with the lower-oxygen concentration mixtures.

In figure 5.2, in nitrogen 6.0 at 25 mbar there is only one channel instead of multiple channels like in figure 5.1. This is caused by the higher voltage (20 kV versus 15.3 kV) and faster risetime ($\sim$10 ns versus $\sim$50 ns) from the Blumlein pulser compared to the C-supply. Such a high voltage could lead to a spark when using the C-supply.

The shapes of all discharges at pressures of 50 mbar and lower correspond to the shapes found by Rep'ev and Repin [176] in discharges in a 100 mm point plane gap in air at atmospheric pressure with 220 kV pulses. This should be no surprise as their reduced background field (E/N) is quite similar to ours. They use a bullet-shaped electrode with a tip radius of 0.2 mm.

Initiation delay and jitter

We have not observed any effects of the gas mixture on initiation delay or jitter as reported by Yi and Williams [243]. In all cases, the streamer initiation jitter was limited to less than 10 ns. This can probably be attributed to our electrode holder geometry, which induces more field enhancement at the tip, our fast voltage risetimes and our overvolted gaps. The protrusion-plane electrode of Yi and Williams has a tip radius of about 100 μm and protrudes only 10 mm from a plane. Our tip has a radius of about 15 μm and is mounted in an elongated holder (see figure 3.4). Van Veldhuizen and Rutgers [222] have shown that such a difference in geometry of the holder and tip can have a large influence on streamer initiation and propagation. Therefore, initiation was always fast in our case and we did not observe differences between the gas mixtures.

5.3.2   Minimal streamer diameter

Briels *et al.* have also shown that the reduced streamer diameter $n_0 \cdot d_{min}$ is constant as function of n_0 for a specific gas mixture [34] (see also figure 2.4). The choice for these thinnest channels has been made because, from experimental data as well
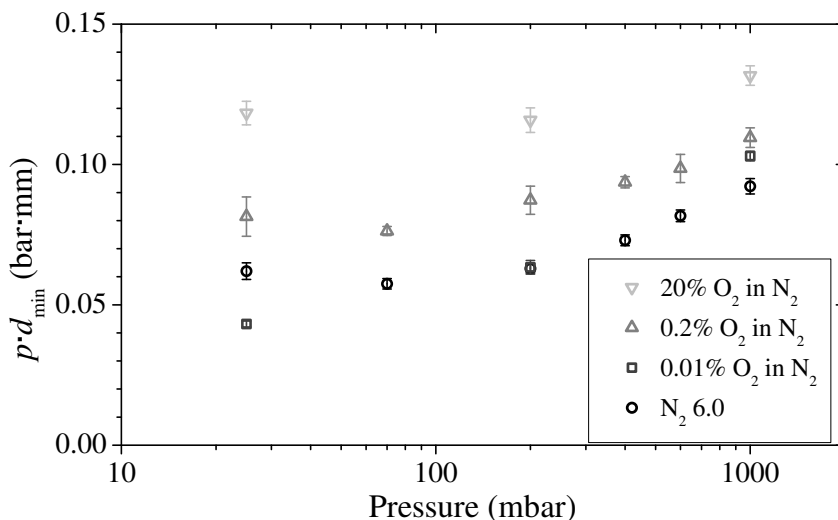
Figure 5.3: Scaling of the reduced diameter ($p \cdot d_{min}$) with pressure (p) for the four different nitrogen oxygen mixtures. Every point represents 4 to 10 measured streamer channels each from a separate discharge image. The error bars give the standard error and do not include systematic errors.

as from theoretical considerations, it has been found that there is a lower limit in streamer diameter, but no upper limit of the streamer diameter with growing voltage has been found yet. In our experiments, the gas temperature is always equal to room temperature (294 K) and therefore we can use the pressure p instead of the density n_0, as they are related through the ideal gas law.

The minimal streamer diameters have been measured on images where the streamer diameter (full width at half maximum of an averaged cross-section) is at least 10 pixels wide. We took zoomed images like the 200 mbar images from figure 5.5 for this purpose, by moving the camera closer to the discharge, and even higher magnifications at higher pressures. Measurements of the minimal streamer diameter are given in figure 5.3. All results have been obtained with the C-supply. Some observations follow:

- The reduced diameter is roughly constant as function of pressure for any single gas mixture, but it does increase slightly at higher pressures.

- The reduced diameter increases as a function of oxygen concentration although there is no significant difference between nitrogen 6.0 and nitrogen with 0.01% oxygen.

The increase of reduced diameter as function of pressure could be a measurement artefact: it is possible that the width of the streamers at high pressures is still

overestimated because of bad focusing (shallow depth of field) and other imaging artefacts [31].

Ono and Oda [153] also find an increase of diameter although they report an increase of a factor 12 between pure nitrogen and a mixture with addition of 20% oxygen. This large factor can be attributed to the fact that Ono and Oda do not specifically look for minimal streamers. They use a pulse of at least 15 kV in gas at atmospheric pressure in a 13 mm point-plane gap. This is an overvolted gap, which generates streamers that are thicker than the minimal streamers we look at. We see as well that air streamers can be thicker than pure nitrogen streamers, but our minimal streamers are much more similar for all mixtures.

When we compare the values from figure 5.3 with the results of Briels *et al.* [34], we see that they are lower in all cases. Briels *et al.* give an average value of $p \cdot d_{min}$ of 0.12 bar·mm for "pure" nitrogen and 0.20 bar·mm for air. We have found 0.07 bar·mm and 0.12 bar·mm respectively. There are several reasons for the differences:

- Influences of other gas components like water vapour and carbon dioxide that are more prevalent in the set-up of Briels than in the new high purity set-up.

- Small differences in voltage pulse risetime and amplitude that could lead to larger than minimal streamers in the case of Briels.

- Overestimation of streamer widths by Briels because of the optical problems explained above.

Note that the pure nitrogen in the work of Briels *et al.* was probably less pure than in the present work. The new set-up is much better suited for work on high purity gasses than the old one used by Briels *et al.* It is estimated that the "pure" nitrogen of Briels *et al.* has a contamination level of less than 0.1%, while here we achieve less than 0.0001%.

5.3.3 Velocity measurements

Streamer velocities have been determined in discharges in all nitrogen-oxygen mixtures. The length of a streamer is determined with the first method discussed in section 3.4.3 and demonstrated in figure 3.17. All results have been obtained with the C-supply. The results of the measurements at 200 mbar are given in figure 5.4.

The reason why we do not present measurements at 1000 mbar is that we were not able to use voltages above 45 kV and therefore, the length of the streamers remained short at 1000 mbar, as is shown in figure 5.1. This short length means that we can not measure the streamer velocity at roughly the middle of the gap.
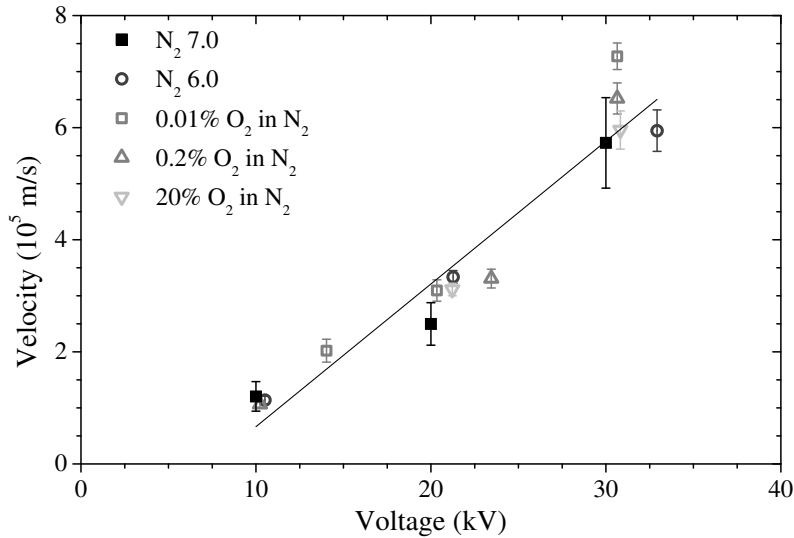
Figure 5.4: Velocity measurement results at 200 mbar for five different gasses, made with the C-supply. The error bars indicate the sample standard deviation. The line is a linear fit through all the points. The velocities are measured roughly in the middle of the gap, except for the cases where the discharge does not reach the middle of the gap (at lower voltages), in these cases, the velocity is determined at a position close to the end of the streamer channels.

We also do not show measurements at 25 mbar. At this pressure, the streamers are so wide, that no fully evolved streamer channel can occur before the cathode plate is reached (see e.g. figure 5.8).

The most striking feature of these measurements is the fact that all five gasses show very similar velocities. This is also observed at other pressures. The measured velocities have a minimum value of $0.5 - 1 \cdot 10^5$ m/s. Although the measurements at 1000 mbar and 25 mbar do not give a complete set of results, like for 200 mbar, we can state that at these pressures the same minimum velocity is found. We did not observe the increase in propagation velocity with increasing oxygen fraction that is reported by Yi and Williams [243]. The increase of velocity with voltage is in accordance with the results found by Briels [33], although she published results measured at 1000 mbar in a 40 mm gap, while we now focus on 200 mbar in a 160 mm gap.
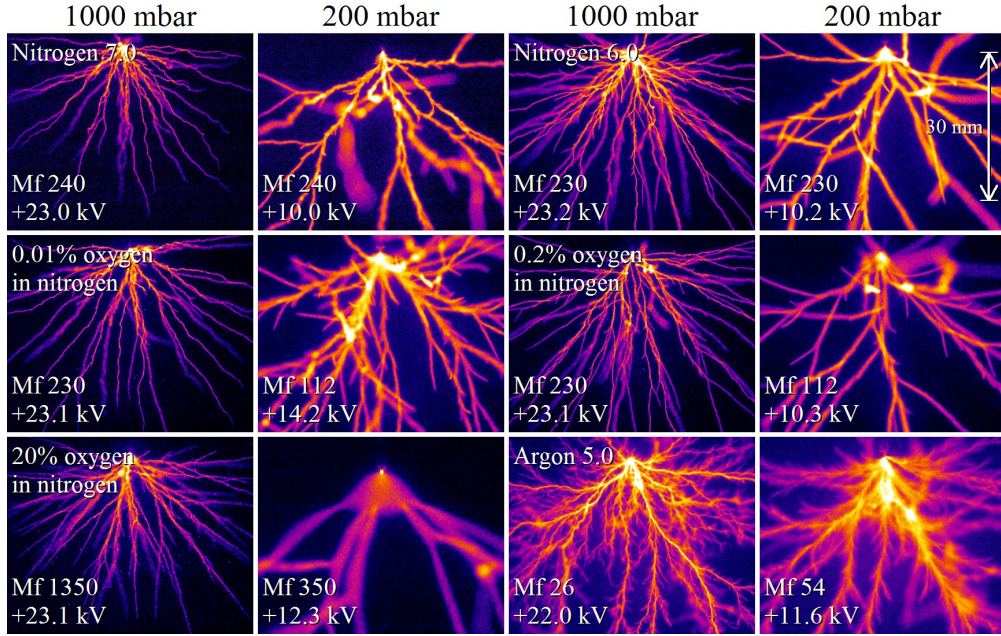
Figure 5.5: Zoomed images produced with the C-supply for six different gasses, at 1000 and 200 mbar around the anode tip region (see length indication at top right image). All other settings are similar to figure 5.1. Note that the image for 0.01% oxygen at 200 mbar has a deviating voltage.
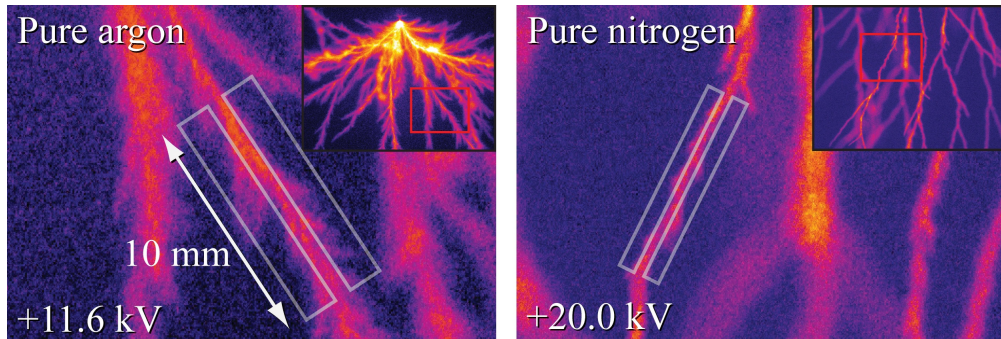
Figure 5.6: Feather like structures in an argon 5.0 and a nitrogen 6.0 discharge. Both images are acquired with the C-supply at 200 mbar. The images as captured by the camera are shown in the boxes in the top right corners with the zoomed areas indicated. The grey rectangles in the zoomed images indicate the area in which the number of small branches was counted. The nitrogen image is on the same scale as the argon image, but lower in the 160 mm gap (roughly halfway).

5.4 Feather-like structures

Figure 5.5 shows images from similar discharges as figure 5.1 but now zoomed to the region closest to the anode tip and with two images from argon 5.0 included. The zooming is achieved by moving the camera closer to the experiment.

We observe again that for lower oxygen concentrations, the streamers branch more often. In nitrogen 6.0 and 7.0 at 200 mbar they form shapes resembling feathers. In argon, these feather-like structures are even more pronounced, especially at 200 mbar. The fact that there are no straight, smooth streamer channels in the argon discharges makes it impossible to determine unambiguous streamer widths in this gas.

We have analysed one channel from an argon image at 200 mbar (figure 5.6). We counted the number of side channels from a 10 mm long section of this channel in a region between 0.5 and 2 mm from the centre of the channel on both sides. Dividing this number by the volume of the counting region (we assume cylindrical symmetry of the streamer channel) leads to a branch density of about 10^2 cm^{-3}.

When we apply the same procedure to the image of a nitrogen discharge from figure 5.6, we find roughly the same branch density. Although the number of small side channels is lower than in the argon image, so is their length. Therefore the counting region reaches to only about 1 mm around the centre of the channel.

In nitrogen 6.0, we have determined that the visible hairs of the feathers have a length of 0.5–1.5 mm. The angle between these hairs and the propagation direction of the streamer is 20 to 50 degrees. This value is determined from a 2D projection of the real hairs, therefore the real angles may be larger than 20 degrees. It can not be distinguished whether the hairs bend away from the streamer channel, bend towards it or are straight. The maximum distance between the tip of a hair and the centre of a streamer channel is about 1 mm, but most hairs do not stick out more than 0.5 mm from the axis of the channel.

About 1–1.5 hairs per mm of streamer channel can be observed. Because hairs in the path of the channel will be overrun by the channel and hairs in the same optical path as the streamer channel will be obscured by the streamer, the total number of avalanches per mm is probably larger than 1.5 hairs per mm. A stereoscopic 3D investigation, like described in chapter 4 would help to increase the accuracy of these values and get more insight in the nature of the feathers.

5.4.1 Interpretation

The photo-ionization mechanism as described by Teich [211] is applicable to oxygen-nitrogen mixtures: the nitrogen concentration determines the number
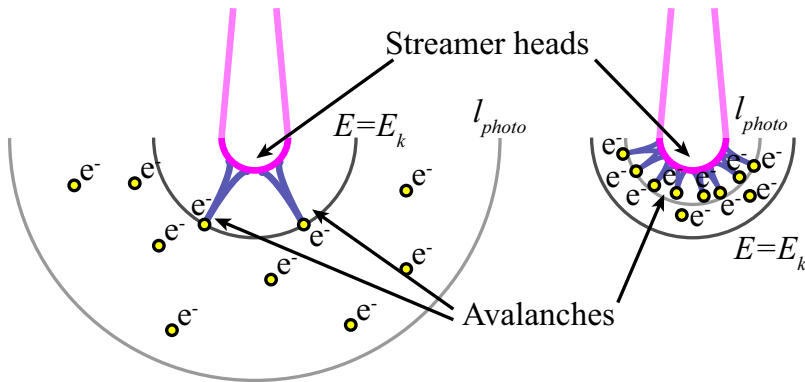
Figure 5.7: Sketch of the mechanism of feather formation. On the left hand side, the photo-ionization length (l_{photo}) is significantly larger than the active region where the local field exceeds the breakdown field ($E > E_k$). The right hand side illustrates the reversed situation.

of available photons in the 98 to 102.5 nm wavelength range; within our experiments where the oxygen concentrations range from below 1 ppm up to 20%, the photon source can be considered as essentially constant (if field enhancement and radius at the streamer tip are the same).

The oxygen concentration determines the absorption length l_{photo} of these photons, and therefore the range of availability of free electrons. The absorption length is about 1.3 mm in air at standard temperature and pressure, and it scales linearly with inverse oxygen density; the oxygen density obviously depends both on the gas density and on the N_2:O_2 mixing ratio [121].

An interpretation for the feather-like structure of the streamer channels in argon and in gas mixtures with low oxygen concentrations is the following. The small branches that form the feathers are in fact avalanches moving towards the streamer head. This is illustrated in figure 5.7, where two extreme cases are shown. In the first case, there is a low O_2 concentration and therefore the photo-ionization length is long. When this length is much larger than the region where the electric field (E) exceeds the critical breakdown field E_k, ionization is mainly created at places where the field is significantly below E_k. Therefore the created free electrons can not form avalanches immediately after creation, or they are lost in the lateral direction where the field never exceeds E_k. Only when the streamer head comes so close that $E \geq E_k$, avalanches form. These separate avalanches are visible in the form of the feathers we see in the images of argon and pure nitrogen.

On the other hand, if there is a sufficiently high oxygen concentration in nitrogen to have a photo-ionization length that is significantly below the radius where

$E = E_k$, all electrons that are created will immediately be accelerated towards the streamer head and create avalanches. Because the density of the seed electrons is much higher (the same amount of UV-radiation is absorbed in a much smaller volume), these avalanches will overlap and become part of the propagating streamer head. Therefore, the streamers will appear smooth, they easily will become broad, and they will not form any feather-like structures.

If photo-ionization is not present at all, but if there is some background ionization, the situation will be similar to the low photo-ionization case (e.g. pure nitrogen or argon). Now the electrons outside the $E \geq E_k$ region will not be created by photo-ionization, but by other processes like cosmic rays or radioactive decay as is discussed in the next chapter.

Figure 5.7 largely resembles textbook concepts of streamer branching due to avalanches caused by single electrons; the first version of such plots stems from Raether [171]. This concept is criticized by Ebert *et al.* in section 5.3 and figure 10 of [51]. Here it is stated that the concept that non-local photo-ionization leads to branching has never been substantiated by further analysis and that even if this avalanche distribution is realized, it has not been shown that it would evolve into several new streamer branches. In contrast, it is stated that the formation of a thin space charge layer is necessary for streamer branching while stochastic fluctuations are not necessary, especially because even in fully deterministic, but nonlinear models, instabilities and branching are possible. These concepts are further elaborated in [46, 86, 119, 137, 208] and were discussed in section 2.4 of this thesis.

Concerning the emergence of feathers rather than branches: there are stochastic avalanches, that we interpret as the "hairs of feathers", but the streamer is apparently not in an unstable situation and does not branch. Of course, this statement is partially semantic - one also could consider the hairs as little side branches that immediately die out again. The real difference between branches and avalanches lies in the question whether the hairs do build up own space charges, or whether they just evolve in the enhanced field of the main streamer. Figure 5.7 suggests that the second is the case. They die out rather after the electron avalanche has reached the main streamer and do not reach a propagating state.

If this interpretation is correct, the number of small branches could be a measure for the background ionization density when no photo-ionization exists. The branch density that was obtained from the measurements at 200 mbar in nitrogen 6.0 and argon 5.0 is about $10^2 \ \text{cm}^{-3}$. Unfortunately, there is very little literature regarding background ionization in pure gasses in containers. Estimations for the maximum equilibrium charge density in air are in the range of $10^3 - 10^4 \ \text{cm}^{-3}$ [156]. However, this value can mainly be attributed to ionization by alpha particles

emitted by decaying radon gas [156]. When we assume that the concentration of radon inside the closed metallic cylinder of our experimental set-up is some orders below the ambient value and the pressure is 200 mbar instead of 1 bar, a background charge concentration of 10^2 cm^{-3} seems reasonable. The natural background density and the effects of pulse repetition rate on the background ionization density will be discussed in the next chapter.

The first Townsend ionization coefficient of argon is much higher than in molecular gasses (at low field strengths) [1] because there are no ro-vibrational states. Therefore the region where the electric field exceeds the breakdown field is larger. This can explain why the feather-like structures are more pronounced in argon discharges than in nitrogen discharges.

Besides photo-ionization, oxygen also plays another role since it is an attaching gas, in contrast to nitrogen or argon. This means that it removes electrons and therefore conductivity from the gas. This mechanism comes in action both ahead of the streamer head and in the streamer channel. Ahead of the streamer head and in the whole non-ionized region, it binds free electrons and makes them essentially immobile, but it also can release them again by detachment when the field exceeds a critical value. In the streamer channel, it limits the conductivity after a sufficiently long propagation time.

If, in our simple model of the feather structure (figure 5.7), the detachment field is higher than the critical breakdown field E_k, then the electrons at the position $E = E_k$ can still be attached to an oxygen molecule and the avalanches will start closer to the streamer head. However, this will only occur at very low pressures. The exact value of the detachment field depends on the vibrational state of oxygen and will therefore be different for background ionization than for photo-ionization. A detailed discussion of the role of detachment can be found in [156].

Aleksandrov *et al.* [10] also find that the addition of 1% of oxygen to a discharge in pure argon leads to a faster decay of the streamer and requires a higher electrical energy input. However, their simulations attribute this not to electron attachment to oxygen, but to quenching of excited argon states by oxygen molecules.

A quantitative analysis, including simulations, of the topics discussed above has been performed by Wormeester *et al.* [236, 237]. We find that at 200 mbar pure nitrogen (1 ppm oxygen), the electric field at about 1 mm from the streamer channel (the length of the feathers found above in pure nitrogen) is around 80 kV/cm, well over the breakdown threshold. At this distance, the electron density is 10^2 mm^{-3}, which is sufficiently low to explain the stochastic occurrence of feathers.
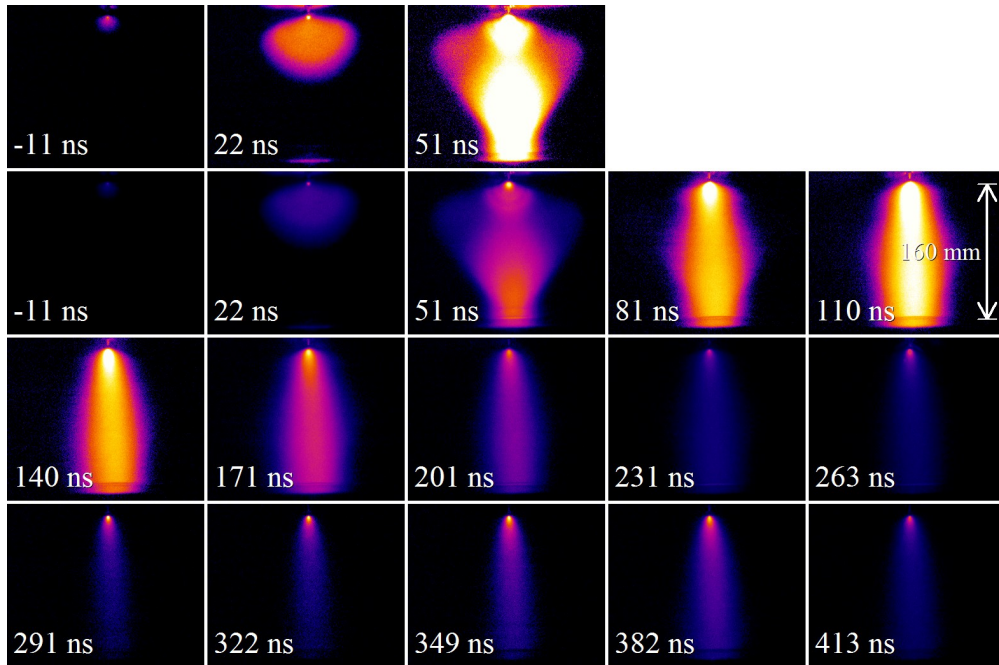
Figure 5.8: Image sequence of streamer discharges in nitrogen 6.0 at 25 mbar. The integration time of each image is 15 ns and the indicated time is the camera delay with respect to the beginning of the voltage pulse. The voltage pulse is similar to the Blumlein pulser from figure 3.12. The images in the top row are identical to the first three in the second row, except for their colour representation. The images in the top row have an *Mf* value of 155, all other images have an *Mf* value of 16.6.
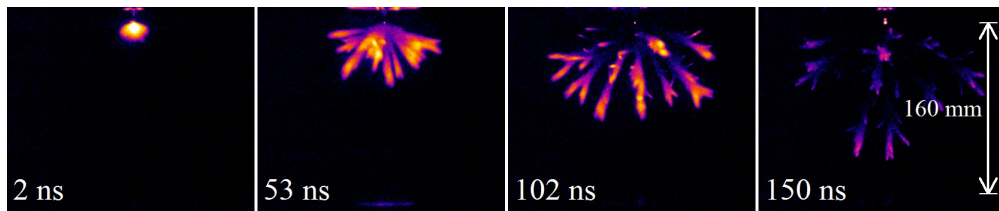
Figure 5.9: Image sequence of streamer discharges in nitrogen 6.0 at 100 mbar. All images have an *Mf* value of 180. All other settings are similar to figure 5.8. Recall that we can not capture more than one image per discharge event. Therefore the images presented here are all from separate discharges.

5.5   Time resolved images

We took time resolved, movie-like image sequences by decreasing the integration time of our camera and varying its internal delay value. Results of these measurements are given in figures 5.8 and 5.9. Note that our camera can only take one image per discharge event and therefore these images are all from separate events. In figure 5.8, the streamer crosses the gap in less than 15 ns. After this time, it evolves into a glow discharge, which is much brighter than the original streamer. This glow discharge remains bright for the duration of the voltage pulse (130 ns), and then starts to extinguish.

After roughly 290 ns, the discharge appears again. This is a negative discharge caused by the reflected pulse in the Blumlein pulser (see figure 3.12). Obviously, at this pressure of 25 mbar, the gap is overvolted at 20 kV, which explains the high propagation velocity of about $3 \cdot 10^6$ m/s.

At 100 mbar, the streamers do not reach the other side of the gap within the pulse duration. Therefore, the light is only emitted by the streamers and no glow discharge is formed, see figure 5.9. The images at 102 and 150 ns clearly show that the light is only emitted by the propagating streamer heads, as was shown before by van Veldhuizen *et al.* [221] and Briels *et al.* [34].

5.6   Conclusions

The most simple and maybe surprising conclusion we can draw from the experiments described here is that streamer properties are quite similar for all nitrogen-oxygen mixtures and pure nitrogen with an impurity level of less than 0.1 ppm. This applies to many of the overview images and zoomed images, but more so for the minimal streamer diameters and velocities. We have tested this on pure nitrogen and four different nitrogen-oxygen mixtures with more than six orders of magnitude difference in oxygen fraction. We do see clear differences when decreasing the oxygen concentration, but the streamers do still propagate with roughly the same velocity and their minimal diameter decreases by less than a factor of two from artificial air to pure nitrogen.

This is remarkable because it means that either the photo-ionization mechanism is not as important in streamer propagation as previously thought, or that this mechanism can still provide enough free electrons, even at very low oxygen concentrations. When we assume that the direct photo-ionization mechanism is not the major source of free electrons there are a few options left for these sources:

- Other photo-ionization mechanisms than direct photo-ionization of oxygen by nitrogen emission are responsible for free electrons. For example, this

could be step-wise ionization of nitrogen molecules, though this is unlikely at the low electron density and high propagation velocity of the streamer tip. The measurements of Penney and Hummert [167] in pure nitrogen and pure oxygen indicate that there is photo-ionization in pure gasses, although in their case, the gasses are orders of magnitude less pure than our gasses.

- Background ionization of the gas due to cosmic radiation, radioactivity or leftover charges from previous discharges can deliver enough free electrons for streamer propagation. The background ionization can lead to free or bound electrons. The bound electrons can be detached by the enhanced electric field of the streamer head [156]. This can be tested by modifying the background charge density in some way (e.g. adding radioactive isotopes) and studying its effect on streamer properties. Results of such studies are discussed in the next chapter.

Numerical simulations of Pancheshnyi [156] show that changing the background ionization of the gas by two orders of magnitude from $10^5 \, \mathrm{cm}^{-3}$ to $10^7 \, \mathrm{cm}^{-3}$ results in only small changes (order 10-30%) of streamer diameter, current and propagation velocity. This is in line with both the hypothesis that a very low amount of oxygen is enough to sustain photo-ionization and the hypothesis that background ionization is the source of the electrons needed for propagation. Note that the literature value for the background ionization in ambient air is $10^3 - 10^4 \, \mathrm{cm}^{-3}$. From the density of feathers, we estimate $10^2 \, \mathrm{cm}^{-3}$ in our 200 mbar pure gasses inside our metal vessel.

Yi and Williams [243] do find an oxygen-fraction dependent streamer velocity. They claim that this is caused by the difference in photo-ionization. An important difference between their measurements and ours is that they have been performed at much higher voltages (70 kV and above) and have a significantly different electrode geometry. Like us, they find that the streamer diameter increases with oxygen fraction. They again attribute this to photo-ionization. More photo-ionization leads to more non-local electron production and thus to a wider streamer head. Besides this, more photo-ionization would also reduce the required field enhancement in the streamer head, which allows the streamer head to have a blunter shape and which reduces branching. Simulations by Luque *et al.* [119] support this, although these simulations treat negative streamers and we have looked at positive streamers.

More detailed descriptions and simulations of these mechanisms are given by Wormeester *et al.* [236]. We find that indeed, at very low concentrations of oxygen in nitrogen (1 ppm), the photo-ionization mechanism can provide enough free charges (electrons and negative ions) to ensure streamer propagation with properties close to air (diameters and velocities within a factor 2 difference). On the other

hand, in our simulations, a realistic background ionization level for 1 Hz repetitive discharges alone (10^7 cm^{-3}) is also enough to ensure positive streamer propagation with roughly the same properties. The effects of background ionization on streamer properties will be treated in more detail in the next chapter.

Although there are some quantitative differences (mainly a $\sim$40% reduction in measured streamer diameter), the qualitative conclusions of Briels *et al.* [34] regarding the similarity laws have been confirmed in this work, also when we take into account the higher purity of the gasses reached here.

Chapter 6

Effects of background ionization

6.1   Introduction

As was discussed in the previous chapter, positive streamers require a source of electrons in front of the streamer in order to sustain their propagation. These electrons can either be created by photo-ionization or be already present in the form of background ionization. Photo-ionization was discussed in detail in the previous chapter. It was found that even in very pure nitrogen, positive streamers are very similar to positive streamers in air. This means that either low levels of oxygen still enable sufficient photo-ionization to enable streamer propagation or that the streamers can propagate by background ionization. Of course a combination of both mechanisms is also possible.

Here we focus on the effects of background ionization by varying its level. Under normal circumstances, there are two probable sources for background ionization: natural background ionization and remaining ionization from previous discharges in repetitive discharges.

In air, electrons produced by any mechanism are quickly attached to oxygen molecules. Therefore the ionization density mostly describes positive and negative ions. At the moderate electric fields outside the streamer head, these positive and negative ions are unable to create secondary ionization (and therefore an avalanche). Only when a streamer head gets close to a negative oxygen atom, the enhanced electric field of the streamer head will detach the electron, which then can create an avalanche.

Natural background ionization levels by radioactivity and cosmic rays are normally around 10^3–10^4 cm^{-3} (Pancheshnyi [156] and references therein). The actual

level depends on many parameters, including building material type, ventilation, room or vessel dimensions and pressure. In our stainless steel vacuum vessel, the ionization levels will probably be lower than in ambient air at the same pressure. This is because the gasses we use are more pure (although we do not have a specification for radon levels), the steel emits less radon than building materials and the vessel may shield part of the cosmic rays. However, it is very difficult to estimate the exact effects on the background ionization level inside the vessel.

The level of background ionization caused by previous discharges in repetitive pulsed discharges depends mainly on the pulse repetition frequency but also on the streamer density. At high streamer densities (when the streamer channels fill most of the discharge volume) a 1 Hz repetition frequency can lead to a background ionization level of about 10^7 cm^{-3} according to simple theoretical estimates by Pancheshnyi [156]. This will be discussed in more detail below.

Hartmann and Gallimberti [78] have experimented with positive streamer discharges in a jet so that rest products of previous discharges are removed before the next discharge. They see a clear effect of the jet on streamer properties, but attribute this to the removal of nitrogen metastables and not of residual ionization.

Simulation results

Simulations on the effects of background ionization on streamers have been performed by Bourdon *et al.* [27] and Wormeester *et al.* [236]. Bourdon *et al.* have simulated both positive and negative streamers in preheated air in which they simulate the effects of repetitive discharges by increasing the background ionization density up to 10^9 cm^{-3} (corresponding to a 10–30 kHz repetition frequency, see below for calculation). They have found that the background ionization density has a small influence on negative streamers, but a significant influence on positive streamers. They find higher propagation velocities as well as shorter initiation delays for higher background ionization densities.

Wormeester *et al.* have found similar results. In that work, we show that photo-ionization and background ionization have roughly the same effect on streamer properties, and that only a low contribution from either of these processes is required to ensure streamer propagation. For example, a concentration of 1 ppm oxygen in nitrogen is enough to make a streamer propagate through photo-ionization, without the need for background ionization. In this case, the propagation velocity is about 20% lower than under similar conditions in air. A similar propagation velocity is found when photo-ionization is turned off and a background ionization level of 10^7 cm^{-3} (positive and negative ions) is assumed.

We find that in air, at streamer repetition frequencies up to 1 kHz, the streamer propagation is dominated by photo-ionization. Finally, we see that streamers branch in "pure" nitrogen, but not in air under otherwise identical conditions.

Arrayás *et al.* [14] have used a slightly different approach: they introduce random fluctuations in the initial ionization density distribution. They show that these random fluctuations can make the front move faster, but do not mention if it also influences streamer branching.

Older simulations, like by Dhali and Williams [48] and Vitello *et al.* [225] model negative streamers. They replace photo-ionization with a uniform background ionization level (order 10^5–10^8 cm^{-3} for Dhali and Williams and 1 cm^{-3} for Vitello *et al.*) in order to simplify calculations.

6.1.1 Experimental methods

We can investigate the importance of background ionization in streamer propagation (and initiation) by artificially increasing this background ionization. There are a few methods to increase ionization levels in gasses. Of course the most simple method is to use (corona) discharges to create the background ionization levels. The effects of leftover ionization from these prior discharges on a new discharge can be investigated by looking at the effects of repetition frequency on streamer initiation and propagation. However, a disadvantage of this method is that it will not create a homogeneous background ionization level and that the exact level is difficult to estimate. We have performed measurements on the effect of repetition frequency. The results of these measurements and related topics are discussed in section 6.2.

Another means to artificially enhance background ionization in a gas is to add radioactive compounds to the gas. The alpha and/or beta particles created in the radioactive decay can ionize many more gas molecules, thereby increasing the background ionization. The advantage of this method is that the resulting ionization level is constant in space and time (charge is created homogeneously). Disadvantages are that the gas mixtures with radioactive additives are expensive and require special handling. We have performed measurements on streamer discharges in nitrogen with a small amount of radioactive krypton-85 added. The results of these measurements are discussed in section 6.3.

There are more methods to increase background ionization. For example irradiation with ultraviolet light (UV). However, UV radiation that is still transmitted by the windows of our vacuum vessel (wavelengths above ∼170 nm) is not able to directly ionize either nitrogen or oxygen molecules. It can be used to free electrons from electrodes and walls, but this is of limited use in our large vessel as it would lead to a very inhomogeneous distribution of ionization density. With special windows, it would be possible to use UV radiation of lower wavelengths. However, both the installation of such windows as well as the generation of enough UV radiation of the right wavelengths would take a lot of effort. Furthermore, this would still result in a quite inhomogeneous distribution of background ionization

with an unknown density.

More exotic methods like electron or ion beams to directly inject charges into the volume have to be discarded for similar reasons.

Measurement of background ionization

Unfortunately, it is very difficult to measure background ionization levels. We have experimented with methods to determine it by measuring the electron and ion drift current in low electric fields (a potential difference of about 100 V over 1 cm distance). If such an electric field is applied in a small volume of a flowing gas and all electrons and ions are removed by this field, we can use the gas flow rate together with the measured current to estimate the density of the electrons and ions in the gas.

At e.g. a (high) background ionization level of 10^8 cm^{-3} and a gas flow rate of 4000 sccm (standard cubic centimetre per minute) at atmospheric pressure, this would lead to a drift-current of about 1 nA. However, this means that the electrical impedance of the system is about 100 GΩ. It is difficult (although far from impossible) to build an electrical system that can measure these low currents at such impedances. Because of limited time, we have not succeeded in setting this up and therefore have not been able to measure background ionization levels.

Experimental conditions

All experiments presented in this chapter have been performed on positive streamers in our new vacuum vessel (see section 3.2.3) with a 160 mm separation point plane geometry. Both the C-supply and the Blumlein pulser have been used. We use some of the same gasses as discussed in the previous chapter (namely nitrogen 7.0 and artificial air, see table 5.1 for specifications) as well as a special gas mixture of pure nitrogen (5.5 purity, see table 6.1) with radioactive krypton-85 added. During use, the gas inside the set-up is flushed with such a flow rate that all gas is replaced every 25 minutes. All experiments are performed at room temperature.

6.1.2   Calculating background ionization levels

Electron attachment

As streamer discharges produce high (local) ionization levels, they can increase the background ionization for subsequent discharges. In gas mixtures with high

oxygen concentrations, electrons quickly attach to oxygen molecules [91, 156]:

$$e + O_2 + O_2 \rightarrow O_2^- + O_2 \qquad\qquad k_{att1} = 2 \cdot 10^{-30}\,\mathrm{cm^6\,s^{-1}} \quad (6.1)$$

or, in gasses with low oxygen concentrations:

$$e + O_2 + N_2 \rightarrow O_2^- + N_2 \qquad\qquad k_{att1} = 8 \cdot 10^{-32}\,\mathrm{cm^6\,s^{-1}}. \quad (6.2)$$

Therefore the free electron density n_e will decrease as function of time as

$$\partial_t n_e = -\, k_{att1} \cdot n_e \cdot [O_2]^2 \qquad\qquad\qquad (6.3)$$
$$-\, k_{att2} \cdot n_e \cdot [O_2] \cdot [N_2]$$

if diffusion is neglected. The attachment time t_{att} can be calculated from this by

$$t_{att1} = \left(k_{att1} \cdot [O_2]^2 \right)^{-1} \qquad\qquad\qquad (6.4)$$

for air, or for oxygen concentrations below a few percent:

$$t_{att2} = \left(k_{att2} \cdot [O_2] \cdot [N_2] \right)^{-1}. \qquad\qquad\qquad (6.5)$$

In air at standard temperature and pressure, t_{att1} is about 20 ns.

Recombination reactions

After that, two- and three-body ion-ion dissociative recombination determines the rate of plasma decay (Pancheshnyi [156]):

$$O_2^- + O_4^+ \rightarrow O_2 + O_2 + O_2 \qquad\qquad k_{rec1} = 10^{-7}\,\mathrm{cm^3\,s^{-1}} \qquad (6.6)$$
$$O_2^- + O_4^+ + M \rightarrow O_2 + O_2 + O_2 + M \qquad k_{rec2} = 2 \cdot 10^{-25}\,\mathrm{cm^6\,s^{-1}} \quad (6.7)$$

where M denotes either a neutral oxygen or a neutral nitrogen molecule. The O_4^+ in these reactions is created quickly after the discharge from reactions of N_2^+ to N_4^+, O_2^+ and finally O_4^+, see e.g. [9]. In other gas mixtures, other recombination reactions will take place.

Homogeneous recombination

Depending on the exact composition of the gas, there can be many different recombination paths and intermediate active species (electrons, ions, atoms, radicals and metastables). However, in spite of this variety, the effective recombination rate is very similar for almost any combination of positive/negative species [158]. This effective recombination rate is roughly

$$k_{rec-air} \approx k_{rec1} + k_{rec2} \cdot [M] \qquad\qquad\qquad (6.8)$$

for air and other electro-negative gas mixtures, with k_{rec1} and k_{rec2} from equations (6.6) and (6.7). For pure electro-positive gasses (gasses without attachment of electrons and therefore without negative ions), we use $k_{rec-N_2} = 5 \cdot 10^{-7}\,\mathrm{cm^3\,s^{-1}}$, which, at room temperature, is equal to $k_{rec-air}$ at a pressure of about 80 mbar ($[M] = 2 \cdot 10^{18}\,\mathrm{cm^{-3}}$).

The decrease of the ionization density n (in a neutral plasma $n = n_+ = n_-$) as function of time t can be described by the following differential equation:

$$\partial_t n = -k_{rec} \cdot n^2, \tag{6.9}$$

with k_{rec} the effective recombination rate, which is dependent on gas composition and density as is described above. Equation (6.9) is solved by

$$n(t) = \left(\frac{1}{n(0)} + t \cdot k_{rec}\right)^{-1}, \tag{6.10}$$

where $n(0)$ is the ionization density at $t = 0\,s$ (for a streamer under standard conditions this is about $10^{14}\,\mathrm{cm^{-3}}$). For all practical values of k_{rec}, high values of $n(0)$ and timescales above milliseconds this can be simplified to

$$n(t) = (t \cdot k_{rec})^{-1}, \tag{6.11}$$

independent of initial ionization density. This means that 1 second after a discharge, the ionization density in air at atmospheric pressure will be roughly $2 \cdot 10^5\,\mathrm{cm^{-3}}$. At 0.1 s and 10 s after a discharge, the ionization density will be ten times as high or low respectively. At other pressures, this number will be different, according to equation (6.8). Therefore, in air, at 200 and 25 mbar, the ionization density 1 second after a discharge will be $9 \cdot 10^5$ and $4 \cdot 10^6\,\mathrm{cm^{-3}}$ respectively.

Note that the reactions shown above are mostly relevant for nitrogen-oxygen mixtures at pressures close to atmospheric pressure. At much lower and higher pressures and in other gasses, other mechanisms start to dominate the recombination reactions. For example, at pressures relevant for sprite discharges (below 1 mbar), dissociative attachment and recombination become very important loss mechanisms [184]. Furthermore, the discharge should occur in an environment where bulk gas recombination is the major ionization loss process. This means that the vessel or environment dimensions have to be sufficiently large so that we can neglect recombination at the wall and that there is no (strong) gas flow which can refresh the gas between repetitive pulses.

Recombination and diffusion

The calculation given above assumes that the ionization is distributed evenly and only changes by recombination. However, as the ionization by streamers is

produced in narrow channels, diffusion will have an influence on ionization levels as well. When we include diffusion, equation (6.9) changes into

$$\partial_t n = D_{ion} \cdot \nabla^2 n - k_{rec} \cdot n^2,$$
(6.12)

with $D_{ion} \approx 5 \cdot 10^{-2}\,\text{cm}^2 \cdot \text{s}^{-1}$ the diffusion coefficient under standard conditions in air [156, 172, 195]. The diffusion coefficient scales inversely with pressure. In section 6.4.1 we will use equation (6.12) to interpret the results of some of the experiments described below. We there show that the more localized ionization distribution in the trails of the streamers will lead to lower final ionization densities than obtained from equation (6.11).

Constant ionization sources

For a gas with a constant source of ionization S, like the natural background ionization (due to natural radioactivity and cosmic rays), or gas mixtures with added radioactive traces, the production rate equals the recombination rate in equilibrium. The ionization density is $n = n_+ = n_-$. As we now have a fixed ionization source and no time dependence, equation (6.12) changes to

$$\partial_t n = S - k_{rec} \cdot n^2 = 0,$$
(6.13)

with the solution for the equilibrium ionization density

$$n = \sqrt{\frac{S}{k_{rec}}}.$$
(6.14)

6.2   Effects of repetition frequency

Both of our pulsed power supplies allow repetition frequencies of about 10 Hz and slower. Therefore we have performed measurements at 10, 1, 0.1 and 0.01 Hz and studied the effect of repetition frequency on streamer morphology. We have not performed detailed quantitative measurements of streamer velocities and diameters.

According to the theoretical estimates given above, the lowest repetition frequency used, 0.01 Hz, will lead to a background ionization level from leftover charges of about $2 \cdot 10^4\,\text{cm}^{-3}$ at 200 mbar. This is close to natural background ionization levels. Therefore we do not expect to see many differences between a completely "fresh" gas fill, and a gas fill 100 seconds after a streamer discharge.
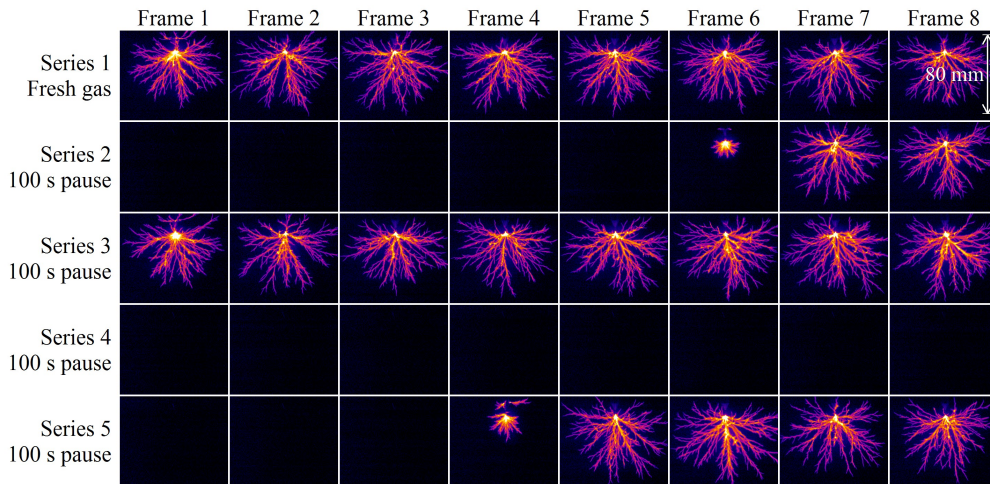
Figure 6.1: Five separate series of eight consecutive frames of streamer discharges (or attempts). The series start at the first pulse of a "fresh" gas filling. In series 1 this is a completely new fill of the vacuum vessel (it was pumped down to 2 mbar before filling). In the other series no pulse was applied for at least 100 s prior to frame 1. The frames have been recorded in nitrogen 7.0 at 200 mbar with 25 kV positive pulses from the Blumlein pulser at a repetition frequency of 1 Hz. The *Mf*-value of the images is about 43. The five series shown comprise the full measurement series.
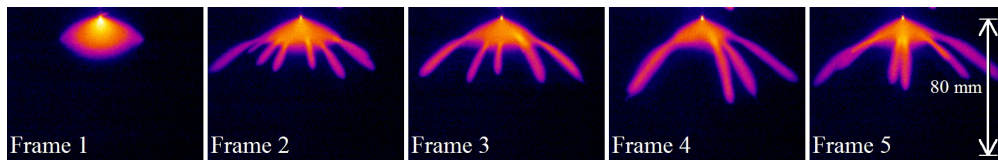
Figure 6.2: The first five frames of streamer discharges after a 100 s pause in artificial air. The frames have been recorded at 200 mbar with 25 kV positive pulses from the Blumlein pulser at a repetition frequency of 1 Hz. The *Mf*-value of the images is about 190.

6.2.1 General results

Initiation, first discharge and subsequent discharges

When studying streamers at different repetition frequencies, we found that streamer discharges in 200 mbar pure nitrogen with 25 kV, 130 ns pulses from the Blumlein pulser, often do not initiate at a pulse repetition frequency of 0.01 Hz. Therefore we have used a different method to investigate streamer propagation at this repetition frequency: After a 100 s pause (no pulses), we switch on the pulse source with a repetition frequency of 1 Hz. ICCD camera frames of the first ten to thirty pulses

are then captured and stored. In this way, the first pulse which results in streamer initiation is nearly always captured as well as some subsequent discharges. In one case, we have taken this approach a bit further and have used a completely fresh gas fill to start with, instead of a 100 s pause. In this case, we first pumped the vacuum vessel down to 2 mbar, before refilling it to 200 mbar. The results of these measurements are given in figure 6.1 for nitrogen 7.0 and figure 6.2 for artificial air.

In nitrogen 7.0 we can observe that indeed the streamers do not always initiate on the first pulse under the specified conditions. In only two of the five attempts did the streamers initiate on the first pulse. One of these two attempts was the case when nearly all of the gas in the vessel was replaced (a fresh gas fill). In another attempt (series 4), no initiation at all was observed during the first ten pulses. In all attempts that show initiation, the morphology of the first discharge is somewhat different from subsequent discharges. The propagation length is usually shorter and there seems to be a denser core of the streamer tree. This is studied in more detail in the next section.

In air, we again see that the first discharge after 100 s waiting is different from subsequent discharges. In the first discharge, only an initiation cloud is visible, while in subsequent discharges, this initiation cloud is smaller and streamers emerge from it. It appears that the initiation cloud of the second frame is still larger than the initiation cloud of subsequent frames. We have observed the same behaviour in all three measurement series we have recorded under these conditions.

Repetition frequency dependence

We have performed measurements on the effect of the pulse repetition frequency with frequencies from 10 Hz down to 0.01 Hz. At least four pulses with the specified repetition frequency have occurred before the capture of the images that are shown here. Again, the measurements at 0.01 Hz have been performed in a slightly different way than the other discharges. In this case, we used a 1 Hz repetition frequency; this was paused for 100 s and then turned back on like discussed in the previous section. Plotted is the first image of such an image series which shows a streamer discharge.

Images of streamer discharges in nitrogen 7.0 and artificial air at these repetition frequencies are shown in figure 6.3. Here, we can see that in both gasses, the streamer morphology depends on repetition frequency. In all cases, the length of the streamers is limited by the short pulse duration ($\approx$130 ns) from the Blumlein pulser.

In nitrogen 7.0, the initiation cloud is very small (as is always the case). Here the main visible effect of variation of the repetition frequency is that for lower

10 Hz	1 Hz	0.1 Hz	0.01 Hz
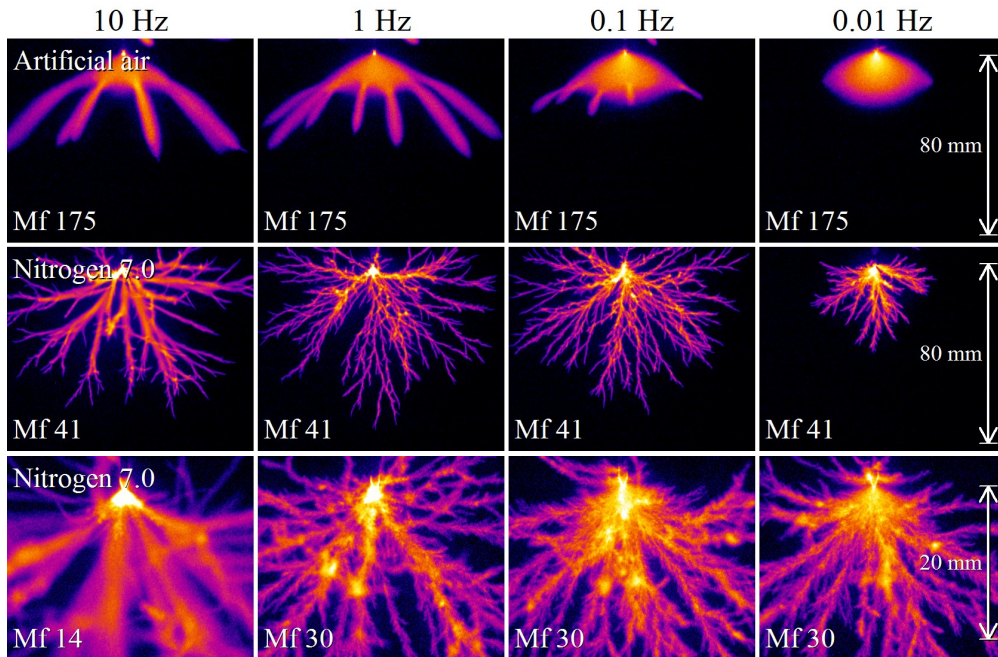
Figure 6.3: Overview (top and middle row) and zoomed (bottom row) images of the effects of pulse repetition frequency on streamer morphology. These images have been acquired in 200 mbar artificial air and nitrogen 7.0 with the Blumlein pulser (pulse length 130 ns) at 25 kV. Note that the images at 0.01 Hz are created in a different manner: after 100 seconds pause, the pulse source was started with a 1 Hz repetition frequency. Shown here is the first image with visible streamers.

frequencies the streamers become thinner and the number of streamers and feathers increases. The bright core that is visible in the first successful discharges in figure 6.1 and in the 0.1 and 0.01 Hz overview images in figure 6.3 consists of many overlapping feather-like streamers, as can be seen in the zoomed images in figure 6.3. Subsequent images in these series are virtually identical to streamers at a 1 Hz repetition frequency.

The total length (and therefore average propagation velocity) does not change much between 10 Hz and 0.1 Hz in nitrogen 7.0. At 0.01 Hz, the streamers are shorter, but this can probably be attributed to late initiation. As was shown in the previous section, streamers mostly do not initiate on the first pulse after a 100 s pause. Therefore we expect that the first streamer discharge that does initiate, does so at a random moment in a pulse. This means that the length of the streamer discharge at 0.01 Hz is not a good indication for its propagation velocity. Except for the difference in discharge length, the general morphology is the same for 0.1 and 0.01 Hz.

We have attempted to measure the propagation velocity in nitrogen 7.0 for the different repetition frequencies, but this turned out to be very challenging and did not give reliable results. The main problem is that we have not been able to use the position correlation method (the second method described in section 3.4.3) because at 10 Hz we can no longer reliably stop our camera and oscilloscope at the same discharge. Therefore we had to use the first method (measuring the length of streamer sections at short integration times). However, this method is not fully suited for the crowded discharges like seen in figure 6.3 and therefore gives quite inaccurate results with a relatively large spread in measured velocities. In our measurement the standard deviation was of the order 10–20%, which is larger than the expected differences between repetition frequencies (as could be estimated by the total size of the discharge). For these reasons, we are not able to draw a definite conclusion on the effect of repetition frequency on streamer propagation velocity, except for the conclusion that the effect is smaller than 20% between 0.1 and 10 Hz.

In air, we see that the initiation cloud becomes larger for lower frequencies. Simultaneously, the streamers emitted from this cloud become shorter and thinner for lower frequencies. At 0.01 Hz, there is only a hint of a streamer coming from this cloud (on the right hand side in this example).
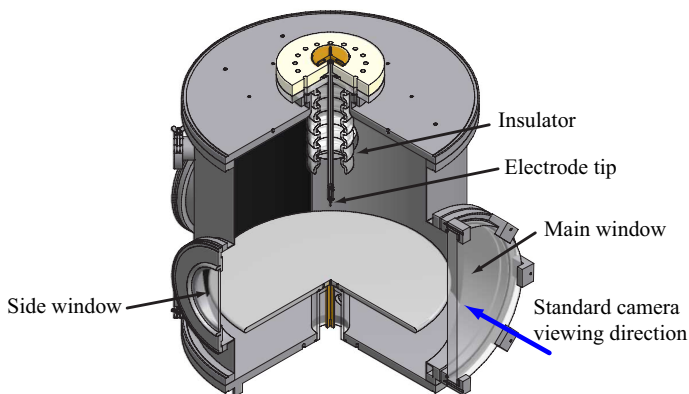
6.2.2   Upward bending streamers

The images of streamers at different repetition frequencies that are shown in the previous sections have all been acquired with (short) pulses from the Blumlein pulser. Figure 6.4 shows some images of streamer morphology as function of repetition frequency for streamers in nitrogen 7.0 generated with the C-supply at a relatively low pulse amplitude (10 kV). In these conditions we see something peculiar occurring: although there is no visible effect of repetition frequency on streamer diameter, there is a large influence on streamer direction. At 10 Hz, all streamer channels are directed upwards, while at lower frequencies more and more streamers are directed downwards. At 1 Hz, all channels are directed downwards up to horizontal, but none are directed upwards. At 4 and 2 Hz, the channels on the right-hand side of the image are more directed upwards than the other streamers.

The images on the bottom row of figure 6.4 are acquired under the same discharge conditions, but with an extra external light source added (through the main window), a much longer camera exposure time (0.5 ms instead of a few µs) and the camera tilted upwards. These three measures enable us to observe both the streamers, as well as the electrode tip holder and the glass insulator around it. An illustration of the set-up with all relevant parts indicated is given in figure 6.5.

It seems that at higher frequencies, either the streamers are repelled by something below the electrode tip, or attracted by something above it. We prefer the
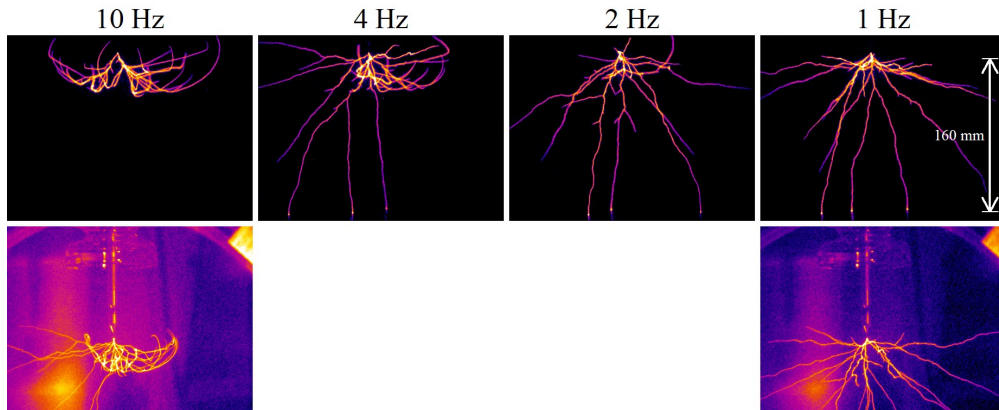
Figure 6.4: Effect of pulse repetition frequency on streamer discharge morphology. All images are in pure nitrogen (7.0 purity) at 200 mbar, 10 kV with the C-supply (risetime ∼100 ns). Top row: standard overview images of the full gap; Bottom row: camera tilted upwards with a lamp turned on and very long (0.5 ms) exposure to show both the streamers as well as the set-up itself.

Figure 6.5: Three-quarter cross section illustration of the vacuum vessel, indicating the important features for the upward bending streamers, including standard camera viewing direction.

latter explanation as it seems from the images of the streamer discharge together with the electrode holder and insulator that the streamers are actually directed towards the glass insulator. As we use positive streamers, they can be electrostatically attracted to the glass if it is negatively charged. Such negative charge could come from previous discharges. If this is the case, then most charge is still there 0.1 s after the discharge, but has mostly disappeared after about 1 s, as there is no visible attraction at 1 Hz.

In measurements under other conditions (mostly at lower pressures), we have often observed that next to the main streamer discharge a parallel discharge occurs over the entire surface of the glass insulator. However, under the conditions of the discharges in figure 6.4, no such surface discharge was visible with the naked eye nor with the ICCD camera.

Furthermore, the fact that for intermediate repetition frequencies (2 and 4 Hz), the streamers on the left-hand side of the image do not bend upwards as much as the ones on the right-hand side may have a similar explanation. On the left-hand side of the vessel (seen from the camera), a glass window is placed while the right-hand side of the vessel is a grounded steel wall (see figure 6.5). Streamers could be attracted to the glass window in a similar way as they are attracted to the glass insulator. However, we have never observed discharges across the glass window, which makes sense, as there is no voltage drop over the window. Therefore, the charging of the surface can only come from the streamers themselves. UV-photons from the streamers can also charge a surface, but as they can only free electrons, this would lead to a positive surface charge instead of the negative charge that is needed to attract streamers. Nevertheless, the freed electrons could form a negative cloud above the surface that may attract the streamers.

6.2.3   Repetition of streamer paths

If positive streamers in pure nitrogen can propagate because of background ionization left by previous discharges, one would expect that streamers in consecutive discharges would follow the same paths, depending on repetition frequency and streamer diameter.

Figure 6.6 shows images from consecutive discharges at 1 Hz repetition frequency, in order to check whether or not streamers will follow the same path. In the bottom row of this figure, we have overlaid images from three subsequent discharges as the red, green and blue channels in two composite images. We can observe in these composite images that, in general, subsequent streamers do not follow the same path. Only some channels (outside the crowded central area) are rendered cyan, yellow, magenta or white, while most channels are either red, green or blue. The channels that appear cyan, yellow, magenta or white can be expected from a statistical point of view, especially considering the fact that we use 2D images representing the 3D streamer tree. Therefore we can conclude that under the conditions from figure 6.6, consecutive discharges do not follow the same path.

In the bottom half of the discharge, the average separation between the channels in one image is over 30 mm if we assume cylindrical symmetry. In section 6.4.1 we calculate that under these conditions, we expect that the ionization trail left by a streamer channel is still somewhat present 1 second later but its ionization density is only 25% higher than in the surrounding volume.
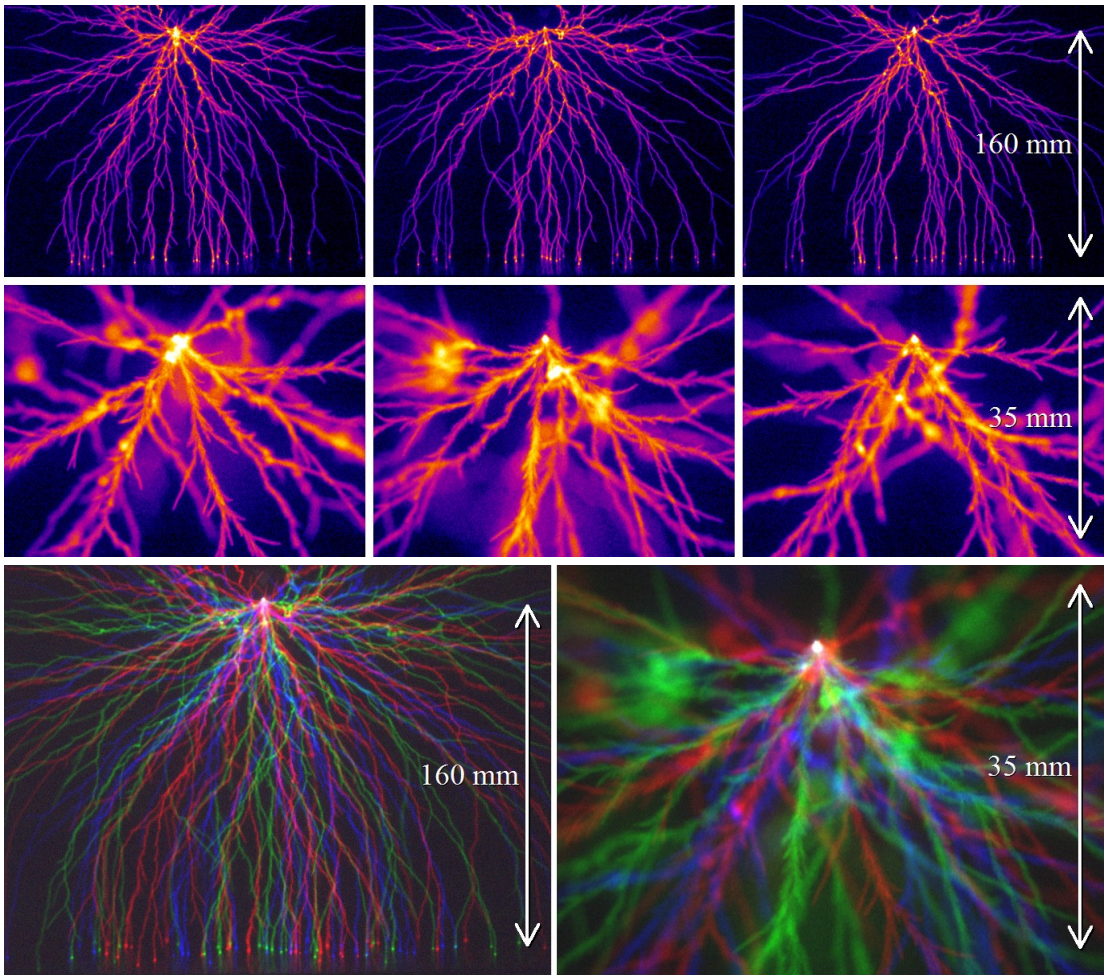
Figure 6.6: Two series of three consecutive images overview (top row) and zoomed (middle row), both at similar conditions and with 1 Hz repetition frequency. The images from the first two rows are represented in a different way in the bottom row. In these representations, the measured intensities of the three consecutive images are overlaid in red, green and blue respectively. This means that repetitive streamer paths are rendered cyan, yellow, magenta or white, while unique streamer paths are rendered red, green and blue. All images have been acquired in 200 mbar nitrogen 7.0 with the C-supply at 15.4 kV. The *Mf*-value of the images is about 170.

Table 6.1: Gas impurity levels of the krypton-mixture as provided by the gas supplier. Impurity levels are given as upper limits, except for ^{85}Kr, which is dosed on purpose, in parts per million (ppm).

N_2	^{85}Kr	O_2	Ar	H_2	H_2O	CO_2	CO	CH_4
≈100%	0.0099	0.5	5	0.5	0.5	1	1	0.5

The results from figure 6.6, confirm our general experience that within a single series of subsequent voltage pulses, streamers follow a new (semi-random) path on every new voltage pulse. It seems that streamer channels do not have a tendency to follow the same path twice nor is there any indication that they are in any way influenced by the shape of the previous discharge (at 0.1 to 10 Hz repetition frequency). This is of course not the case for conditions that lead to only one streamer channel (short gaps or low pressures, see the 25 mbar images in figure (5.2)). In this case, the one channel is always located on the symmetry axis of the experimental setup. But, under all conditions where multiple channels are observed, the streamers take a new path on each instance.

6.3 Addition of radioactive ^{85}Kr

In order to increase the background ionization density in pure nitrogen without changing the repetition frequency, we have performed experiments with a pre-mixed gas mixture consisting of pure nitrogen with 500 kBq/litre of radioactive krypton-85 added. Details of the impurities in this mixture as specified by the gas supplier are given in table 6.1. Krypton-85 (^{85}Kr) is a radioisotope of krypton with a half-life of 10.756 years. The most common decay (99.57%) is by emission of a beta particle to form ^{85}Rb (a stable isotope). The emitted beta particles have a maximum energy of 687 keV and an average energy of 251 keV. We will use the average energy for our calculations. Krypton 85 has the advantage that it is an inert gas. Therefore it is used in many applications like for example leak detection [59] or mixed in low densities in argon as an ignition aid for high intensity discharge (HID) lamps [61].

We use a mixture of 9.9 ppb (parts per billion) of ^{85}Kr in pure nitrogen at standard pressure and temperature. This mixture has a specified decay rate of 500 Bq cm^{-3} (= 500 kBq/litre) or about 13.5 nCi cm^3 (nCi = nanocurie = 37 decays per second). In our vessel with a volume of about 100 litre, this leads to about $5 \cdot 10^7$ decays per second at atmospheric pressure. The average time between decays is 20 ns which means that during a streamer discharge of duration 100 ns–1 µs five to fifty decays will take place in our gas volume.

	1000 mbar	200 mbar	25 mbar
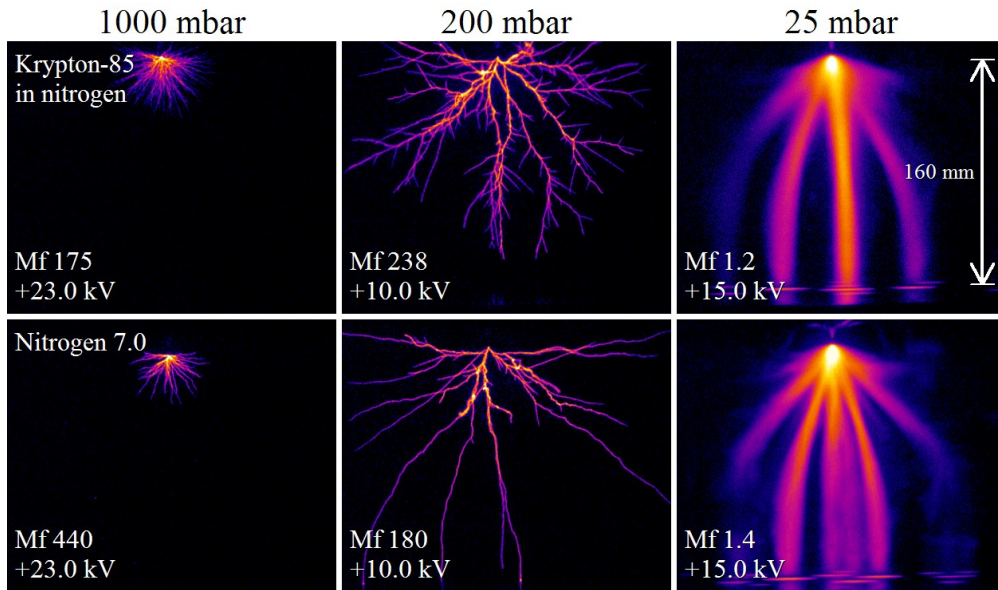
Figure 6.7: Comparison of streamer discharges in nitrogen with [85]Kr added and in pure nitrogen. The discharges are produced with the C-supply. Discharges in other gas mixtures under the same conditions are given in figure 5.1.
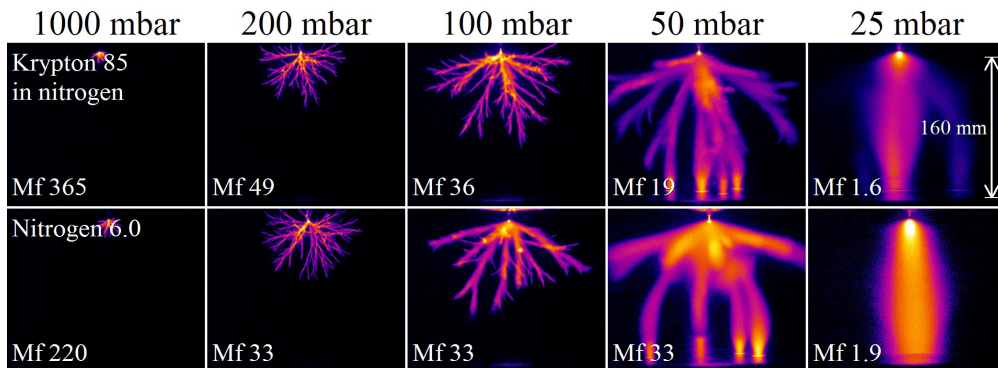
Figure 6.8: Comparison of streamer discharges in nitrogen with [85]Kr added and in pure nitrogen. The discharges are produced with the Blumlein pulser at about 20 kV.

According to an empirical formula by Glendenin [66, 98], the penetration length of a 251 keV beta particle in air at atmospheric pressure is about 50 cm which is nearly equal to the dimensions of our vacuum vessel. The average path length before an emitted particle hits the wall is about 25 cm. Therefore we assume that

only half of the energy of the particle is absorbed inside the gas.

When we assume that half of the energy loss of the particle inside the gas is used to ionize molecular nitrogen (ionization energy 15.6 eV) we can estimate the electron-ion pair production at about 4000 pairs per emitted beta particle. Combined with the decay rate given above, this gives an ion-electron pair production rate S of about $2 \cdot 10^6 \, \mathrm{s}^{-1} \mathrm{cm}^{-3}$.

We can use this production rate together with the recombination rate for pure nitrogen $k_{rec-N_2} = 5 \cdot 10^{-7} \, \mathrm{cm}^3 \, \mathrm{s}^{-1}$ and equation 6.14 to calculate the equilibrium ionization density. At 1000 mbar this gives an equilibrium ionization density of $2 \cdot 10^6 \, \mathrm{cm}^{-3}$, which is clearly higher than the background ionization density in air, which ranges between 10^2 and $10^4 \, \mathrm{cm}^{-3}$ depending on circumstances (e.g. radon concentration, presence of walls, cosmic radiation shielding).

At lower pressures, the ion-electron pair production rate decreases for two reasons: a lower absolute density of ^{85}Kr and a longer path length of the beta particles. In other words, the ion-pair production rate scales with n_0^2 for gas densities n_0 when the penetration length is larger than the dimensions of the vessel. The equilibrium ionization densities will be roughly $4 \cdot 10^5$ and $1 \cdot 10^4 \, \mathrm{cm}^{-3}$ at 200 and 25 mbar respectively.

6.3.1 General results

We have compared discharges in the krypton-85 nitrogen mixture with discharges in pure nitrogen like discussed in section 5.3. Results of these comparisons are given in figures 6.7, 6.8 and 6.9. In general, the discharges are very similar to discharges in pure nitrogen. However, there are some clear differences: In the krypton-mixture, more branches occur. These "extra" branches are longer than the feathers observed in pure nitrogen and pure argon, but they do not reach much farther than about 10 streamer diameters. This is especially clear in the 200 mbar images from figure 6.7 and the 50 and 100 mbar images from figure 6.8. The zoomed images at 200 mbar from figure 6.9 also show longer branches in the krypton-mixture than the short "feathers" in pure nitrogen. In the same figure, at 1000 mbar, the number of channels is about two times higher in the krypton-85 mixture than in pure nitrogen, which may be attributed to the same reason.

However, the differences in general morphology between the krypton-mixture have little influence on propagation velocities and minimal streamer diameters. As is shown in figure 6.11, the measured propagation velocities and minimal streamer diameters in this mixture are very similar to values in other gas mixtures (see figures 5.3 and 5.4). In this case, velocities have been measured in the centre of the gap and diameters have been determined from minimal streamers at relatively low voltages. More details about such measurements can be found in sections 3.4.3, 5.3.2 and 5.3.3.
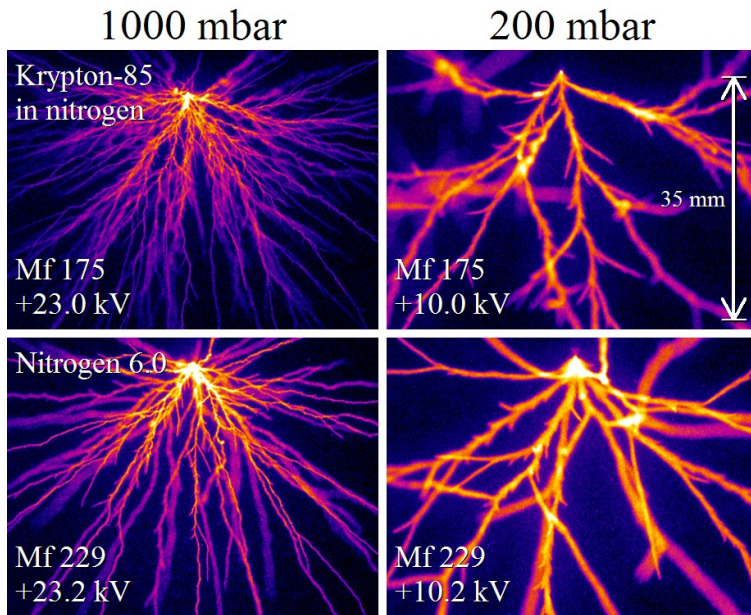
Figure 6.9: Comparison of zoomed streamer discharge images in nitrogen with [85]Kr added and in pure nitrogen. The discharges are produced with the C-supply. Discharges in other gas mixtures at the same conditions are given in figure 5.5.
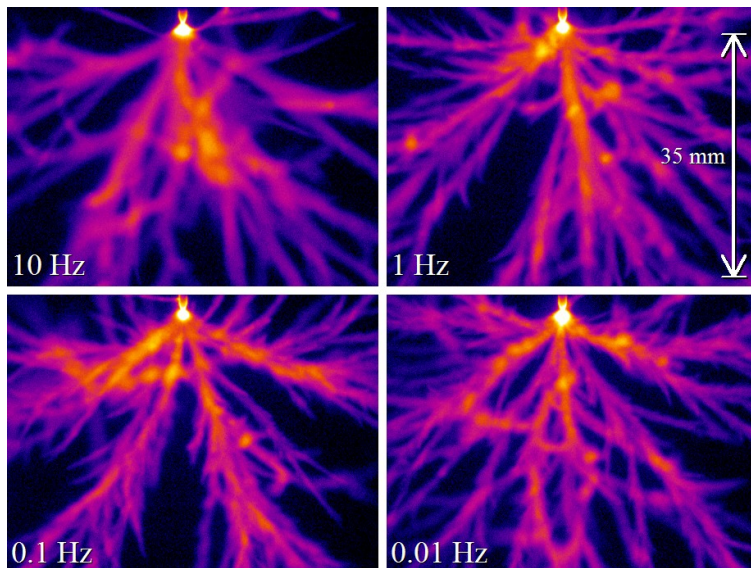
Figure 6.10: Zoomed images of the effects of pulse repetition frequency on streamer morphology in the nitrogen-krypton-85 gas mixture. These images have been acquired at 200 mbar with the Blumlein pulser at 25 kV.
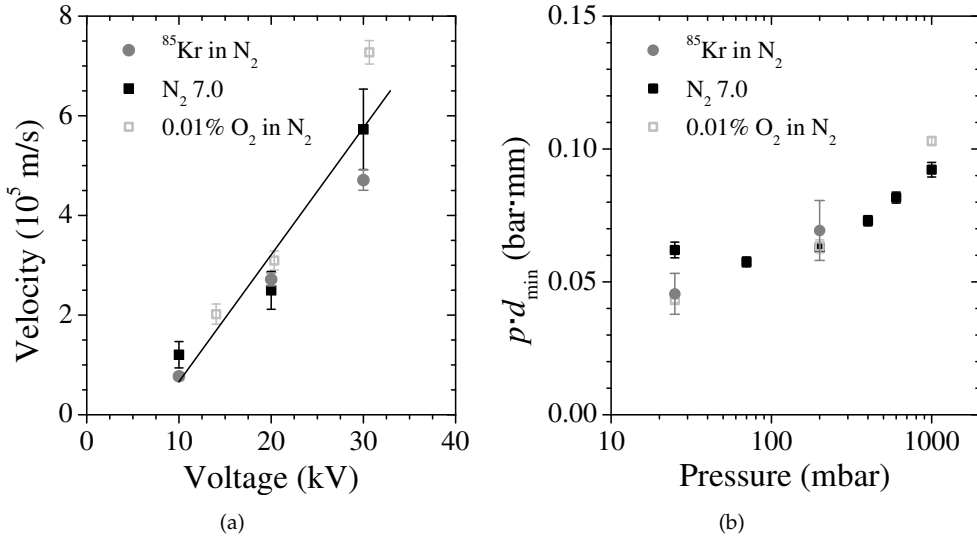
Figure 6.11: Streamers created with the C-supply: a) velocities as a function of voltage at 200 mbar and b) minimal streamer diameters as a function of pressure for the nitrogen-krypton mixture as well as for two other gasses. The error bars indicate the sample standard deviation. The line in a) is a linear fit through all the points from figure 5.4. More diameter measurements in nitrogen-oxygen mixtures are shown in figure 5.3.

6.3.2   Effects of repetition frequency with ^{85}Kr

With the krypton-85 nitrogen mixture, we have performed similar experiments as discussed in section 6.2. Results of these experiments are given in figure 6.10. Initiation is very easy in this gas-mixture. In all cases a full discharge was observed on the first pulse, also with lower voltage pulses (not shown here). This is no surprise, as the radioactive decay of the krypton-85 guarantees a constant source of free electrons.

In figure 6.10, the morphology of discharges is very similar for 0.01, 0.1 and 1 Hz pulse repetition frequency. The high density of feathers that is observed at 0.1 and 0.01 Hz in pure nitrogen (see figure 6.3) is not visible in the krypton-mixture. However, the thicker branches and less feathers at 10 Hz that are observed in pure nitrogen are also visible in the krypton-mixture. From this, we can conclude that at 10 Hz repetition frequency, the background ionization by previous discharges dominates over the background ionization by radioactivity.

If we use equation (6.11) to calculate the leftover ionization density at 200 mbar 1 second after a discharge, we get $2 \cdot 10^6 \, \text{cm}^{-3}$. This is about five times higher than our estimation of background ionization caused by the krypton-85 in our gas

mixture, which is $4 \cdot 10^5$ cm^{-3} at 200 mbar. At 10 Hz repetition frequency however, the ionization left by previous discharges may dominate as the radioactive ionization remains constant, while the leftover ionization increases by a factor of 10 (compared to 1 Hz). At repetition frequencies below 0.2 Hz, the ionization density is dominated by charge produced by krypton-85. Therefore, it is no surprise that we can no longer distinguish discharges at 1 Hz repetition frequency from discharges at lower repetition frequencies, but that we still do see differences between discharges at 1 Hz and 10 Hz repetition frequency.

Note that all these numbers are rough estimates and can have an uncertainty up to one order of magnitude. Therefore, the exact repetition frequency at which krypton-85 induced ionization dominates over leftover ionization can vary as well.

6.4   Discussion and conclusions

6.4.1   Effects of repetition frequency

We have observed that at higher pulse repetition frequencies (e.g. 10 Hz) there are fewer but thicker streamer channels than at lower repetition frequencies (e.g 0.1 Hz). This effect is more prominent close to the electrode tip than in the outer edges of the streamer discharge. We have not observed any difference in streamer morphology between repetition frequencies of 0.1 Hz, 0.01 Hz and discharges in a fresh gas fill. However, in nitrogen 7.0, streamers do initiate more easily at 0.1 Hz than at 0.01 Hz. In artificial air, the initiation cloud is larger at lower repetition frequencies.

According to Pancheshnyi [156], streamers branch less often in higher background ionization conditions. This is in accordance with the observations described above and with observations by others (e.g. [67]). Pancheshnyi explains this by the stochastic nature of branching. In conditions with high background ionization levels, there are so many free charges available that the discharge is no longer dominated by stochastic processes. Furthermore, Wormeester *et al.* [236] show that the strong photo-ionization in air will lead to a smoother distribution of free electrons in front of the streamer (see figure 6.12). This smoother distribution also suppresses branching.

This is related to the interpretation of feather-like structures that is discussed in section 5.4.1. At high repetition frequencies, the background ionization level is increased, which means that there will be many free electrons (or negative ions from which electrons can be detached) in front of the streamer head. Such a high concentration will lead to a thick, smooth streamer. At lower repetition frequencies, there are much fewer (free or attached) electrons available. These few electrons can then form avalanches which can be observed separately and cause stochastic
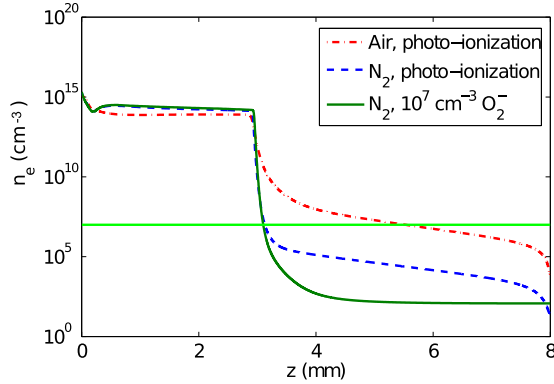
Figure 6.12: Simulated electron densities on the streamer axis. The streamers propagate from left to right with their heads at about $z = 3$ mm. The solid curve shows N_2 with 1 ppm O_2 with a background ionization of 10^7 cm^{-3} and no photo-ionization, the dashed curve shows N_2 with 1 ppm O_2 with photo-ionization and the dashed-dotted curve shows air with photo-ionization. Also included is the initial level of O_2^- background ionization (horizontal line). Figure from Wormeester *et al.* [236].

branching. This also explains the feather-like structure in the centre of the discharge region that is observed in streamers in pure nitrogen at low repetition frequencies (see e.g. the zoomed images at 0.1 and 0.01 Hz in figure 6.3).

In air this mechanism is much less important, as the high level of photo-ionization will prevent most of the stochastic instabilities that are present in mixtures with low oxygen concentrations. At these high levels of photo-ionization, there are so many electrons in front of the streamer head that they can be treated as a homogeneous density, instead of a very low density with stochastic behaviour. Nevertheless, we still see that the initiation cloud in air becomes smaller at higher repetition frequencies, for which we have no good explanation yet.

The fact that streamers bend upwards at high pulse repetition rates in a discharge with relatively long pulses (≈ 5 μs) from the C-supply can probably be explained by electrostatic attraction of streamers by surface charges on the glass insulator.

The fact that we observe much easier initiation in artificial air than in pure nitrogen seems to contradict the results of van Veldhuizen and Rutgers [223]. They found that both ambient air, dry air and pure nitrogen exhibit roughly similar inception probabilities as function of voltage. However, the purity of their nitrogen gas is specified as 4.0, compared to our 7.0 nitrogen (three orders of magnitude less impurities). Furthermore, they use a low repetition frequency with a manually triggered discharge every 10 to 60 seconds (according to a trainee

report by Hermans [82]).

According to Panchesnhyi [156], the probability P of streamer initiation in air-like gasses is

$$P = \frac{n_{max} \cdot 2\pi}{L} \left(\frac{U \cdot R_{el}}{E_{det}} \right)^2 \tag{6.15}$$

where n_{max} is the background ionization density in the middle of the gap, L the length of the gap (160 mm), U the applied voltage, R_{el} the radius of the electrode tip (15 μm) and E_{det} the minimum electric field needed for electron detachment from O_2^- (38 kV/cm). This estimate has been derived by calculating the probability that a negative ion exists in the effective volume where the electric field is so high that it can lead to a streamer start. This effective volume is bounded by the distance from the electrode tip where the tip field enhancement leads to a field that is equal to E_{det}. The ionization density in this volume is estimated by assuming a diffusion balance of ionization from the centre of the gap (with $n = n_{max}$) to the electrodes. This approach neglects time dependent phenomena like ionization, recombination and diffusion and is therefore only suitable to calculate initiation probabilities for short voltage pulses. Furthermore, its diffusion model is one-dimensional and may therefore not be perfectly suited for a sharp electrode tip. Lastly, this model neglects that the streamer density near the tip is usually the highest in the domain and that therefore the charge density close to the tip may be higher than anywhere else.

When we use equation (6.15) with an applied voltage of 25 kV and a background ionization density of $2 \cdot 10^4 \, \text{cm}^{-3}$ (corresponding to a 0.01 Hz repetition frequency at 200 mbar according to equation (6.11)), we get $P = 0.76\%$. This is clearly lower than the initiation probabilities that we observe, which lie above 10% for nitrogen 7.0 and at about 100% for artificial air. For higher repetition rates P should increase linearly. This would mean that $P = 7.6\%$ at 0.1 Hz, while we observe that it is close to 100% for both gasses at this repetition frequency. At 1 Hz and higher, we always observe a 100% initiation rate, which seems reasonable as the calculated probability is 76%, but these calculations are not expected to be better than order of magnitude accuracy.

The discrepancy between calculations and observations can not be attributed to natural background radiation as this will lead to ionization densities of $10^3 - 10^4 \, \text{cm}^{-3}$, equal to or lower than the assumed ionization density at 0.01 Hz repetition frequency. Furthermore, it also does not explain the observed differences between artificial air and nitrogen 7.0. However, the difference between these gasses may indicate that the estimation of k_{rec} for electropositive gasses by Pancheshnyi [158] is not fully correct for our conditions.

Channel repetition

We do not observe that streamers follow (nearly) the same path as in the previous discharge. This can be caused by two reasons: there is just no preference for the previous path or the streamers are actually repelled by the previous path. However, in situations where only one streamer channel occurs (at low pressures), this channel always follows the closest path between tip and plate. It does not avoid the path of the previous discharge. Therefore we assume that there is no preference for the previous path. This would mean that either streamer channels are not attracted to higher concentrations of leftover ionization from a previous discharge, or that the ionization has been redistributed and recombined so effectively that the previous channels are no longer a preferred path.

In order to estimate which of these scenarios is most likely, we have calculated the effects of recombination and diffusion on the distribution of the ionization trail left by a streamer channel. In this calculation we will neglect space charge and fields, as both will be gone fast after the discharge has occurred. For the conditions of the discharges from figure 6.6 we assume that a streamer channel leaves a trail in the form of a gaussian ionization distribution with a FWHM (full width at half maximum) of 0.3 mm and a maximum ionization density of 10^{14} cm^{-3}. In 200 mbar pure nitrogen, the diffusion coefficient will be $D_{ion} \approx 0.25$ cm^2 s^{-1} and the recombination rate $k_{rec-N_2} \approx 5 \cdot 10^{-7}$ cm^3 s^{-1}. For simiplicity, we assume that the streamers are distributed in a hexagonal grid with 30 mm distance to their neighbours.

We solve $n(t, r)$ from equation (6.12) numerically for a cylindrical symmetric system with $\frac{\partial n}{\partial r} = 0$ as boundary condition. The initial conditions include the gaussian streamer channel around $r = 0$ added to a fixed background ionization level:

$$n(0, r) = n_{ini} + n_{channel} \cdot e^{-\frac{r^2}{\sigma^2}}, \qquad (6.16)$$

where n_{ini} is the background ionization level, $n_{channel}$ the maximal ionization density left in the centre of the channel and σ a measure for the width of the channel ($\sigma = \text{FWHM}/2\sqrt{\ln 2}$).

First we study the case where the initial background level is $n_{ini} = 10^3$ cm^{-3}, representative for the first discharge in virgin gas (figure 6.13a). In this case, the ionization density at $t = 1$ s at the centre of the original channel ($r = 0$) is about 3.4 times higher than on the edge of the domain ($r = 15$ mm). This means that the channel is still clearly present. However, its width has become quite large (FWHM ≈ 15 mm), as can be seen from the figure.

In order to know the background ionization level after many shots, we have looked for a value of n_{ini} where the spatially averaged calculated ionization density n_{ave} at $t = 1$ s (averaged over cylindrical coordinates), is equal to n_{ini}. We call
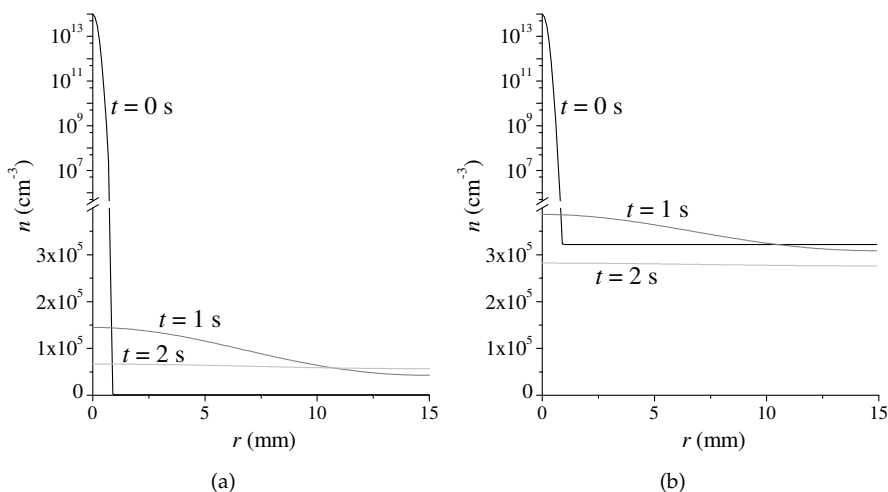
Figure 6.13: Ionization density as function of distance r to a streamer channel for different times t after the discharge. Results are for pure nitrogen at 200 mbar with 30 mm streamer spacing. Initial conditions include a background ionization level $n_{ini} = 1 \cdot 10^3$ cm^{-3} for (a) and $n_{ini} = 3.2 \cdot 10^5$ cm^{-3} for (b), both with the same central gaussian streamer trail at $r = 0$ (FWHM = 0.3 mm and $n_{channel} = 10^{14}$ cm^{-3}). Note that the vertical axis changes from a linear to a logarithmic scale at $n = 4 \cdot 10^5$ cm^{-3}.

this the equilibrium background ionization density, $n_{eq} = n_{ave} = n_{ini}$. Under the given conditions this is about $n_{eq} \approx 3 \cdot 10^5$ cm^{-3}. Results for the ionization density distribution with n_{eq} as initial background level are given in figure 6.13b. Here, at $t = 1$ s the ratio between centre and edge ionization density is only 1.25 and the FWHM of the trail is again about 15 mm. After 2 seconds, the profile is nearly flat with only 2% difference between the centre and the edge.

From these calculations, we can conclude that in a 1 Hz repetitive discharge, the ionization trail left over by the streamers from the previous discharge is quite weak. At its centre its ionization density is only 25% higher than in the periphery. One pulse (or second) later, the trail has completely disappeared.

At higher repetition frequencies, the trail remains more prominent. At 10 Hz, the equilibrium background ionization level is about $n_{eq} \approx 1.1 \cdot 10^6$ cm^{-3}. When keeping all other parameters the same as in the previous calculations, this will give a centre-to-edge ratio of about 5.

However, also at these higher repetition frequencies (e.g. 10 Hz) in our experiments we never observe that streamers take the same paths in subsequent discharges. Our camera system can only process about 1.4 frame per second so we can not record consecutive discharges at 10 Hz. Still, if streamers would (nearly)

always follow the same path between two discharges, one would expect that they (often) still follow the same path seven discharges later. So, even when we cannot record all discharge events, we can still conclude that there is no strong tendency for streamers to follow the path of their predecessors, even at 10 Hz repetition frequency where the centre of the previous channels has an ionization density that is about five times higher than the minimal ionization density.

Note that the equilibrium ionization densities n_{eq} as defined above are close to an order of magnitude lower than the ionization levels calculated with equation (6.11) for a homogeneous initial distribution. This because at the streamer core the ionization density and therefore the recombination rate are higher while for the homogeneous distribution assumed by equation (6.11) the rates will be lower for the same total amount of charged species. At 200 mbar nitrogen and 1 Hz, the result from equation (6.11) is $n \approx 2 \cdot 10^6$ cm^{-3} while for the same conditions $n_{eq} \approx 3 \cdot 10^5$ cm^{-3}. At 10 Hz repetition frequency, these values are $2 \cdot 10^7$ cm^{-3} and $n_{eq} \approx 9 \cdot 10^5$ cm^{-3} respectively. However, the value of n_{eq} depends on the assumptions for streamer channel width, channel separation and maximal streamer ionization density. For high streamer densities (wide channels or small channel separation), n_{eq} becomes equal to $(t \cdot k_{rec})^{-1}$. Furthermore, photo-ionization can also increase ionization levels outside of the streamer channels. As we do not have good estimates for channel densities and photo-ionization for all conditions, we have not calculated or used n_{eq} for other conditions and use values from $(t \cdot k_{rec})^{-1}$ with the realization that this is an upper bound.

6.4.2   Addition of ^{85}Kr

An explanation for the extra branches observed in pure nitrogen with added ^{85}Kr can be that they are in fact traces of ionization left by the fast electrons (beta-particles) from a radioactive decay of krypton-85 (see page 117 for decay rates). However, in this case one would expect that their orientation is fully isotropic. We do not observe this isotropic behaviour. The extra branches are always orientated in a small angle (less than 45°) to the propagation direction of the streamer channel they are connected to. Still, this can mean that the streamer channels orient themselves in such a way that they always connect to such a trace of leftover ionization, but this seems unlikely.

Another, more convincing explanation is that the main difference between the krypton-85 mixture and any other gas mixture we have used is that the krypton-mixture always contains "fresh" free electrons. With this mixture in our vessel, a radioactive decay occurs on average every 20 ns at 1000 mbar and every 100 ns at 200 mbar. These electrons are lost by attachment to trace amounts of oxygen in the gas mixture (equations (6.1) and (6.2)).
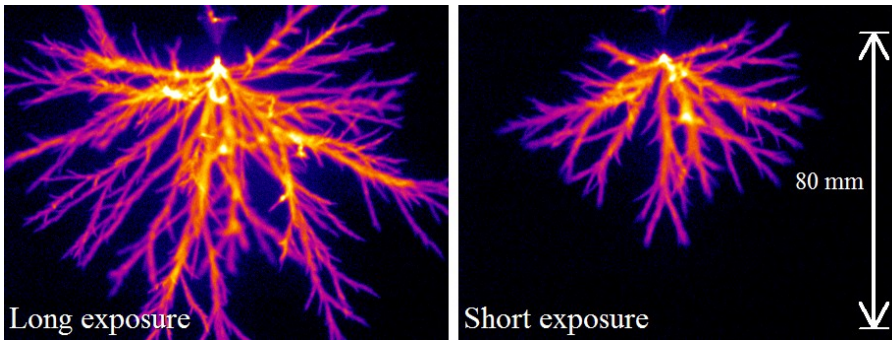
Figure 6.14: Overview images of streamer discharges in the nitrogen-krypton-85 gas mixture at 200 mbar made with the Blumlein pulser at 25 kV. The left-hand side image is made with a long exposure so that the whole discharge evolution is visible. For the right hand-side image, the camera exposure duration was reduced to roughly 65 ns (half of the pulse duration).

If we assume an oxygen concentration of 1 ppm, the attachment time at 200 mbar is about 0.5 s (see equation (6.5)). Therefore, most secondary electrons created by the beta particles are still free when a streamer discharge occurs. In other gas mixtures, most electrons that are left over after a previous discharge will be attached to ambient oxygen molecules and therefore require a higher electric field before they can start to create an avalanche towards the streamer head. Only electrons created by photo-ionization are free, but, at low oxygen concentrations, their density is low as well.

However, when we image a discharge in the krypton-mixture with a short exposure time, like in figure 6.14, we never see any "disconnected" parts of a streamer channel. If the long side channels in the krypton-mixture would be avalanches moving towards the streamer head, one would expect to see small starting channels visually separated from the main channels. This does not occur in our images; we see short and long channels that are always connected to another channel. This would indicate that the longer side-channels in the krypton-mixture are not avalanches themselves. Nevertheless, it is possible that if they are avalanches, they are not yet visible on the short exposure images because the lifetime of the excited states can be longer than the avalanche propagation duration. Therefore the avalanches have not yet emitted enough light to be observed before they attach to the parent streamer.

6.4.3   Conclusions

We have found that the background ionization levels can have a significant influence on streamer initiation, morphology and propagation. In pure gasses, at lower pulse repetition frequencies (which means lower background ionization levels), streamers branch more often and are more "feather-like" in appearance. This is probably due to the more stochastic nature of the discharge at lower background ionization levels. Lower ionization densities will lead to a lower avalanche density which more easily leads to instabilities in the streamer front and therefore to branching or feathers.

Background ionization left by previous discharges also influences the initiation probability. We have not performed an elaborate investigation into this phenomenon, but have found from our limited measurements that in nitrogen 7.0 at 0.01 Hz repetition frequency (estimated leftover ionization density $n \approx 2 \cdot 10^4 \, cm^{-3}$), the initiation probability is in the order of 10%, while at 0.1 Hz ($n \approx 2 \cdot 10^5 \, cm^{-3}$) it is more than close to 100%.

Theoretically, adding 10 ppb of ^{85}Kr to pure nitrogen at 200 mbar in our vessel should lead to a background ionization level of about $4 \cdot 10^5 \, cm^{-3}$. This value lies between the estimated background ionization levels corresponding to 1 and 0.1 Hz repetition frequency (closer to 1 Hz if we use n_{eq} which takes diffusion into account). In our measurements, we only observe differences in streamer morphology in the ^{85}Kr mixture between 1 and 10 Hz repetition frequency and not between lower repetition frequencies. This is in agreement with the estimated background ionization levels when one takes the expected accuracies of these estimations into account.

We observe that in the ^{85}Kr mixture more short streamer sections appear. These may be explained by the relatively high number of free electrons in this mixture. Electrons created by previous discharges will mostly be bound to oxygen atoms (even at very low oxygen concentrations) because of the relatively long time between two discharges. However, as radioactive decay occurs constantly, there will always be a higher number of "fresh" un-attached electrons available in a gas with radioactive additions than in a gas mixture without such additions. Nevertheless, as we have not observed separate avalanches moving towards the streamer stem in short exposure imagery, we are not fully convinced that this hypothesis can explain the extra branches in the ^{85}Kr mixture.

We have not observed any tendency of streamer channels to follow the same path as streamers in preceding discharges. Therefore, we must conclude that streamer channels are relatively insensitive to exact background ionization levels. They do not follow paths of increased negative ion density. From calculations of diffusion and recombination after a streamer discharge, we have found that 1 second after a streamer discharge, the path of increased ionization left by a

streamer has become much wider than the original streamer and that the maximal ionization density on this path is only slightly above the space-averaged value.

In general, our findings are in agreement with theoretical and modelling observations by Pancheshnyi [156], Bourdon *et al.* [27] and Wormeester *et al.* [236]. They all find large contributions of background ionization (mainly due to attached electrons) on different aspects of streamer propagation and initiation. Our experiments with adding radioactive ^{85}Kr to pure nitrogen and the comparison with streamer discharges at different repetition frequencies have confirmed that indeed background ionization levels play an important role in streamer propagation, but that their influence on propagation velocity and minimal streamer diameter is very limited. Unfortunately, we have not been able to measure background ionization levels directly and we can only use theoretical estimations for the charge density levels.

Chapter 7

Streamers in other gasses

7.1 Introduction

In order to get more insight into positive streamer propagation, we have studied more than just the nitrogen-oxygen mixtures discussed in the previous chapters. We have studied pure oxygen, argon, helium, hydrogen and carbon dioxide. Each of these gasses has different properties like ionization levels, excitation levels, cross sections and electronegativity. Molecular mass and ionization levels of these gasses are given in table 7.1.

Nitrogen is a non-attaching gas and argon and helium are not electronegative. Free electrons will therefore not attach to these three gasses. Oxygen, carbon dioxide and (to a lesser extent) hydrogen have cross sections for dissociative attachment which can remove electrons and influence electron kinetics significantly. At high pressures, 3-body attachment in oxygen can be an additional source of negative ions, which can, through auto-detachment, be the additional source of free electrons necessary for positive streamer propagation as was discussed in the previous chapters.

The compositions of the gasses and mixtures that are used in this chapter are given in table 7.2. We refer to gas purity in a notation that gives the number of nines in the purity, so 4.0 purity means >99.99% purity.

Besides helping us understand the physics of streamers, some of these measurements can also help in the study of extra-terrestrial sprites. We therefore investigate sprites on Venus and Jupiter by means of creating streamer discharges in gas mix-

---

Sections 7.2 and 7.3 in this chapter are largely based on Nijdam *et al.*, J. Phys. D: Appl. Phys. **43**, 145204 (2010), while section 7.7 is largely based on Dubrovin *et al.*, J. Geophys. Res. - Space Physics **115**, A00E34 (2010).

Table 7.1: Properties of the pure gasses discussed in this thesis. Data from [106, 107].

Gas	Mass (a.u.)	Ionization level (eV)
N_2	28.01	15.58
O_2	32.00	12.07
Ar	39.95	15.76
He	4.00	25.59
H_2	2.01	15.43
CO_2	44.01	13.77

Table 7.2: Gas impurity levels of relevant gasses as provided by the gas supplier. Impurity levels are given as upper limits in parts per million (ppm), n/a indicates that no number is specified by the supplier. Helium is excluded from this table as it is never specified as impurity by the supplier. It is dosed at ≈100% for helium 6.0 and at ≈10.2% for Jupiter.

Gas	N_2	O_2	Ar	H_2O	H_2	CO_2	CO	C_nH_m
Oxygen 5.0	5	≈100%	3	3	n/a	n/a	0.2	0.1
Oxygen 6.0	0.5	≈100%	1	0.5	n/a	0.1	0.1	0.1
Argon 5.0	5	2	≈100%	3	n/a	n/a	n/a	0.2
Helium 6.0	0.4	0.2	n/a	0.5	100	n/a	n/a	0.1
Hydrogen 6.0	0.3	0.2	n/a	0.5	≈100%	0.05	0.05	0.1
CO_2 5.3	3	1	n/a	3	n/a	≈100%	n/a	1
Venus mixture	≈3.5%	1	n/a	3	n/a	≈96.5%	n/a	1
Jupiter mixture	0.3	0.2	n/a	0.5	≈89.8%	0.05	0.05	0.1

tures that correspond to the planetary atmospheres of Venus and Jupiter, CO_2-N_2 (96.5%-3.5%) and H_2-He (89.8%-10.2%), respectively. The mixtures' compositions are based on the National Space Science Data Center (compiled by Williams [228]). Results from these measurements are discussed in section 7.7. The measurements in pure carbon dioxide, nitrogen, hydrogen and helium can assist in understanding the properties of these planetary discharges as well.

7.2   Pure oxygen

The images of pure oxygen (figure 7.1) are more noisy than all other overview images because of the low brightness of the streamers, which requires high multiplication factors. To take the images we had to increase the gain of the ICCD camera close to its maximum level. The intensity of the streamers in pure oxygen is two to three orders lower than in most other gasses. When the voltage of the pure oxygen measurement at 1000 mbar would have been around 25 kV as it is for

the other gasses, this difference would have been even larger. However, at 25 kV nothing could be seen and therefore we have used a 59.4 kV image. At 200 mbar, the situation was similar. Here we used 28.9 kV for oxygen and around 10 kV for other gasses.

Because of the low intensity of the streamers, we were unable to determine streamer diameters or propagation velocities. Note that the measured intensity also depends on the emission spectrum, as a camera (always) has a wavelength dependent response. Our camera is sensitive between 200 and 800 nm. However, because of the ITO glass in our Faraday cage, radiation below 300 nm is cut off (see figure 3.16).

The low intensity of the streamers in oxygen can be explained by the lack of emission lines from oxygen in the sensitive region of the camera (see also sections 3.4.2 and 8.4.1). The strongest line at 777 nm is close to the limit of the camera sensitivity curve. This makes it nearly impossible to do any quantitative research on streamers in pure oxygen with our camera. The images at pressures above 50 mbar are not suitable for diameter or velocity measurements. At high pressures it is often even difficult to determine if streamers are present or not. Therefore we will not present any other data on pure oxygen streamers.

7.3 Pure argon

Aleksandrov *et al.* [10] have performed experiments on streamers in pure argon (4.0 purity) and a mixture of 1 to 5% oxygen in argon, all at atmospheric pressure. They present streak photography of discharges in a 250 mm rod-plane gap with 10 to 60 kV voltage pulse with 1 µs risetime. They conclude that a non-thermal mechanism of streamer breakdown in the case of argon discharges gives way to leader breakdown when 1% or more of oxygen is added. This addition also leads to a decay of the streamer channel that is an order of magnitude faster and therefore a noticeable higher electric field is needed for the streamers to bridge the gap. Their simulations show that this can be explained by the quenching of excited argon molecules by oxygen molecules. Note that what Aleksandrov *et al.* call a leader may in fact better be described as a secondary streamer (see section 2.3.3).

Van Veldhuizen and Rutgers [222] have used air and argon. They found that streamers in argon branch less and can only be produced in a narrow voltage range which is lower than in air and pure nitrogen. This low maximal voltage is required to prevent breakdown. With shorter voltage pulses like those produced by our Blumlein pulser it is possible to use higher voltages and still prevent breakdown.
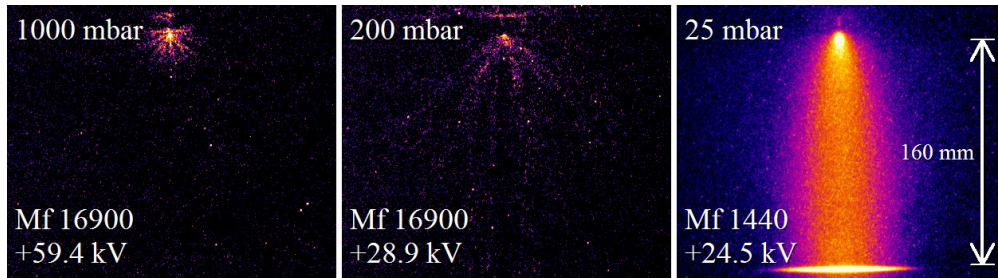
Figure 7.1: Overview of streamer discharges in oxygen 6.0, produced with the C-supply at 1000, 200 and 25 mbar. The measurements have a long exposure time and therefore show one complete discharge event, including transition to glow for 25 mbar.
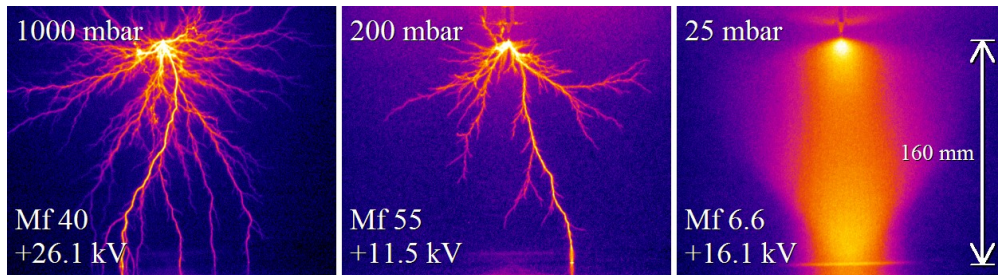
Figure 7.2: Overview of streamer discharges in argon 5.0, produced with the C-supply at 1000, 200 and 25 mbar. The measurements have a long exposure time and therefore show one complete discharge event, including transition to glow for 25 mbar. Additional images with other voltages are given in figure B.1.

Results and discussion

Pure argon has a significant light emission intensity and yields good quality camera images. In comparison to the other gasses, it branches much more, but most branches are very short (see figure 7.2 as well as figure 5.5). It also develops easily into a spark, which means that we have to take care that the voltage pulse remains short enough to avoid this (we did not use the Blumlein pulser with its short pulses to create images in argon). In the 1000 and 200 mbar images it can already be seen that one channel is much brighter than the others. This bright channel is the reason why we could use the relatively low *Mf* values for argon at these pressures. This near-sparking behaviour is frequently observed in argon discharges.

The feather-like structure of streamers in argon (see section 5.4) makes it impossible to determine a clear diameter of streamer channels. In order to determine the propagation velocity in argon, the second method discussed in section 3.4.3 must be used due to the long emission time after impact excitation. It must be noted

that the usable voltage range (for the C-supply) is limited to only a few kilo-volts: if the voltage is too low there is no discharge at all and if the voltage is too high we get a spark that can potentially damage the camera. Therefore, we only have measured the velocity at one voltage for argon (see figure 7.4). This velocity is a bit lower than in most other gas mixtures, but not much more than the measurement uncertainty.

The easy sparking and heavy branching is probably due to the fact that argon is a noble gas without rotational or vibrational degrees of freedom. Therefore there are few inelastic collisions at low electron energies, and hence impact ionization becomes effective at much lower field strengths $|E|$ than in nitrogen or oxygen. The impact ionization coefficient $\alpha_i\left(|E|\right)$ is more than 2 orders of magnitude larger for argon than for nitrogen at fields below 30 kV/cm at atmospheric pressure [1].

7.4   Pure helium

Akishev *et al.* [7] have studied corona barrier discharges in pure nitrogen, argon and helium as well as in air. In their experiments, they use a paraboloidal tip mounted 1.5–30 mm above a metal disk that is covered with a polymer film. They use the gasses at atmospheric pressure and apply a 50 Hz to 50 kHz sinusoidal voltage with amplitudes up to 35 kV to the tip. They have found that the radius of the discharge in helium is smaller than in argon at elevated voltages. However, as they do not use a fast camera, their images include all discharge stages of multiple pulses (including glow discharges) and therefore this radius can not be compared to the diameters of minimal streamer channels that we measure.

Éfendiev and Aliverdiev [53] have also studied streamer-like discharges in helium, but they did not investigate streamer properties like diameter and propagation velocity.

Many experiments have been performed on other non-thermal atmospheric pressure plasmas in helium, like glow discharges (e.g. Bruggeman *et al.* [37]), microjet discharges (e.g. Kim *et al.* [88]) or dielectric barrier discharges (e.g. Abolmasov *et al.* [4]). However, these discharges are very different from the streamer discharges discussed here.

Results

We have found that streamers in pure helium (6.0 purity) are generally bright and wide. They initiate at low voltages. Even at 1000 mbar we have observed streamer initiation with a 6 kV pulse[1] in our 160 mm gap. Overview images of streamers in

---

[1]5–6 kV is about the minimum practical voltage of our C-supply.
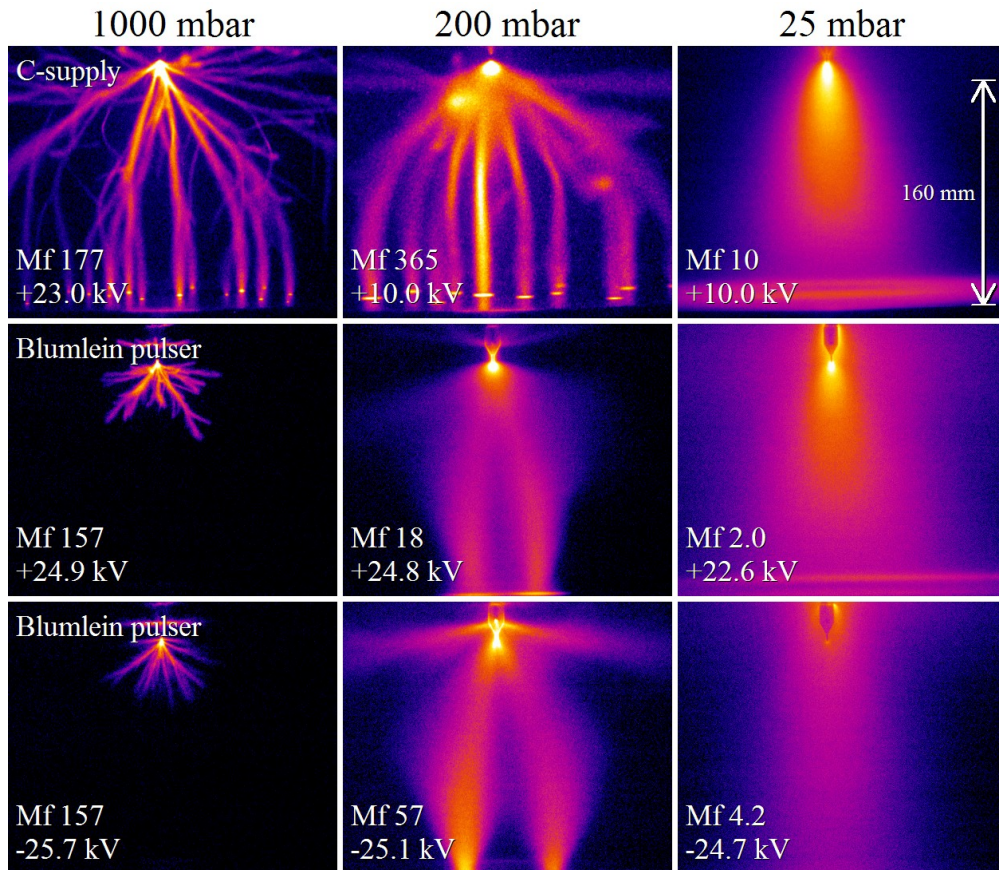
Figure 7.3: Overview of positive (top and middle) and negative (bottom) streamer discharges in helium 6.0, produced with the C-supply (top) and Blumlein (middle and bottom) pulsers at 1000, 200 and 25 mbar. The measurements have a long exposure time and show one complete discharge event, including transition to glow.

pure helium are given in figure 7.3. In this image sequence, the 1000 mbar images resemble streamer discharges in other gas mixtures at 200 mbar (e.g. air and pure nitrogen), while the 200 mbar images resemble 25 mbar images in other gasses.

At 25 mbar, 22 kV, there is no longer a real streamer channel (it probably has a diameter comparable to our discharge vessel). Instead, we only observe a transient glow discharge that encompasses the complete vessel and is especially bright around the needle tip and needle holder (the anode) in the positive discharge. Since the streamer is so wide, it is impossible to determine its diameter at this pressure. At 25 mbar, 10 kV similar behaviour is observed, although to a lesser extent.

136
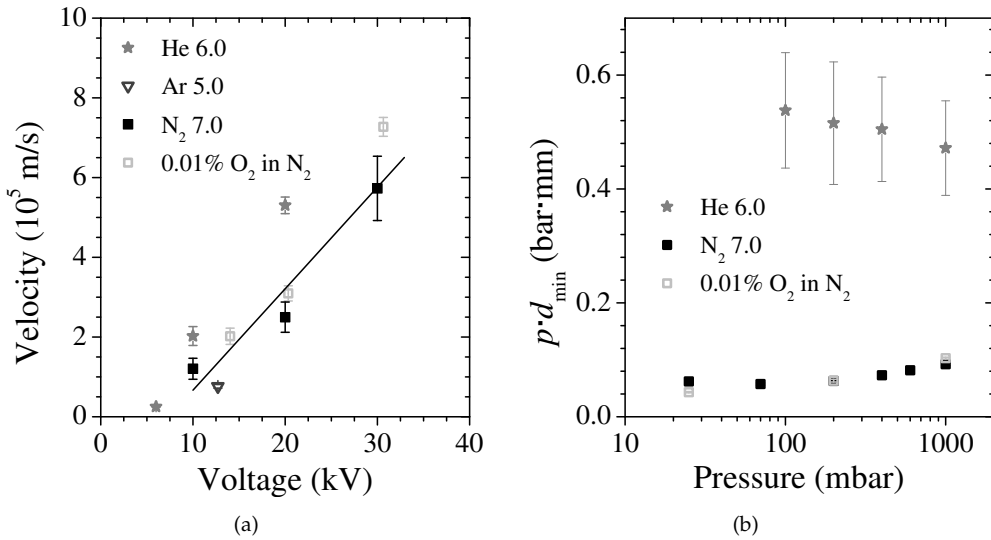
Figure 7.4: Streamers created with the C-supply: a) velocities as a function of voltage at 200 mbar and b) reduced minimal streamer diameters as a function of pressure for helium 6.0, argon 5.0 (only velocity) as well as for two other gasses, all made with the C-supply. The error bars indicate the sample standard deviation. The line in a) is a linear fit through all the points from figure 5.4. More diameter measurements in nitrogen-oxygen mixtures are shown in figure 5.3.

At 1000 mbar the streamer channels in pure helium are relatively straight and do not branch much (when compared with e.g. pure nitrogen or argon). However, in contrast to most other pure gasses we have tested, the channels become wider as they travel away from the anode tip. In all other gas mixtures, streamer widths remain roughly constant between branching events. An exception may be hydrogen, but the low intensity of the discharges in this gas makes it difficult to observe whether the streamers widen. The negative streamers are visually quite similar to the positive streamers.

The propagation velocity and minimal diameter of streamers in helium are shown in figure 7.4. It is clear that both velocity and diameter are larger in helium than in any of the other gas mixtures we have tested. The propagation velocity is roughly double that of other gasses, while the reduced diameter is a factor 4 to 8 higher. Note that helium is the only gas for which we have been able to measure the propagation velocity at 6 kV (at 200 mbar) because of its very low inception voltage. The minimal diameters of streamers in helium have all been determined at 5–6 kV (for other gasses higher voltages were used to ensure streamer inception). We have not been able to measure the reduced diameter below 100 mbar as this resulted in an initiation cloud that covered most of the gap distance and therefore

no real streamer channels occurred. The same is observed with other gasses below 25 mbar.

Some more results from measurements in pure helium can be found in the traineeship report by Guillaume Caillault [39].

Discussion and conclusions

The reason for the large width of the streamers in helium is probably related to the small cross-section for elastic electron-neutral collisions of helium atoms (below 5×10^{-19} cm^2 at electron energies below 20 eV [1]). Other species, especially molecules, have larger cross-sections at lower electron energies. The species that we have investigated that is closest to helium is argon. Its elastic cross-section is still about 1×10^{-17} cm^2 at 12 eV electron energy. However, because of the very high ionization potential of helium (24.6 eV), we also expect higher electron energies in helium-dominated streamer discharges than in other gas mixtures.

Because of the small cross-section, the mean free path for electrons will be large. As the mean free path scales with inverse density, the large mean free path in helium explains why the helium streamers appear like streamers in other gasses at lower pressures.

The large width of streamers in helium contradicts the findings by Akishev *et al.* [7]. They observe smaller diameters in helium than in argon discharges. However, their total discharge duration is much longer than ours (milliseconds versus microseconds). Therefore they only observe time-integrated images. Furthermore, they study the radius at the surface of a dielectric instead of in the bulk gas. For these reasons their results can not really be compared one on one with our results.

7.5 Pure hydrogen

Streamer discharges in pure hydrogen have been studied in the past by Weissler [226]. He found that streamers did occur in this gas in a 31 mm gap at atmospheric pressure with 3.5 kV DC supplied.

Unfortunately, we have only a small set of measurements in pure hydrogen. The main reason for this is the small amount of hydrogen gas that was available for our experiments. Therefore we have only been able to perform some quick experiments. Nevertheless, we still want to show the results of these measurements, as they can be useful in the understanding of the properties of streamers in Jupiter atmosphere that is discussed in section 7.7.

We have found that streamer discharges in pure hydrogen are fainter than similar discharges in most other gasses, although they are not as faint as discharges
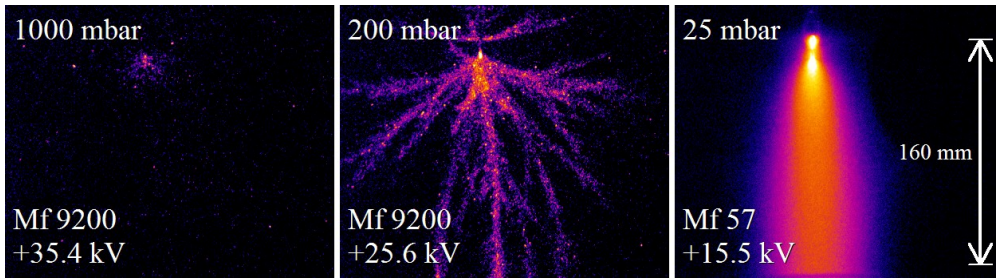
Figure 7.5: Overview of streamer discharges in hydrogen 6.0, produced with the Blumlein pulser at 1000, 200 and 25 mbar. The measurements have a long exposure time and show one complete discharge event, including transition to glow for 25 mbar.
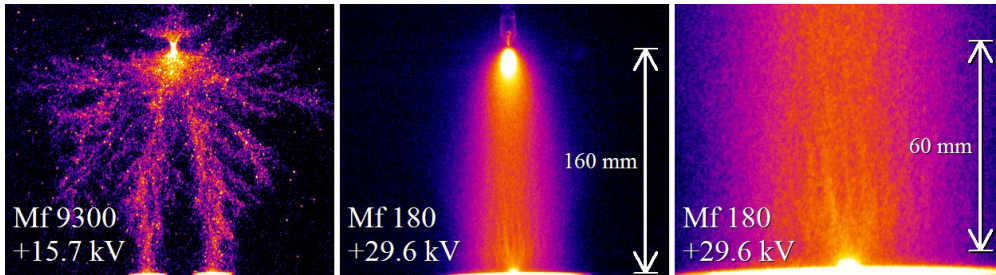
Figure 7.6: Overview of streamer discharges in CO_2 5.3, produced with the Blumlein pulser at 25 mbar. The first two images show the full discharge gap while the rightmost image is a zoomed version of the bottom area of the central image.

in pure oxygen. However, the general morphology (see figure 7.5) of these discharges is similar to streamers in air and nitrogen-oxygen mixtures. No feather-like structures have been observed, although they could be hidden by the low intensity of the emitted light.

7.6 Pure CO_2

Streamers in pure CO_2 are again very dim (see figure 7.6). Because of limited time and gas-supply, we have only investigated streamers at 25 mbar in this gas. In this gas, at lower pulse voltages (below ∼20 kV), a multichannel streamer tree is observed with feather-like characteristics, somewhat similar to discharges in pure argon, but without the tendency to have one channel that is brighter than all others.

At pulse voltages above 20 kV, a single channel is formed, without a feather-like structure. However, in contrast to channels at similar conditions in other

gasses, this single channel contains a filament-like internal structure and ends in a constricted spot within a larger spot. We have not investigated the exact nature or cause of this structure. Similar filamentation in CO_2 was seen by Janda and Machala [85] in high frequency (1–10 kHz) discharges above a water surface. However, their images are obtained with long (1–4 s) exposure times and therefore may not represent a single pulse discharge very well.

Like oxygen, carbon dioxide has a high electron affinity and therefore impedes formation of discharges, especially transient discharges, as free electrons are easily lost. More results from measurements in pure CO_2 can be found in the traineeship report by Karsten Miermans [133].
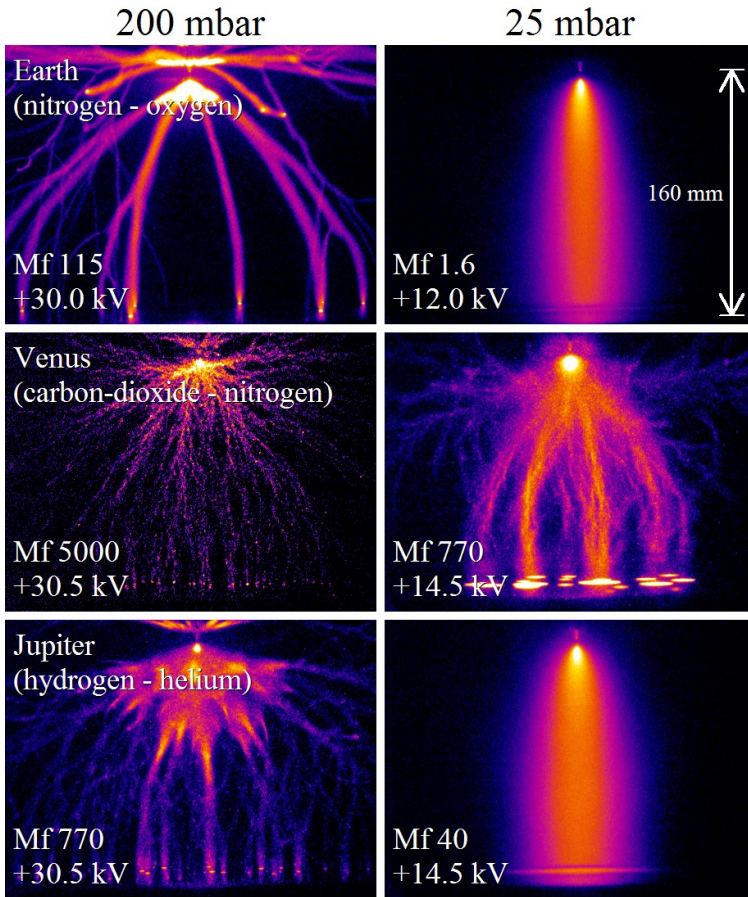
7.7   Planetary gasses

We have used two different gas mixtures to simulate streamer (or sprite) discharges on other planets. The mixtures are pre-mixed by the supplier: a mixture (Venus) that consists of 96.5% CO_2 and 3.5% N_2 and a mixture (Jupiter) that consists of 89.8% H_2 and 10.2% He. According to the specifications, the contamination level is below 1 ppm for both mixtures (see table 7.2).

We were able to observe streamers in both Venus and Jupiter atmosphere gas mixtures. In figure 7.7 we show examples of the streamers we observed. The voltages in this figure are well above the inception voltage, the minimal applied voltage that is required to create a streamer. Examples of streamers close to the inception voltages are shown in figure 7.8. Increasing voltage, or decreasing pressure causes the discharge to be brighter and less filamentary. When planetary mixtures are compared, we notice that the initiation of streamers in both our gasses requires higher voltages than in air at the same pressure. In the Venusian mixture streamers are particularly difficult to create. For example, at 800 mbar a minimal voltage of approximately 20 kV is required to initiate a streamer discharge. At this voltage the streamer dies out before it bridges the gap. At the same pressure, streamers in the Jovian mixture are created at voltages below $\sim$15 kV. These streamers do not cross the gap either. Likewise, streamers at 1 bar in dry air can form when the applied voltage is as low as $\sim$10 kV, as was shown by Briels *et al.* [33] in a similar set-up.

Both in air and in the Jovian mixture, H_2-He, a single wide channel is formed when the pressure is below 50 mbar. In the Venusian mixture, CO_2-N_2, the filamentary streamer structure persists at the lowest pressures, very similar to the observations in pure CO_2 as discussed above. Several channels conduct most of the current in the glow phase, as indicated by their strong intensity in the images. The light emission is usually too weak to be observed by the naked eye, except at the lowest pressures, below 100 mbar. In the Venusian mixture the streamers tend

Figure 7.7: Overview of streamer discharges produced with the C-supply for artificial air and the two planetary gas mixtures, at 200 and 25 mbar. All measurements have a long exposure time and therefore show one complete discharge event, including transition to glow for 25 mbar.

to be bluish-green in colour, and in the Jovian mixture they seem to be pink.

The images in figure 7.7 are long exposure images taken at voltages that are relatively high when compared to the minimal inception voltages at the corresponding pressures. Under such conditions the streamers bridge the gap and conduct enough current to create the glow phase. When voltage is set as close as possible to the inception voltage value, the glow phase does not appear. An example is shown in figure 7.8, that shows the streamer channels, and no indication of a glow phase. Note the different applied voltages, indicated at the bottom of each image, in the Venusian mixture the inception voltage is higher than in the Jovian mixture. This difference persists in other pressures as well. We note that
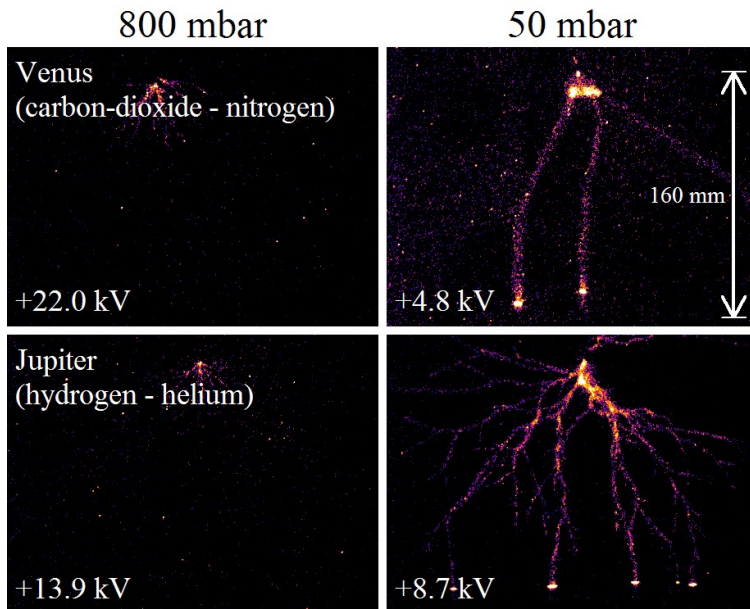
Figure 7.8: Overview of streamers at or slightly above inception voltage at pressures of 50 and 800 mbar in the Venus and Jupiter gas mixtures. The light emitted by the streamer is very weak, which required the use of the maximum gain voltage (950V) in our camera. Therefore all images have an *Mf* value of about 18500. This also accounts for the many specs in the images, which are most likely due to noise from the ICCD camera. The bright dots at the bottom of the picture are the points where the streamers reach the plate electrode.

the Jovian streamers have much less branches than the Venusian streamers, under very similar conditions.

The morphological differences between the streamers in the two mixtures are probably due to two properties of the gasses, (*i*) their atomic or molecular structure, and (*ii*) the photo-ionization mechanism. We here recall the basic mechanisms, that will have to be elaborated further in future work. (*i*) A noble gas like He or Ar consists of single atoms, N_2 and H_2 are molecular gasses consisting of two atoms, and CO_2 consists of three atoms. The molecular gasses, and in particular CO_2, have many rotational and vibrational states at low energies that can absorb the energy of colliding electrons; therefore the electrons experience more friction than in noble gasses. Furthermore, He and H_2 have only two electrons each which results in only few electronic excitation states. For this reason, streamer propagation is much easier in Jovian than in Venusian or terrestrial atmospheres. (*ii*) Positive streamers as investigated here move approximately with the electron drift velocity, but against the direction of electron drift; therefore they depend on a source of free

electrons ahead of the ionization front. These free electrons can be supplied either by a non-local photo-ionization effect or by background ionization.

In nitrogen-oxygen mixtures the photo-ionization process is attributed to several nitrogen emission lines in the wavelength range 98-102.5 nm. These photons are energetic enough to ionize oxygen molecules at $\sim$12 eV. This photo-ionization takes place after some travel distance that depends on the oxygen concentration; thus it is a non-local process. On Venus, CO_2 requires a slightly higher ionization energy of $\sim$13 eV. The nitrogen molecule does not have emission lines that are energetic enough to ionize this molecule in a one-step process. Therefore other, less effective processes like background ionization or two-step photo-ionization must account for streamer propagation in the Venusian mixture. With the low photo-ionization efficiency in the streamer head, it becomes less stable and more likely to branch. The picture in the Jovian H_2-He mixture is completely different. There is a large gap between the ionization energies of the hydrogen molecule and helium. A photon with a wavelength below 77.5 nm is energetic enough to ionize the hydrogen molecule at $\sim$16 eV. The helium atomic spectrum has a group of lines in the range 50.7-58.4 nm that can produce photons with enough energy to ionize the hydrogen molecule in a one step process. Assuming that the photo-ionization process is effective in the H_2-He mixture, one is not surprised to find that the streamer heads are as stable as they are. Nevertheless, for both gas mixtures, it is possible that impurities play an important role in streamer propagation, as they do in "pure" nitrogen (see chapter 5). Ionization and atomic spectral data in this paragraph are taken from the NIST database ([174] and [107]).

The optical brightness of the streamers in both gasses is considerably weaker than many other of the gasses used (ambient air, nitrogen–oxygen mixtures and argon). Our setup is not calibrated to estimate absolute optical brightness, however a rough estimation of the relative intensity of planetary streamers to streamers in air is possible. The pixel grey level in an image is proportional to the light intensity and depends on the camera settings. We can estimate the ratios between average intensities per area in different gasses, with the following method: we record short exposure images using the same equipment and under the same pressure and voltage conditions. We evaluate the averaged grey level per area of the streamer sections in these images. Our estimation shows that the optical brightness of both Jovian and Venusian streamers appears to be about a 100 times weaker than of streamers in air at similar pressures. A similar method is used to estimate the brightness of terrestrial sprites [242]. Averaged intensity per area depends on pressure, at lower pressures streamer images are brighter in all gasses. These findings depend on equipment choice, since they are measured with the specific wavelength sensitivity curve of our equipment. So a very bright line at the edges or outside of this curve is not observed, but could be observed when other equipment is used, as was discussed above for pure oxygen.
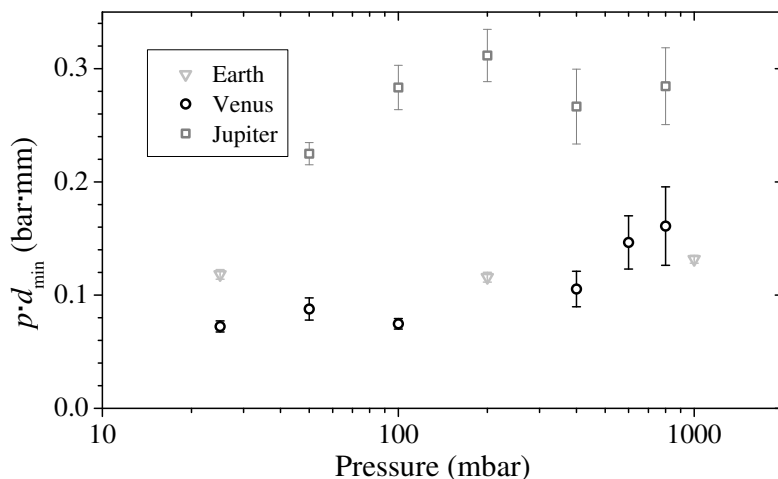
Figure 7.9: Minimal diameter, $p \cdot d_{min}$, of streamers created with the C-supply as a function of pressure, at room temperature in binary gas mixtures representing earth, Venus and Jupiter. The errors are determined as the maximum between the image resolution and the standard error. Higher pressure measurements are dominated by the resolution error, while lower pressure measurements are dominated by the standard error. More diameter measurements in nitrogen-oxygen mixtures are shown in figure 5.3.

Diameter and Velocity

Figure 7.9 shows the reduced minimal diameter, $p \cdot d_{min}$, as function of pressure in the two gas mixtures and air. As expected, the reduced minimal diameter depends very weakly on pressure. In the Jovian mixture $p \cdot d_{min} \approx 0.26$ mm·bar and in the Venusian mixture $p \cdot d_{min} \approx 0.09$ mm·bar. These values are of the same scale as values measured by Briels *et al.* [34] in air and nitrogen and reported above in argon and in oxygen–nitrogen mixtures of varying concentration. The average reduced diameter in dry air is ~ 0.12 mm·bar (see section 5.3.2).

We can summarize that the values of $p \cdot d_{min}$ of the streamer head in the CO_2-N_2 mixture, in air and in pure nitrogen are quite similar. In the H_2-He mixture the value of $p \cdot d_{min}$ is twice to three times as large, but still only half as large as in pure helium (see figure 7.4). We have not been able to measure streamer diameters in pure hydrogen or CO_2. It is likely that the Jovian mixture is ionized more easily than the mixtures that represent Venus and Earth, as well as pure nitrogen, creating wider and possibly faster streamers.

We made preliminary measurements to estimate the minimal streamer velocity. We recall that theoretically the streamer velocities do not depend on density when similarity laws apply, as discussed in section 2.3.2. In all the pressures, in both

mixtures, the measured minimal velocity is of order of 10^5 m/s. Our best estimation in the Venusian mixture is $\sim 0.80 \pm 0.04 \times 10^5$ m/s in 800 mbar, and in the Jovian mixture it is $1.00 \pm 0.05 \times 10^5$ m/s in 50 mbar. Briels *et al.* [34] report similar values in other gas mixtures, such as air as have we shown in section 5.3. Velocities of 10^5 to 10^7 m/s were measured in sprite tendrils by means of high temporal resolution observations of terrestrial sprites ([128, 140, 199]).

Measurements by Briels *et al.* [33] in air as well as the measurements presented in section 5.3.3 demonstrate that the velocity depends more strongly on the applied voltage, than the diameter.

According to Yair *et al.* [240], sprites are expected on Venus at altitudes between 80 and 90 km above the surface, and on Jupiter at $\sim$300 km above the 1 bar level. At these altitudes the pressure is 5 to 0.4 mbar on Venus, and of the order of 10^{-3} mbar on Jupiter. The streamer minimal diameter at such pressures according to our measurements are expected to be 0.2-0.02 m, and 300 m respectively. The sprite tendrils may in fact be quite wider, as they do not need to be minimal. For example, based on the value of $p \cdot d_{min}$ measured by Briels *et al.* [34] in air, minimal sprite tendrils on Earth should be roughly 20 m wide. However observations report tendrils as wide as $\sim$150 m (Gerken and Inan [64]). On the other hand, sprite or streamer channel diameters are easily overestimated. We have observed that measured diameters depended on zoom ratio (they became smaller at higher zoom levels) up to a streamer diameter (FWHM) of about 10 pixels. The width of smaller streamers is usually overestimated.

7.8   Conclusions

We have observed streamers in a previously unexplored set of gasses in controlled laboratory settings. These gasses include the atmospheres of Venus and Jupiter-like planets as well as pure oxygen, argon, helium, hydrogen and carbon-dioxide. We have compared this to results in air, pure nitrogen and other nitrogen-oxygen mixtures. We have demonstrated that streamer discharges are possible in all of these gasses. For the planetary gasses, this gives firmer ground to our hope of observing sprites on these planets. We have explored some features of these discharges, such as the inception voltages, the minimal diameter and velocity of the streamer heads and their intensity as compared to the optical brightness of streamers in air. We find that the streamers in these gasses follow scaling laws as expected. We demonstrate that the reduced minimal diameter, $p \cdot d_{min}$ does not depend on pressure.

With regards to brightness, we can recognize three rough groups: nitrogen-oxygen mixtures, nitrogen, argon and helium are all relatively bright, hydrogen and the Jovian mixture are one to two orders of magnitude dimmer and oxygen,

CO_2 and the Venusian mixture are again one to two orders dimmer. Note that this brightness comparison is only valid for the wavelength range of our optical system. The main reason for the variations in brightness between different gasses are the positions of relevant emission lines. As nearly all radiation in a streamer discharge is produced by atomic or molecular emission lines, lack of lines in the visible region (like e.g. in pure oxygen) will lead to very dim streamers. Another major factor that can influence brightness is quenching of excited states by collisional de-excitation. This process is pressure dependent and becomes more important at higher pressures. The emitted spectra of all gasses discussed here will be shown in the next chapter.

We can recognize two groups with regards to streamer shapes. Nitrogen-oxygen mixtures, helium, hydrogen and the Jovian mixture all show quite straight streamer channels while argon, pure nitrogen, CO_2 and the Venusian mixture show feather-like behaviour like discussed in section 5.4. Because of their very low brightness we can not judge the exact shape of streamers in pure oxygen.

The reduced minimal diameter in all the gasses is of the same order of magnitude except for pure helium which has a minimal diameter that is about four to eight times larger than the other investigated gasses. In the Venusian mixture it is very close to the reduced diameter in air that was reported by Briels *et al.* [34] and found in this chapter, but it is twice as wide in Jupiter. Hence, the diameter is influenced by the composition of the gas. Some considerations on the physical origin of these differences, like electron friction and photo-ionization versus background ionization, are discussed above. Based on our reduced minimal diameter measurements, and the sprite altitudes estimated by Yair *et al.* [240], we predict that sprite tendrils on Jupiter will be at least 300 m wide, and of the order of a meter wide on Venus.

Most important in terms of the search for planetary sprites is the fact that the streamers in both planetary mixtures emit much less light than in air, and that they require higher inception voltages, particularly in the Venusian mixture. Therefore, planetary sprites can be expected to have similar morphology to terrestrial sprites, but they might be significantly weaker in optical brightness and require a larger charge moment of the parent lightning. Recently, Takahashi *et al.* [205] have shown that there is a high correlation between sprite optical intensity and the charge moment change of its parent flash. These considerations should be taken into account if a more detailed scheme for predicting sprite altitudes than the one proposed by Yair *et al.* [240], is to be employed.

Chapter 8

Spectroscopic measurements

8.1   Introduction

An often employed method for studying properties of plasmas is optical emission spectroscopy. It yields information regarding many different plasma parameters like composition, different temperatures (e.g. electron, rotational, vibrational), electric field and densities of species. Some well-known examples of passive optical spectroscopy methods are absolute and relative line intensity measurements, absolute continuum measurements and line broadening determination.

General advantages of optical emission spectroscopy are that it is non-intrusive and relatively simple and inexpensive. Therefore, this technique can also be employed to study natural phenomena like sprite discharges, where active techniques are difficult or impossible to apply. The main disadvantage of such passive measurements is that they integrate emission over the entire line of sight and that the processing is indirect and therefore often needs assumptions or models which may be debatable.

Lines in spectra of atomic gasses are often easy to determine, especially for lighter elements. They come from electronic transitions between excited atomic levels and are usually quite narrow (too narrow to resolve with the equipment we used). Molecular spectra, on the other hand, can be much more complex. Their lines (in the visible and neighbouring wavelengths) are also primarily created by transitions between electronic excitational levels. However, these lines are heavily affected by vibrational and rotational quantum levels of the molecules. Therefore, a single electronic transition is often split in many vibrational and rotational lines.

The sections regarding planetary gas mixtures in this chapter are largely based on Dubrovin *et al.*, J. Geophys. Res. - Space Physics **115**, A00E34 (2010).

These lines can have large widths and overlap, together forming a complex band system.

Here we use optical emission spectroscopy for a combination of purposes. First, we use the spectra to get information about the important species in the discharge and about the role of impurities. Second, we fit some spectra of streamers in air to get a rough estimate of relevant temperatures. Finally, the spectra of streamers and sparks in air and gas mixtures that simulate the atmospheres of Venus and Jupiter can be used for the planning of (space) missions to study lightning and sprites on theses planets, as well as for the interpretation of the data gathered during these missions. I.e. they make it possible to distinguish between sprites and lightning by carefully chosen wavelength filters on detectors.

8.1.1   Spectroscopic measurements on streamers

As is visually shown in many images in the preceding chapters, most streamer discharges emit enough light to be clearly visible by an intensified CCD (ICCD) camera. However, in most cases, the total amount of light is still very low; most streamers are hardly visible to the naked eye in a darkened room.

Another challenge in streamer spectroscopy is the fact that they move very fast. The propagation velocity of the streamers treated in this thesis is of the order 10^5–10^6 m/s. Furthermore, the size of the streamer heads is quite small, from tens of micrometres to a few millimetres thickness. This means that all spectroscopic measurements with exposures longer than some tens of nanoseconds will detect emissions not only from the streamer head, but also from the tail. For exposures longer than the crossing time of the streamers, additional emissions from a glow discharge that follows the streamer discharge will also be acquired. At lower pressures (e.g. 25 mbar), such a glow discharge often emits much more light than the streamers. This can be seen clearly in figure 5.8.

Finally, at higher pressures (or larger gap distances) streamer discharges can contain many separate streamer channels that follow unpredictable paths. In our set-up with a 16 cm point plane gap we mostly observe one channel at 25 mbar and more channels at higher pressures (the number of channels also depends on the applied voltage amplitude and shape). This makes it impossible to capture the emission spectrum of one streamer at these higher pressures, as it is impossible to determine which path the streamers will follow exactly. Only at short gap distances or low pressures, when there is only one channel present (see for example the 25 mbar images in figure 5.2) is it possible to predict the exact position of the streamer channel.

All three challenges discussed above (low intensity, short timescales and multiple channels) make it difficult to measure a good spectrum of a propagating

streamer. If one wants to acquire the signal of a single streamer, only a small gap or low pressure can be used ($p \cdot d$ should be small). If one wants to only acquire light emitted by the propagating streamer head, a fast gate-able detector like an ICCD or photo-multiplier is required. The low amount of emitted radiation leaves two options for acquiring a good spectrum of a streamer discharge: capturing a lot of discharges or using a very sensitive spectrometer. Mostly, both solutions have to be used together.

As we did not have the opportunity to use a light sensitive spectrometer together with an ICCD camera, we have chosen to expose our spectrometer for the full duration of a large number of subsequent discharges (up to 600[1]). The details of this equipment are discussed below. We also chose to measure primarily at 25 mbar as this resulted in the brightest discharges and therefore the best signal to noise ratio.

As the pressure is low and the exposure can not be triggered exactly to the streamer propagation, the measured spectrum will contain light emitted by all processes and discharges that occur during (and shortly after) the voltage pulse. In most cases, this includes the glow discharge. Such a compound spectrum makes it impossible to determine one electron energy distribution function with the Boltzmann method from the spectrum, as it is made up from sources with presumably different average electron energies. However, as we will show in section 8.3.1, the general shape of the spectrum is not very sensitive to changes in pressure.

In our measurements, we mainly look for the presence of atomic, ionic and molecular lines and systems to get better insight in the processes and species inside the discharge. Only for spectra in air did we perform temperature calculations. This is discussed in section 8.3.2.

Others have performed calculations on measured streamer spectra, although only for a limited set of gasses. For example, Tochikubo and Teich [215] have investigated time-dependent spectra of corona discharges intended for the conversion of nitrogen oxides. Sun *et al.* [203] have studied O, H and OH radicals from optical emission by corona discharges in water. An often employed method to determine the electric field in nitrogen containing discharges is to measure the ratio between a line of the first negative system of N_2^+ and the second positive system of N_2. This method is employed for example by Kozlov *et al.* [92] for laboratory scale discharges and for sprites by Liu *et al.* [111].

Šimek *et al.* [191] have used time-resolved emission spectroscopy to study pulsed positive streamers in high-purity nitrogen (5.0 purity). They find that the maximum density of $N_2(A\,^3\Sigma_u^+)$ metastables occurs during the early post-discharge

---

[1]The maximal practical repetition rate of our pulse sources is 10 Hz and the maximum practical exposure of our spectrometer is 60 s.

period (0.5–1 μs) and that the densities of NO($X^2\Pi$) and OH($X^2\Pi$) radicals (from oxygen and water impurities) peak at 9 and 5 μs after the discharge respectively.

Shcherbakov and Sigmond [187] have measured absolute intensities of the second positive system (SPS) of N_2 and the first negative system (FNS) of N_2^+. They used a cross-correlation synchronization mechanism to get a good time-resolved signal with sub-nanosecond temporal resolution. They find risetimes of the waveforms of the order 0.2–0.4 ns for both systems and durations of 1.4–1.5 ns and 0.5–0.6 ns for the SPS and FNS systems respectively. In a second paper [188] they show a model that can explain these measured results. With this model they estimate the electric field and electron number density at 70–80 kV/cm and $(2–3)\cdot10^{14}$ cm^{-3} respectively (at 450 K temperature and atmospheric pressure).

Staack *et al.* [197] have studied spectra of atmospheric pressure DC glow discharges in a variety of atomic and molecular gasses (all with 4.0 purity). We will compare their results to our spectra when relevant. They used trace additions of nitrogen in all gasses to determine vibrational temperatures and Boltzmann plots to determine the excitation temperature in pure hydrogen and helium.

8.1.2   Planetary sprite spectra

In looking for planetary sprites, the expected spectrum of their optical emissions is of major importance. Such knowledge allows identifying sprites and constructing observation devices. Laboratory settings are convenient for performing such measurements. Terrestrial sprites' spectrum was successfully simulated by Williams *et al.* [229], who have created a "sprite in the bottle" in a glow discharge tube. This experiment was repeated by Goto *et al.* [68]. Note that these are performed on a DC glow discharge. Therefore they do not necessarily have the same chemistry and emission spectrum as the sprites they try to simulate, which are pulsed streamer discharges. Nevertheless, the spectrum measured by this method agrees quite well with the spectrum of terrestrial sprites, measured by Mende *et al.* [131] and Hampton *et al.* [76]. To our knowledge, the simulation of planetary sprites' spectra was not attempted yet.

We remark that several research groups have measured spectra of hot plasmas to simulate lightning in planetary atmospheres. Borucki *et al.* [25] created hot plasma using a laser pulse and measured the emission spectrum. The conditions in that experiment resemble those in the hot plasma lightning channel, where many chemical processes take place due to high temperature rather than due to a high electric field. Goto and Ohba (unpublished report, 2008), simulated the lightning spectrum in pure CO_2 using spark discharges. Below, we report our measurements of the spectrum of sparks in the gas mixture that represents Venus' atmosphere. The spectrum of the cold plasma streamer and glow discharge is significantly different from that of the hot plasma spark discharge in this mixture, and the same

Table 8.1: Specifications of the different Ocean Optics spectrometers. The designations given here are used to identify the different spectrometers in this thesis.

Designation	Type	Wavelength range (nm)	Slit width (μm)	Resolution FWHM (nm)	Bit depth
UV-Vis	HR2000	172-624	50	0.9	12
Vis	HR2000+	415-855	10	0.4	14
Vis-NIR	HR4000	497-946	50	0.9	14
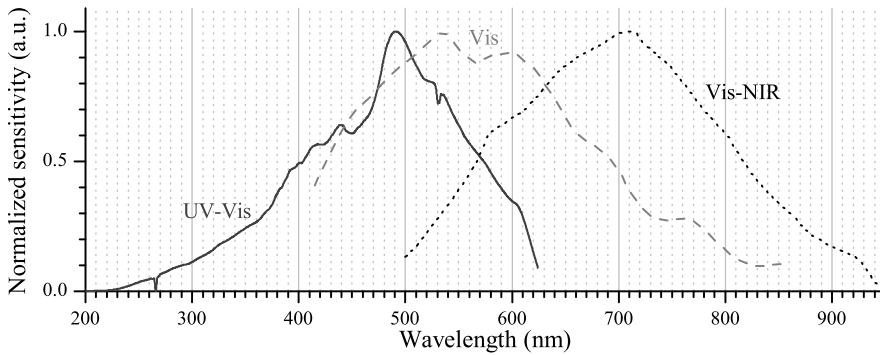
Figure 8.1: Normalized sensitivity curves of the three spectrometers. The sensitivity curves have been acquired by means of calibrated deuterium and halogen lamps.

is probably true in other gas mixtures. Unfortunately we have not been able to produce a spark in the Jovian mixture with our set-up. We observed that the glow discharge became stronger, but did not transform into a spark discharge.

8.2 Experimental techniques

We have used three spectrometers to determine the spectra emitted by the various discharges under investigation. These spectrometers are sensitive in different wavelength regions. Some specifications of the spectrometers are shown in table 8.1.

All three are Czerny-Turner spectrometers with a fixed slit, a fixed reflective grating and a CCD array detector. The sensitivity curves of the spectrometers are shown in figure 8.1. Note that these are normalized curves. An optical fibre is used to get the light into the spectrometer. The acceptance angle of this fibre is enough to capture light from the entire discharge region, when placed behind the large quartz window. The end of the optical fibre is placed within the Faraday cage (protecting
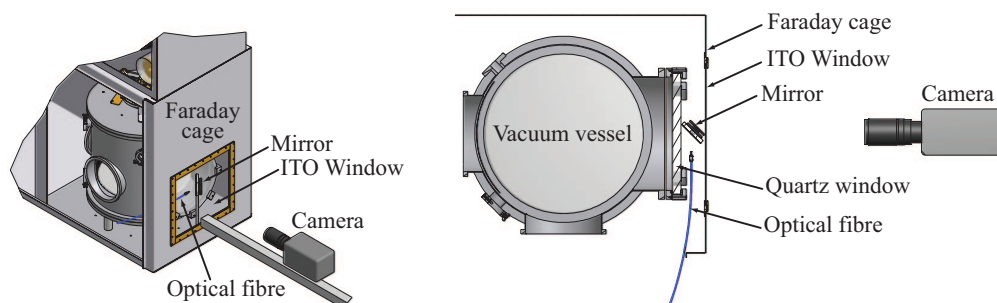
Figure 8.2: Schematic depiction of fibre position with regards to the vacuum vessel (3D view and horizontal cross-section). When the ICCD camera is in use, the optical fibre and the mirror are removed.

our camera and other electronics), parallel to the quartz window of the vacuum vessel (see figure 8.2). A mirror is used to direct the light from the discharge to the fibre. This is needed to measure at wavelengths below 300 nm, which are absorbed by the ITO window that is part of the Faraday cage. The construction with the mirror is necessary because of the small space between the ITO and the quartz windows.

In our experiments, the discharges are created by voltage pulses of hundreds of nanoseconds to microseconds duration. The streamers emit more light at lower pressures, where they also easily transit into stationary glow, that is even brighter. These are the conditions where the spectrum can be measured in a reasonable time span. Thus, most of the spectra reported in this chapter are in fact spectra of discharges that start as a streamer and quickly transform into a glow column.

In order to get enough radiation from the discharge to produce a spectrum with an acceptable signal to noise ratio, we needed to use long measurement times (up to 100 minutes) and a relatively high discharge repetition rate (10 Hz). Most measurements are averaged curves of 1 to 100 intervals of 60 s integration time.

The spectra presented in this chapter are corrected for the sensitivity of the spectrometers. The intensity scale is equal between the different spectra and spectrometers. Therefore intensities can be compared between different spectra and wavelengths (except for the air and nitrogen spark discharges that were created in other set-ups). However, we have no absolute intensity calibration. In some spectra small parts of the spectrum are missing. This is due to the mapping out of known bad pixels of the spectrometers. Especially at long integration times these bad pixels can give incorrect results and therefore they have been mapped out.

Most spectroscopic measurements have been performed with the Blumlein-pulser at a peak voltage of about 20 kV and a pulse duration of about 130 ns (like shown in figure 3.12). The short pulse from the Blumlein pulser ensures a

short discharge time. Exceptions are the planetary discharges and some spark measurements. The planetary discharges have been performed with the C-supply and some spark measurements have been performed with entirely different set-ups, as is discussed in the text.

Lines have been identified with Pearse and Gaydon [166] and the NIST atomic line database [174]. In the presented spectra, relevant lines are indicated on top of the figures. The length of each indicated line corresponds with its strength according to literature. For atomic lines the length is proportional to the logarithm of the relative intensity as indicated by the NIST atomic line database. For molecular lines this length is proportional to the intensity value as given by Pearse and Gaydon. Note that in both cases the relative intensities can differ between the literature values and our measurements. This is expected as the literature values have been acquired in very different discharges than ours. Nevertheless, within one atom or one molecular system, the line strength according to literature is a good indication whether a line is strong or weak.

The composition and purity of the gasses and mixtures that are discussed in this chapter are summarized in tables 5.1 and 7.2. We refer to gas purity in a notation that gives the number of nines in the purity, so 4.0 purity means >99.99% purity. Some more explanation about our spectroscopic methods can be found in the traineeship report by Romuald Blanc [21].

8.3   Pure nitrogen and artificial air

The nitrogen 6.0 and oxygen-nitrogen spectra in figures 8.3 and 8.4 are both dominated by molecular nitrogen lines, mainly from the so-called second positive system. This has been found by many others like Stritzke *et al.* [202]. We have also measured streamer spectra in dry air and they are virtually indistinguishable from the 20% oxygen mixture spectra although we did not look specifically for weak lines of other components like CO_2 or argon.

Striking is the disappearance of the lines from Gaydon's green system and Herman's infra-red system (exact transitions unknown according to [166]) in artificial air. This confirms a remark in Pearse and Gaydon [166] that Gaydon's green system is visible in pure nitrogen discharges, but not in air discharges. No remarks of this nature have been found for Herman's infra-red system. The disappearance of these lines can probably be attributed to efficient quenching of some of the molecular nitrogen states by molecular oxygen. Besides this difference, the two spectra are very similar. A weak atomic oxygen line at 777 nm may be visible on the flank of one of the FPS lines in artificial air.

We have attempted to measure the electric field by studying the ratio between lines from the first negative system of N_2^+ and lines from the second positive
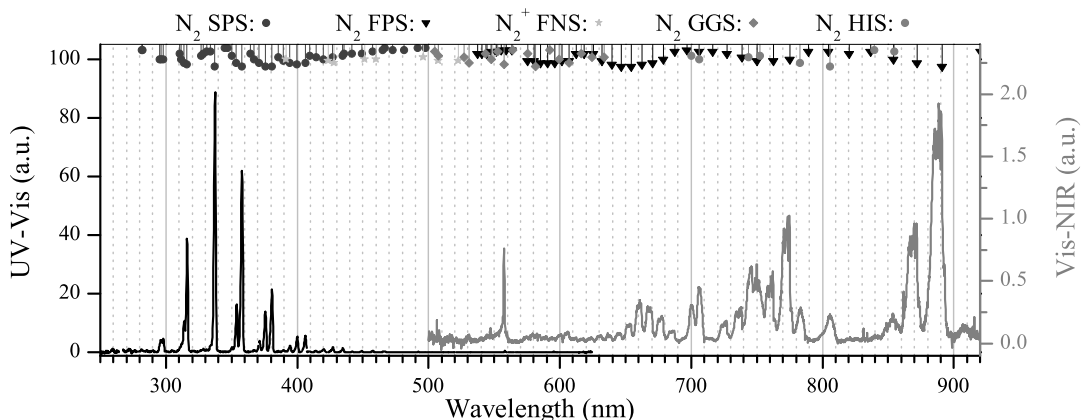
Figure 8.3: Spectra of discharges in 25 mbar nitrogen 6.0, acquired with the *UV-Vis* and *Vis-NIR* spectrometers. The discharges are operated with the Blumlein pulser at about 20 kV. The following line and band systems are indicated: the first and second positive system (FPS & SPS), Gaydon's green system (GGS) and Herman's infra-red system (HIR), all of neutral molecular nitrogen as well as the first negative system (FNS) of N_2^+.
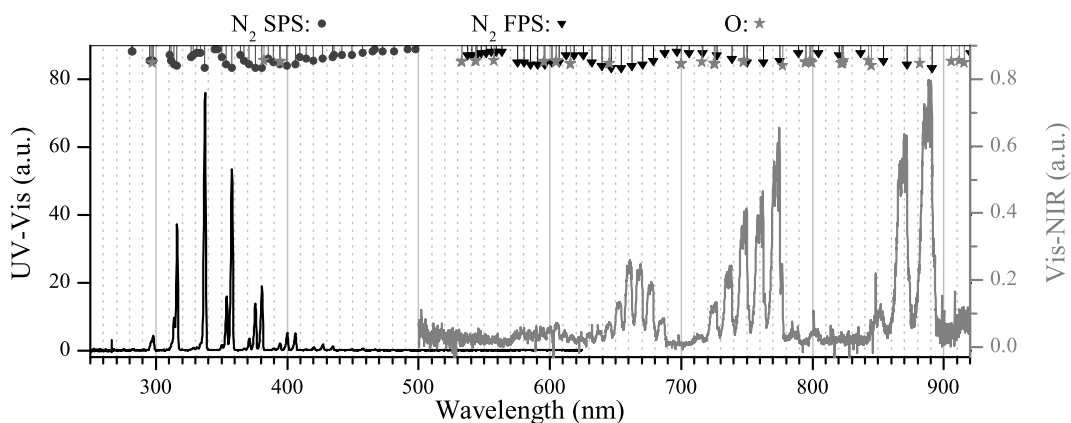
Figure 8.4: Spectra of discharges in 25 mbar artificial air, acquired with the *UV-Vis* and *Vis-NIR* spectrometers. The discharges are operated with the Blumlein pulser at about 20 kV. The following line and band systems are indicated: the first and second positive system (FPS & SPS) of molecular nitrogen and the strongest atomic lines of atomic oxygen.

system of N_2 (like performed by [92, 111, 159, 187]). Unfortunately, no ionic line can be clearly distinguished. The strongest line from the first negative system of N_2^+ is located at 391.4 nm. In our spectrum, we probably do see this line, but our spectral resolution is too low to use it for quantitative measurements.

We have not observed any NO bands, as are reported by Teich [213]. One reason for this is our reduced sensitivity in the UV-region (below 300 nm). Another reason may be that Teich uses a much higher repetition rate, resulting in much more effective chemistry with produced species surviving until the next pulse. He also uses a negative corona instead of a positive one.

The general shape of the *Vis-NIR* part of artificial air is quite similar to the sprite spectrum measured by Stenbaek-Nielsen *et al.* [200] and Hampton *et al.* [76] as well as the "sprite-simulating" glow discharges of Williams *et al.* [229]. However, our spectral resolution is significantly better than that of Williams *et al.* and we can clearly distinguish the different spectral lines within the band systems. Stenbaek-Nielsen *et al.* do not present data below 640 nm, mainly because of attenuation by Rayleigh scattering. Williams *et al.* do show part of the second positive system. However, in their case, its intensity is lower than the intensity of the first positive system. In our case this is just the other way around, the second positive system is much more intense than the first positive system. This difference can be explained by differences in quenching of the excited states, scattering of the blue part of the spectrum by air and the much longer path length in the sprite measurements.

The measured spectra at 25 mbar have much in common with the atmospheric glow spectra in ambient air and nitrogen 4.0 by Staack *et al.* [197]. However, the ratio between SPS and FPS peak heights is much higher in our measurements. Furthermore, Staack *et al.* [197] find strong atomic oxygen peaks (especially 777 nm) in ambient air, while we only see a trace of this peak on the edge of the FPS bands. This can be attributed to the fact that they use a DC plasma, and therefore all reaction products remain inside the plasma, while we study a fast transient discharge.

8.3.1   Dependence on pressure

Most spectra presented in this chapter are from discharges at 25 mbar. However, it is also possible to measure at higher pressures albeit with lower signal to noise ratios. An example of the effect of pressure on spectral shape for pressures between 25 and 200 mbar is given in figure 8.5. The shape of the spectrum is very similar for the different pressures, only small differences in ratios between lines are visible; for increasing pressure, lines from levels with vibrational quantum number $v' > 0$ are decreasing relative to lines from $v' = 0$. This indicates that the vibrational temperature decreases with increasing pressure. This can be explained by faster
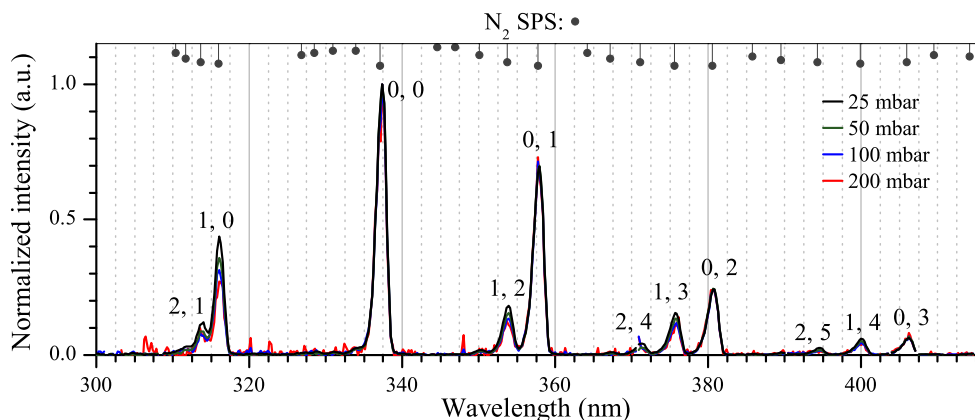
Figure 8.5: Effect of pressure on spectral shape in a nitrogen 6.0 discharge acquired with the *UV-Vis* spectrometer. The spectral shapes have been normalized on the strongest line (337.1 nm). The upper (v') and lower (v'') vibrational levels of the transitions of clearly visible lines of the second positive system (SPS) are indicated above the peaks.
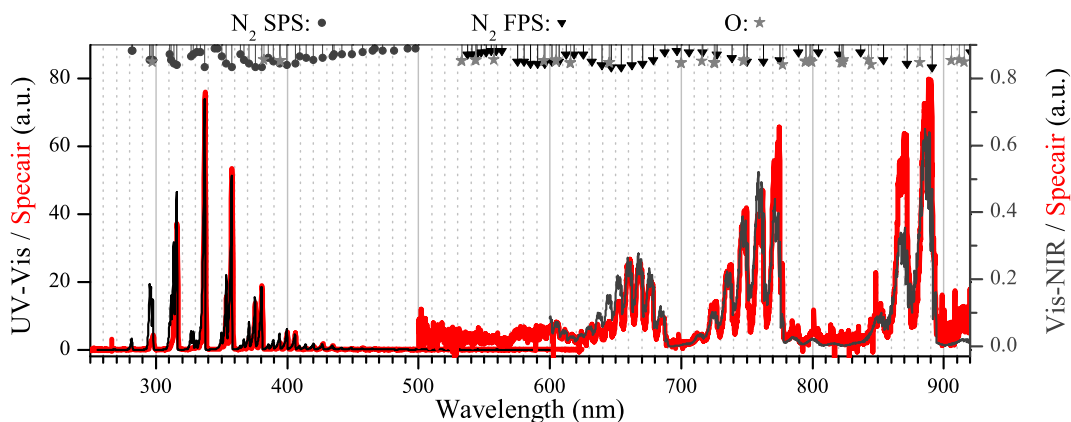
Figure 8.6: Simulated spectra of discharges in air by the Specair 2.2 model (in black) with the settings given in table 8.2. The measured spectrum from figure 8.4 is shown on the background in red with larger line-width. Note that the two different parts of the simulated spectrum (250–600 nm and 600–920 nm) have been scaled differently and do not fit simultaneously on both parts of the measured spectrum.

quenching of the excited vibrational states at higher pressures. The similarity of the spectra at different pressures proves that the spectra of fast transient glow discharges can be used to qualitatively simulate streamer discharges.

The total spectral intensity decreases very rapidly with pressure (see e.g. the *Mf*-values in figure 5.2). Therefore, the spectra obtained at higher pressures are very noisy, even when long integration times are used. This is especially the case for wavelengths above 500 nm in the nitrogen oxygen mixtures, as lines in this region are much weaker than the nitrogen lines between 300 and 500 nm (see vertical scales in figure 8.3). For this reason we have only presented spectra obtained at 25 and 50 mbar.

This low pressure does bring a disadvantage though: at 25 mbar, the streamer channel has already crossed the 160 mm gap within the 130 ns pulse duration. This is shown in figure 5.8, where the streamer crosses the gap in less than 51 ns and most radiation is produced after that time by a glow discharge.

At higher pressures, the streamers are not able to cross the gap in the first half of the pulse duration; at 50 mbar the channel crosses the gap in about 100 ns, but most light is emitted by the streamers, not by a glow discharge (see figure 5.2). At pressures above 50 mbar, the streamers do not cross the gap at all within (or after) the pulse duration, see figure 5.9. As is discussed above, the spectral shape is not significantly influenced by the pressure, except for a small difference in vibrational temperature, even though the discharge morphology is quite different.

We can conclude that the spectra shown here are a good qualitative representation of sprite spectra. Also, because the spectrum of the combined streamer-glow discharge is very similar to the streamer-only spectra, this glow discharge is not in equilibrium, as was to be expected.

8.3.2   Comparison with the Specair model

In order to get some more information from the spectra of streamers in air, we have tried to reproduce them with the Specair 2.2 spectral model [100]. Specair is a freely available [99] model that can calculate a spectrum of air-like gas mixtures with different electronic, rotational, translational and vibrational temperatures. Unfortunately, there is no documentation available about the algorithms, reactions, cross sections and other parameters used in the model. Furthermore, the program regularly crashes and is not able to calculate all parameter variations without indications of the reasons for these crashes. Finally, Specair is not able to fit a measured spectrum, nearly all calculations have to be performed manually and it is cumbersome to compare them with measured spectra.

Despite these shortcomings, a calculation with Specair can give some insight in the streamer temperatures. As was discussed in the introduction of this chapter, the measured spectrum is produced by time integration of a transient process far from equilibrium with no well defined temperature and fastly changing local electric fields. Therefore it is not expected that the spectrum can be fitted completely with the temperatures. Our best effort to fit the measured spectrum of a streamer

Table 8.2: Settings of Specair 2.2 used for the simulation shown in figure 8.6. Only the indicated species and transitions have been used.

Temperatures (K)		Partial pressures (mbar)	
Electronic	40000	N_2	20
Rotational	800	N_2^+	0.00025
Translational	300	O_2	5
Vibrational	5000		
General		Radiative transitions	
Absorption	Yes	N_2	First positive system
Air lambda	0	N_2	Second positive system
Generate mole fractions	No	N_2^+	First negative system
Air absorbers	False		

discharge in air is shown in figure 8.6. The corresponding settings of the Specair model for this calculation are given in table 8.2.

We have not been able to find model settings that result in a ratio between first positive system (FPS) and second positive system (SPS) radiation which is similar to our measurements and still gives a reasonable fit within these systems as well. The ratio between the strongest SPS and FPS lines in our measurements is about 100, while the model results with the settings shown in table 8.2 give a ratio of about 4000. Nevertheless, within these systems, the model results are quite close to the measured spectrum. The difference in SPS/FPS-ratio can probably be attributed to quenching of the FPS system in air but we can not be sure of this as we have no information on the exact inner workings of the Specair model. One hypothesis is that quenching rates in the model are calculated for atmospheric pressure and therefore may be 40 times too high for the FPS at 25 mbar if we assume that quenching scales with inverse density.

The settings given in table 8.2 include only a very limited amount of species and radiative transitions. However, we have found that adding small molar fractions of other expected species (e.g. 10 ppm of O or N atoms) and including all available radiative transitions to the model hardly influences the calculated emission spectrum.

As is clear from the discussion above, the temperatures found above and shown in table 8.2 are only a very rough indication for the following reasons:

- As indicated in the introduction, the spectral measurements are integrated over time and position and therefore include multiple regions with different temperatures at once.

- The electrons energies are not distributed according to a Boltzmann distribution (see e.g. Li *et al.* [103]) that is probably assumed in the Specair
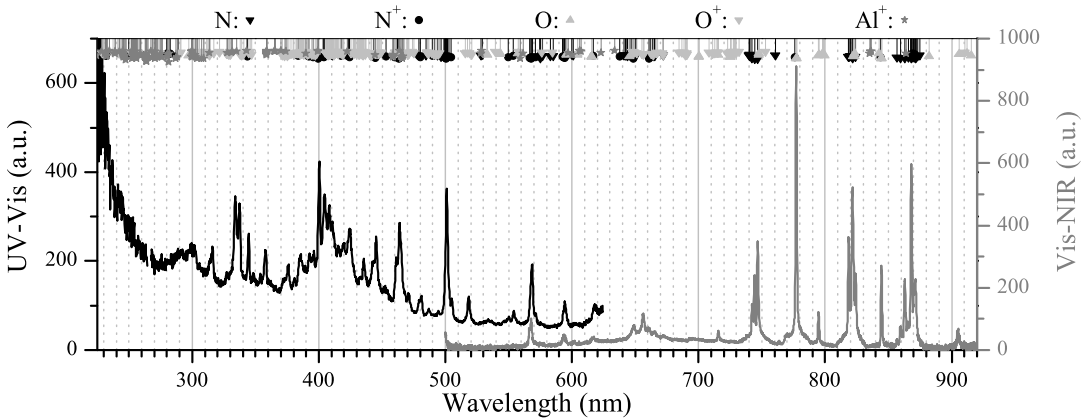
Figure 8.7: Spectra of strong spark discharges in ambient air, acquired with the *UV-Vis* and *Vis-NIR* spectrometers. The discharges are operated with the Marx generator at 900 kV. We have indicated the atomic and ionic lines of nitrogen, oxygen and aluminium.

calculations.

The relative decrease of lines from levels with vibrational quantum number $v' > 0$ that was found in the previous section for an increase in pressure has been confirmed by calculations with the Specair model. We found that indeed, for a vibrational temperature of 4000 K instead of the 5000 K used in the other calculations, these higher vibrational levels decrease relative to the $v' = 0$ levels.

The vibrational temperature of 5000 K is close to the findings of Staack *et al.* [197] who find vibrational temperatures of 4000–4500 K (depending on discharge current) in their DC glow discharges.

8.3.3 Sparks in air and nitrogen

Besides streamer and transient glow discharges, we have also measured the emission spectrum of spark discharges in air. The strongest spark we have investigated is a lightning-like discharge at the Department of Electrical Engineering of the Eindhoven University of Technology operated by Nguyen *et al*. [145]. The voltage pulse for this discharge is generated by a Marx generator. It has an amplitude of 900 kV, and produces a discharge of about 5.5 kA during 3 μs in a 70 cm gap in ambient air.

Spectra of this discharge are given in figure 8.7. Because this discharge emits much more light than the streamer discharges discussed above and below, we did not integrate over multiple discharges. The intensities in the measured results can
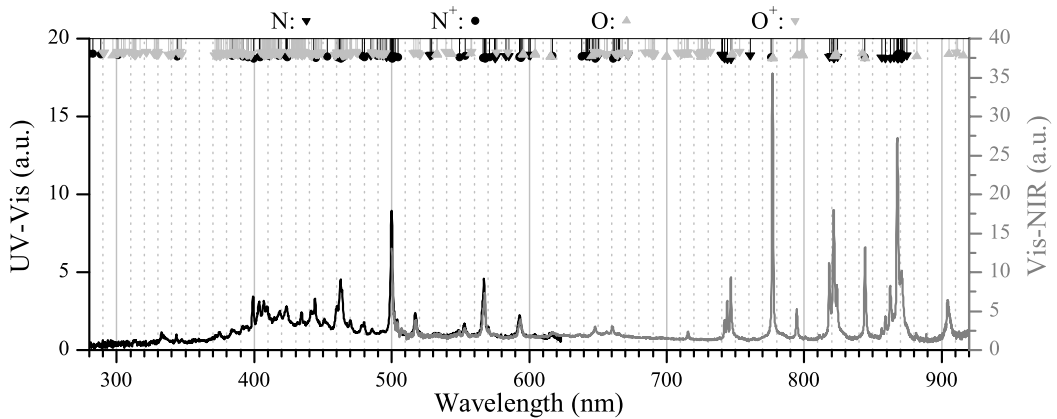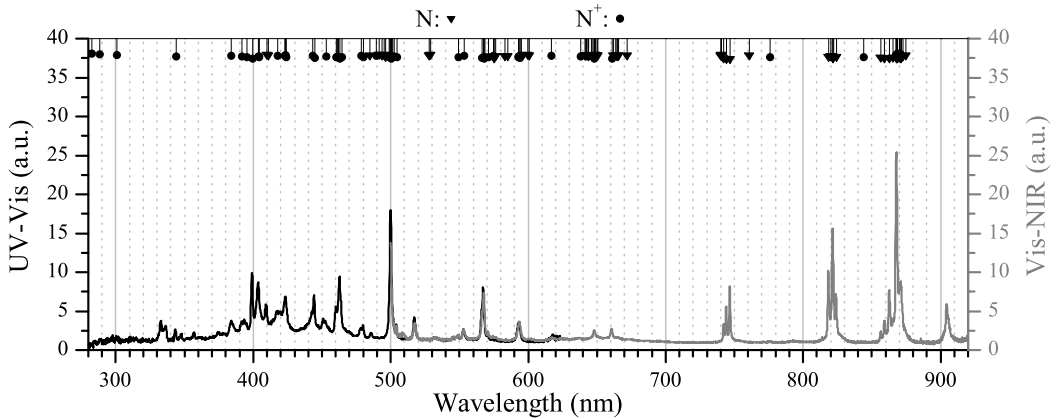
Figure 8.8: Spectra of spark discharges inside the single sparkgap switch of the C-supply while flushed with compressed air, acquired with the *UV-Vis* and *Vis-NIR* spectrometers. The discharges are operated at about 55 kV. We have indicated the atomic and ionic lines of nitrogen and oxygen.

not be compared with other spectra in this thesis because the positioning of the optical fibre with respect to the discharge is very different.

The spectrum of this strong spark is very different from spectra of streamer like discharges in artificial air (e.g. figure 8.4). The spark discharge is dominated by a strong continuum, combined with atomic and ionic lines of nitrogen, oxygen and possibly aluminium (from the electrode material). None of the molecular nitrogen systems that dominate the streamer discharge can be found in this spark spectrum.

Quite similar spectra are emitted by the less powerful sparks inside the sparkgap of our C-supply (see section 3.3). These sparks have been produced by using the sparkgap in its normal operating mode (in the C-supply circuit) at a voltage of 56 kV with a gap distance of about 20 mm. The sparkgap is usually flushed with nitrogen in order to prevent oxidation of the electrodes. However, for the experiment shown in figure 8.8 we have used compressed air to flush the sparkgap. A spectrum emitted by the spark under similar conditions but flushed with nitrogen (estimated purity 3.0–4.0) is given in figure 8.9. Note that the housing of the sparkgap is made from poly(methyl methacrylate) (PMMA) which has a low transmittance for UV radiation with a cut-off that is dependent on the exact material properties and is unknown in our case. Therefore, the relative lack of intensity below 400 nm in figures 8.8 and 8.9 may be partly caused by absorption by the PMMA casing.

When comparing the sparkgap-produced spectrum from figure 8.8 with the lightning-like spectrum from figure 8.7 we can observe many similarities. Most strong emission lines are present in both spectra. The main difference between

Figure 8.9: Spectra of spark discharges inside the single sparkgap switch of the C-supply while flushed with nitrogen from building infrastructure (purity 3.0–4.0), acquired with the *UV-Vis* and *Vis-NIR* spectrometers. The discharges are operated at about 55 kV. We have indicated the atomic and ionic lines of nitrogen.

the two spectra is the intense continuum at lower wavelengths that is much more pronounced in the strong spark and not in the sparkgap-spark spectrum. However, as is stated above, absorption by the PMMA casing of the sparkgap may suppress part of this feature below 400 nm. Nevertheless it is to be expected that the more powerful spark will emit more continuum radiation[2] as the powerful sparks are expected to have much higher gas temperatures and electron densities. Higher electron densities will result in a larger continuum to line intensity ratio (see [38]). This effect may be enhanced by black body radiation emitted from the spark.

The differences between the sparkgap spark spectra in air and in pure nitrogen are quite small; only the atomic oxygen lines are missing from the pure nitrogen spectrum, as could be expected.

A final spectrum of a spark-like discharge that was investigated is a spectrum in a 2 mm point-point gap with a 10 kV voltage pulse with a repetition frequency of 400 Hz in atmospheric air and nitrogen. These spectra (not shown here) contain features from both the spark spectra shown in this section as from the streamer spectra shown in figures 8.4 and 8.3. They contain strong lines from the second positive system of N_2 that dominates the streamer spectra as well as the atomic and ionic lines that dominate the other spark spectra. Therefore we can conclude that in this discharge, the streamer-phase contributes more to the spectrum than in the other investigated sparks.

---

[2]We only measured relative intensities, so this comparison is only between continuum and line intensities, not for absolute continuum intensities.
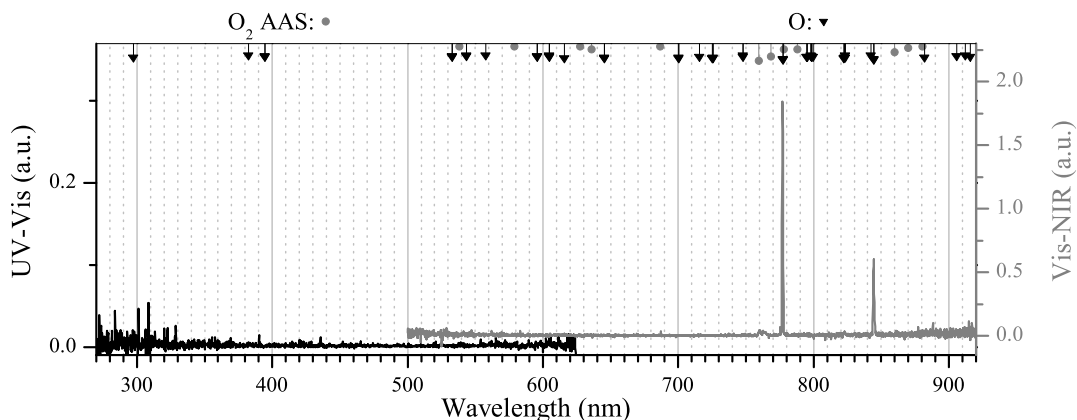
Figure 8.10: Spectra of discharges in 25 mbar oxygen 5.0 acquired with the *UV-Vis* and *Vis-NIR* spectrometers. The discharges are operated with the Blumlein pulser at about 20 kV. The following line and band systems are indicated: the atmospheric absorption spectrum (AAS) of molecular oxygen and lines of atomic oxygen.

Unfortunately, we have not been able to produce a spark in air or nitrogen inside our *new* vacuum vessel setup (see section 3.2.3). The fixed long gap distance of 160 mm requires higher voltages or currents than our C-supply is able to deliver in order to produce a spark in air or nitrogen at pressures between 10 and 1000 mbar. We have been able to produce a spark in the Venus atmosphere gas mixture (see figure 8.16 and discussion in section 8.16).

The lines found in the two spark-spectra in air are very similar to the ones found by Orville and Salanave in a spectrum of lightning [154]. They use photographic techniques so it is difficult to compare relative intensities, but the general distribution of line intensities seems to be similar to our measured spectra.

8.4   Other gasses

8.4.1   Pure oxygen

The *UV-Vis* part of the spectrum of oxygen shown in figure 8.10 is completely empty. We only see two clear (but relatively weak) atomic lines and one weak molecular band (atmospheric absorption system) in the NIR region. The line at 777 nm is clearly the strongest. This line is in fact a triplet, but we are not able to resolve this with our spectrometer. It is also visible in the spectrum of sparks in air (figure 8.7) and weakly in the spectrum of streamers in air (figure 8.4).
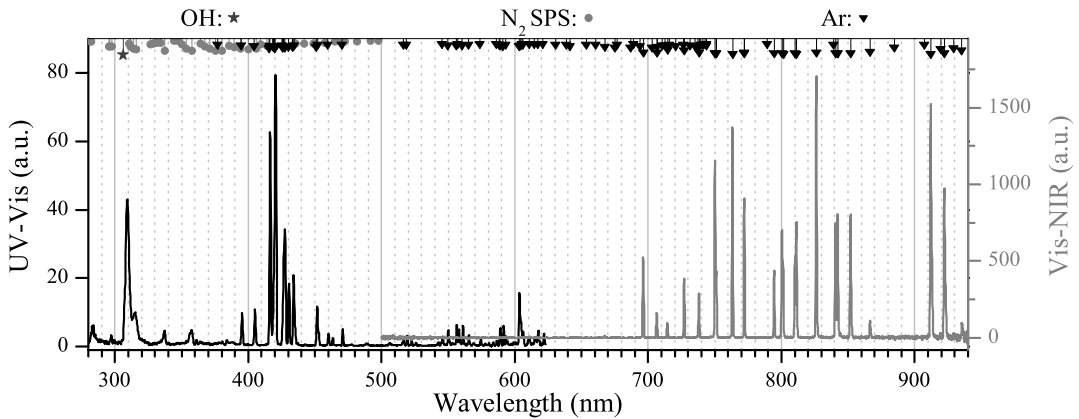
Figure 8.11: Spectra of discharges in 25 mbar argon 5.0 acquired with the *UV-Vis* and *Vis-NIR* spectrometers. The discharges are operated with the Blumlein pulser at about 20 kV. The following line and band systems are indicated: the 3054 Å system of OH, the second positive system (SPS) of molecular nitrogen and the strongest atomic lines of argon.

The lack of radiation below 750 nm explains the low intensity of the images of oxygen streamer discharges; the only available radiation is just at the edge of the sensitivity curve of the camera (see figure 3.16). A camera with a different photo-cathode would be needed to more effectively image streamers in pure oxygen.

8.4.2 Pure argon

In the spectrum of pure argon from figure 8.11 many atomic argon lines are visible, which are especially strong in the red and infrared region. However, also two lines from the second positive system of molecular nitrogen are present as well as the 3054 Å system from OH-molecules. This demonstrates that the argon is not really pure but also contains nitrogen and water vapour, although we do not know in which concentrations. According to the specifications from the supplier, the gas should contain less than 5 ppm water and oxygen and less than 0.2 ppm nitrogen.

It should be noted that in the case of an argon discharge, a significant part of the radiation does not originate from the streamer discharge, but from a surface discharge on the glass insulator surrounding the feedthrough and holder of the cathode pin. This glass insulator can be seen at the top of the vacuum vessel in figures 3.4 and 6.5. In many cases, at low pressures, a surface discharge can be observed over this insulator. However, in the case of argon, this discharge is especially intense (to the naked eye) and produces more light than the bulk streamer discharge. In this case we also observe spark-like discharges between

the cathode holder and this surface. We have shielded our fibre so that it does not receive direct radiation from the surface discharge, but it can still observe reflected radiation.

The argon lines in our spectrum are very similar to the ones found by Staack *et al.* [197]. However, they do not show the less intense lines below 650 nm that we find.

8.4.3   Pure helium

The spectrum of a streamer/transient glow discharge in helium 6.0 (figure 8.12) is the most complex spectrum treated in this thesis. Apart from lines from He, He^+ and He_2^+, it contains lines of many contaminants, including nitrogen, oxygen, carbon and carbon monoxide. Oxygen and nitrogen are only visible in atomic form and as molecular ions. No lines of neutral oxygen and nitrogen molecules have been identified in this spectrum. A somewhat similar spectrum was found by others like Ricard *et al.* [177]. They use pure helium (with unspecified purity) in an atmospheric glow discharge with microsecond-scale pulse duration.

The reason why there are so many lines of contaminants visible in the spectrum must be the high excitation and ionization levels of helium. The upper levels of most helium transitions are about 23-24eV above the ground state, while helium metastables and He_2 dimers also have relatively high excitation levels (~20 eV and ~16 eV respectively). For most of the contaminants, the upper levels of electronic transitions are between 5 and 14 eV above the ground state (e.g. N ~13 eV). This means that the excited states of helium will be very sparsely populated due to the Boltzmann factor $\exp(-\frac{E_i}{k_B T})$, where E_i is the energy of the upper level, k_B the Boltzmann's constant and T the temperature, in this case (far from thermodynamic equilibrium) the effective excitation temperature. At expected electron energies (order 1 eV), the Boltzmann factor can be many orders of magnitude lower for helium energy levels than for levels of the contaminants.

This is consistent with the finding in the previous chapter that streamers in pure helium are much wider than in any of the other investigated gasses. The larger width is probably also caused by the low cross sections for collisions between lower energy electrons (below ~20 eV) and helium atoms and the therefore longer electron mean free path in helium.

Besides the differences in energy levels, there is an extra reason why some lines, like the ones of N_2^+ and OH, are so strong in the spectrum. For example, excited $N_2^+(B)$ species can easily be formed through a charge transfer or Penning effect (see Ricard *et al.* [177]). Furthermore, reactions of impurities with helium metastables (with energies of 19.8 eV and higher) can lead to dissociation, ionization and excitation of many species.
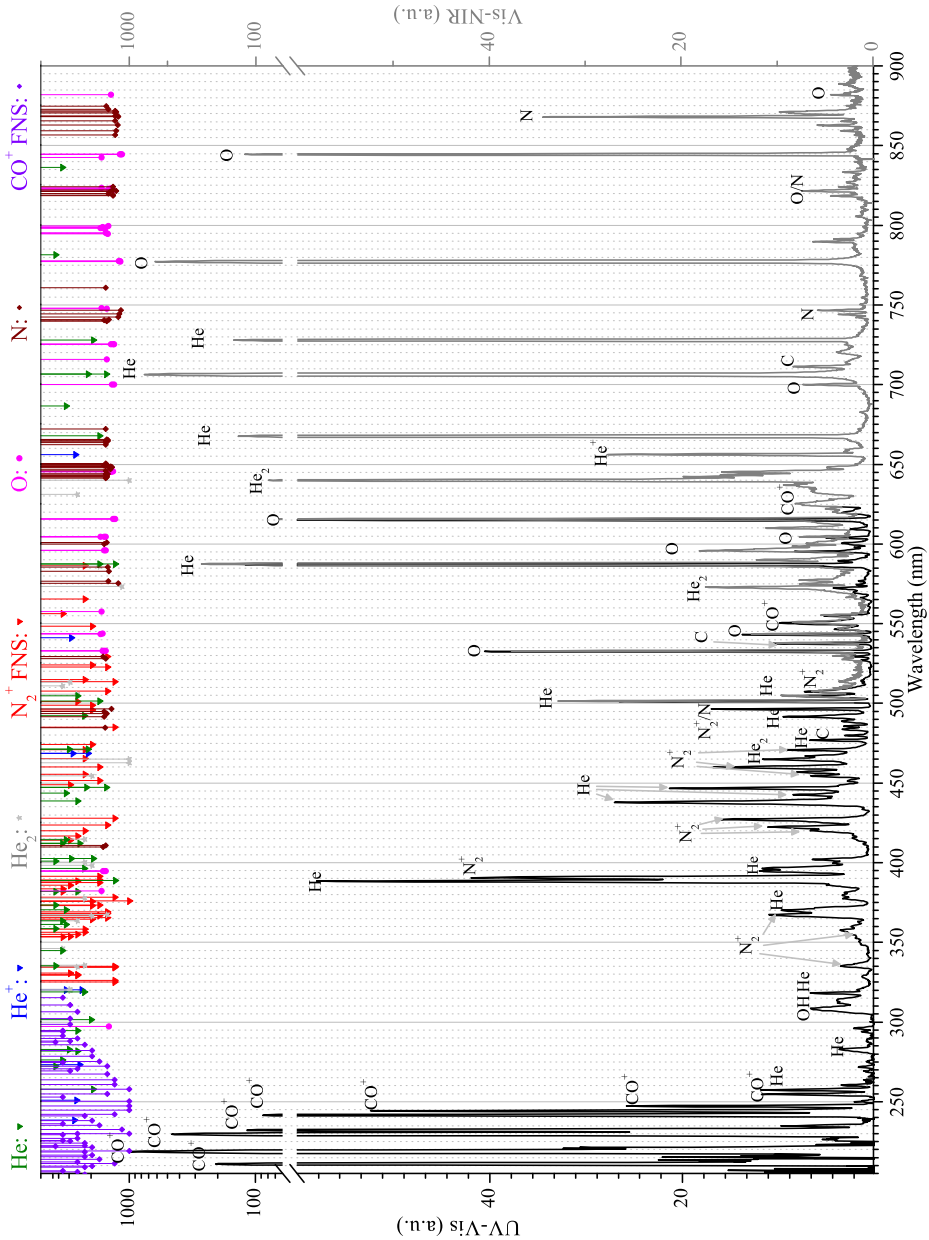
Figure 8.12: Spectra of discharges in 25 mbar helium 6.0 acquired with the *UV-Vis* and *Vis-NIR* spectrometers. The discharges are operated with the Blumlein pulser at about 22 kV. The following line and band systems are indicated: the first negative system (FNS) of molecular nitrogen ions and molecular CO ions, lines of molecular helium (He_2) and the strongest lines of He^+ and atomic helium, oxygen and nitrogen. Note that the vertical axis has a linear scale for low values and a logarithmic scale for high values.

Because of the two mechanisms discussed above, the presence of the contaminant lines in the spectrum is no indication of high contamination levels. Even very low concentrations (below 1 ppm) can lead to significant line amplitudes in the emission spectrum. To check this, we have performed an experiment in which we included a few promille of nitrogen gas into a helium discharge. The spectrum of this discharge is very different from the "pure" helium discharge. It clearly shows many lines of molecular nitrogen (the second positive system, as shown in figure 8.3) that are not visible in the spectrum of figure 8.12. Verreycken *et al.* [224] also report that in He-N$_2$ mixtures, molecular nitrogen lines (like 337 nm from the SPS) are clearly visible from 1‰ nitrogen concentration. Therefore, we conclude that the impurity level is much better than 1‰. We are not able to determine exactly how much better, but judging on our experience with other gasses, we expect to have less than 10 ppm impurities.

In any case, the purity in our experiment is probably higher than in the experiments by Ricard *et al.* [177]. In their spectrum, the ratio between the 391.4 nm N$_2^+$-line and the 706.4 nm He-line is about 20:1, while in our spectrum it is 1:18, a difference of a factor 360. However, Ricard *et al.* do not give any indication of their expected gas purity and work at a much higher pressure (1000 mbar compared to our 25 mbar). At higher pressures three-particle Penning effects will become more prominent.

Staack *et al.* [197] also observe the lines of N$_2^+$ and OH in their helium DC glow discharge spectrum, although they are very weak (the 391.4 nm N$_2^+$-line is about 150 times less intense than the 706.4 nm He-line).

8.4.4 Pure hydrogen

The *UV-Vis* spectrum of a discharge in hydrogen 6.0 is given in figure 8.13. Unfortunately, we only had a limited amount of hydrogen gas available and therefore have not been able to measure the higher wavelength region of this spectrum.

The dominant feature of this spectrum is the continuum in the *UV-Vis* range, with a higher intensity at the lower wavelengths. It is similar in form to the UV continuum emission in H$_2$ reported by Lavrov *et al.* [101], and references therein. The continuum is associated with the $a^3\Sigma_g^+ \rightarrow b^3\Sigma_u^+$ electronic transition in H$_2$. Besides this continuum, we can recognize a few lines from the Balmer series of atomic hydrogen and many small other molecular hydrogen lines.

Staack *et al.* [197] also report the Balmer lines as well as the molecular hydrogen bands in their DC atmospheric glow discharge. However, they do not observe the strong continuum at lower wavelengths.
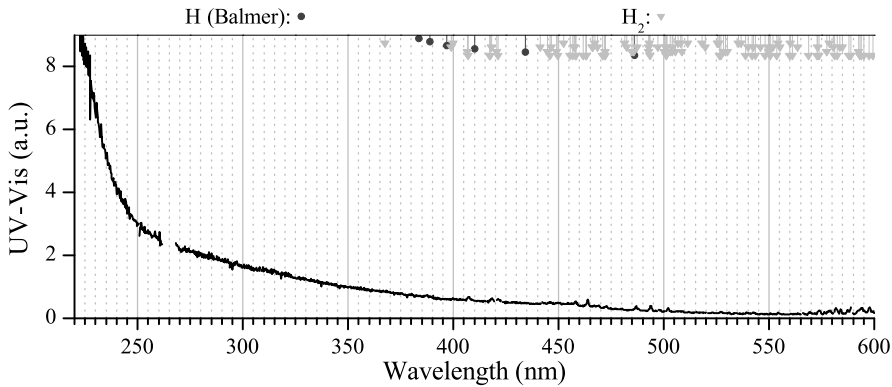
Figure 8.13: Spectrum of discharges in 25 mbar hydrogen 6.0 acquired with the *UV-Vis* spectrometer. The discharges are operated with the Blumlein pulser at about 20 kV. The following line and band systems are indicated: the Balmer line series of atomic hydrogen and a series of molecular H_2 lines from [60].
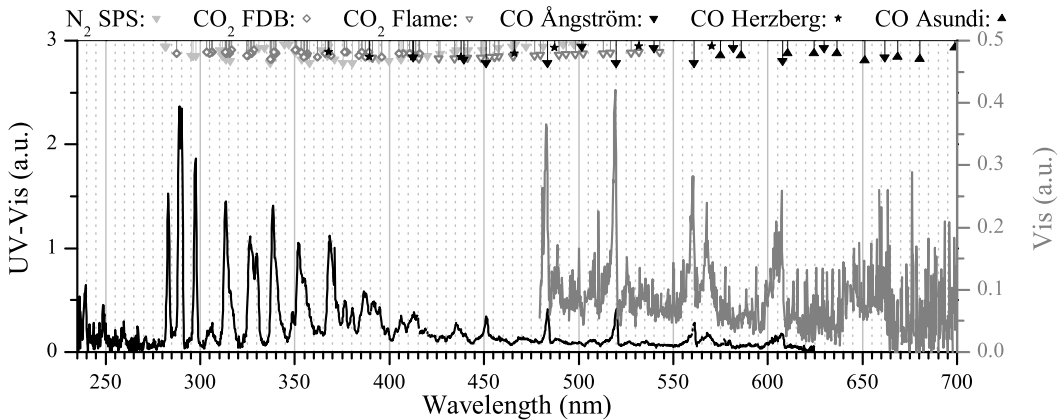
Figure 8.14: Spectra of discharges in 25 mbar CO_2 5.3 acquired with the *UV-Vis* and *Vis* spectrometers. The discharges are operated with the Blumlein pulser at about 25 kV. The following line and band systems are indicated: the first and second positive system (SPS) of neutral molecular nitrogen, the Fox, Duffendack and Barker's system (FDB) and the carbon monoxide flame spectrum (Flame) both from CO_2 (despite its name), the Ångström, Herzberg and Asundi systems of CO.

8.4.5 Pure CO_2

The spectrum of a streamer/fast glow discharge in CO_2 with 5.3 purity is, unsurprisingly, dominated by molecular bands of CO_2 and CO (see figure 8.14). Especially the CO_2 Fox, Duffendack and Barker's system and the CO Ångström system are clearly present.

8.4.6 Venus atmosphere

Figure (8.15) shows the spectrum obtained in a mixture that simulates the Venusian atmosphere (CO_2/N_2 with a 96.5/3.5 ratio), at a pressure of 50 mbar and applied voltage of $\sim$43 kV. The optic fibre is placed behind the ITO window, so no spectral lines can be observed below the wavelength of 300 nm.

The most dominant feature of this spectrum is the N_2 second positive band of triple heads in the range 300 to 450 nm (N_2-SPS). The CO Ångström system is clearly visible in the *Vis* spectrum, with lines at 451 nm, 483 nm, 519 nm, 561 nm, 607 nm and 662 nm, all degraded to the violet. This system is considerably weaker that the N_2-SPS band. The line at 567 nm is possibly one of the triplets of the CO triplet system. Other triplets of this system might be present as well, but many of them are very close to CO Ångström lines, making it difficult to identify them (such as the wide line at 600-607 nm), others are too weak to be unequivocally identified. Several very weak heads of the N_2 first positive band (N_2-FPS), are found at the upper edge of the spectrum, at the wavelength range 725-790 nm. When comparing the measured Venus spectrum with the spectrum from pure CO_2 (figure 8.14), we can observe that above 400 nm, the spectra match quite closely[3]. Below 400 nm, the Venus spectrum is dominated by the nitrogen lines which are of course absent in the pure CO_2 spectrum.

It is somewhat surprising that we observe primarily nitrogen lines in this spectrum. Previous work by Goto and Ohba (unpublished report 2008) in hot plasma, found a significant CO_2 signature in the spectrum, while Borucki *et al.* [25] found mainly atomic oxygen and carbon lines. However, according to the literature ([166]) even a very small amount of nitrogen mixed into a gas can produce strong N_2 lines in some circumstances, and these nitrogen lines can be considerably stronger than any other feature of the spectrum. This seems to be the case with the streamer spectrum in the Venusian atmosphere examined here. This is an indication that pure CO_2 may not be the best choice when one wishes to simulate such discharges in the Venusian atmosphere, and nitrogen must be taken into account. The hot plasma spectrum is discussed in more detail in the following section.

8.4.7 Venus spark

By a simple modification, the system described in section 3.3.1 can create sparks in the discharge gap. The resistor R_3 in figure 3.7, through which most of the current during a voltage pulse, is replaced by a resistor with a higher resistance (a 1 kΩ

---

[3]Note that the CO_2 spectrum has been averaged from a lower number of discharges and therefore has a worse signal-to-noise ratio. This bad signal-to-noise ratio masks some lines that are clearly visible in the Venus spectrum, especially above 650 nm.

N$_2$ SPS: •   N$_2$ FPS: ▪   CO$_2$ Flame: ▽   CO Ångström: ▼   CO Herzberg: ⋆   CO Asundi: ▲   O: ∗
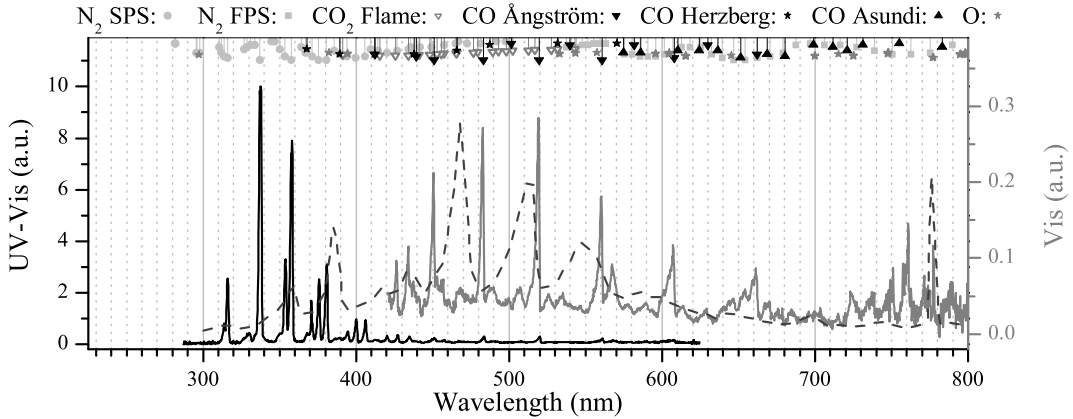
Figure 8.15: Spectra of streamer/glow discharges in 50 mbar Venus atmosphere mixture acquired with the *UV-Vis* and *Vis* spectrometers. The discharges are operated with the C-supply at about 43 kV. The following line and band systems are indicated: the first and second positive system (FPS & SPS) of neutral molecular nitrogen, the carbon monoxide flame spectrum (Flame) from CO$_2$ (despite its name), the Ångström, Herzberg and Asundi systems of CO. Finally, the atomic lines of oxygen are indicated. The dashed grey line indicates the results of Goto and Ohba [69].

CO$_2$ FDB: ▫   CO$_2$ Flame: ▽   CO Ångström: ▼   CO$^+$ FNS: ▽   O: ∗
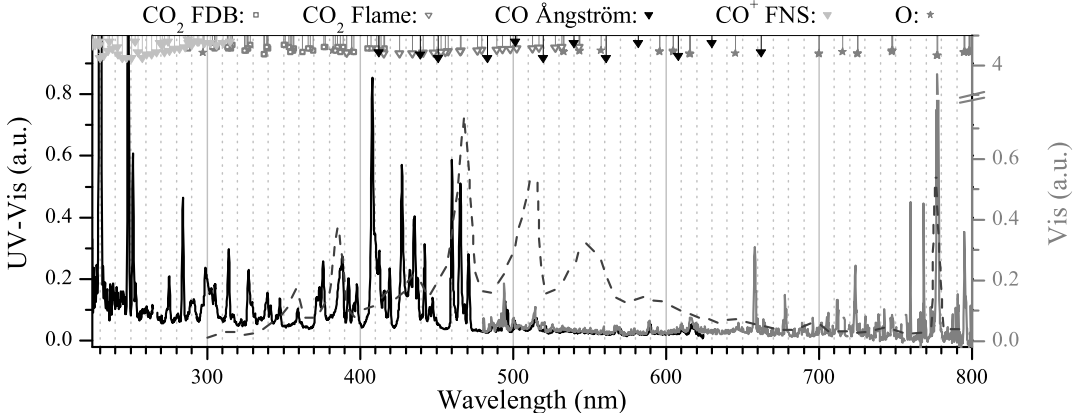
Figure 8.16: Spectra of spark discharges in 200 mbar Venus atmosphere mixture acquired with the *UV-Vis* and *Vis* spectrometers. The discharges are operated with the C-supply at about 50 kV. The following line and band systems are indicated: the Fox, Duffendack and Barker's system (FDB), the carbon monoxide flame spectrum (Flame) both from CO$_2$ (despite its name), the Ångström system of CO, the first negative system (FNS) of CO$^+$ and the atomic lines of oxygen. The dashed grey line indicates the results of Goto and Ohba [69]. Note the broken vertical axis for the *Vis* spectrometer results.

resistor is replaced by a 6 MΩ resistor). The original resistor is chosen in such a way that most of the current flows through the R_3 branch of the circuit, rather than through the discharge gap, therefore the high voltage on the discharge gap falls very rapidly, within several micro-seconds. With the stronger resistor in place, the high voltage on the electrodes persists for a time long enough for a spark discharge to occur, if the gas in the vessel is dense enough. The spark discharge is akin to lightning on a small scale.

We used this setting to create sparks in the mixture that represents Venus' atmosphere, CO_2-N_2, and recorded its spectrum using the equipment and methods described above. The optic fibre was placed between the vessel quartz window and the ITO window (as indicated in figure 8.2), so wavelengths shorter than 300 nm were observed. The pressure in the vessel was 200 mbar, and a voltage of ~50 kV was used. The sparks created in this way are significantly brighter than the cold plasma discharges discussed above. As a result we could measure the spectrum with considerable shorter exposure times; 10 seconds for the *UV-Vis* range, and 30 seconds for the *Vis* range were used. The curves shown in figure 8.16, are the averaged result of 10 measurements.

When one compares the spectra in figures 8.15 and 8.16, the difference is apparent. The strongest lines of the cold plasma spectrum are concentrated in the wavelength range 300-400 nm, and these are nitrogen lines. There are no CO_2 lines, and the CO lines are very weak. The spark spectrum, on the other hand, has a concentration of lines between 400 and 500 nm, and several strong and narrow lines; the atomic oxygen line at ~777 nm, and two lines in the UV, ~230 nm and ~250 nm, that probably belong to the CO^+ first negative system. Many of the other lines in this spectrum correspond with the carbon monoxide flame bands ($^1B_2 - X^1\Sigma^+$), which are in fact CO_2 emissions, and also with the Fox-Duffendack and Barker's system ($A^2\Pi - X^2\Pi$), which are CO_2^+ emissions.

Goto and Ohba (unpublished report 2008) performed measurements of the hot plasma spectrum in pure CO_2 at several pressures. Their results are quite similar to the spark spectrum shown here. They identified several wide CO_2 lines. The spectrum in figure 8.16 has a higher resolution, and therefore many more lines are observed. These lines are grouped into several bands that agree well with the wide lines of the 100 Torr (133 mbar) spectrum measured by Goto and Ohba. These bands in our spectrum are located roughly at 375 nm, 390 nm, 415 nm, 440 nm and 470 nm, and all have widths between 10 and 20 nm. We also observe a strong oxygen line at 777 nm which was also reported by Goto and Ohba as well as by Borucki *et al.* [25]. However, the structures observed by Goto and Ohba between 500 and 600 nm do not appear prominently in our spark spectrum. Goto and Ohba attribute them to CO_2 band emission. The wavelengths of 512.9 and 543.0 nm they indicate do belong to the CO_2 flame system, but, according to Pearse and Gaydon [166], are not the strongest lines in this region. In our streamer spectrum
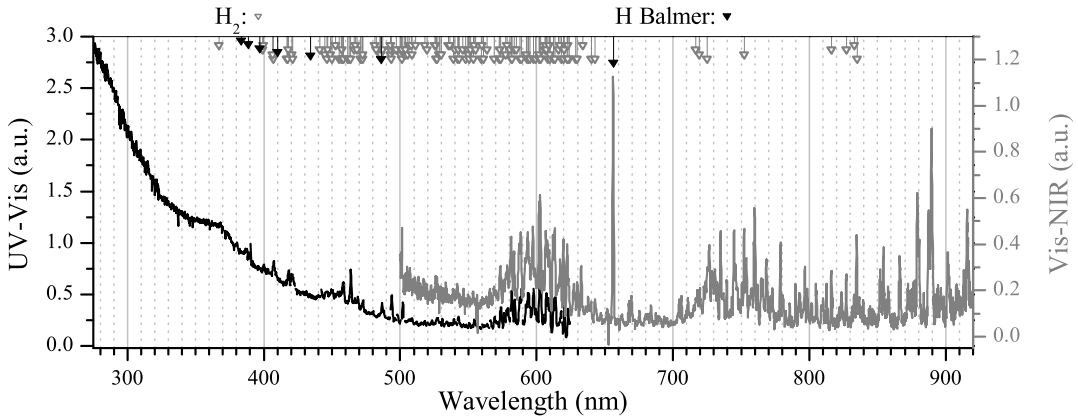
Figure 8.17: Spectra of discharges in the Jovian atmosphere mixture acquired with the *UV-Vis* and *Vis-NIR* spectrometers. The two spectra are obtained under slightly different conditions: the UV spectrum was obtained at 50 mbar with the C-supply at about 26 kV while the *Vis-NIR* spectrum was obtained at 25 mbar with the Blumlein pulser at about 19 kV. The following line and band systems are indicated: the Balmer line series of atomic hydrogen and a series of molecular H_2 lines from [60].

these lines are not clearly visible at all and in our spark spectrum only the 512.9 nm line is weakly visible.

It is interesting to note in this respect, that 6 of the 7 flashes reported by Hansell *et al.* [77] in their ground observation of Venus' night-side were found using a 777.4 nm filter and one more flash was observed using a 656.3 nm filter. Our spectrum has a strong oxygen line at ∼777 nm, and a clear and narrow line at about 658 nm (probably CO Ångström).

8.4.8 Jupiter atmosphere

Figure 8.17 shows the spectrum obtained in the mixture that simulates Jupiter's atmosphere (H_2/He with a 89.8/10.2 ratio), at a pressure of 50 mbar and a voltage peak of ∼25 kV. Under these conditions the discharge is dominated by a glow discharge. These measurements were taken with the optic fibre placed between the discharge vessel window and the ITO glass, so radiation below 300 nm was recorded.

Like in pure hydrogen, the spectrum is dominated by the continuum from the $a^3\Sigma_g^+ \rightarrow b^3\Sigma_u^+$ transition in H_2. In addition to this continuum, there are many spectral lines. We focus here on the most distinctive features of the spectrum. The strong and narrow line at 656 nm, is the H_α line. The second line of the Balmer series (H_β at 486.1 nm), much less intense (as it usually is), is present as well. There

are two regions of particularly strong and dense lines, one at the wavelength range of 575-625 nm and another at 700-800 nm. These bands probably belong to H_2 molecular systems. No trace of helium lines or contaminants can be found in the spectrum. This means that electron energy levels in the Jupiter atmosphere mixture are much lower than in the helium streamers that are discussed in section 8.4.3. The ionization level of molecular hydrogen (15.43 eV) is so much lower than the excitation and ionization levels of helium (23 eV and above) that the discharge is dominated by hydrogen.

8.5   Conclusions

Air and pure nitrogen discharges

The visible and near UV/IR spectra of all streamer discharges in air and other nitrogen-oxygen mixtures (with a nitrogen concentration of at least 80%) at pressures between 25 and 1000 mbar are dominated by radiation from the second positive system (SPS) of molecular nitrogen. Lines from this system are stronger than any other atomic or molecular lines. At higher pressure we observe a relative decrease of lines coming from higher vibrational levels in this system, which indicates a decrease of the vibrational temperature with increasing pressure.

Besides the SPS system, also the first positive system of N_2 is visible in these streamer discharges, although nearly a factor 100 less intense (for peak values). In pure nitrogen, Herman's infrared system and Gaydon's green system are (dimly) visible but in air they are absent, probably because of quenching of the excited nitrogen states by molecular oxygen. Tentative fitting of the spectra with modelling results from the Specair program has resulted in the following rough temperatures: $T_{electronic} = 40000$ K, $T_{rotational} = 800$ K, $T_{translational} = 300$ K and $T_{vibrational} = 5000$ K for a streamer spectrum in 25 mbar air.

Note that in all discharges at 25 mbar, part of the radiation is emitted by the glow discharge that follows the streamer discharge, even though most of the spectra discussed in this chapter have been acquired with the short (~130 ns) pulses from the Blumlein pulser. We have not been able to determine local electric fields because the lines of the second negative system of N_2^+ could not be distinguished with our equipment.

Spectra of sparks are very different from streamer spectra. They hardly contain any radiation from the molecular systems discussed above, but only show line radiation from dissociated atoms and atomic ions. For a very powerful spark (70 cm, 5.5 kA), we also observe a strong continuum, especially at lower wavelengths. This continuum is caused by free-free radiation (Bremsstrahlung), recombination and black-body radiation and is an indication of the very high temperature of this

thermal plasma (at least several thousand Kelvin).

Other gasses

The other gasses that were investigated all have very different spectra. The spectrum of a streamer in oxygen is nearly empty, except for a few atomic oxygen lines (the strongest around 777 nm). The spectrum of a discharge in argon is dominated by atomic argon lines. However, in our case it also showed some lines of molecular nitrogen and OH-molecules; these are indications of contaminations.

The spectrum of a streamer discharge in helium is very complex. In this spectrum lines from contaminations (N_2^+, N, O, CO^-) are nearly as intense as atomic and ionic helium lines. This can be attributed to the high excitational and ionization levels of helium. These require high electron energies, which can easily excite and ionize all other species, even if they are only present in trace amounts. Furthermore, reactions between helium species (ions, metastables) and impurities can lead to excited states of impurity species.

The spectrum of a hydrogen streamer is dominated by a near continuum starting in the UV (we measure from about 220 nm). This continuum is associated with the molecular H_2 transition $a^3\Sigma_g^+ \to b^3\Sigma_u^+$. Finally, the spectrum of a CO_2 streamer discharge is again dominated by molecular band systems, like in nitrogen. In CO_2 the most prominent systems are Fox, Duffendack and Barker's system and the CO Ångström system.

Planetary discharges

To maximize the chances of discovering planetary sprites by optical observations, one should focus on the specific spectral lines expected in these discharges. We have examined the optical spectra of streamers and glow in the two atmospheres, in the visual and the near UV range. In the Venusian atmosphere we find strong N_2 lines from the second positive band, as well as considerably weaker CO lines. In contrast, Borucki *et al.* [25] have investigated a hot plasma in a similar gas mixture. They find that the spectrum is populated by many more spectral lines. It is also significantly different from the spectrum measured by Goto and Ohba (unpublished report 2008) in pure CO_2, and from our own measurements of the spark spectrum in the N_2-CO_2 mixture. We find that in the case of a cold plasma discharge the presence of nitrogen in the atmospheric gas is important and should not be neglected. In case of a hot plasma discharge, a spark, CO_2 and CO lines are dominant. Among the strongest lines in our spark spectrum, it is worth mentioning the lines at 777 nm and 658 nm. These lines are close to the wavelengths proposed by Hansell *et al.* [77] for lightning observations on Venus. We observe also two very strong lines at 230 nm and 250 nm, which may be useful as well. However,

these two lines are at the edge of our spectrum, where the apparatus sensitivity is low. It is worthwhile to look more closely at this wavelength.

In Jupiter's atmosphere the spectrum is more complex, consisting both of continuum radiation and very dense spectral lines. The Balmer alpha line is a common feature of spectra of gasses that contain hydrogen and can not be considered a characteristic of the cold plasma spectrum. For example, Borucki *et al.* [25] find this line as the strongest feature of the hot plasma spectrum in a similar gas mixture. On the other hand, we see a dominant continuum spectrum, which is not found in Borucki's work. Moreover, there are several regions of dense band structure, which are characteristic of the hydrogen molecular spectrum. No lines or bands from helium have been found.

Chapter 9

Conclusions and outlook

9.1   Overview

As reviewed in the introduction, streamers are a general dynamical phenomenon that occurs when a high electric potential is applied to ionizable matter. They are an essential element in the formation of sparks and lightning in our atmosphere as well as in the atmospheres of other planets. And they play an important role in many technical applications.

This is because streamers are an exceptionally efficient way of transferring high electric voltages into a very localized and transient field enhancement at the tips of the streamer fingers and further into electron energy distributions with very pronounced tails at high energies within an essentially cold gas. These electrons generate chemical transitions in a very energy efficient way and can also be the cause of very energetic radiation.

A key ingredient in understanding the energy conversion process from high voltage into chemical products is the relation between applied potential, electrode configuration and gas composition on the one hand and the number, distribution and properties of the streamer tips on the other hand. Tip radius and voltage determine the local field enhancement as well as energy and number of free electrons. Understanding these relations is a challenge for theory. But theory needs to explain clear observations. And these observations were largely lacking.

First, most all experiments up to this thesis were performed in ambient air. But air is a composed gas where microscopic interaction parameters are not known with sufficient accuracy. Investigating other and also very pure gasses therefore is important for two reasons: it gives additional input to test the relation between microscopic parameters and macroscopic structures further, and it predicts streamer

behavior in other gasses, either for technical applications or in the atmospheres of other planets. Within this thesis, much progress has been made on all questions.

Second, streamers form complex branched trees, and radius and voltage at the streamer tips depend on the voltage distribution within the tree and on the current through the tree. And the tree structure depends also on whether different branches can reconnect or merge. The full three-dimensional structure of these trees and the possibility of reconnections were investigated for the first time in this thesis.

Third, recent progress in pulsed power circuits and fast imaging as well as spectroscopy have been used in this thesis to characterize streamer inception and reactive species better, and to investigate new parameter regimes, in particular, the phases immediately before leader or spark formation without endangering the sensitive ICCD camera by these bright discharges.

9.2   Summary of the investigations in detail

To improve our understanding of the physics of positive pulsed streamers by means of laboratory experiments, we first have used an existing vacuum set-up which has been modified and later replaced by a new vacuum vessel for work with high purity gasses. In these vacuum set-ups, streamers have been generated by means of a pulsed power source, of which we have used two types. We have studied the streamer discharges by means of a fast ICCD-camera as well as three spectrometers. From these experiments we have been able to draw the following conclusions.

Interaction and branching

- It is possible to use stereo-photography to investigate streamer discharges and get more insight into processes like branching, reconnection and merging. In our application of stereo photography we are able to (manually) process images with up to about 50 separate streamer channels.

- Some cases of apparent streamer reconnection and merging in 2D streamer images are in fact artefacts of the 2D representation of the 3D streamer tree.

- Reconnection of late streamer channels to earlier channels can occur. However, within our experiments, this was only observed when the early channel has already connected to the other side. Therefore we interpret this as a change in polarity of the earlier streamer channel that then attracts the late streamer electrostatically.

- Merging of two existing streamer channels of the same polarity was observed only when these channels are so close that they virtually overlap. This occurred only when the streamers start from two points that were very close to each other (much closer than the streamer diameters and of the same order as the photo-ionization length).

- Positive streamers in air in an overvolted gap of 14 cm have a branching angle of 43° with a standard deviation of 12°, nearly independent of pressure (between 220 and 1000 mbar).

Photo- and background ionization

- Even in high purity nitrogen (less than 0.1 ppm contamination), streamers are able to propagate with velocities and diameters that vary by not more than a factor of two compared to similar streamers in air. This means that a reduction of the oxygen concentration by more than six orders of magnitude hardly influences the major streamer properties.

- Streamers in pure nitrogen and argon show a feather-like structure with many short hairs attached to the main channels, this contrasts with streamers in air which are smooth. Based on theoretical estimates we interpret them as ionization avalanches started by single electrons. Due to the low photo-ionization rates in very pure gasses, these avalanches appear on few random locations and can be distinguished individually. This is the first time that these theoretically postulated avalanches are observed experimentally.

- Background ionization levels have a significant influence on streamer initiation, morphology and propagation. This was shown by varying the pulse repetition frequency between 0.01 and 10 Hz and by using pure nitrogen with added radioactive ^{85}Kr.

- In pure nitrogen, the feathers discussed above appear more often and more pronounced at lower pulse repetition frequencies, i.e. at lower background ionization levels. This reinforces the theory that the feathers are created by the stochastic occurrence of the few free electrons in front of positive streamers.

- Streamer initiation is also influenced by pulse repetition frequency: at lower frequencies the chance of initiation is lower because there are less (attached or free) electrons available in the high field region around the electrode tip.

- In pure nitrogen with an addition of radioactive ^{85}Kr (which should theoretically lead to a background ionization level of about $4 \cdot 10^5 \, \text{cm}^{-3}$ at 200 mbar) we can no longer observe any differences between streamers at 1 and 0.1 Hz pulse repetition frequency. This indicates that the background ionization level

from the ^{85}Kr is of the same order as is normally left over 0.1 to 1 seconds after a streamer discharge. This is in accordance with rough theoretical estimates about recombination rates.

- Streamer channels do not follow the same path as their predecessors from preceding discharges, at least not for pulse repetition frequencies of 1 Hz and lower. This can be explained by the combination of recombination and diffusion, which causes the trail of the streamer to be hardly distinguishable from the background 1 second after the discharge.

Other conclusions

- We have successfully built a Blumlein pulser that is able to produce quasi-rectangular voltage pulses with a duration of about 130 ns and a risetime of about 10 ns. The short duration of the pulse allows us to produce streamer discharges with relatively high voltages that would transform into a spark when a longer pulse is applied. The exact amplitude of the pulse during streamer initiation and propagation is better defined than with previous pulse sources, due to the faster risetime of the Blumlein pulser.

- Positive streamer discharges can occur in all gasses investigated: air, nitrogen-oxygen mixtures, nitrogen, oxygen, argon, helium, hydrogen, CO_2 and simulated Venus and Jupiter atmospheres.

- For all gasses for which we were able to reliably measure streamer diameters (i.e. all N_2-O_2 mixtures, the two planetary gas mixtures and pure nitrogen and helium) we have found that they obey the similarity law that states that $p \cdot d_{min}$ (with p the pressure and d_{min} the diameter of the thinnest streamers) does not depend on pressure. The value for $p \cdot d_{min}$ is around 0.05–0.15 bar·mm for most gasses, except for helium (~0.5 bar·mm) and the Jovian mixture (~0.3 bar·mm). This allows laboratory investigations of many properties of tens of kilometers large sprite discharges that appear at low gas densities.

- We have again confirmed that streamer propagation velocity is nearly proportional to applied voltage. The measured propagation velocities in the middle of the gap for all investigated gasses lie within a factor 2 from each other for a fixed voltage.

- Optical streamer brightness differs greatly between different gasses. Streamers are brightest in nitrogen-oxygen mixtures, argon and helium and dimmest in oxygen, CO_2 and the Venusian mixture. The difference between the brightest and dimmest gasses is about three to four orders of magnitude.

- All streamer spectra in molecular gasses are characterized by molecular bands. In gasses containing a significant amount of nitrogen (including

the Venusian mixture), the nitrogen second positive system dominates the emission spectrum. This in contrast to spark-like discharges, which are dominated by radiation from neutral and ionized atoms.

- In pure helium the spectrum contains many lines of contaminations (N_2^+, N, O, CO^-) which are nearly as intense as the strongest atomic helium lines. This can be attributed to the high excitation and ionization levels of helium as well as to some reactions between helium species and impurities. The discharge might actually be dominated by the impurities that are easier to ionize. This also explains the larger diameter of streamers in helium.

- Hydrogen and Jovian discharge spectra are dominated by a large continuum in the UV region from the molecular H_2 transition $a^3\Sigma_g^+ \rightarrow b^3\Sigma_u^+$.

- Spectra of streamers and sparks largely differ in terrestrial as well as in the Venusian atmosphere. This gives a clue for how to distinguish sprites from lightning spectroscopically from satellites, planetary missions or ground.

9.3   Broader implications

Although most of the conclusions discussed above are not aimed at specific applications or occurrences of streamers, they have implications on our knowledge and future research.

Streamer models

The most direct application of the results from the work presented in this thesis is the improvement of streamer models. These models are used in the development and study of all applications and occurrences of streamers. Both the macroscopic 3D streamer tree models and the microscopic streamer propagation models can benefit from the knowledge gained. The measured branching angles and conclusions about streamer merging and reconnection are a key ingredient for macroscopic streamer tree models. Such models currently are fractal-like and often depend on wrong assumptions about streamer branching and interaction. Furthermore, our conclusions can also be used to test predictions of microscopic modelling of streamer branching and streamer interaction. The same is true for the results on photo- and background ionization. In fact, the important conclusion that streamers are quite insensitive to the exact amount of photo-ionization, has recently been reproduced in a streamer model by Wormeester *et al.* [236]. The results of these simulations would not have been accepted this easily without our corresponding experimental results.

Sprites and lightning

The results obtained on structure, brightness and spectra streamers in simulated (extraterrestrial) atmospheres are of great value in the design of (space) missions to study (extraterrestrial) sprites and in the interpretation of their results. Most importantly, we found that streamers in the Venus and Jupiter atmosphere emit relatively little light; this makes it very challenging to detect sprites on these planets if they actually occur.

Thunderstorms are an important source of green house gasses, mostly due to lightning. In literature, there has been debate about the relevance of sprites on atmospheric chemistry (see for example [151, 168]). One of the unknowns in sprite research that is relevant for the prediction of e.g. NO_x production by sprites, is the exact volume occupied by one sprite. Our new knowledge gained by the study of branching and reconnection of streamers can improve the estimations of the geometric volume of sprites.

The re-confirmation of the similarity laws for different gasses strengthens our confidence that carefully designed laboratory experiments are able to simulate many aspects of lightning and sprites.

Streamer applications

The measurements on streamers in a variety of gasses have shown that streamers do occur in all gasses studied. This fact can be very relevant in the industrial application of streamers for gas cleaning, surface treatment and flow control, as it broadens the scope of gasses that can be used in these applications. The knowledge about streamer branching and interaction is valuable in estimating the active streamer volume fraction of an industrial streamer reactor. The spectral measurements presented here, and more specifically the results regarding the presence of certain chemical species can be a first step in the determination whether a streamer discharge in a particular gas is useful for a specific application.

The re-confirmation of the similarity laws in many gasses enables us to use small-scale, high pressure laboratory prototypes in the development of large industrial streamer applications. Finally, as was discussed above, the verification of streamer models with the results presented here can have an impact on all streamer application development.

9.4   Recommendations for future work

Despite the many new results presented in this thesis, a lot of open questions remain. Below, we list a few experiments that we recommend for future investigations on the physics of streamers.

- Better measurement of the photo-ionization process in air and other (pure) gasses. Up to now, most streamer models rely on photo-ionization data that was acquired experimentally by Penney and Hummert in 1970 [167]. Penney and Hummert looked at air, pure oxygen and pure nitrogen. However, the purity of their gasses was not very good (probably 0.1–1% impurities). Furthermore, they were not able to determine the wavelength-range of the UV-photons that cause the photo-ionization. This is even more important for other gasses than nitrogen-oxygen mixtures, where there is no empirical data and hardly any good theoretical knowledge about possible photo-ionization mechanisms. For this purpose, a set-up should be built that can measure photo-ionization directly and that can measure the UV-spectrum that is responsible for the photo-ionization. Photo-ionization can be measured with the method employed by Penney and Hummert, but with much higher demands on gas purity.

- Extensive measurements of branching angles and distances. In order to better understand branching, branching angles and distances should be measured methodically over a wide range of pressures, voltages and gasses. This will be very beneficial for both the theoretical branching models as well as for the development of fractal-like 3D streamer tree models.

- Measure background ionization density directly. By applying a low (50–100 V) voltage over a gas, and then measuring the current, it is possible to measure the background ionization density directly. However, for the low background ionization densities that are relevant in this work (10^3–10^7 cm^{-3}), this involves very low currents, and therefore very high impedances. Therefore, such measurements are a technical challenge, but their results are very useful in the interpretation of measured streamer phenomena.

- Investigate streamer brightness. A straightforward parameter of streamers that has never been investigated in detail is the brightness of the channels (or in fact the streamer head, as in most gasses, only the streamer head emits light). For this, one would need a camera that is calibrated for absolute intensity over a certain wavelength region. This can be extended to more wavelength regions in order to get temporally and spatially resolved spectral information from the streamers. Knowledge about streamer brightness can help to compare experiments to models and is also very welcome for future planetary sprite missions.

- Extension of the study of streamers in other gasses. We have found interesting new properties in streamers in for example helium. In order to better understand the exact mechanisms responsible for streamer propagation in such a gas, one would need a more in-depth experimental investigation combined with modelling. Such an investigation should include a methodical study of streamer properties over a wide parameter range (pressure and pulse voltage, polarity and duration) combined with a brightness study as described above.

Appendix A

A peculiar streamer morphology created by a complex voltage pulse
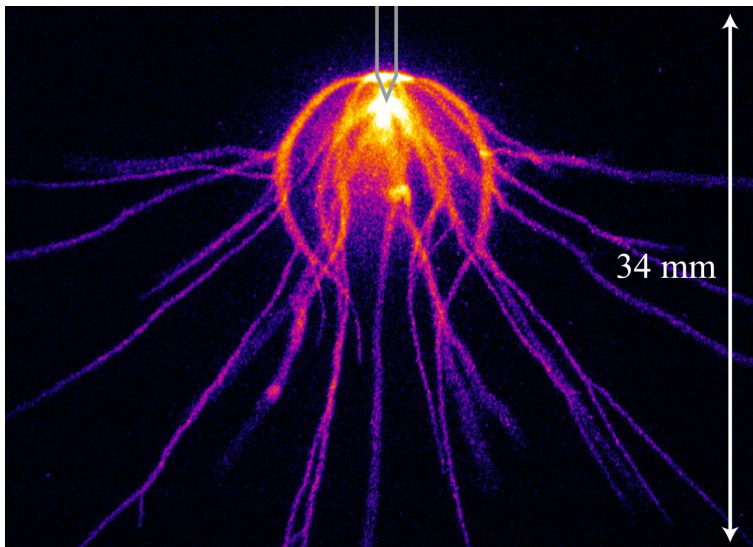
Figure A.1: Time integrated image of a streamer discharge operated with the Blumlein pulser with a negative pulse of 35 kV in 600 mbar artificial air. The grey shape at the top represents the electrode tip. *Mf* =765 (see section 3.4.2 for definition).

While investigating streamer discharges in artificial air, we have found a very peculiar streamer morphology. When we applied a negative voltage pulse from the
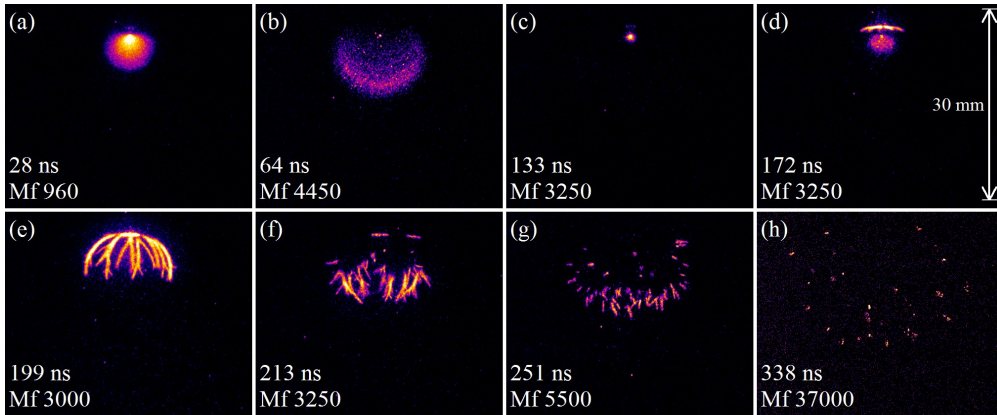
Figure A.2: Time resolved image sequence of streamer discharges with the same settings as in figure A.1. The exposure time of each frame is 20 ns. The approximate start time of the exposure after the start of the voltage pulse as well as the *Mf* values are given on the images.

Blumlein pulser (see section 3.3.2) in 600 mbar artificial air, we observed streamer discharges like the one that is shown in figure A.1. These discharges only fill a small part of the 160 mm gap between point and plane.

Time resolved images together with knowing the voltage pulse shape lead to a hypothesis on why the discharge has this strange morphology. A time resolved image sequence of similar discharges is given in figure A.2. The approximate timing of these images[1] combined with the voltage pulse shape is given in figure A.3.

We will follow the phases of the given image sequence in an attempt to explain the morphology of the discharge:

a-b   The discharge starts as a more or less standard negative polarity discharge. An initiation cloud is formed, which expands to a light emitting shell. The size of this shell is close to the expected theoretical maximum. At a voltage of 35 kV the maximum radius will be 11.6 mm at atmospheric pressure according to equation (2.22). When we scale this to 600 mbar with equation (2.14) we get a maximum radius of 19.4 mm. The measured size of the cloud is about 13 mm. The expansion velocity is of the order 10^5 m/s, which is a typical velocity of an ionization wave. Similar clouds for positive pulses are shown in figure 6.3. We do not observe break-up of the cloud and formation of negative streamers.

---

[1]Unfortunately, we have found that the measurement of the timing of these time-resolved images is not perfect. Apparently, the automated measurement of the start of the voltage pulse was not tuned well, which results in jitter of the measured start time with respect to the camera start time. We estimate this jitter at about 20 ns. However, we have tried to select the images in figure A.2 so that the relative timing error is less than 20 ns (order 5–10 ns). There can still be a timing offset that we did not take into account properly.
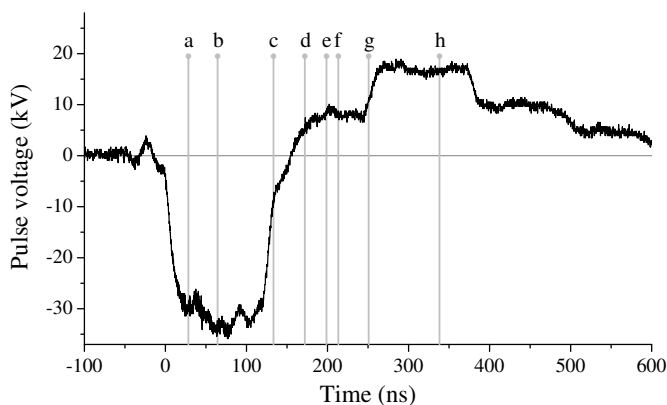
Figure A.3: Electrode tip voltage as function of time for the discharges shown in figures A.1 and A.2. The approximate exposure start times of the sub-figures of figure A.2 are indicated (the end times are 20 ns later).

c   Eventually the shell stops expanding and extinguishes. Only a glowing area around the electrode tip is left. The end of the shell propagation can either be caused by the decrease of the voltage pulse or because the shell size has become so large that it can no longer propagate.

d   The voltage changes to positive polarity as a result of the design of the Blumlein pulser. A new small cloud is formed below the electrode tip. This is probably an electron extraction cloud. The free electrons formed by the previous initiation cloud are now attracted to the tip and move inwards. However, thin streamers channels are formed as well. These new thin channels do not originate from the real tip of the electrode, but from the edge between the conical region and cylindrical region of the electrode tip (see figure A.1).

e-g   The new initiation cloud extinguishes, but the new thin (positive) streamers start to move towards the plate electrode. They do not travel straight towards this electrode, but seem to go around the area that was previously occupied by the expanding negative initiation cloud and shell.

h   When the streamers have reached the lower side of the negative discharge, they move more down and outwards, become thinner and start to decelerate. They keep moving until the end of the high amplitude part of the positive pulse.

Until phase c, the discharge follows a well known pattern. However, as soon as the voltage pulse changes polarity, something different occurs. New streamers

are formed, even though the positive pulse is much lower than the negative pulse. From other streamer experiments, it is well known that positive streamers propagate easier than negative streamers (see [33, 122]). This explains why we do see positive streamers after a negative voltage pulse, but no negative streamers after a positive voltage pulse. These new positive streamers only occur when the amplitude of the positive reflected pulse is high enough, which means that the original negative pulse should have a high amplitude, as it is always significantly higher than the reflected pulse. For some reason, the reflected pulse is relatively high in the discharges discussed here (more than 50% of the original pulse).

The small new positive streamer channels are formed on the edge between the conical and cylindrical regions of the electrode tip. Apparently, streamers form more easily from this edge than from the tip even though the field enhancement is much lower on the edge than on the real tip. This preference for the edge is not observed in discharges with a positive main voltage pulse. Therefore, it must be related to leftover ionization from the negative discharge. In all previous simulations by Ebert *et al.* [119, 135, 175], the space charge density $(n_e - n_+)$ is always much smaller than the ionization density $n_e \approx n_+$. At the short timescales of the voltage pulse, diffusion, attachment and recombination have not modified the electron and ionization density much (see section 6.1.2). One therefore can assume that electrons and ions are present inside the ball, also when the polarity changes. A streamer cannot propagate inside such a heavily ionized region, you only can see rather homogeneous waves – the currents might generate their own space charges as, e.g. inside a sprite streamer [124].

Note that we are not entirely sure that the newly emitted positive streamers originate exactly from the edge of the needle tip. They could also emerge from positions a bit above or below the sharp edge. If this is the case, then the position of these new streamers is not determined by field enhancement on the edge, but by the size of the shielding ionization cloud that also extends slightly upwards from the tip.

In phases e to g, the newly formed positive streamers move over the surface of the old initiation cloud. They are either attracted by the cloud edge, or repelled by the cloud interior. Both can be the case, streamers need free charges to propagate (see e.g. chapters 5 and 6), but, as discussed above, too much free charge may block streamer propagation as it will screen the streamer and prevent field enhancement. Therefore, there are stable bulk waves inside the ball and "sliding surface streamers" at the edge of the ball. They are probably kept in the neighbourhood of the sphere because free electrons are available there. It seems unlikely that they follow the electric field lines but this needs to be investigated further. To fully understand the propagation of the positive streamers on the shell, we need to know the exact electric field configuration and space charge distribution during this stage.

Finally in phase h, when the positive streamers have reached the lower side

of the old initiation cloud, they start to move down and outwards, like positive streamers in air usually do (see e.g. figure 5.2).

Conclusions

An unintended reflection of the voltage pulse shape, caused by the design of our Blumlein pulser, leads to a very peculiar streamer discharge morphology. The combination of a high negative voltage pulse, followed by a lower positive voltage pulse creates positive streamers that run over the surface of the nearly spherical, previous negative discharge. This can very likely be explained by leftover ionization from the negative discharge, but the exact mechanism should be investigated further. This would be a good test case to validate streamer discharge models and to understand the influence of electrical field and structured background ionization on the direction of streamer propagation.

Appendix B

Additional images

This appendix contains additional images of streamer discharges, supplementing the images already available in chapters 5 and 7, especially figures 5.1 and 7.2.
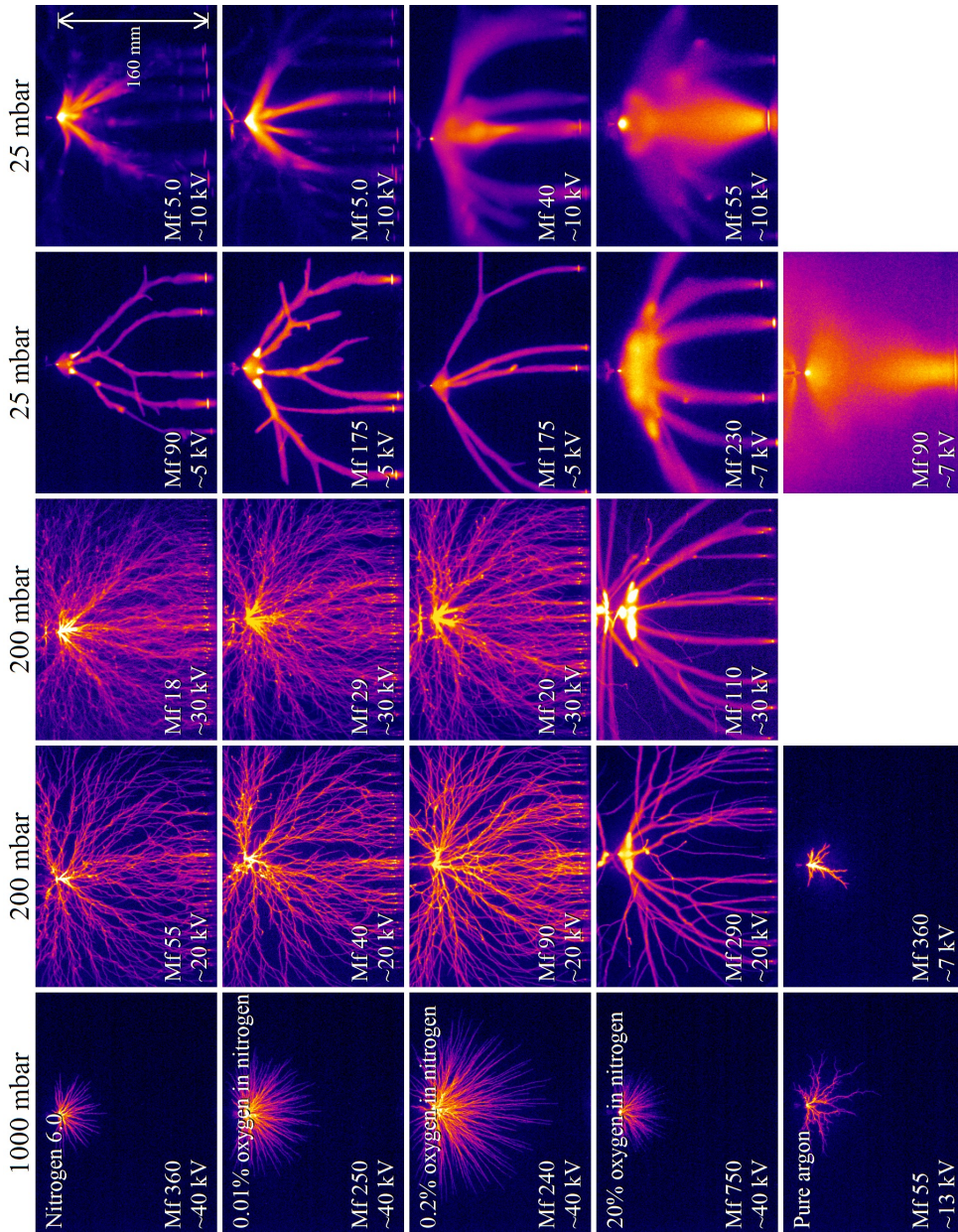
Figure B.1: Extra images of streamer discharges produced with the C-supply for five gas mixtures used (rows), at 1000, 200 and 25 mbar (columns). All measurements have a long exposure time and therefore show one complete discharge event, including transition to glow for 25 mbar. The multiplication factor (*Mf*) gives an indication of the real intensity of the discharge. The white arrow at the top right image indicates the vertical position of the anode point and the cathode plane. At 25 mbar the discharge is partly in the glow-phase instead of the streamer-phase.

Bibliography

[1] The Siglo Data base, CPAT and Kinema Software. url: www.siglo-kinema.com.

[2] *Cluster issue on streamers, sprites and lightning*. J. Phys. D: Appl. Phys. **41**, 234001–234031 (2008).

[3] *Special section on effects of thunderstorms and lightning in the upper atmosphere*. J. Geophys. Res. - Space Physics **114 & 115** (2009 & 2010), guest editor: D. Sentman, link.

[4] Abolmasov, S. N., Shirafuji, T. and Tachibana, K. *Submillimeter dielectric barrier discharges at atmospheric pressure: edge effect*. IEEE T. Plasma. Sci. **33**, 941 – 948 (2005), doi: 10.1109/TPS.2005. 845093.

[5] Agneray, A. *et al. Fast imaging of oscillatory streamer discharge in dense air*. In Proc. Int. Conf. Phenom. Ioniz. Gases, 823–826 (2007).

[6] Aints, M., Haljaste, A., Plank, T. and Roots, L. *Absorption of Photo-Ionizing radiation of corona discharges in air*. Plasma Process. Polym. **5**, 672 – 680 (2008), doi: 10.1002/ppap.200800031.

[7] Akishev, Yu., Dem'yanov, A., Karal'nik, V., Monich, A. and Trushkin, N. *Comparison of the AC barrier corona with DC positive and negative coronas and barrier discharge*. Plasma Phys. Rep. **29**, 82–91 (2003), 10.1134/1.1538505, doi: 10.1134/1.1538505.

[8] Akyuz, M., Larsson, A., Cooray, V. and Strandberg, G. *3D simulations of streamer branching in air*. J. of Electrostat. **59**, 115 (2003), doi: 10.1016/S0304-3886(03)00066-4.

[9] Aleksandrov, N. L. and Bazelyan, E. M. *Ionization processes in spark discharge plasmas*. Plasma Sources Sci. T. **8**, 285 (1999), doi: 10.1088/0963-0252/8/2/309.

[10] Aleksandrov, N. L., Bazelyan, E. M. and Novitskii, G. A. *The effect of small O_2 addition on the properties of a long positive streamer in Ar*. J. Phys. D: Appl. Phys. **34**, 1374–1378 (2001), doi: 10.1088/0022-3727/34/9/314.

[11] Amarasinghe, D. and Sonnadara, U. *Fractal characteristics of simulated electrical discharges*. J. Natl. Sci. Found. Sri **36**, 137–143 (2008), doi: 10.4038/jnsfsr.v36i2.145.

[12] Arrayás, M., Ebert, U. and Hundsdorfer, W. *Spontaneous branching of anode-directed streamers between planar electrodes*. Phys. Rev. Lett. **88**, 174502 (2002), doi: 10.1103/PhysRevLett.88.174502.

[13] Arrayás, M., Fontelos, M. A. and Trueba, J. L. *Mechanism of branching in negative ionization fronts*. Phys. Rev. Lett. **95**, 165001 (2005), doi: 10.1103/PhysRevLett.95.165001.

[14] Arrayás, M., Baltanás, J. P. and Trueba, J. L. *Fluctuation charge effects in ionization fronts*. J. Phys. D: Appl. Phys. **41**, 105204 (2008), doi: 10.1088/0022-3727/41/10/105204.

[15] Babaeva, N. Yu., Bhoj, A. N. and Kushner, M. J. *Streamer dynamics in gases containing dust particles*. Plasma Sources Sci. T. **15**, 591 (2006), doi: 10.1088/0963-0252/15/4/001.

[16] Babaeva, N. Yu. and Kushner, M. J. *Streamer branching: The role of inhomogeneities and bubbles*. IEEE T. Plasma. Sci. **36**, 892 –893 (2008), doi: 10.1109/TPS.2008.922434.

[17] Baines, K. H., Simon-Miller, A. A. and Orton, G. S. *Polar lightning and decadal-scale cloud variability on Jupiter*. Science **318**, 226–229 (2007), doi: 10.1126/science.1147912.

[18] Barrington-Leigh, C. P., Inan, U. S., Stanley, M. and Cummer, S. A. *Sprites triggered by negative lightning discharges*. Geophys. Res. Lett. **26**, 3605–3608 (1999), doi: 10.1029/1999GL010692.

[19] Bazelyan, E. M., Raizer, Yu. P. and Aleksandrov, N. L. *Corona initiated from grounded objects under thunderstorm conditions and its influence on lightning attachment*. Plasma Sources Sci. T. **17**, 24015 (2008), doi: 10.1088/0963-0252/17/2/024015.

[20] Beckers, J., Manders, F., Aben, P. C. H., Stoffels, W. W. and Haverlag, M. *Pulse, dc and ac breakdown in high pressure gas discharge lamps*. J. Phys. D: Appl. Phys. **41**, 144028 (2008), doi: 10.1088/0022-3727/41/14/144028.

[21] Blanc, R. *Exploring effects of UV radiation and spectroscopic overview on streamers*. Trainee report, Eindhoven University of Technology (2009). EPG 09-09.

[22] Blom, P. P. M., Smit, C., Lemmens, R. H. P. and van Heesch, E. J. M. *Combined optical and electrical measurements on pulsed corona discharges*. Gaseous Dielectrics **7**, 609 (1994).

[23] Blom, P. P. M. *High-power pulsed coronas*. Ph.D. thesis, Eindhoven University of Technology (1997). link.

[24] Borucki, W. J. and Magalhaes, J. *Analysis of Voyager 2 images of jovian lightning*. Icarus **96**, 1–14 (1992), doi: 10.1016/0019-1035(92)90002-O.

[25] Borucki, W. J., McKay, C. P., Jebens, D., Lakkaraju, H. S. and Vanajakshi, C. T. *Spectral irradiance measurements of simulated lightning in planetary atmospheres*. Icarus **123**, 336–344 (1996), doi: 10.1006/icar.1996.0162.

[26] Bourdon, A. *et al. Efficient models for photoionization produced by non-thermal gas discharges in air based on radiative transfer and the helmholtz equations*. Plasma Sources Sci. T. **16**, 656 (2007), doi: 10.1088/0963-0252/16/3/026.

[27] Bourdon, A., Bonaventura, Z. and Celestin, S. *Influence of the pre-ionization background and simulation of the optical emission of a streamer discharge in preheated air at atmospheric pressure between two point electrodes*. Plasma Sources Sci. T. **19**, 034012 (2010), doi: 10.1088/0963-0252/19/3/034012.

[28] Bradley, C. D. and Snoddy, L. B. *Ion distribution during the initial stages of spark discharge in nonuniform fields*. Phys. Rev. **47**, 541 (1935), doi: 10.1103/PhysRev.47.541.

[29] Brewster, D. *The stereoscope: its history, theory and construction* (Morgan & Morgan, 1856).

[30] Briels, T. M. P., van Veldhuizen, E. M. and Ebert, U. *Branching of positive discharge streamers in air at varying pressures*. IEEE T. Plasma. Sci. **33**, 264 (2005), doi: 10.1109/TPS.2005.845939.

[31] Briels, T. M. P., Kos, J., van Veldhuizen, E. M. and Ebert, U. *Circuit dependence of the diameter of pulsed positive streamers in air*. J. Phys. D: Appl. Phys. **39**, 5201 (2006), doi: 10.1088/0022-3727/39/24/016.

[32] Briels, T. M. P. *Exploring streamer variability in experiments*. Ph.D. thesis, Eindhoven University of Technology (2007). link.

[33] Briels, T. M. P., Kos, J., Winands, G. J. J., van Veldhuizen, E. M. and Ebert, U. *Positive and negative streamers in ambient air: measuring diameter, velocity and dissipated energy*. J. Phys. D: Appl. Phys. **41**, 234004 (2008), doi: 10.1088/0022-3727/41/23/234004.

[34] Briels, T. M. P., van Veldhuizen, E. M. and Ebert, U. *Positive streamers in air and nitrogen of varying density: experiments on similarity laws*. J. Phys. D: Appl. Phys. **41**, 234008 (2008), doi: 10.1088/0022-3727/41/23/234008.

[35] Briels, T. M. P., van Veldhuizen, E. M. and Ebert, U. *Positive streamers in ambient air and a N_2:O_2-mixture (99.8: 0.2)*. IEEE T. Plasma. Sci. **36**, 906–907 (2008), doi: 10.1109/TPS.2008.924510.

[36] Briels, T. M. P., van Veldhuizen, E. M. and Ebert, U. *Time resolved measurements of streamer inception in air*. IEEE T. Plasma. Sci. **36**, 908–909 (2008), doi: 10.1109/TPS.2008.920223.

[37] Bruggeman, P., Iza, F., Lauwers, D. and Gonzalvo, Y. A. *Mass spectrometry study of positive and negative ions in a capacitively coupled atmospheric pressure RF excited glow discharge in He-water mixtures*. J. Phys. D: Appl. Phys. **43**, 012003 (2010), doi: 10.1088/0022-3727/43/1/012003.

[38] Cabannes, F. and Chapelle, J. C. *Reactions under plasma conditions I*, chap. Spectroscopic plasma diagnostics (Wiley-Interscience, New York, 1971).

[39] Caillault, G. *Characterizing streamer channels in Helium*. Trainee report, Eindhoven University of Technology (2010). EPG 10-02.

[40] Clements, J. S., Mizuno, A., Finney, W. C. and Davis, R. H. *Combined removal of SO_2, NO_x, and fly ash from simulated flue gas using pulsed streamer corona*. IEEE T. Ind. Appl. **25**, 62 –69 (1989), doi: 10.1109/28.18870.

[41] Cravath, A. M. *Photoelectric effect and spark mechanism*. Phys. Rev. **47**, 254 (1935), (abstract for APS december meeting).

[42] Creyghton, Y. *Pulsed Positive Corona Discharges: Fundamental Study and Application to Flue Gas Treatment*. Phd thesis, Technische Universiteit Eindhoven (1994). link.

[43] Creyghton, Y. L. M. and van Veldhuizen, E. M. *Diagnostic techniques for atmospheric streamer discharges*. IEE Proceedings Science, Measurement & Technology **141**, 141 (1994), doi: 10.1049/ip-smt:19941017.

[44] Cummer, S. A. *et al. Submillisecond imaging of sprite development and structure*. Geophys. Res. Lett. **33**, L04104 (2006), doi: 10.1029/2005GL024969.

[45] Czichy, M., Hartmann, T., Mentel, J. and Awakowicz, P. *Ignition of mercury-free high intensity discharge lamps*. J. Phys. D: Appl. Phys. **41**, 144027 (2008), doi: 10.1088/0022-3727/41/14/144027.

[46] Derks, G., Ebert, U. and Meulenbroek, B. *Laplacian instability of planar streamer ionization fronts – an example of pulled front analysis*. J. NonLinear Sci. **18**, 551–590 (2008), doi: 10.1007/s00332-008-9023-0.

[47] Desch, S. J., Borucki, W. J., Russell, C. T. and Bar-Nun, A. *Progress in planetary lightning*. Rep. Prog. Phys. **65**, 955 (2002), doi: 10.1088/0034-4885/65/6/202.

[48] Dhali, S. K. and Williams, P. F. *Two-dimensional studies of streamers in gases*. J. Appl. Phys. **62**, 4696–4707 (1987), doi: 10.1063/1.339020.

[49] Dilecce, G., Ambrico, P. F. and Benedictis, S. D. *On the collision quenching of $N_2^+ (B\,^2\Sigma_u^+, v = 0)$ by N_2 and O_2 and its influence on the measurement of E/N by intensity ratio of nitrogen spectral bands*. J. Phys. D: Appl. Phys. **43**, 195201 (2010), doi: 10.1088/0022-3727/43/19/195201.

[50] Dyudina, U. A. *et al. Detection of visible lightning on Saturn*. Geophys. Res. Lett **37**, L09205 (2010), doi: 10.1029/2010GL043188.

[51] Ebert, U. *et al. The multiscale nature of streamers*. Plasma Sources Sci. T. **15**, S118 (2006), doi: 10.1088/0963-0252/15/2/S14.

[52] Ebert, U. *et al. Review of recent results on streamer discharges and discussion of their relevance for sprites and lightning*. J. Geophys. Res. - Space Physics **115**, A00E43 (2010), doi: 10.1029/2009JA014867.

[53] Éfendiev, A. Z. and Aliverdiev, A. A. *Multichannel helium discharge in a nonuniform field*. Radiophys. Quantum El. **20**, 850–855 (1977), 10.1007/BF01038796, doi: 10.1007/BF01038796.

[54] Eichwald, O. *et al. Experimental analysis and modelling of positive streamer in air: towards an estimation of O and N radical production*. J. Phys. D: Appl. Phys. **41**, 234002 (2008), doi: 10.1088/0022-3727/41/23/234002.

[55] Faugeras, O. D. *Three-Dimensional Computer Vision: A Geometric Viewpoint* (MIT Press, 1993).

[56] Flegler, E. and Raether, H. *Untersuchung von gasentladungsvorgängen mit der nebelkammer*. Zeitschrift für technische Physik **11**, 435 (1935).

[57] Franz, R. C., Nemzek, R. J. and Winckler, J. R. *Television image of a large upward electrical discharge above a thunderstorm system*. Science **249**, 48 (1990), doi: 10.1126/science.249.4964.48.

[58] Fridman, A., Chirokov, A. and Gutsol, A. *Non-thermal atmospheric pressure discharges*. J. Phys. D: Appl. Phys. **38**, R1 (2005), doi: 10.1088/0022-3727/38/2/R01.

[59] Fries, B. A. *Krypton-85. a versatile tracer for industrial process applications*. Int. J. Appl. Radiat. Is. **28**, 829 – 832 (1977), doi: 10.1016/0020-708X(77)90022-9.

[60] Gale, H. G., Monk, G. S. and Lee, K. O. *Measurements of wave-lengths in the secondary spectrum of hydrogen*. Astrophys. J. **67**, 89–113 (1928), doi: 10.1086/143095.

[61] Gallagher, T. *et al. Krypton-85 gas mixture radioactivity comparisons*. In Proceedings of the 12th International Symposium on the Science and Technology of Light Sources, Eindhoven, The Netherlands (2010).

[62] Gallimberti, I., Hepworth, J. K. and Klewe, R. C. *Spectroscopic investigation of impulse corona discharges*. J. Phys. D: Appl. Phys. **7**, 880 (1974), doi: 10.1088/0022-3727/7/6/315.

[63] Gerken, E. A., Inan, U. S. and Barrington-Leigh, C. P. *Telescopic imaging of sprites*. Geophys. Res. Lett. **27**, 2637 (2000), doi: 10.1029/2000GL000035.

[64] Gerken, E. A. and Inan, U. S. *Observations of decameter-scale morphologies in sprites*. J. Atmos. Sol.-Terr. Phy. **65**, 567 (2003), doi: 10.1016/S1364-6826(02)00333-4.

[65] Geurts, C. G. C. *Reconnection and merging of streamer channels*. Trainee report, Eindhoven University of Technology (2008). EPG 08-23.

[66] Glendenin, L. E. *Determination of the energy of beta particles and photons by absorption*. Nucleonics **2**, 12 (1948).

[67] Goldman, M. and Goldman, A. *Corona discharges*. In Gaseous Electronics, Volume 1: Electrical Discharges, 219 (1978).

[68] Goto, Y., Ohba, Y. and Narita, K. *Optical and spectral characteristics of low pressure air discharges as sprite models*. J. Atmos. Elec. **27**, 105–112 (2007).

[69] Goto, Y. and Ohba, Y. *Spectroscopic characteristics of the long gap CO_2 discharges as the model of Venus lightning discharges.* (2008). Unpublished.

[70] Grabowski, L., van Veldhuizen, E., Pemen, A. and Rutgers, W. *Corona above water reactor for systematic study of aqueous phenol degradation*. Plasma Chem. Plasma Process. **26**, 3–17 (2006), 10.1007/s11090-005-8721-8, doi: 10.1007/s11090-005-8721-8.

[71] Grabowski, L. R., Briels, T. M. P., van Veldhuizen, E. M. and Pemen, A. J. M. *Streamers in pulsed positive corona: low and high current regimes*. In Proceedings of the 27th ICPIG Conference (Eindhoven), vol. 27, 04–425 (2005). link.

[72] Gurnett, D. A. *et al. Lightning and plasma wave observations from the Galileo flyby of Venus*. Science **253**, 1522–1525 (1991), doi: 10.1126/science.253.5027.1522.

[73] Gurnett, D. A. *et al. Non-detection at Venus of high-frequency radio signals characteristic of terrestrial lightning*. Nature **409**, 313 (2001), doi: 10.1038/35053009.

[74] Gurnett *et al. Non-detection of impulsive radio signals from lightning in Martian dust storms using the radar receiver on the Mars Express spacecraft*. Geophys. Res. Lett. **37**, L17802 (2010), doi: 10.1029/2010GL044368.

[75] Hallac, A., Georghiou, G. E. and Metaxas, A. C. *Secondary emission effects on streamer branching in transient non-uniform short-gap discharges*. J. Phys. D: Appl. Phys. **36**, 2498 (2003), doi: 10.1088/0022-3727/36/20/011.

[76] Hampton, D. L., Heavner, M. J., Wescott, E. M. and Sentman, D. D. *Optical spectral characteristics of sprites*. Geophys. Res. Lett. **23**, 89–92 (1996), doi: 10.1029/95GL03587.

[77] Hansell, S. A., Wells, W. K. and Hunten, D. M. *Optical detection of lightning on Venus*. Icarus **117**, 345–351 (1995), doi: 10.1006/icar.1995.1160.

[78] Hartmann, G. and Gallimberti, I. *The influence of metastable molecules on the streamer progression*. J. Phys. D: Appl. Phys. **8**, 670 (1975), doi: 10.1088/0022-3727/8/6/010.

[79] He, J. L., Zhang, X. W., Dong, L., Zeng, R. and Liu, Z. H. *Fractal model of lightning channel for simulating lightning strikes to transmission lines*. Science in China Series E-technological Sciences **52**, 3135–3141 (2009), doi: 10.1007/s11431-009-0259-1.

[80] Heavner, M. J. *et al. Near-ultraviolet and blue spectral observations of sprites in the 320–460 nm region: N_2 (2PG) emissions*. J. Geophys. Res. **115**, A00E44, 5 PP. (2010), doi: 201010.1029/2009JA014858.

[81] van Heesch, E. J. M., Winands, G. J. J. and Pemen, A. J. M. *Evaluation of pulsed streamer corona experiments to determine the O* radical yield*. J. Phys. D: Appl. Phys. **41**, 234015 (2008), doi: 10.1088/0022-3727/41/23/234015.

[82] Hermans, P. J. *Een studie naar het gedrag van corona-ontladingen in verschillende gassen*. Trainee report, Eindhoven University of Technology (2004). EPG 04-01.

[83] Hu, W., Cummer, S. A., Lyons, W. A. and Nelson, T. E. *Lightning charge moment changes for the initiation of sprites*. Geophys. Res. Lett. **29**, 1279 (2002), doi: 10.1029/2001GL014593.

[84] Hu, W., Cummer, S. A. and Lyons, W. A. *Testing sprite initiation theory using lightning measurements and modeled electromagnetic fields*. J. Geophys. Res. **112**, 13115 (2007), doi: 10.1029/2006JD007939.

[85] Janda, M. and Machala, Z. *Transient-spark discharge in N_2/CO_2/H_2O mixtures at atmospheric pressure*. IEEE T. Plasma Science **36**, 916–917 (2008), doi: 10.1109/TPS.2008.917172.

[86] Kao, C. Y., Brau, F., Ebert, U., Schäfer, L. and Tanveer, S. *A moving boundary model motivated by electric breakdown: II. Initial value problem*. Physica D **239**, 1542–1559 (2010), arxiv preprint arXiv:0908.2521, doi: 10.1016/j.physd.2010.03.011.

[87] Kashiwagi, Y. and Itoh, H. *Positive surface streamers by VUV*. J. Phys. D: Appl. Phys. **39**, 113–118 (2006), doi: 10.1088/0022-3727/39/1/017.

[88] Kim, D. B., Rhee, J. K., Moon, S. Y. and Choe, W. *Study of geometrical and operational parameters controlling the low frequency microjet atmospheric pressure plasma characteristics*. Appl. Phys. Lett. **89**, 061502 (2006), doi: 10.1063/1.2335956.

[89] Kocik, M. *et al. Reconstruction of 3D structure of positive corona streamer by local methods*. In Hakone XII, 12th International Symposium on High Pressure Low Temperature Plasma Chemistry (2010).

[90] Kogelschatz, U. *Atmospheric-pressure plasma technology*. Plasma Phys. Contr. F. **46**, B63 (2004), doi: 10.1088/0741-3335/46/12B/006.

[91] Kossyi, I. A., Kostinsky, A. Y., Matveyev, A. A. and Silakov, V. P. *Kinetic scheme of the non-equilibrium discharge in nitrogen-oxygen mixtures*. Plasma Sources Sci. T. **1**, 207 (1992), doi: 10.1088/0963-0252/1/3/011.

[92] Kozlov, K. V., Wagner, H.-E., Brandenburg, R. and Michel, P. *Spatio-temporally resolved spectroscopic diagnostics of the barrier discharge in air at atmospheric pressure*. J. Phys. D: Appl. Phys. **34**, 3164 (2001), doi: 10.1088/0022-3727/34/21/309.

[93] Krasnochub, A. V., Mintoussov, E. I., Nudnova, M. M. and Starikovskii, A. Y. *Interference between streamers in bunch of streamers*. In Proceedings of the XXVIIth ICPIG, vol. 27, 04–312 (Eindhoven, The Netherlands, 2005). link.

[94] Krasnopolsky, V. A. *A sensitive search for nitric oxide in the lower atmospheres of Venus and Mars: detection on Venus and upper limit for Mars.* Icarus **182**, 80–91 (2006), doi: 10.1016/j.icarus.2005.12.003.

[95] Ksanfomality, L. V. *Venera 9 and 10: thermal radiometry.* Icarus **41**, 36–64 (1980), doi: 10.1016/0019-1035(80)90158-X.

[96] Kulikovsky, A. A. *The role of photoionization in positive streamer dynamics.* J. Phys. D: Appl. Phys. **33**, 1514–1524 (2000), doi: 10.1088/0022-3727/33/12/314.

[97] Kupershtokh, A. and Karpov, D. *Simulation of the development of branching streamer structures in dielectric liquids with pulsed conductivity of channels.* Tech. Phys. Lett. **32**, 406–409 (2006), doi: 10.1134/S1063785006050129.

[98] L'Annunziata, M. F. *Handbook of radioactivity analysis* (Academic Press, San Diego, 2003).

[99] Laux, C. Specair website. url: www.specair-radiation.net/.

[100] Laux, C. *Radiation and nonequilibrium collisional-radiative models.* In Fletcher, D., Charbonnier, J.-M., Sarma, G. and Magin, T. (eds.) von Karman Institute Lecture Series 07, Physico-Chemical Modeling of High Enthalpy and Plasma Flows (Rhode-Saint-Genèse, Belgium, 2002).

[101] Lavrov, B. P., Melnikov, A. S., Käning, M. and Röpcke, J. *UV continuum emission and diagnostics of hydrogen-containing nonequilibrium plasmas.* Phys. Rev. E **59**, 3526–3543 (1999), doi: 10.1103/PhysRevE.59.3526.

[102] Levin, Z., Borucki, W. B. and Toon, O. B. *Lightning generation in planetary atmospheres.* Icarus **56**, 80–115 (1983), doi: 10.1016/0019-1035(83)90129-X.

[103] Li, C., Brok, W. J. M., Ebert, U. and van der Mullen, J. J. A. M. *Deviations from the local field approximation in negative streamer heads.* J. Appl. Phys. **101**, 123305 (2007), doi: 10.1063/1.2748673.

[104] Li, C., Ebert, U. and Brok, W. *Avalanche-to-streamer transition in particle simulations.* IEEE T. Plasma. Sci. **36**, 910 –911 (2008), doi: 10.1109/TPS.2008.922487.

[105] Li, C., Ebert, U. and Hundsdorfer, W. *3D hybrid computations for streamer discharges and production of run-away electrons.* J. Phys. D: Appl. Phys. **42**, 202003 (2009), doi: 10.1088/0022-3727/42/20/202003.

[106] Lide, D. R. (ed.) *CRC Handbook of Chemistry and Physics, 90th Edition (Internet Version 2010)* (CRC Press/Taylor and Francis, Boca Raton, FL., 2010).

[107] Linstrom, P. J. and Mallard, W. G. (eds.) NIST Chemistry WebBook, NIST Standard Reference Database Number 69 (retrieved Oktober 25, 2009). url: webbook.nist.gov/chemistry.

[108] Liu, N. and Pasko, V. P. *Effects of photoionization on propagation and branching of positive and negative streamers in sprites.* J. Geophys. Res. **109**, 1 (2004), doi: 10.1029/2003JA010064.

[109] Liu, N. and Pasko, V. P. *Molecular nitrogen LBH band system far-UV emissions of sprite streamers.* Geophys. Res. Lett **32**, 05104 (2005), doi: 10.1029/2004GL022001.

[110] Liu, N. and Pasko, V. P. *Effects of photoionization on similarity properties of streamers at various pressures in air.* J. Phys. D: Appl. Phys. **39**, 327 (2006), doi: 10.1088/0022-3727/39/2/013.

[111] Liu, N. *et al. Comparison of results from sprite streamer modeling with spectrophotometric measurements by ISUAL instrument on FORMOSAT-2 satellite.* Geophys. Res. Lett **33**, 01101 (2006), doi: 10.1029/2005GL024243.

[112] Liu, N. *et al. Photoionization and optical emission effects of positive streamers in air at ground pressure.* IEEE T. Plasma. Sci. **36**, 942–943 (2008), doi: 10.1109/TPS.2008.927088.

[113] Liu, N. *Model of sprite luminous trail caused by increasing streamer current.* Geophys. Res. Lett **37**, L04102 (2010), doi: 10.1029/2009GL042214.

[114] Liu, Z., Yan, K., Winands, G. J. J., Heesch, E. J. M. V. and Pemen, A. J. M. *Novel multiple-switch blumlein generator*. Rev. Sci. Instrum. **77**, 033502 (2006), doi: 10.1063/1.2176080.

[115] Liu, Z. *et al. Multiple-gap spark gap switch*. Rev. Sci. Instrum. **77**, 073501–4 (2006), doi: 10.1063/1.2216792.

[116] Lock, E. H., Saveliev, A. V. and Kennedy, L. A. *Initiation of pulsed corona discharge under supercritical conditions*. IEEE T. Plasma. Sci. **33**, 850 – 853 (2005), doi: 10.1109/TPS.2005.845302.

[117] Loeb, L. B. *The problem of the mechanism of static spark discharge*. Rev. Mod. Phys. **8**, 267 (1936), doi: 10.1103/RevModPhys.8.267.

[118] Loeb, L. B. and Meek, J. M. *The mechanism of spark discharge in air at atmospheric pressure. i.* J. Appl. Phys. **11**, 438–447 (1940), doi: 10.1063/1.1712792.

[119] Luque, A., Ebert, U., Montijn, C. and Hundsdorfer, W. *Photoionization in negative streamers: Fast computations and two propagation modes*. Appl. Phys. Lett. **90**, 081501 (2007), doi: 10.1063/1.2435934.

[120] Luque, A. and Ebert, U. *Interacting streamers in air: The evolution of the space-charge layer in their heads*. IEEE T. Plasma. Sci. **36**, 914 (2008), doi: 10.1109/TPS.2008.925706.

[121] Luque, A., Ebert, U. and Hundsdorfer, W. *Interaction of streamer discharges in air and other oxygen-nitrogen mixtures*. Phys. Rev. Lett. **101**, 075005 (2008), doi: 10.1103/PhysRevLett.101.075005.

[122] Luque, A., Ratushnaya, V. and Ebert, U. *Positive and negative streamers in ambient air: modeling evolution and velocities*. J. Phys. D: Appl. Phys. **41**, 234005 (2008), doi: 10.1088/0022-3727/41/23/234005.

[123] Luque, A. and Ebert, U. *Emergence of sprite streamers from screening-ionization waves in the lower ionosphere*. Nature Geoscience **2**, 757–760 (2009), doi: 10.1038/ngeo662.

[124] Luque, A. and Ebert, U. *Sprites in varying air density: Charge conservation, glowing negative trails and changing velocity*. Geophys. Res. Lett **31**, L06806 (2010), doi: 10.1029/2009GL041982.

[125] MacAlpine, J. M. K., Qiu, D. H. and Li, Z. Y. *An analysis of spark paths in air using 3-dimensional imageprocessing*. IEEE T. Dielect. El. In. **6**, 331–336 (1999), doi: 10.1109/94.775619.

[126] Marode, E. *The mechanism of spark breakdown in air at atmospheric pressure between a positive point and a plane. i. experimental: Nature of the streamer track*. J. Appl. Phys. **46**, 2005–2015 (1975), doi: 10.1063/1.321882.

[127] Marshall, R. A. and Inana, U. S. *High-speed measurements of small-scale features in sprites: Sizes and lifetimes*. Radio Science **41**, RS6S43 (2006), doi: 10.1029/2005RS003353.

[128] McHarg, M. G., Stenbaek-Nielsen, H. C. and Kammae, T. *Observations of streamer formation in sprites*. Geophys. Res. Lett. **34**, L06804 (2007), doi: 10.1029/2006GL027854.

[129] Meek, J. M. and Craggs, J. D. *Electrical breakdown of gases* (John Wiley and Sons, 1978).

[130] Meek, J. M. *A theory of spark discharge*. Phys. Rev. **57**, 722–728 (1940), doi: 10.1103/PhysRev.57.722.

[131] Mende, S. B., Rairden, R. L., Swenson, G. R. and Lyons, W. A. *Sprite Spectra; $N\tilde{2}$ 1 PG band identification*. Geophys. Res. Lett **22**, 2633–2636 (1995), doi: 10.1029/95GL02827.

[132] Meulenbroek, B., Rocco, A. and Ebert, U. *Streamer branching rationalized by conformal mapping techniques*. Phys. Rev. E **69**, 67402 (2004), doi: 10.1103/PhysRevE.69.067402.

[133] Miermans, K. *Influence of gas composition on streamer morphology*. Trainee report, Eindhoven University of Technology (2010). EPG 10-01.

[134] Moerman, J. *EUV spectroscopy of hydrogen plasmas*. Trainee report, Eindhoven University of Technology (2008). EPG 07-14.

[135] Montijn, C., Meulenbroek, B., Ebert, U. and Hundsdorfer, W. *Numerical simulations and conformal analysis of growing and branching negative discharge streamers*. IEEE T. Plasma. Sci. **33**, 260 (2005), doi: 10.1109/TPS.2005.845951.

[136] Montijn, C. and Ebert, U. *Diffusion correction to the Raether and Meek criterion for the avalanche-to-streamer transition*. J. Phys. D: Appl. Phys. **39**, 2979 (2006), doi: 10.1088/0022-3727/39/14/017.

[137] Montijn, C., Ebert, U. and Hundsdorfer, W. *Numerical convergence of the branching time of negative streamers*. Phys. Rev. E **73**, 65401 (2006), doi: 10.1103/PhysRevE.73.065401.

[138] Moreau, E. *Airflow control by non-thermal plasma actuators*. J. Phys. D: Appl. Phys. **40**, 605 (2007), doi: 10.1088/0022-3727/40/3/S01.

[139] Morrow, R. and Lowke, J. J. *Streamer propagation in air*. J. Phys. D: Appl. Phys. **30**, 614 (1997), doi: 10.1088/0022-3727/30/4/017.

[140] Moudry, D. R., Stenbaek-Nielsen, H. C., Sentman, D. D. and Wescott, E. M. *Velocities of sprite tendrils*. Geophys. Res. Lett. **29**, 1992 (2002), doi: 10.1029/2002GL015682.

[141] Naidis, G. V. *On photoionization produced by discharges in air*. Plasma Sources Sci. T. **15**, 253–255 (2006), doi: 10.1088/0963-0252/15/2/010.

[142] Nakamura, M. *et al. Planet-C: Venus climate orbiter mission of Japan*. Planet. Space Sci. **55**, 1831 – 1842 (2007), the Planet Venus and the Venus Express Mission, Part 2, doi: 10.1016/j.pss.2007.01.009.

[143] Namihira, T., Wang, D., Katsuki, S., Hackam, R. and Akiyama, H. *Propagation velocity of pulsed streamer discharges in atmospheric air*. IEEE T. Plasma. Sci. **31**, 1091 (2003), doi: 10.1109/TPS.2003.818765.

[144] Ng, W. B. and Zhang, Y. *Stereoscopic imaging and reconstruction of the 3D geometry of flame surfaces*. Exp. Fluids **34**, 484–493 (2003), doi: 10.1007/s00348-002-0585-6.

[145] Nguyen, C. V., van Deursen, A. P. J. and Ebert, U. *Multiple X-ray bursts from long discharges in air*. J. Phys. D: Appl. Phys. **41**, 234012 (2008), doi: 10.1088/0022-3727/41/23/234012.

[146] Niemeyer, L., Pietronero, L. and Wiesmann, H. J. *Fractal dimension of dielectric breakdown*. Phys. Rev. Lett. **52**, 1033 (1984), doi: 10.1103/PhysRevLett.52.1033.

[147] Niemeyer, L., Ullrich, L. and Wiegart, N. *The mechanism of leader breakdown in electronegative gases*. IEEE T. Electr. Insul. **24**, 309 (1989).

[148] Nijdam, S., Moerman, J. S., Briels, T. M. P., van Veldhuizen, E. M. and Ebert, U. *Stereo-photography of streamers in air*. Appl. Phys. Lett. **92**, 101502 (2008), doi: 10.1063/1.2894195.

[149] Nijdam, S., Geurts, C. G. C., van Veldhuizen, E. M. and Ebert, U. *Reconnection and merging of positive streamers in air*. J. Phys. D: Appl. Phys. **42**, 045201 (2009), doi: 10.1088/0022-3727/42/4/045201.

[150] Nijdam, S., van de Wetering, F. M. J. H., Blanc, R., van Veldhuizen, E. M. and Ebert, U. *Probing photo-ionization: Experiments on positive streamers in pure gases and mixtures*. J. Phys. D: Appl. Phys. **43**, 145204 (2010), doi: 10.1088/0022-3727/43/14/145204.

[151] Nijdam, S., van Veldhuizen, E. M. and Ebert, U. *Comment on "NO_x production in laboratory discharges simulating blue jets and red sprites" by H. Peterson et al.* J. Geophys. Res. - Space Physics **115**, A12305 (2010), accepted, doi: 10.1029/2010JA015861.

[152] Nudnova, M. M. and Starikovskii, A. Yu. *Streamer head structure: role of ionization and photoionization*. J. Phys. D: Appl. Phys. **41**, 234003 (2008), doi: 10.1088/0022-3727/41/23/234003.

[153] Ono, R. and Oda, T. *Formation and structure of primary and secondary streamers in positive pulsed corona discharge–effect of oxygen concentration and applied voltage*. J. Phys. D: Appl. Phys. **36**, 1952–1958 (2003), doi: 10.1088/0022-3727/36/16/306.

[154] Orville, R. E. and Salanave, L. E. *Lightning Spectroscopy—Photographic Techniques*. Appl. Opt. **9**, 1775–1781 (1970), doi: 10.1364/AO.9.001775.

198

[155] Pai, D. Z., Lacoste, D. A. and Laux, C. O. *Transitions between corona, glow, and spark regimes of nanosecond repetitively pulsed discharges in air at atmospheric pressure*. J. Appl. Phys. **107**, 093303 (2010), doi: 10.1063/1.3309758.

[156] Pancheshnyi, S. *Role of electronegative gas admixtures in streamer start, propagation and branching phenomena*. Plasma Sources Sci. T. **14**, 645 (2005), doi: 10.1088/0963-0252/14/4/002.

[157] Pancheshnyi, S., Nudnova, M. and Starikovskii, A. *Development of a cathode-directed streamer discharge in air at different pressures: Experiment and comparison with direct numerical simulation*. Phys. Rev. E **71**, 016407 (2005), doi: 10.1103/PhysRevE.71.016407.

[158] Pancheshnyi, S. Private communications (2010).

[159] Paris, P. *et al. Intensity ratio of spectral bands of nitrogen as a measure of electric field strength in plasmas*. J. Phys. D: Appl. Phys. **38**, 3894 (2005), doi: 10.1088/0022-3727/38/21/010.

[160] Pasko, V. P., Inan, U. S. and Taranenko, Y. N. *Sprites produced by quasi-electrostatic heating and ionization in the lower ionosphere.* J. Geophys. Res. **102**, 4529 (1997), doi: 10.1029/96JA03528.

[161] Pasko, V. P., Inan, U. S. and Bell, T. F. *Spatial structure of sprites*. Geophys. Res. Lett **25**, 2123–2126 (1998), doi: 10.1029/98GL01242.

[162] Pasko, V. P., Inan, U. S. and Bell, T. F. *Fractal structure of sprites*. Geophys. Res. Lett **27**, 497–500 (2000), doi: 10.1029/1999GL010749.

[163] Pasko, V. P., Inan, U. S. and Bell, T. F. *Mesosphere-troposphere coupling due to sprites*. Geophys. Res. Lett. **28**, 3821 (2001), doi: 10.1029/2001GL013222.

[164] Pasko, V. P. *Sprites, Elves and Intense Lightning Discharges*, vol. 225 of *NATO Science Series II: Mathematics, Physics and Chemistry*, chap. Theoretical modeling of sprites and jets, 253–311 (Springer Netherlands, 2006), link.

[165] Pasko, V. P. *Red sprite discharges in the atmosphere at high altitude: the molecular physics and the similarity with laboratory discharges*. Plasma Sources Sci. T. **16**, S13 (2007), doi: 10.1088/0963-0252/16/1/S02.

[166] Pearse, R. W. B. and Gaydon, A. G. *The identification of molecular spectra* (Chapman & Hall Ltd, London, 1965).

[167] Penney, G. W. and Hummert, G. T. *Photoionization measurements in air, oxygen, and nitrogen*. J. Appl. Phys. **41**, 572 (1970), doi: 10.1063/1.1658715.

[168] Peterson, H., Bailey, M., Hallett, J. and Beasley, W. *NOx production in laboratory discharges simulating blue jets and red sprites*. J. Geophys. Res. **114**, A00E07 (2009), doi: 10.1029/2009JA014489.

[169] Przybylski, A. *Untersuchung über die "gasionisierende" Strahlung einer Entladung*. Zeitschrift für Physik **151**, 264 (1958), doi: 10.1007/BF01338382.

[170] Raether, H. *Über eine gasionisierende Strahlung einer Funkenentladung*. Zeitschrift für Physik **110**, 611 (1938), doi: 10.1007/BF01340219.

[171] Raether, H. *Die Entwicklung der Elektronenlawine in den Funkenkanal*. Zeitschrift für Physik A Hadrons and Nuclei **112**, 464–489 (1939), doi: 10.1007/BF01340229.

[172] Raizer, Yu. P. *Gas discharge physics* (Springer-Verlag Berlin, 1991).

[173] Raizer, Yu. P., Milikh, G. M., Shneider, M. N. and Novakovski, S. V. *Long streamers in the upper atmosphere above thundercloud*. J. Phys. D: Appl. Phys. **31**, 3255 (1998), doi: 10.1088/0022-3727/31/22/014.

[174] Ralchenko, Yu., Kramida, A. E., Reader, J. and NIST ASD Team. NIST atomic spectra database (2008). url: physics.nist.gov/asd3.

[175] Ratushnaya, V., Luque, A. and Ebert, U. *Electrodynamic characterization of long positive streamers in air* (2011), to be submitted to J. Phys. D: Appl. Phys.

[176] Rep'ev, A. G. and Repin, P. B. *Dynamics of the optical emission from a high-voltage diffuse discharge in a rod-plane electrode system in atmospheric-pressure air.* Plasma Phys. Rep. **32**, 72–78 (2006), doi: 10.1134/S1063780X06010077.

[177] Ricard, A., Décomps, P. and Massines, F. *Kinetics of radiative species in helium pulsed discharge at atmospheric pressure.* Surf. Coat. Technol. **112**, 1 – 4 (1999), doi: 10.1016/S0257-8972(98)00797-X.

[178] Rocco, A., Ebert, U. and Hundsdorfer, W. *Branching of negative streamers in free flight.* Phys. Rev. E **66**, 35102 (2002), doi: 10.1103/PhysRevE.66.035102.

[179] Roth, J. R. *Industrial plasma engineering: Principles* (Institute of Physics Publishing, London, 1995).

[180] Ruf, C. *et al. Emission of non-thermal microwave radiation by a Martian dust storm.* Geophys. Res. Lett **36**, L13202 (2009), doi: 10.1029/2009GL038715.

[181] Russell, C. T. *et al. Lightning on Venus inferred from whistler-mode waves in the ionosphere.* Nature **450**, 661–662 (2007), doi: 10.1038/nature05930.

[182] Russell, C., Strangeway, R., Daniels, J., Zhang, T. and Wei, H. *Venus lightning: Comparison with terrestrial lightning.* Planet. Space Sci. (2010), in Press, Corrected Proof, doi: 10.1016/j.pss.2010.02.010.

[183] Sao Sabbas, F. T. *et al. Statistical analysis of space-time relationships between sprites and lightning.* J. Atmos. Sol.-Terr. Phy. **65**, 525–535 (2003), doi: 10.1016/S1364-6826(02)00326-7.

[184] Sentman, D. D., Stenbaek-Nielsen, H. C., McHarg, M. G. and Morrill, J. S. *Plasma chemistry of sprite streamers.* J. Geophys. Res. - Atmospheres **113**, D11112 (2008), doi: 10.1029/2007JD008941.

[185] Sentman, D., Wescott, E., Osborne, D., Hampton, D. and Heavne, M. *Preliminary results from the Sprites94 aircraft campaign: 1. Red sprites.* Geophys. Res. Lett. **22**, 1205 (1995), doi: 10.1029/95GL00583.

[186] Settaouti, A. *Monte carlo simulation of avalanche formation and streamer discharge.* Electrical Engineering (Archiv fur Elektrotechnik) **92**, 35–42 (2010), doi: 10.1007/s00202-010-0157-3.

[187] Shcherbakov, Y. V. and Sigmond, R. S. *Subnanosecond spectral diagnostics of streamer discharges: I. basic experimental results.* J. Phys. D: Appl. Phys. **40**, 460 (2007), doi: 10.1088/0022-3727/40/2/023.

[188] Shcherbakov, Y. V. and Sigmond, R. S. *Subnanosecond spectral diagnostics of streamer discharges: Ii. theoretical background.* J. Phys. D: Appl. Phys. **40**, 474 (2007), doi: 10.1088/0022-3727/40/2/024.

[189] Sigmond, R. S. *The residual streamer channel: Return strokes and secondary streamers.* J. Appl. Phys. **56**, 1355–1370 (1984), doi: 10.1063/1.334126.

[190] Šijačić, D. D. and U., E. *Transition from townsend to glow discharge: Subcritical, mixed, or supercritical characteristics.* Phys. Rev. E **66**, 066410 (2002), doi: 10.1103/PhysRevE.66.066410.

[191] Šimek, M., Babický, V., Člupek, M. and Šunka, P. *Observation of the N_2 Herman infrared system in pulsed positive streamer induced emission at atmospheric pressure.* J. Phys. D: Appl. Phys. **34**, 3185 (2001), doi: 10.1088/0022-3727/34/21/311.

[192] Šimek, M. *Streamer-induced emission and spectrometric determination of basic plasma parameters.* Czechoslovak Journal of Physics **54**, C778–C783 (2004), doi: 10.1007/BF03166486.

[193] Sinkevich, O. A. *Anode streamer branching.* High Temp. **41**, 609–618 (2003), doi: 10.1023/A:1026136426473.

[194] Smith, P. W. *Transient Electronics: Pulsed Circuit Technology* (Wiley, Chichester, 2002).

[195] Snuggs, R. M., Volz, D. J., Schummers, J. H., Martin, D. W. and McDaniel, E. W. *Mobilities and longitudinal diffusion coefficients of mass-identified potassium ions and positive and negative oxygen ions in oxygen.* Phys. Rev. A **3**, 477–487 (1971), doi: 10.1103/PhysRevA.3.477.

200

[196] Sobota, A., van Veldhuizen, E. M. and Stoffels, W. W. *Discharge ignition near a dielectric*. IEEE T. Plasma. Sci. **36**, 912 (2008), doi: 10.1109/TPS.2008.924614.

[197] Staack, D., Farouk, B., Gutsol, A. and Fridman, A. *DC normal glow discharges in atmospheric pressure atomic and molecular gases*. Plasma Sources Sci. T. **17**, 025013 (2008), doi: 10.1088/0963-0252/17/2/025013.

[198] Starikovskii, A. *et al. Nanosecond-pulsed discharges for plasma-assisted combustion and aerodynamics*. J. Propul. Power **24**, 1182 (2008), doi: 10.2514/1.24576.

[199] Stenbaek-Nielsen, H. C., McHarg, M. G., Kanmae, T. and Sentman, D. D. *Observed emission rates in sprite streamer heads*. Geophys. Res. Lett. **34**, L11105 (2007), doi: 10.1029/2007GL029881.

[200] Stenbaek-Nielsen, H. C. and McHarg, M. G. *High time-resolution sprite imaging: observations and implications*. J. Phys. D: Appl. Phys. **41**, 234009 (2008), doi: 10.1088/0022-3727/41/23/234009.

[201] Stenbaek-Nielsen, H., Haaland, R., McHarg, M. G., Hensley, B. A. and Kanmae, T. *Sprite initiation altitude measured by triangulation*. J. Geophys. Res. **115**, A00E12 (2010), doi: 10.1029/2009JA014543.

[202] Stritzke, P., Sander, I. and Raether, H. *Spatial and temporal spectroscopy of a streamer discharge in nitrogen*. J. Phys. D: Appl. Phys. **10**, 2285–2300 (1977), doi: 10.1088/0022-3727/10/16/019.

[203] Sun, B., Sato, M. and Clements, J. S. *Optical study of active species produced by a pulsed streamer corona discharge in water*. J. of Electrostat. **39**, 189 – 202 (1997), doi: 10.1016/S0304-3886(97)00002-8.

[204] Takahashi, Y., Yoshida, J., Yair, Y., Imamura, T. and Nakamura, M. *Lightning detection by LAC onboard the Japanese Venus climate orbiter, Planet-C*. Space Sci. Rev. **137**, 317–334 (2008), doi: 10.1007/s11214-008-9400-x.

[205] Takahashi, Y. *et al. Absolute optical energy of sprites and its relationship to charge moment of parent lightning discharge based on measurement by ISUAL/AP*. J. Geophys. Res. **115**, A00E55 (2010), doi: 10.1029/2009JA014814.

[206] Takaki, K., Hosokawa, M., Sasaki, T., Mukaigawa, S. and Fujiwara, T. *Production of atmospheric-pressure glow discharge in nitrogen using needle-array electrode*. Appl. Phys. Lett. **86**, 151501 (2005), doi: 10.1063/1.1905801.

[207] Tan, Y. B., Tao, S. C. and Zhu, B. Y. *Fine-resolution simulation of the channel structures and propagation features of intracloud lightning*. Geophys. Res. Lett **33**, L09809 (2006), doi: 10.1029/2005GL025523.

[208] Tanveer, S., Schäfer, L., Brau, F. and Ebert, U. *A moving boundary problem motivated by electric breakdown, I: Spectrum of linear perturbations*. Physica D **238**, 888–901 (2009), doi: 10.1016/j.physd.2009.02.012.

[209] Tao, S., Tan, Y., Zhu, B., Ma, M. and Lu, W. *Fine-resolution simulation of cloud-to-ground lightning and thundercloud charge transfer*. Atmospheric Research **91**, 360–370 (2009), doi: 10.1016/j.atmosres.2008.05.012.

[210] Tardiveau, P., Marode, E., Agneray, A. and Cheaib, M. *Pressure effects on the development of an electric discharge in non-uniform fields*. J. Phys. D: Appl. Phys. **34**, 1690 (2001), doi: 10.1088/0022-3727/34/11/321.

[211] Teich, T. H. *Emission gasionisierender Strahlung aus Elektronenlawinen I. Messanordnung und Messverfahren. Messungen in Sauerstoff*. Zeitschrift für Physik **199**, 378–394 (1967).

[212] Teich, T. H. *Emission gasionisierender Strahlung aus Elektronenlawinen II. Messungen in O_2– He-Gemischen, Daempfen, CO_2 und Luft; Datenzusammenstellung*. Zeitschrift für Physik **199**, 395–410 (1967).

[213] Teich, T. H. *Emission spectroscopy of corona discharges*. NATO ASI series G ecological sciences **34**, 231–231 (1993).

[214] Thomas Jr, E., Williams, J. D. and Silver, J. *Application of stereoscopic particle image velocimetry to studies of transport in a dusty (complex) plasma*. Phys. Plasmas **11**, L37 (2004), doi: 10.1063/1. 1755705.

[215] Tochikubo, F. and Teich, T. H. *Optical emission from a pulsed corona discharge and its associated reactions*. Jpn. J. Appl. Phys **39**, 1343–1350 (2000), doi: 10.1143/JJAP.39.1343.

[216] Townsend, J. S. E. *Electricity in gases* (Clarendon Press, Oxford, 1915).

[217] Tren'kin, A. A. *Fractal spatial structure of lightning discharge and its relation to the structures of high-voltage discharges of other types*. Tech. Phys. Lett. **36**, 299–301 (2010), doi: 10.1134/S1063785010040036.

[218] Uehara, H. and Kud, K. *Three-dimensional tree simulation utilizing a three-layer model*. Electrical Engineering in Japan **168**, 1–9 (2009), doi: 10.1002/eej.20808.

[219] Uman, M. A. *Lightning* (Dover Publications, New York, 1984).

[220] van Veldhuizen, E. M. *Electrical Discharges for Environmental Purposes: Fundamentals and Applications* (Nova Science Publishers, New York, 2000).

[221] van Veldhuizen, E. M., Kemps, P. C. M. and Rutgers, W. R. *Streamer branching in a short gap: the influence of the power supply*. IEEE T. Plasma. Sci. **30**, 162 –163 (2002), doi: 10.1109/TPS. 2002.1003974.

[222] van Veldhuizen, E. M. and Rutgers, W. R. *Pulsed positive corona streamer propagation and branching*. J. Phys. D: Appl. Phys. **35**, 2169 (2002), doi: 10.1088/0022-3727/35/17/313.

[223] van Veldhuizen, E. M. and Rutgers, W. R. *Inception behaviour of pulsed positive corona in several gases*. J. Phys. D: Appl. Phys. **36**, 2692 (2003), doi: 10.1088/0022-3727/36/21/015.

[224] Verreycken, T., Schram, D. C., Leys, C. and Bruggeman, P. *Spectroscopic study of an atmospheric pressure dc glow discharge with a water electrode in atomic and molecular gases*. Plasma Sources Sci. T. **19**, 045004 (2010), doi: 10.1088/0963-0252/19/4/045004.

[225] Vitello, P. A., Penetrante, B. M. and Bardsley, J. N. *Simulation of negative-streamer dynamics in nitrogen*. Phys. Rev. E **49**, 5574–5598 (1994), doi: 10.1103/PhysRevE.49.5574.

[226] Weissler, G. L. *Positive and negative point-to-plane corona in pure and impure hydrogen, nitrogen, and argon*. Phys. Rev. **63**, 96 (1943), doi: 10.1103/PhysRev.63.96.

[227] van de Wetering, F. M. J. H. *Characterizing streamer channels in N_2:O_2 mixtures and pure Ar*. Trainee report, Eindhoven University of Technology (2008). EPG 08-22.

[228] Williams, D. R. Planetary fact sheets. url: nssdc.gsfc.nasa.gov/planetary/planetfact.html.

[229] Williams, E., Valente, M., Gerken, E. and Golka, R. *Sprites, Elves and Intense Lightning Discharges*, vol. 225 of *NATO Science Series II: Mathematics, Physics and Chemistry*, chap. Calibrated radiance measurements with an air-filled glow discharge tube: application to sprites in the mesosphere., 237–247 (Springer Netherlands, 2006).

[230] Wilson, C. T. R. *The electric field of a thundercloud and some of its effects*. Proc. Phys. Soc. London **37**, 32D (1925), doi: 10.1088/1478-7814/37/1/314.

[231] Winands, G. J. J. *et al. Temporal development and chemical efficiency of positive streamers in a large scale wire-plate reactor as a function of voltage waveform parameters*. J. Phys. D: Appl. Phys. **39**, 3010 (2006), doi: 10.1088/0022-3727/39/14/020.

[232] Winands, G. J. J. *et al. An industrial streamer corona plasma system for gas cleaning*. IEEE T. Plasma. Sci. **34**, 2426–2433 (2006), doi: 10.1009/TPS.2006.881278.

[233] Winands, G. J. J. *Efficient Streamer Plasma Generation*. Ph.D. thesis, Technische Universiteit Eindhoven (2007). link.

[234] Winands, G. J. J., Liu, Z., Pemen, A. J. M., van Heesch, E. J. M. and Yan, K. *Analysis of streamer properties in air as function of pulse and reactor parameters by iccd photography*. J. Phys. D: Appl. Phys. **41**, 234001 (2008), doi: 10.1088/0022-3727/41/23/234001.

[235] Winands, G. J. J., Liu, Z., van Heesch, E. J. M., Pemen, A. J. M. and Yan, K. *ADS and CDS streamer generation as function of pulse parameters*. IEEE T. Plasma. Sci. **36**, 926 (2008), doi: 10.1109/TPS.2008.924097.

[236] Wormeester, G., Pancheshnyi, S., Luque, A., Nijdam, S. and Ebert, U. *Probing photoionization: Simulations of positive streamers in varying N_2:O_2-mixtures*. J. Phys. D: Appl. Phys. **43**, 505201 (2010), accepted, doi: 10.1088/0022-3727/43/50/505201.

[237] Wormeester, G., Nijdam, S. and Ebert, U. *Feather-like structures in positive streamers*. Jpn. J. Appl. Phys. (2011), submitted.

[238] Yair, Y., Levin, Z. and Tzivion, S. *Lightning generation in a Jovian thundercloud: Results from an axisymmetric numerical cloud model*. Icarus **115**, 421 – 434 (1995), doi: 10.1006/icar.1995.1108.

[239] Yair, Y., Fischer, G., Simoes, F., Renno, N. and Zarka, P. *Updated review of planetary atmospheric electricity*. Space Sci. Rev. **137**, 29–49 (2008), doi: 10.1007/978-0-387-87664-1_4.

[240] Yair, Y., Takahashi, Y., Yaniv, R., Ebert, U. and Goto, Y. *A study of the possibility of sprites in the atmospheres of other planets*. J. Geophys. Res. **114**, E09002 (2009), doi: 10.1029/2008JE003311.

[241] Yan, K. *et al. A high-voltage pulse generator for corona plasma generation*. IEEE T. Ind. Appl. **38**, 866–872 (2002), doi: 10.1109/TIA.2002.1003442.

[242] Yaniv, R., Devir, A., Yair, Y., Price, C. and Ziv, B. *Calibration of CCD cameras for measurements of sprites and elves*. In AIP Conference Proceedings, vol. 1118, 92 (2009).

[243] Yi, W. J. and Williams, P. F. *Experimental study of streamers in pure N_2 and N_2/O_2 mixtures and a $\approx$13 cm gap*. J. Phys. D: Appl. Phys. **35**, 205–218 (2002), doi: 10.1088/0022-3727/35/3/308.

[244] Zhelezniak, M. B., Mnatsakanian, A. K. H. and Sizykh, S. V. *Photoionisation of nitrogen and oxygen mixtures by radiation from a gas discharge*. High Temp. **20**, 357 (1982), link.

Index

Acknowledgments

Before I left my position at Philips Lighting to pursue a more scientific career, I was often told that the work of a PhD-student is boring and solitary. I can definitely disagree with this statement. All of the work I have done during the past four years was done together with other people, whose company I enjoyed very much, both during work hours as well as on business trips and social occasions. Furthermore, I have never been bored with my work at all.

First and foremost I would like to thank Eddie van Veldhuizen and Ute Ebert. They were my direct supervisors in this project and have helped me understand streamers and streamer research. Furthermore, they were of great value in assisting me while writing papers and finally this thesis. My second promotor, Gerrit Kroesen, made it possible for me to work on two very different projects, of which only one is discussed in this thesis. He helped me a lot, especially in the project that is outside the scope of this work, namely research on exotic effects in hydrogen discharges.

Working on two entirely different projects at the same time would not have been possible without the help of a large group of students. The trainee students that worked on streamers are Joeri Moerman, Christian Geurts, Ferdi van de Wetering, Romuald Blanc, Karsten Miermans and Guillaume Caillault. All of these students performed experiments of which the results are represented in some way in this thesis. I again want to thank them for this work.

A second group of students worked on exotic effects in hydrogen discharges. These include six students that did more theoretical work as part of their honors-program: Ilse van der Heijden, Marloes van der Heijden, Jarno van Roosmalen, Sander Verdonschot, Jaron Sanders and Bauke Conijn. Experimental work on this topic was done by eight internal and external trainees: Tim Righart, Andreas van den Brink, Gerrit Sitters, Alexis Leray, Ruud Joosten, Jeroen van der Put, Remco Poulus and Emilie Bahette. Finally, much experimental and theoretical work was done by four students working on their masters theses: Ruud Wijtvliet, Bram van Gessel, Benjamin de Maat and René van Bussel. Especially this last group has

achieved a lot and made it easy for me to spend enough time on streamers while they investigated the interesting hydrogen discharges. Furthermore, they made working on this topic a pleasure.

Besides the support from the people mentioned above, that worked directly for my projects, I have also gotten a lot of support from other people within the EPG group. The list would be too long to name them all, so I will only mention some special ones: Tanja Briels, whose work was the basis for my work and helped me to start my project, Hjalmar Mulders, my room-mate for most of the time and who was always there for a nice discussion, Ana Sobota, who works on a related topic and therefore shared a lot of equipment and information with me, Rina Boom, whose help is needed and welcomed by all EPG members and finally, our technicians, Evert, Loek and Huib who were always ready to troubleshoot and fix my problems. In the workshop of the physics department, much work was done to build and modify set-ups used in both of my projects. I specifically want to thank Jan van Asten, who came back from retirement to build a complicated calorimetric set-up.

Outside of our department I was helped by many people from the Electrical Engineering department, most notably Guus Pemen who helped us design and improve our pulsed power supplies and by people working for the CWI in Amsterdam like Alejandro Luque, Li Chao and Gideon Wormeester. Geographically even further away are the nice people in Tel Aviv, namely Yoav Yair and Daria Dubrovin. Daria visited us twice to perform the planetary sprite experiments that are treated in this work. These two visits were a pleasure and have lead to some good results and discussions.

Besides Eddie, Ute, Gerrit and Yoav, I also want to thank the other members of my PhD committee, namely Thomas Christen, Takashi Fujii, Niek Lopes Cardozo and Klaas Kopinga. Thank you for taking the time to carefully read my thesis and to attend the defence.

Finally, I would like to thank Yvonne van Andel for supporting me in my decision to quit my job at Philips and start with this PhD project and for your continuing support during the project.

Curriculum Vitae

Born in Nuenen, the Netherlands, 4 December 1974

1987-1993

Secondary education (VWO) at Eckart College Eindhoven.
Courses in final exams: Dutch, English, Math A, Physics, Chemistry, Biology, Geography.
Participated in the national and international biology Olympiad (1992 and 1993).
Finished 4th nationally and 10th internationally (1993).

1993-2000

M.Sc. in Applied Physics at the Eindhoven University of Technology (TU/e):

- Traineeship at the Eindhoven University of Technology in the group Cryogenic Technology.
  Subject: *Electronen op vloeibaar helium in besloten geometriën* (Electrons on liquid helium in enclosed geometries), supervised by ir. A.M.C. Valkering and dr. R.W. van der Heijden. Grade: 8/10

- Traineeship at the Philips Lighting, Eindhoven.
  Subject: *Dynamic behaviour of metal halide lamps in PCA*, supervised by dr. R. Keijser and prof.dr. J.J.A.M. van der Mullen. Grade: 9/10

- Master's thesis project at the Eindhoven University of Technology in the group Vortex Dynamics.
  Subject: *Concentration Measurements in a Stratified Fluid using Laser Induced Fluorescence*, supervised by ing. G.A.J. van der Plas, drs. S.R. Maassen and prof.dr.ir. G.J.F. van Heijst. Grade: 8.5/10

Extracurricular activities include membership of the board of the Student Association Demos, Eindhoven University 1995-1996. Active as treasurer and responsible for organization of large activities.

2000-2006

Development Engineer at the Central Development Lighting laboratory, Philips Lighting, Eindhoven.
Participation in and leading of projects within the group HID Lamp Ballast interactions (previously HID physics).
Amongst project tasks was the development of a computer model of electrodes in HID lamps.
Teacher of course *HID lamp physics* in the internal Philips HTO Lighting training program.

2006-2010

PhD project at the Eindhoven University of Technology in the group Elementary Processes in Gas Discharges of the Department of Applied Physics.
Subjects:

- *Experimental Investigations on the Physics of Streamers*, supervised by dr.ir. E.M. van Veldhuizen and prof.dr. U. Ebert.

- *Experiments on exotic effects in Hydrogen Discharges*, supervised by dr.ir. E.M. van Veldhuizen and prof.dr.ir. G. Kroesen.

In these projects, supervision of 24 trainee students (4 master projects, 10 bachelor projects, 4 exchange students from Orleans and 6 honors program projects).
Task as supervisor of first year practical work students. Nominated as best supervisor by students.
Outstanding Student Paper Award at the Fall Meeting of the American Geophysical Union 2009.

Other activities and skills

Scuba diving
Level PADI Dive Master (first professional level).
Assists regularly in training of new divers.